Active Filtering of AC Harmonics from HVDC Converters.

by

André Luiz da Rosa Plaisant

A thesis
presented to the University of Waterloo
in fulfillment of the
thesis requirement for the degree of
Doctor of Philosophy
in
Electrical Engineering

Waterloo, Ontario, Canada, 1997

The University of Waterloo requires the signatures of all persons using or photocopying this thesis. Please sign below, and give address and date.

Abstract

HVDC converter stations, being non-linear loads for the AC system, have been relying on the use of shunt AC passive filters to reduce the harmful effects that the harmonic AC currents impose on the AC system. AC passive filters, however, present several characteristics that redeem their performance to levels far from excellent.

Concerns about harmonic-related problems caused by the of use of large-capacity non-linear loads have led to the use of active filters in the industry. Active filters cancel the aimed harmonic content of a non-linear load by injecting harmonic currents with the same magnitude but in complete phase opposition. Active filters present superior performance than that offered by the traditional AC passive filters.

Although there have been proposals of the application of AC-side active filtering in HVDC systems, the present ratings of the power semiconductor switches commercially available do not permit the straightforward implementation of these proposals yet. Besides the high power rating that characterizes HVDC systems, some of their operation characteristics have been posing further obstacles to the use of active filters.

This thesis proposes an active-filter topology that decouples the reactive-power supply and filtering functions that characterize the traditional HVDC AC passive filters and all the active-filter proposals presented to date. The complete devotion to the filtering function offer several advantages that might overshadow its potentially higher initial costs.

The application of modern control theory is proposed as the basis of the control scheme. This technique suits more adequately the complexity of the control problem at hand than classical methods do, and provides a common framework for comparison of different control approaches. The optimal-control technique is the approach used in this thesis.

The CIGRÉ HVDC benchmark system has been chosen as the platform on which to test the performance of the proposed AC active filter. A simplified version of this system, that still maintains the weak AC system and the AC- and DC-frequency resonances of the original system, has been used, and poses a good degree of difficulty to the proposed active-filter operation.

Acknowledgments

I would like to express my gratitude to Professor John Reeve for the opportunity to do this research, for his expertise, guidance, encouragement and support.

I am also profoundly indebted to Geraldo Leite Torres, whom I am now a sincere friend of, for his help in typing this thesis, expertise with LaTeX and personal support.

A special thanks is due to Edvina Uzunovic, an office colleague who, by capricious fate, became a close friend, and whose personal support was very important to this accomplishment.

Thanks to Prof. David Wang for the valuable advice on Control Theory, to Antonio G. G. Lima and Luiz A. S. Pilotto, from CEPEL, for their recommendations and guidance, and to all of my office colleagues for many helpful and interesting discussions.

I would like to thank the Brazilian people through CAPES, for their financial support and trust. I also appreciate the support from the University of Waterloo, especially towards the end of the program.

The Brazilian community of Waterloo, particularly my close friends Antonio, Marli and Matheus, also deserve my deep gratitude for easing my homesickness by providing personal support and by keeping the Brazilian spirit always present.

A big "thanks" go to Everton, Fernando, Geraldo and Pedro, the "night-shift" group who, during the last months of preparing this manuscript, provided me with support and relaxing moments at the coffee breaks in the early, and late morning hours.

Finally, most of all, I would like to thank my parents, Cecilia and Geraldo, for caring, for their love, and for the life guidance and support that made this achievement possible.

André Luiz da Rosa Plaisant.

Glossary of Terms

ABB	ASEA Brown Boveri
AC	Alternating current
BIL	Basic insulation level
CEPEL	Centro de Pesquisas de Energia Elétrica
CCI	Current-controlled inverter
CIGRÉ	Conferénce Internationale des Grands Réseaux Electriques
CR-VSI	Current-regulated voltage-source inverter
CSI	Current-source inverter
DC	Direct current
DSP	Digital signal processor
ESCR	Effective short-circuit ratio
ESR	Equivalent series resistance
FACTS	Flexible AC transmission systems
FBSOA	Forward-biased safe operating area
FFT	Fast Fourier transform
HDL	Hardware-description language
HVDC	High voltage direct current
IHD	Individual harmonic distortion
MTBF	Mean-time between failures
NPT	Non-punch-through
PC	Phase comparator
PI	Proportional-integral
PLL	Phase-locked loop
p.u.	Per-unit
PWM	Pulse-width modulator

RBSOA	Reverse-biased safe operating area
RMS	Root-mean-square
SCR	Short-circuit ratio
SISO	Single-input, single-output
SPWM	Sinusoidal pulse-width modulator
SVC	Static VAr compensator
VCI	Voltage-controlled inverter
VCO	Voltage-controlled oscillator
VDCOL	Voltage-dependent current-order limiter
VSI	Voltage-source inverter
THD	Total harmonic distortion
TIF	Telephone interference factor

Contents

List of Tables

List of Figures

Chapter 1

Introduction

1.1 Introduction

Harmonics are qualitatively defined as sinusoidal waveforms of any frequency; they may be voltages or currents. Harmonic number h is the ratio between a harmonic and the fundamental frequencies. The AC power-system fundamental frequency has "1" as its harmonic number. If the harmonic number is greater than one, the harmonic is termed a superharmonic (or just "harmonic", for short); if less than one, a subharmonic. The DC component of a waveform is sometimes referred to as of order "0".

Harmonics arise whenever non-sinusoidal currents and/or voltages are generated in the power system, they are generally referred to as harmonic distortion. The basic conditions that give rise to harmonic-related problems in power systems are, in brief, as follows [1,2]:

- Non-linear loads;
- Phase imbalance;
- High input voltage or current;
- Resonance.

The harmonic-related problems caused by the wide spread use of large-capacity

non-linear loads such as rectifiers, inverters and cycloconverters in industries [3] and, on an individual basis, lower capacity ones in modern office-automation equipment [4], lead to the relatively recent creation of a new area in the power electronics field: Power Quality. Power quality is, nowadays, a major topic in the electric-power generation, distribution, and user arenas.

The use of such types of loads is ever increasing [5]. Therefore, power quality concerns already play a very important role in the electric-energy scenario, imposing harmonic power consumption constraints on the adoption of new power electronic technologies.

The IEEE Working Group on Power-System Harmonics listed the following areas and the harmonic problems [6]:

- Failure of capacitor banks due to dielectric breakdown or reactive-power overload;
- Interface with ripple control and power-line carrier systems, causing misoperation of systems which accomplish remote switching, load control, and metering;
- Excessive losses resulting in heating of induction and synchronous machines;
- Overvoltages and excessive currents on the system from resonance to harmonic voltages or currents in the network;
- Dielectric breakdown of insulated cables resulting from harmonic overvoltages in the system;
- Inductive interference with telecommunication systems;
- Errors in meter reading;
- Signal interference and relay malfunction, particularly in solid-state- and microprocessor-controlled systems;
- Interference with large motor controllers and power-plant excitation systems;
- Mechanical oscillations of induction and synchronous machines;
- Unstable operation of firing circuits based on zero-crossing detecting or latching.

In what concerns utility companies, since it is difficult to identify all the sources of harmonic distortion and take wide-range measures, it is more practical and cost-effective to lessen the effects of these distortions right at the equipment that causes them. At consumer levels, this practice is motivated by the imposition of extra taxes and/or fines on the infractor.

Traditionally, besides careful design of the equipment that causes harmonics and, if applicable, of its control, shunt passive filters have been widely used by energy utilities and consumers to minimize harmonic generation [7]. They consist of passive energy-storing elements (inductors and capacitors) arranged in such a topology as to provide a low-impedance path to the ground just for the harmonic frequency (or frequencies) to be reduced. It is said that the filters are "tuned" at these frequencies.

High-voltage-direct-current (HVDC) converter stations are, by their very nature, non-linear loads and their operation deals with all of the conditions which cause harmonics in power systems. Their high level of harmonic generation requires the installation of filters. Shunt passive AC filters, as will be seen in Chapter 3, have the added benefit of providing reactive-power compensation at the power (fundamental) frequency and, thus, improve the power factor of the converter station.

Since passive filters are expensive, tend to overload, and require a considerable amount of space, consideration has been given to yet another power-electronic equipment to solve these problems: the active filter. An active filter is a device that injects harmonic currents into the utility AC system with the same magnitudes but opposite phases as the harmonic currents generated by a given non-linear load.

For several years, the available ratings of power semiconductor switches have permitted their use in low- and medium-power active filtering (industrial applications). As a consequence, pulse-width-modulated (PWM) amplifiers have become available during recent years with ever increasing power capability and with very low losses. Concurrently, digital signal processors (DSP), a key technology, have recently become available with the capability of processing data at speeds commensurate with harmonic filtering [5].

Compared with industrial applications, until very recently, the available power-handling capabilities of power semiconductor switches have been inadequate for the needs of active filters at HVDC converter stations. As it will be clear from the

sections ahead, this limitation has been having the application of active filters in HVDC systems hindered.

Yet, new ideas for active filtering applied to HVDC systems have been proposed in recent years both in universities and in industry. This has been motivated by the existence of problems related to the design and use of passive filters, together with more and more stringent requirements from power utilities on limiting interference caused by harmonic currents from HVDC transmission lines [8–10], and recent breakthroughs in power-handling capabilities and speed of power semiconductor switches [11]. Some of these ideas will be briefly described in the subsequent sections.

1.2 Magnetic-Flux Compensation

The first method for actively filtering harmonics generated by an HVDC converter station was originally proposed by H. Sasaki and T. Machida in 1971 [12,13]. Their method was based on the principle of the magnetic-flux compensation in the converter-transformer core. The principle is illustrated in Figure 1.1.

The currents in the valves are detected on the secondary of the converter transformer and fed into a tertiary winding by high-fidelity-type linear amplifiers. The amplified signals then induce the same amperes-turns as those induced by the secondary current. The harmonic components in the magnetic flux are therefore theoretically cancelled by perfect compensation. Normal steady-state theoretically predictable (or "characteristic") harmonics as well as abnormal (or "non-characteristic") ones can be actively filtered.

It can be noted from Figure 1.1 that the tertiary windings of three phases are connected in delta. The linear amplifiers are bypassed by series resonant circuits that provide zero impedance at the fundamental frequency. This prevents the high fundamental frequency voltage from being applied to the linear amplifiers. The current injected by the amplifiers does not circulate through the tuned filters either. The wye-connected capacitors provide the path for the output currents and supply reactive power to the HVDC converter.

Although the method is very elegant, several aspects rendered it impractical for implementation at that time. Since the current to be injected has several harmon-

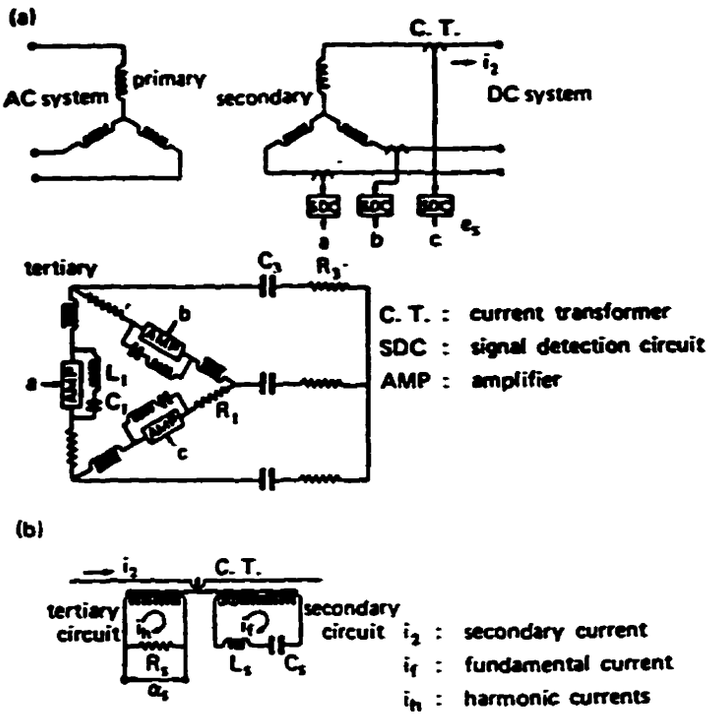

Figure 1.1: Circuit diagram of the magnetic-flux compensation method (extracted from [14]).

ics, the linear amplifiers should have a large power bandwidth. The use of a linear amplifier was unreasonable due to very low efficiency. The detection circuit had to detect and amplify these harmonics without any phase delay and with a uniform gain. It is an open-loop control scheme and, therefore, although stable, is susceptible to precision problems when detuning of the several passive filters components is considered. It reportedly had problems with low-order-harmonic amplification in the output circuit [14].

The problems perhaps could be surmounted with today's technologies. However, the main drawback of this method is in the special design of the converter transformer [15]. The converter transformers are among the most expensive components of an HVDC converter station. The use of special three-winding transformers besides increasing its price and copper losses, adds complexity to dealing with the practical effects of mutual impedances and saturation.

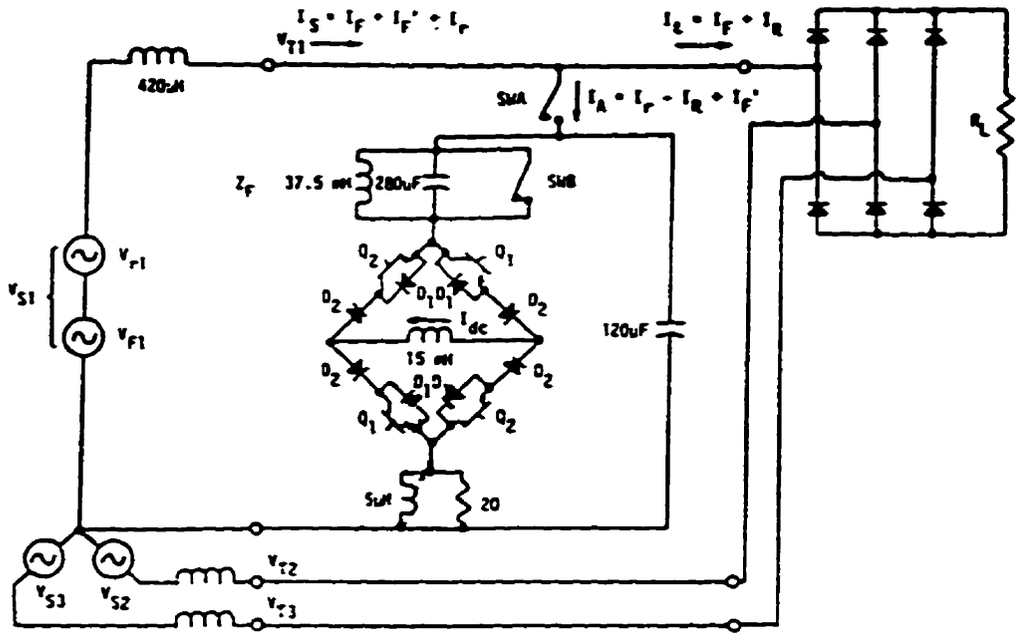

Figure 1.2: Circuit of laboratory model of a current-source active filter (extracted from [16]).

1.3 Current-Source PWM Inverter as an Active Source

In 1976, L. Gyugyi and E. C. Strycula presented the concept of PWM inverters using power semiconductor switches [16]. In their work, a laboratory model was set up. The circuit can be seen in Figure 1.2. The active filter was shunt-connected to a single phase of a three-phase 220 V source feeding a six-pulse rectifier circuit with a resistive load current of 55 A. Instead of using a DC current source as the active source of the PWM inverter, a 15 mH inductor was used. The power semiconductor switches were power transistors rated 375 V, 70 A.

The block diagram of the control scheme can be seen in Figure 1.3. The terminal voltage V_T is passed through a fundamental-frequency-tuned (60 Hz) filter so that a reference signal is obtained. The actual terminal voltage is then subtracted from this

reference so that the error signal V_E is generated. Depending on the instantaneous error, either pair of transistors Q_1 or Q_2 will be turned on. The use of the inductor as a DC current source implies that the AC system must supply its losses through the only connection to it; that is through the power transistors. The fundamental voltage across the active filter is reduced by placing a 50-Hz parallel-tuned LC filter in series with it. A second input signal, V_{LOSS}, is intended to compensate for the internal losses of the active element. The error amplifier is a bistable device with a hysteresis loop. It reverses its state only when input V_E is reduced to zero and then appears with sufficient opposite polarity. The terminal voltage is thus forced to follow the established reference waveform. In the experiment, the power transistors were operated at an average switching frequency of 10 kHz.

The problem with this scheme in an eventual application in HVDC converter stations is that a considerable part of the typically large fundamental voltage would have to be applied to the active filter. This is due to the necessary charging of the inductor (because of its losses) used as the current source and to the compensation for the PWM switching losses. Note that the type of nonlinear load used in the test, different from an HVDC converter station, makes use of diodes and, therefore, does not require reactive power compensation.

1.4 Capacitor-Commutated Inverter with a PLL-Generated Reference Signal

In 1977, N. Mohan et al. proposed the use of a capacitor commutated inverter (or, as it was referred to, harmonic inverter) consisting of thyristors [17, 18]. The complete circuit diagram is in Figure 1.4.

The inverter thyristors are commutated by three series output capacitors. Once the capacitors have been charged during a start-up procedure, the inverter thyristors would be sequentially fired at every 120 degrees of the harmonic frequency. As opposed to Gyugyi and Strycula's approach, the DC current source was a current-controlled DC rectifier (or harmonic rectifier). The rectifier-inverter set is nowadays referred to as a current-regulated voltage-source inverter (CR-VSI).

It can also be seen in Figure 1.4 that the fundamental-voltage reduction across

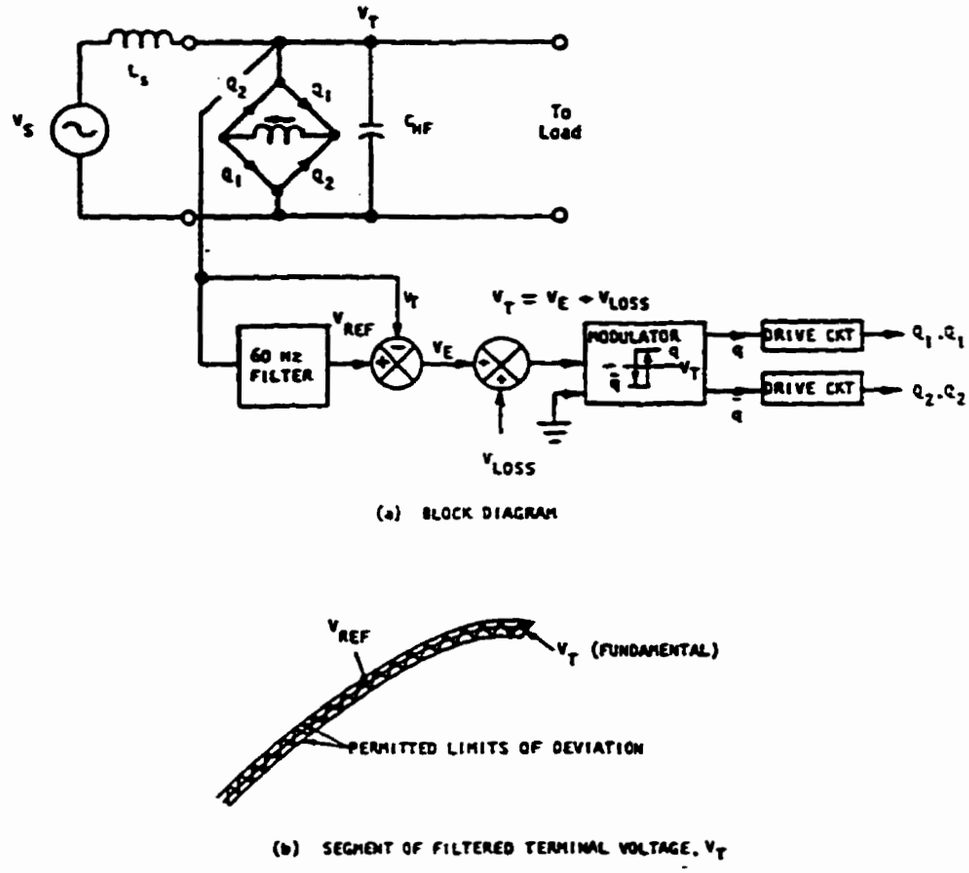

Figure 1.3: Block diagram of the control scheme of the current-source shunt active filter (extracted from [16]).

the active filter is achieved by the single-tuned filter connected between the active source and the AC system. The lower parallel-tuned filter is tuned to the harmonic frequency to avoid "sinking". The parallel resistor provides damping and facilitates the start-up process.

Figure 1.5 shows the control scheme for the proposed capacitor-commutated active filter. The current sensors were designed using phase-locked loops (PLL). Amplitudes and phases for a given harmonic frequency of the injected current and of the non-linear-load current are determined. With the magnitude and phase errors,

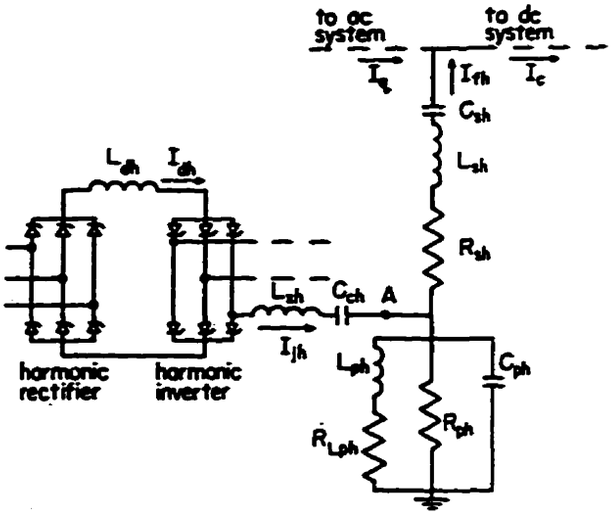

Figure 1.4: Capacitor-commutated active filter for harmonic h (extracted from [17]).

the generated active-filter current would then be accordingly controlled to reduce the specific harmonic content of the AC-system current to an arbitrarily small value.

Later, in 1979, N. Mohan suggested a new topology for the passive part of this active-filter concept [19]. The "modified high-pass filter", as it was referred to, would allow both the 11th and the 13th harmonics to be actively filtered at the same time (still by two separate harmonic rectifier-inverter sets), while higher-order harmonics were deviated by passive filters. Figure 1.6 shows the corresponding circuit diagram.

In 1981, G. Dreifuerst, in his Ph. D. Thesis [18], built the same original basic circuit. The test set-up was controlled by several microprocessor algorithms running in parallel. They were controlling the DC current provided by the harmonic rectifier and the firing angle of the harmonic inverter. In this case, a 12-pulse non-linear load current was generated by means of digital-analog electronics. The phase-locked-loop detection sensors would lock on a harmonic component of the synthesized 12-pulse current waveform. Either the 11th or the 13th harmonics were actively filtered by changing control parameters.

One of the reported problems was that the harmonic-inverter generated noise

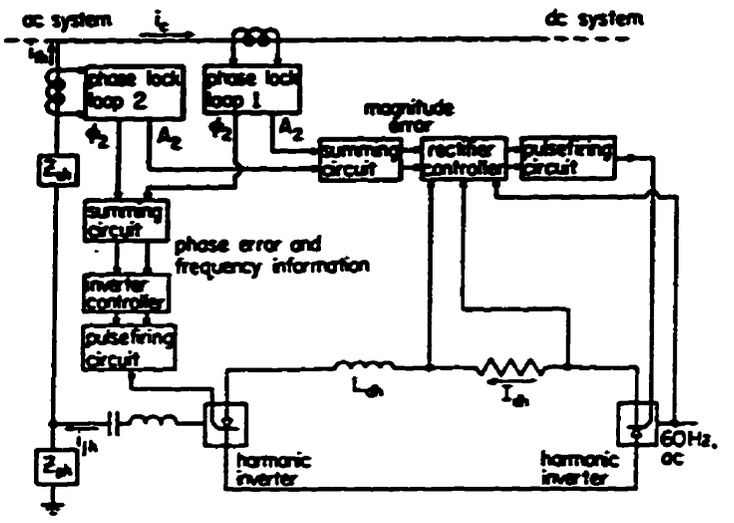

Figure 1.5: Control scheme of the capacitor-commutated active filter (extracted from [17]).

affected the data-acquisition system, the measurement devices and the PLL current sensor [18, 20]. Also, as later mentioned by C. Wong et al. [21], although this active filter worked well in steady-state operation, it had difficulties handling current-order changes in the DC-system control. These transients would cause overvoltages in the active-filter circuit itself.

1.5 PWM CR-VSI and Economic Feasibility

In 1989, C. Wong et al. evaluated the economic feasibility for active filtering of AC-side current harmonics and DC-side voltage harmonics produced by a typical HVDC converter station [21]. Both designs were cost-compared with existing schemes at the Dickinson terminal of the CU HVDC transmission line project (1000 MW, ± 400 kV). Both designs were based on the use of transformer-coupled PWM CR-VSI as active sources. Although the work presented a digital simulation of the steady-state operation in a electromagnetic transients program for the DC-side active filter, the authors did not present any simulation results for the AC side.

The controlled injected currents would actively filter both the 11th and the 13th

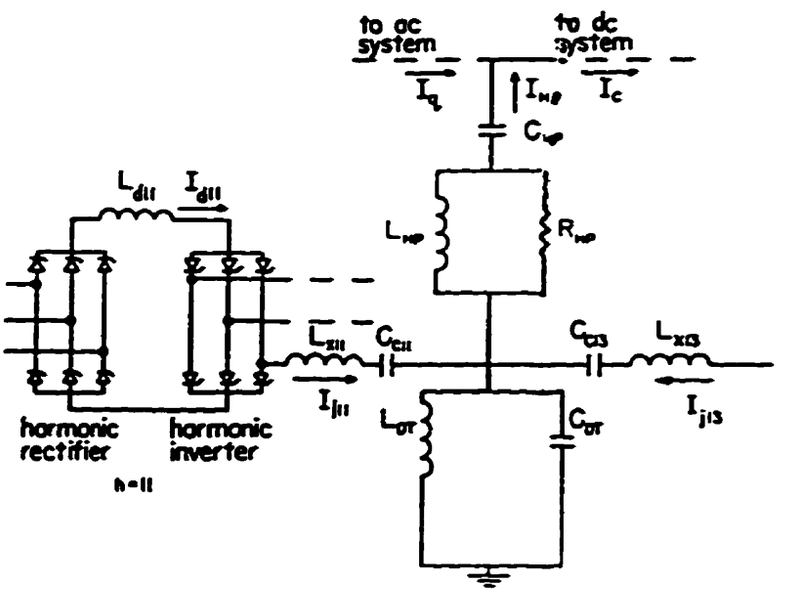

Figure 1.6: Capacitor-commutated active filter with "modified high-pass filter", for both the 11th and the 13th harmonics (extracted from [19]).

harmonic currents. Based on measurement of site harmonic currents, the harmonic current required to drive the terminal harmonic voltage to zero was calculated as a reference value. The suggested control method was similar to that of the previous proposal, that is, the actual injection current is forced to remain within a prescribed tolerance band around the reference value by controlling the inverter switches.

Since the passive components provide partial filtering of the AC current harmonics, the rating of the active current-injection source can be reduced. Furthermore, the kVA rating of the harmonic-current injection is conservatively estimated by neglecting individual harmonic phases by adding each individual harmonic RMS voltages together, as well as individual RMS harmonic currents, as if all the harmonic components were in phase with each other.

The passive-topology part of the active filter is Mohan's "modified high-pass filter" [19,21] and is shown in Figure 1.7.

It is essentially composed of two portions. The design of the upper portion, Z_{HP}, led it to exhibit the following characteristics:

- Low impedance to the 11th and to the 13th harmonics;
- Low impedance to the 23rd and higher order harmonics (comparable or lower than that of the existing high-pass filter);
- Same capacitive VAr's at the fundamental frequency as the existing bank of filters.

The tuned frequency and the quality factor were selected to be the same as those in the existing high-pass filter. The design of the lower impedance, Z_j, in parallel with the active source, led to the following characteristics:

- Low impedance at 60 Hz to reduce the voltage across the injection source;
- High impedance at the 11th and at the 13th harmonic frequencies to minimize the "sinking" of the injection current;
- Low impedance at higher frequencies to achieve overall high-pass feature.

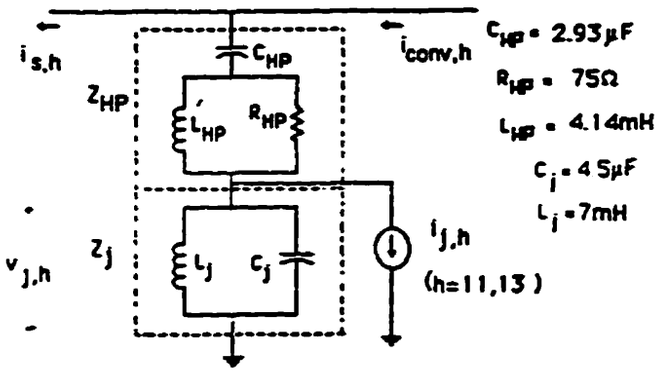

Figure 1.7: PWM CR-VSI active filter with "modified high-pass filter", for the 11th and the 13th harmonics (extracted from [21]).

It was concluded that the cost of both AC-side and DC-side active-filter designs were comparable to those of the existing passive filters. Hence, if it were a future project, the choice should be considered based on the potential for a better filtering performance, favoring the active-filtering solution.

Although the system's impedance and the bank of shunt capacitors were absent from the calculations of the ratings of the active source, they might have had little influence in the result of the cost comparisons. As load varies, it is common practice to have some arms of the passive filters connected or disconnected to control the AC fundamental voltage at the converter terminal. This could complicate the operation of such scheme. The economic advantage of using one single impedance Z_{HP} to inject the harmonic currents would disappear if different arms had to be installed to allow fine control of the supply of reactive power. Another approach, without any directly-connected passive elements, was proposed by Thanh-Nam Lê et al. in 1994 [22].

1.6 Combined Use of Series Active Filters and a Traditional Bank of Shunt Passive Filters

F. Peng et al. proposed the use of a small-capacity series active filter to operate in conjunction with a traditional bank of shunt passive filters in 1990 [20,23,24]. Their work also presented a theoretical analysis of the stability of the suggested control scheme. The role of their series active filter is to improve the filtering characteristics of the shunt passive filters. The circuit diagram of the laboratory model which was built can be seen in Figure 1.8.

The shunt passive filters, formed by a 10-kVA bank of passive filters, consisting of arms tuned at the 5th- and at the 7th-order harmonics and a high-pass filter, is in parallel with a 20-kVA harmonic source (a three-phase six-pulse thyristor converter).

The series active filter consists of three 450-VA/15-kHz single-phase PWM-VSI units. They are each connected in series with the AC system through single-phase current transformers with 1:20 as the turns ratio. The energy corresponding to the switching and copper losses of the active filter is provided through a 50-VA single-phase diode rectifier. Figure 1.9 presents details of the active-source design.

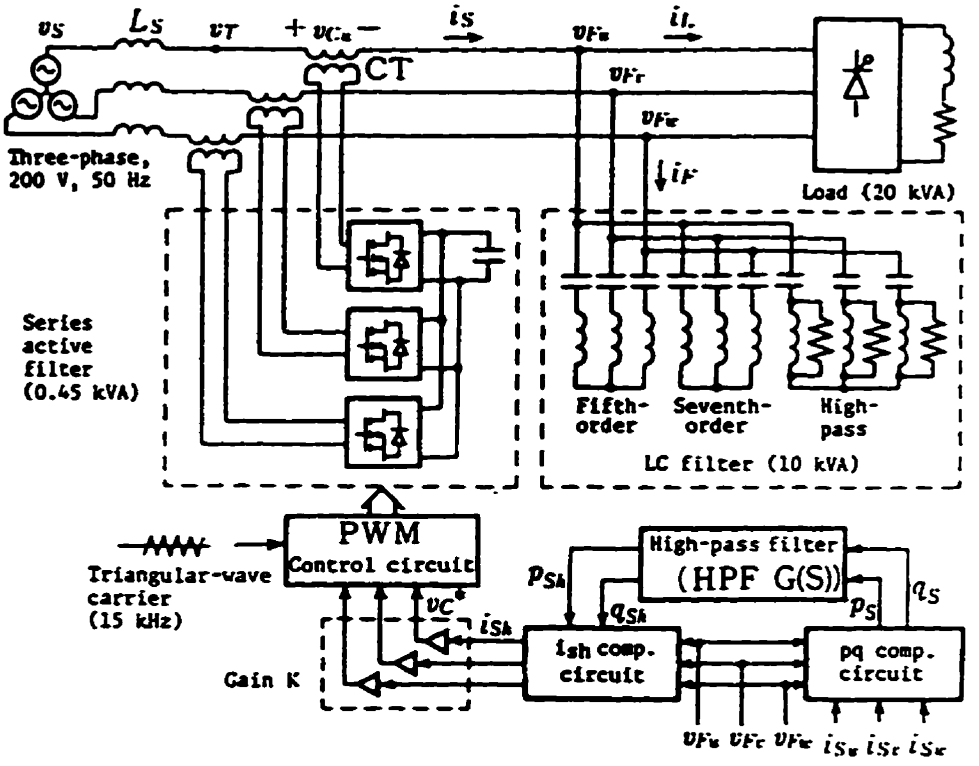

Figure 1.8: Combined use of series active filters and the traditional shunt passive filters (extracted from [20]).

Later, in 1993, H. Fujita and H. Akagi optimized the values of the capacitances of the single-tuned shunt passive filters by means of a graphical method [25]. The same topology and control scheme were then used in a 12-pulse converter laboratory model. As a consequence, the required rating of the series active filter was further reduced.

The desired overall behavior of the series active filter is to exhibit zero impedance at the fundamental frequency, and of the order of kilohms at harmonic frequencies. The control scheme that achieves this is also shown in Figure 1.8.

The reference output voltage varies proportionally (K) with the residual harmonic

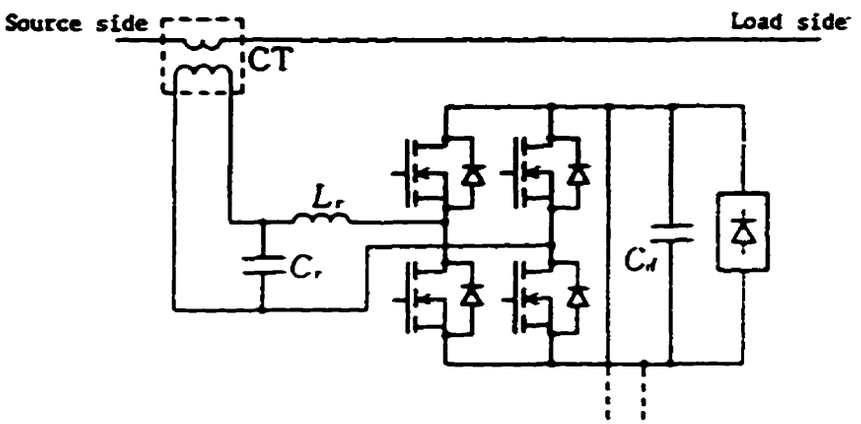

Figure 1.9: Details of one of the active sources of the series active filters (extracted from [20]).

current not removed by the bank of shunt filters. This reference output voltage is then compared to a triangle carrier, producing the PWM switching patterns that will generate the output voltage of the active filter.

The determination of the harmonic current to be injected by the active filter is based on the theory of the instantaneous reactive power (or *p-q* theory) developed by H. Akagi [26] in conjunction with a high-pass filter $G(s)$. The desired dynamic performance of the control scheme is obtained by varying the the gain K and the high-pass filter $G(s)$ characteristics.

The main problem with this control scheme is that the instantaneous quantities being filtered by the high-pass filter $G(s)$ also contains the fundamental frequency. Since the magnitude of the fundamental-frequency component is several times larger than the magnitude of the lowest-order harmonic component to be filtered, the design of $G(s)$ becomes delicate.

The harmonic currents can be compensated more accurately by reducing the cut-off frequency f_c of the high-pass filter. However, unfortunately, the harmonic-compensation effectiveness at frequencies close to fundamental worsens as f_c decreases. The consequence is that the output voltage of the active filter increases as f_c decreases when the load current contains side-band components close to the fundamental frequency or when the load suddenly changes. In this case, the active-

filter elements would be overloaded. This problem can be minimized by increasing the order of $G(s)$. However, the transient characteristics also deteriorate as the order of the filter is increased. That is, if a fast response is required, a low-order filter should be preferred.

Analysis done by F. Peng et al. also indicated that although the system is always stable if $G(s)$ is of the first order, there would be limits imposed on its cut-off frequency f_c and gain K if a higher-order filter were used.

The proposed series connection of the active filter seems to have been an attempt to make use of the existing bank of shunt passive filters without modifications. Unfortunately, the series active filter is unfeasible both in cost and reliability. In such configuration, protection against large switching transients and lightening surges, would demand that the basic insulation level (BIL) of the coupling transformer to be very high. Another significant point is that the current carried by the active filter will also include the fundamental component of the load current and the fundamental leading power factor current of the shunt passive filters.

1.7 Combined Use of Active Filters in Series with a Traditional Bank of Shunt Passive Filters

In 1990, H. Fugita and H. Akagi presented another combined system [27]: a small-rated active filter in series with existing passive shunt filter banks. Again, the aim is the reduction of the required rating of the active filter. The circuit diagram of the experimental prototype model is shown in Figure 1.10.

This proposal had the three single-phase PWM CR-VSI replaced by one three-phase PWM VSI. The diagram also shows that a typical LC output filter was used to filter the harmonics generated by the high frequency switching (20 kHz) of the power semiconductor switches.

Another characteristic of this circuit is that the energy corresponding to the switching and conducting losses of the active filter is now provided through the power semiconductor switches and stored in a DC capacitor, which plays the role of a DC voltage source.

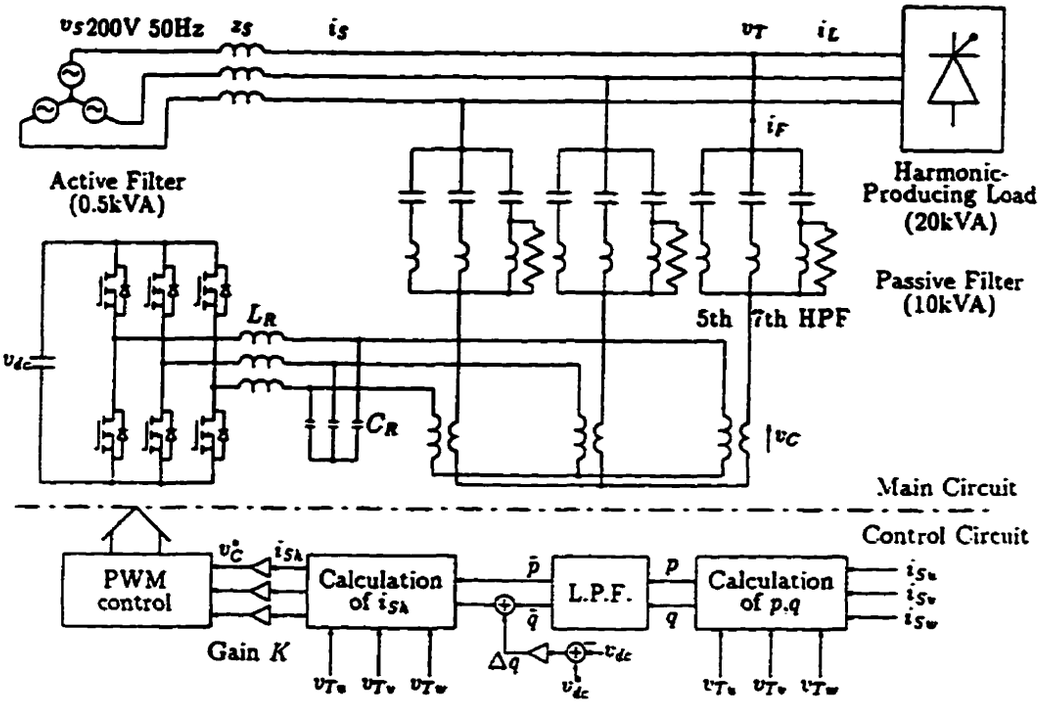

Figure 1.10: Combined use of active filters in series with traditional shunt passive filters (extracted from [27]).

The control scheme is similar to that of Section 1.6. This time, since the voltage-source capacitor must have its voltage built up and regulated throughout the operation, an additional control input signal was provided. In order to draw active power from the AC system, the output of the active filter must contain a fundamental-frequency voltage component that is in phase with the leading reactive current that flows through the shunt passive filter. Therefore, the electrical quantity to be controlled in the DC-voltage feedback loop is the instantaneous reactive power Δq.

A following paper, [28] by the same authors, revisited the same circuit with a diode rectifier as the DC voltage source for the PWM inverter.

The weakness of this scheme is that the active filter always carries the capacitive fundamental component of the current through the shunt passive filter.

1.8 Combined Use of Active Filters in Series with Shunt Single-Tuned Filters

The scheme shown in Figure 1.11 was proposed by I. Takahashi and Y. Omura in 1993 [29]. Their main purpose was to reduce the complexity of the harmonic inverter switches and their control.

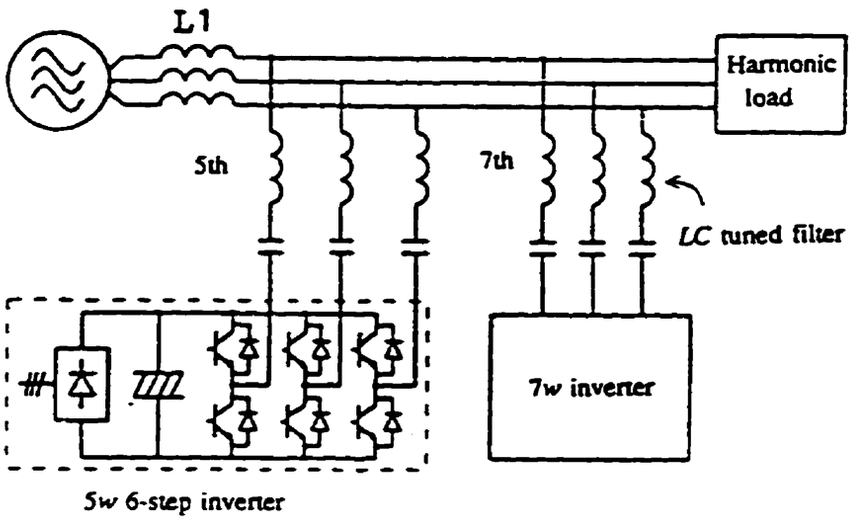

Figure 1.11: Combined use of active filters in series with traditional shunt single-tuned passive filters (extracted from [29]).

The inverter used was of the square-wave voltage type and, therefore, there could be only one frequency being actively filtered by each active filter. They were placed in series with the existing shunt single-tuned passive filters of the corresponding harmonic order. The frequency of the switching of the inverter must correspond to the order of the harmonic which is to be actively filtered. This way, reducing the number of switchings, reduction of losses is also achieved.

The inputs that control the switching of the inverter are the amplitude and phase of the harmonic voltage to be compensated. To obtain these quantities, the actual voltage waveform first has its fundamental frequency eliminated by an analog/digital notch filter. This has the effect of improving the resolution of the A/D converters that feed the digital processing unit. The DSP performs a Fourier analysis of the

harmonic content and provides the actuators with their required inputs.

The process of reading the data into the DSP takes approximately 20 ms and about 4 ms for the FFT computation and the computation of the command values. The repetition period of the control is 40 ms.

As in the previous approach, this active filter also carries the fundamental capacitive current of the shunt passive filters.

1.9 Active Filters for the DC side of HVDC Converter Stations

The DC side of the HVDC system deals with less harmonics and does not involve reactive power compensation issues. This seems to have favored research centers and the main power-equipment manufacturers to become interested in this side of the HVDC system first [30–33]. Results of the operation of a prototype of an active DC-side filter in an HVDC converter station was published in 1993 [31, 32]. The manufacturer, ABB, installed the active filter at the Lindome converter station of the Konti-Skan 2 HVDC link between Sweden and Denmark at the end of 1991.

Figure 1.12 shows a simplified circuit diagram for the hybrid solution of active and shunt passive filters, connected in series, on the DC side of the converter station. The active filter comprises the part of the circuit within the dashed line. The passive filter is tuned to the first two characteristic DC-line harmonics (of the 12th and the 24th orders). The objective of the installation is to compensate for all the remaining line harmonic voltages.

The active source includes a PWM power amplifier whose losses are supplied by a rectifier. The inverter is isolated from the power circuit by a high frequency transformer. The objective of capacitor C_1 is to provide the active filter with isolation from the high DC transmission voltage.

Figure 1.13 shows a simplified block representation of the control scheme. The controller is digitally implemented in a high speed computer. The main parts of this scheme are the second block, which holds the digital models of the converter station and the DC line, and the third block, the controller itself.

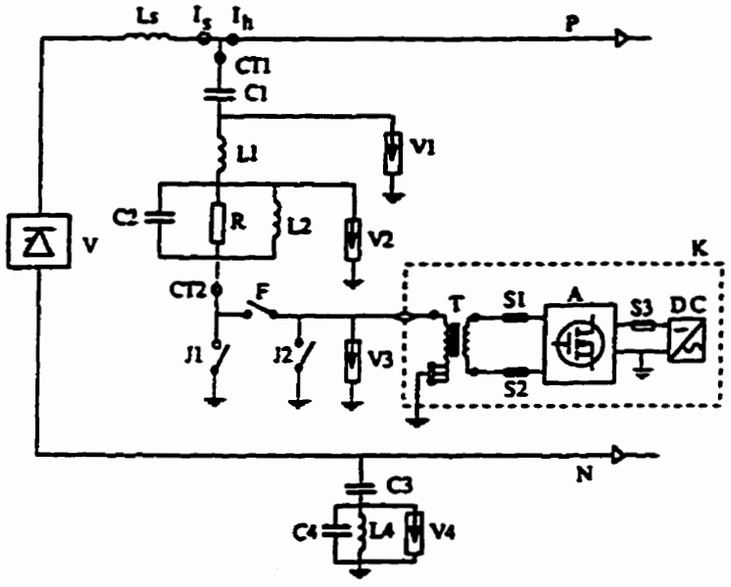

Figure 1.12: Active filter for the DC side of the Lindome HVDC-converter station (extracted from [31]).

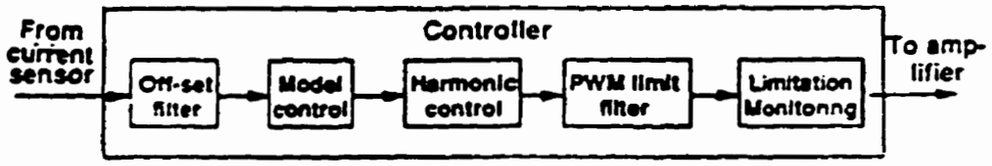

Figure 1.13: Control scheme of the active filter for the DC side of the Lindome HVDC-converter station (extracted from [31]).

The report mentions that to achieve comparable results by passive filters alone would require something like ten times more high voltage equipment. It is also reported that is was easy to integrate the active filter to the existing passive filter, it has small physical size, little installation work, short HVDC outage requirement for its installation and no outage requirement for maintenance and testing. The stan-

dardized fashion in which the digital control was designed allows easy implementation in other installations.

1.10 Conclusion

It is apparent that the main obstacle to the implementation of active filters in HVDC converter stations is the high ratings that such application demands. Therefore, power requirement seems to be the most important element of the design. A few approaches to rating reduction in active filters have been proposed on the basis of a combination of active filters and passive filters.

Except for the ABB report, all of the previous works tested their approaches on laboratory models. An important aspect that has not been mentioned in any of the proposals is that the circuits in question would probably demand series and/or parallel connection of the semiconductor switches. This poses additional problems in the selection and characteristic matching of the switches as well as to the gating circuitry.

Nevertheless, increasing needs for filter performance and economic considerations will maintain interest in an active-filter solution. Practical evidence that the concept is indeed applicable to HVDC transmission systems and that this is a better alternative to the traditional passive filter banks (albeit restricted to DC-side filtering) has been provided by the Lindome converter-station prototype.

Certainly, the broad range of potential advantages over the traditional passive filters, and their subsequent impact in terms of the performance of HVDC systems, justify the consideration of further specific research associated with this technology. This thesis is concerned with further exploration of AC active filters for HVDC converter stations.

Chapter 2

Harmonics in HVDC Systems

2.1 The HVDC System

Figure 2.1 shows one of the poles of a conventional configuration of a bipolar two-terminal HVDC transmission system [13, 34–36]. Since the steady-state operating point of the other pole is the same as the one shown (except for the opposite DC-voltage polarity), its representation has not been considered in this work. The pole controls are designed to keep either the DC power or the DC-current in the DC line constant.

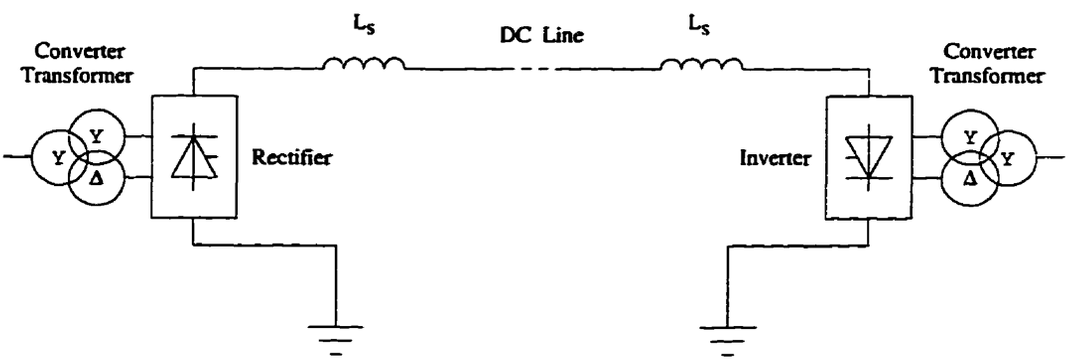

Figure 2.1: Conventional configuration of one pole of a bipolar two-terminal HVDC system.

The HVDC converters are each connected to one end of the DC transmission line, at the converter stations, through smoothing reactors L_s. The power flows from the converter station being operated as a rectifier to the converter station which is being operated as an inverter. Both converter stations can operate either as a rectifier or as an inverter, and their basic operation is determined by the control philosophy of the firing pulses to the power semiconductor switches (thyristors), which depends upon the desired DC power-flow direction.

Each of these converters typically consists of two three-phase six-pulse bridges connected in series per pole, and this combination results in a twelve-pulse arrangement. This can be seen in Figure 2.2.

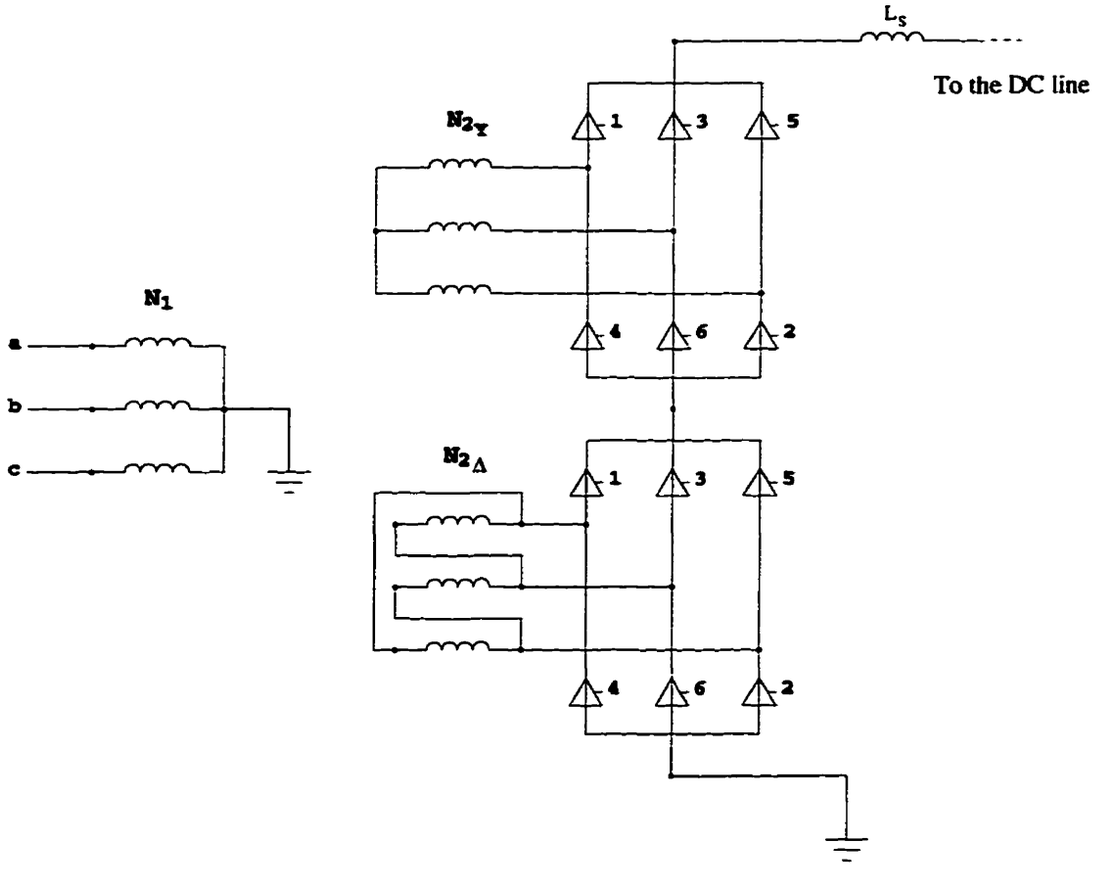

Figure 2.2: Conventional configuration of an HVDC-system converter terminal.

The number assigned to the valves (semiconductor switches) show the order in

which they are fired in normal operation. At a given converter station, the AC voltage is supplied from the AC system to each one of the six-pulse bridges by means of Y-Y and Y-Δ three-phase transformer banks. The connection of each six-pulse bridge to a differently connected three-phase transformer bank provides the bridges with 30° -phase-shifted three-phase voltages between them. Naturally, the transformer turns ratio of the Y-Δ transformer is increased by a factor of $\sqrt{3}$ in relation to the Y-Y transformer so that their individual DC output power remains the same.

2.2 AC-Current Characteristic Harmonics

Considering a perfectly balanced 60 Hz AC/DC system, with a steady state DC current of $I_d = 2000$ A and a commutation (or overlap) angle of $\mu = 23.17°$ (period of time elapsed from the moment of the firing of a valve until the DC current is completely transferred from another valve to it), Figure 2.3 shows one theoretical fundamental-frequency period of the currents in both the Y- and Δ-connected secondary windings of the three-winding single-phase transformer connected to phase a. Figure 2.4 shows the resulting line current in the primary winding considering turn ratios of $N_{2_Y}/N_1 = 0.6126$ for the Y-Y connection and $N_{2_\Delta} \; / \; N_1 = 1.0610$ for the Y-Δ connection.

Just by means of a visual analysis of the AC line current waveform, it is readily concluded that, besides the fundamental component, such a twelve-pulse converter arrangement also draws harmonic current components from the AC system. Theoretical Fourier analysis of such current waveform shows that, in a twelve-pulse converter, the AC-side current consists of a fundamental 60 Hz component plus the currents at the so called characteristic harmonics of the orders

$$h = 12k \pm 1, \qquad \text{for } k = 1, 2, 3, \ldots .$$

For a given AC line current waveform for which the commutation angle μ is less than 60°, the RMS magnitude of each characteristic harmonic can be calculated by [12,35]

$$I_h = K\sqrt{K_{-_{sin}}^2 K_{+_{sin}}^2 - 2K_{-_{sin}}^2 K_{+_{sin}}^2 \cos(2\alpha + \mu)}, \tag{2.1}$$

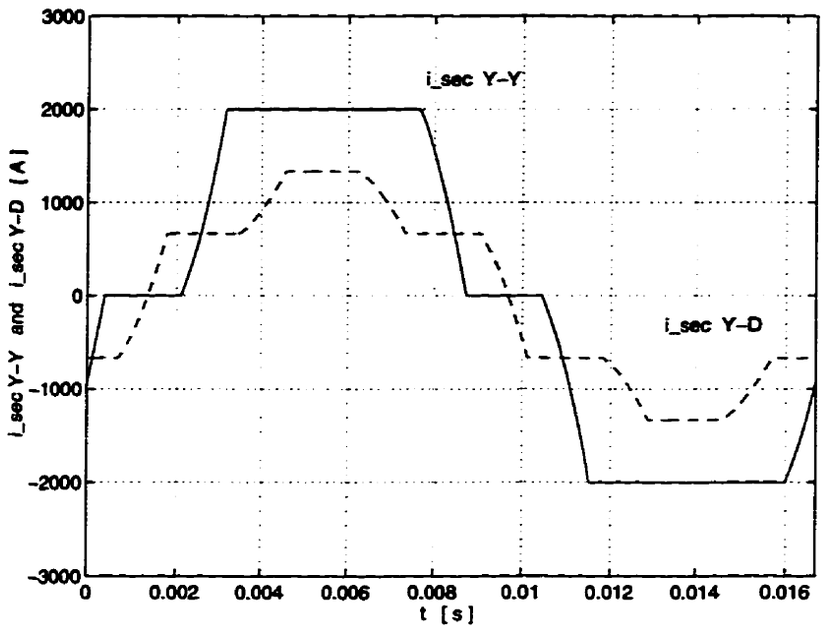

Figure 2.3: AC currents in the secondary windings of the converter transformer connected to phase a (— Y-Y, — Y-Δ).

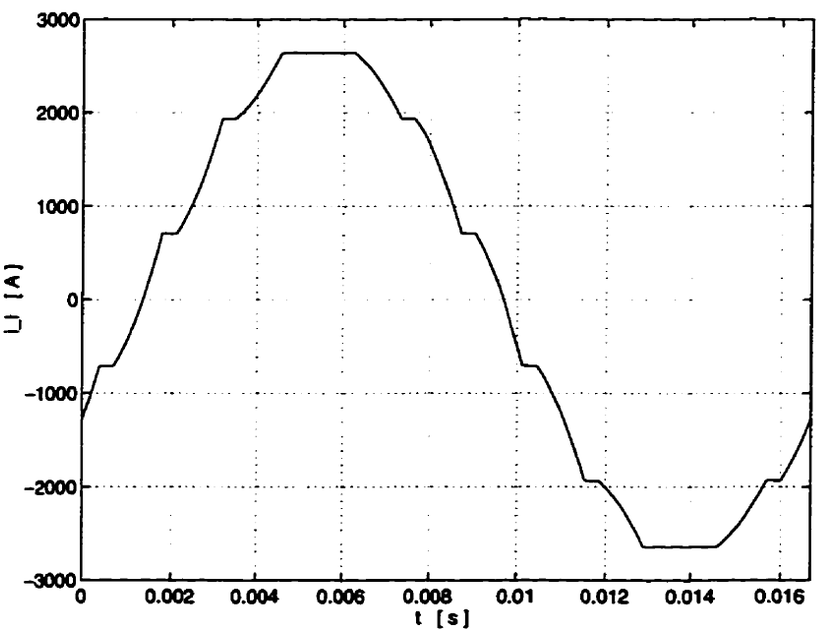

Figure 2.4: HVDC-converter AC line current in phase a.

where

$$K = \frac{\sqrt{6}\sqrt{2}E_{\phi\phi}}{2\pi X_c h};$$

$$K_{-_{\sin}} = \frac{\sin\frac{(h-1)\mu}{2}}{h-1};$$

$$K_{+_{\sin}} = \frac{\sin\frac{(h+1)\mu}{2}}{h+1};$$

α firing (or delay) angle (measured from the zero crossing instant of the respective commutation voltage of each valve);

μ commutation (or overlap) angle;

h characteristic-harmonic order;

$E_{\phi\phi}$ commutation voltage;

X_c leakage reactance of the converter transformer (commutation reactance).

It can be seen that the magnitudes of the characteristic harmonics depend mainly on the commutation angle μ, and that they tend to reduce as it increases. Basically, a change in the firing angle α just corresponds to a shift of the transformers' secondary currents. Due to this delay angle in the firing of the valves, a certain amount of reactive power is then required by the HVDC converter. Figure 2.5 repeats the waveform of Figure 2.4 and includes its fundamental and harmonic components. This harmful harmonic component is put into evidence in Figure 2.6.

Figure 2.7 shows the dependence of the magnitudes of the first eight characteristic harmonics, as percentages of the fundamental component, on the commutation angle μ, for a firing angle of $\alpha = 15°$ [35]. It can be easily noted from the graph that the two dominant current characteristic harmonics are the 11th and the 13th ones. The worst theoretical case takes place when $\mu = 0°$. In this case, the waveform is the most distorted it can possibly be from the perfect sinusoid (see Figure 2.8). The maximum theoretical magnitude of a characteristic harmonic h for such a case ($\mu = 0°$) is given by [13,35]:

$$I_{h_0} = \frac{\sqrt{6}}{\pi h} I_d, \tag{2.2}$$

where I_d is the DC-line current.

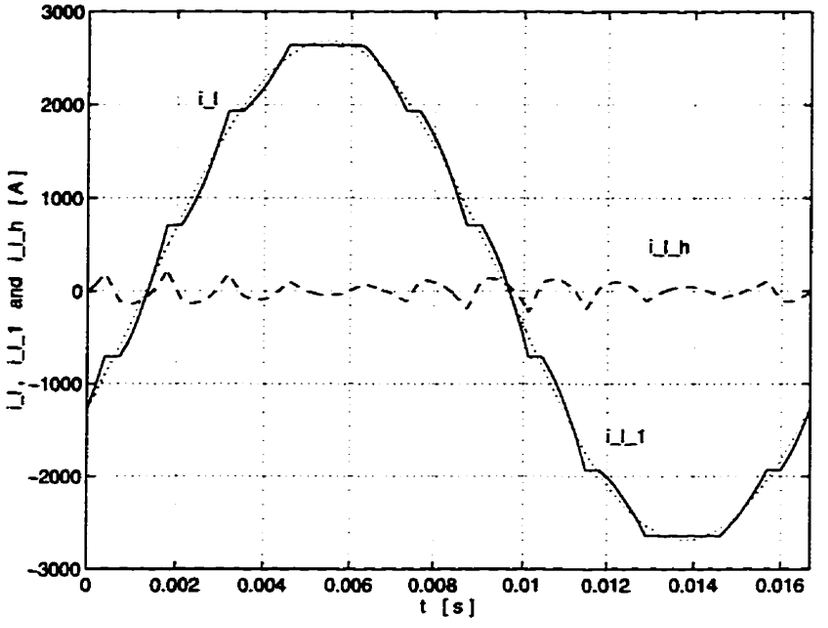

Figure 2.5: Fundamental and harmonic components of the HVDC-converter AC line current in phase a (— line current, ··· fundamental component, — total harmonic content).

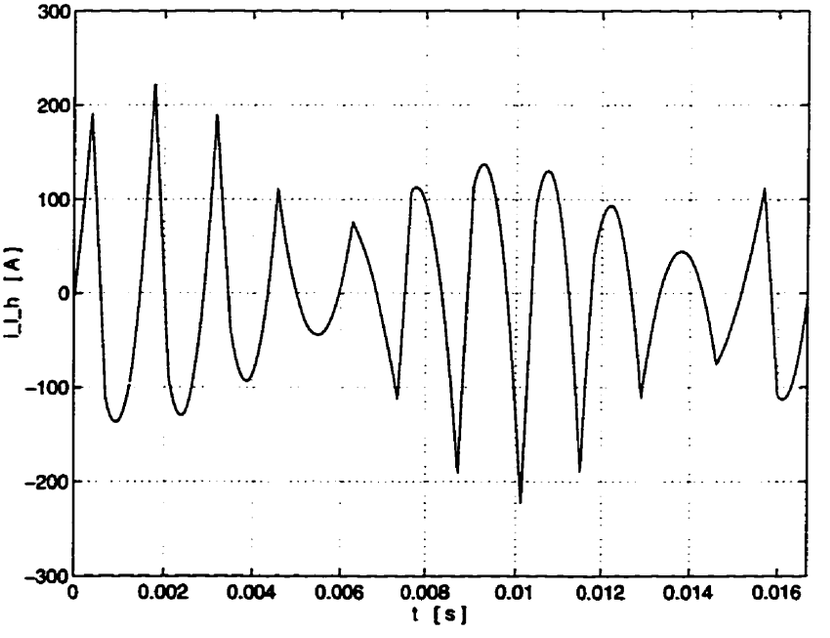

Figure 2.6: Harmonic component of the HVDC-converter AC line current in phase a.

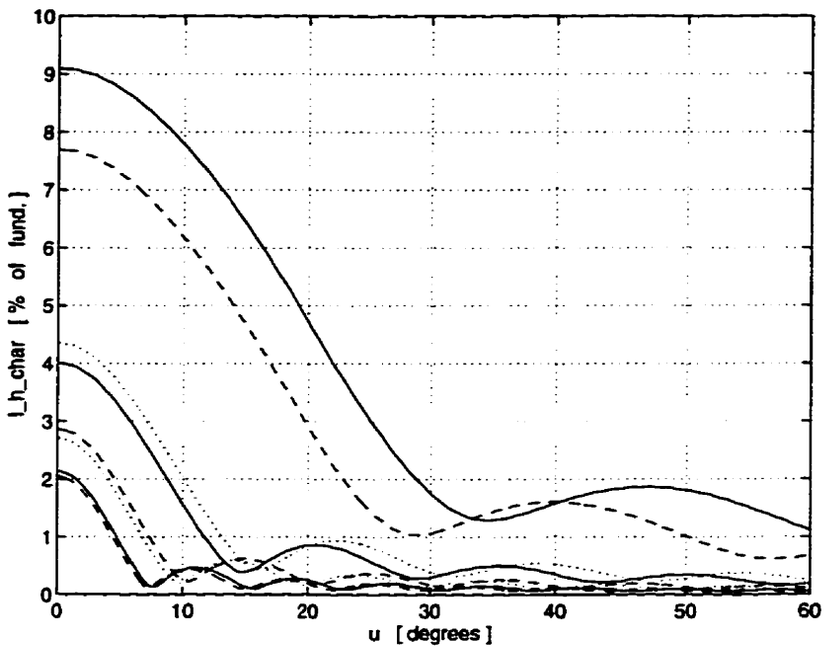

Figure 2.7: Percentage of AC harmonics as a function of the overlap angle. From top to bottom, on the $\mu = 0°$ axis, the 11th, 13th, 23rd, 25th, 35th, 37th, 47th and 49th harmonic-current components.

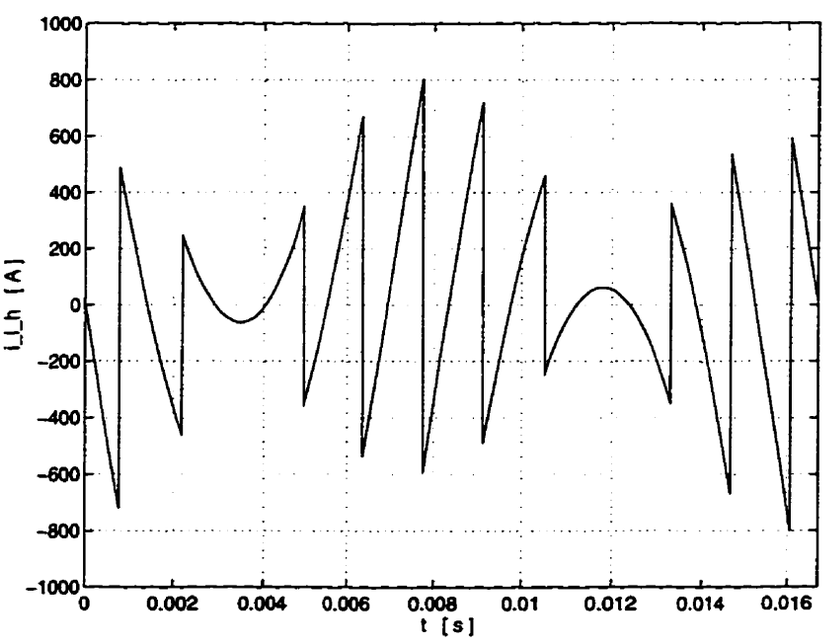

Figure 2.8: Maximum harmonic component of the AC line current.

2.3 AC-Current Non-Characteristic Harmonics

A real HVDC system deviates from the assumption "perfectly balanced AC/DC system" made for the derivation of the AC line current waveform in Figure 2.4. Therefore, expressions for the characteristic harmonics are not completely accurate (especially for higher frequencies) and non-characteristic harmonics are also present in the AC line current [37–39]. Actually, HVDC systems draw harmonic currents of all orders from the AC system and the non-characteristic harmonic content is, in general, around 7% of the characteristic harmonics [12].

The main factors that cause non-characteristic AC harmonics are [2]:

- Differences in the commutation inductances between phases, within one bridge, and between those of different bridges. These can vary in a complex manner;
- Firing angle variations (non-equidistant firing pulses to the valves and/or firing errors). These can vary in a complicated pattern and are determined by the control scheme of the pole;
- AC voltage unbalance (negative sequence) and/or distortion. These can be produced by an amplitude difference between phase voltages and/or by a phase difference from the 0/120/240 degrees among the phase voltages;
- Operation of the converter transformers near magnetic saturation.

Another important cause of concern is the possibility of occurrence of the phenomenon known as "harmonic instability". This phenomenon will be further explained in Chapter 3, but a preliminary explanation about DC-side voltage harmonics generation as relevant to harmonic instability is given in the following section.

2.4 DC-Voltage Harmonics

In the same way as the non-linear nature of operation of the HVDC converter draws current harmonics from the AC system, it causes the converter to supply voltage harmonics to the DC transmission line together with its direct voltage [35]. One

fundamental period of the theoretical DC voltage waveform across a twelve-pulse converter of a 60 Hz AC/DC system, 500 kV/2000 A, and commutation angle $\mu = 23.17°$ is shown in Figure 2.9. The individual voltage waveforms across each one of the six-pulse bridges that add up to form the DC-line voltage are also included in this figure.

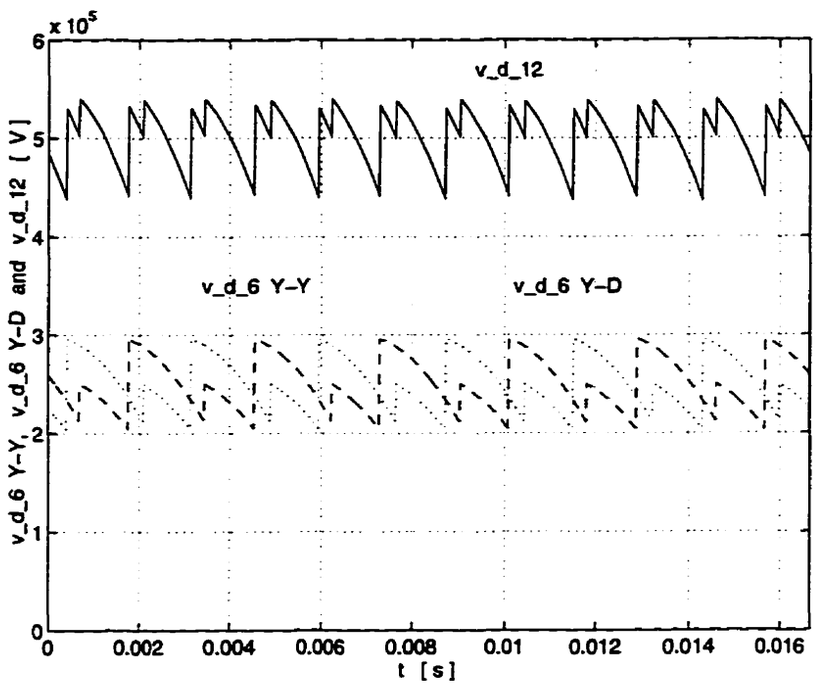

Figure 2.9: DC voltages of an HVDC-converter twelve-pulse bridge (— 12-pulse, -- 6-pulse Y-Y, ··· 6-pulse Y-Δ).

Theoretical Fourier analysis of the 12-pulse-converter DC-voltage waveform shows that it consists of a DC component plus the voltages at characteristic harmonics. Their orders are given by

$$h = 12k, \qquad \text{for } k = 1, 2, 3, \ldots .$$

For a given DC-voltage waveform for which the commutation angle μ is less than 60°, the RMS magnitude of each characteristic harmonic can be calculated by [35].

$$V_h = V_{d_0} \sqrt{K_{-_{\cos}}^2 K_{+_{\cos}}^2 - 2K_{-_{\cos}}^2 K_{+_{\cos}}^2 \cos(2\alpha + \mu)}, \tag{2.3}$$

where

$$K_{-_{\cos}} = \frac{\cos \frac{(h-1)\mu}{2}}{h-1};$$

$$K_{+\cos} = \frac{\cos\frac{(h+1)\mu}{2}}{h+1};$$

and V_{d_0} is the maximum average DC voltage (no load and $\alpha = 0°$) that is given by

$$V_{d_0} = \frac{3\sqrt{2}E_{\phi\phi}}{\pi}.$$

Figure 2.10 shows the dependence of the 4 first DC-line-voltage characteristic harmonics (with respect to the fundamental component) on μ when $\alpha = 15°$.

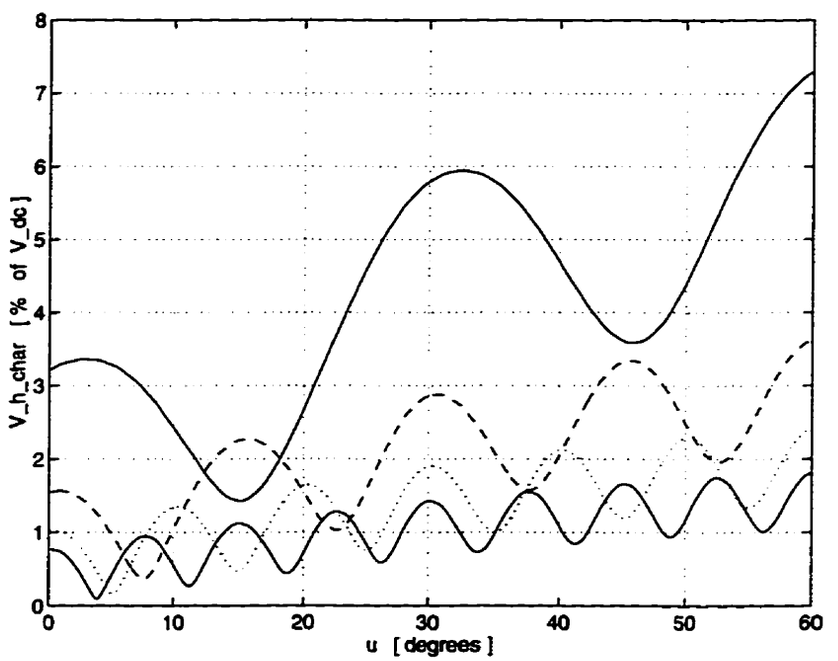

Figure 2.10: Percentage of DC harmonics as functions of the overlap angle ($\alpha = 15°$). From top to bottom, on the $\mu = 0°$ axis, the 12th, 24th, 36th and 48th harmonic-voltage components.

It is interesting to note that, unlike the AC current harmonics, in the case when $\mu = 0°$ the harmonics still depend on α. Harmonic contents (especially the higher order ones) increase with α. The maximum generation of voltage harmonics in the DC transmission line occurs when $\alpha = 90°$ and the individual harmonic level in this case is given by [13]

$$V_h = \frac{\sqrt{2}}{h}V_{d_0}. \tag{2.4}$$

2.5 DC-Voltage Non-Characteristic Harmonics

The same causes of the AC current non-characteristic harmonics apply to the DC-line voltage [40]. The normal operation of each 6-pulse bridge requires that each commutating inductance will be commutated twice per period of the fundamental frequency; once due to the commutation of its upper valve, and once due to the commutation of its lower valve. These events are displaced by half a period of the fundamental frequency. This defines the maximum interval of DC-line current wave train repetition as the half period of fundamental frequency (2nd harmonic). Therefore, the commutating inductance variations can only generate even non-characteristic harmonics (the 2nd, 4th, 6th, etc.). Hence, the most significant non-characteristic harmonics are all of even orders [35, 41].

2.6 AC-DC Harmonic-Order Transferences

An AC-current harmonic of order h_{ac} somehow flowing in the AC system at the converter station causes an AC-voltage harmonic of the same order h_{ac} on the AC system [42, 43]. On the DC side of the converter station, a DC voltage harmonic of order h_{dc} causes a DC current harmonic of the same order h_{dc} on the DC side. The conversion function, determined by the non-linear characteristic of operation of the converter bridge on the AC- and DC-current and voltage harmonics are as follows.

AC $\rightarrow$ DC: The converter modulates an AC harmonic voltage at a frequency f_h into harmonic voltages at frequencies $f_h \pm 60$ Hz (fundamental frequency) on the DC side. For example, the presence of a 2nd- order non-characteristic harmonic in the AC system voltage would cause the fundamental- and the 3rd-order components on the DC side.

DC $\rightarrow$ AC: A harmonic current at frequency f_h on the DC side will reflect onto the AC side as a harmonic current at frequencies $f_h \pm 60$ Hz. For example, a fundamental component on the DC side causes DC and the 2nd-order components on the AC side.

The complete cycle of the above harmonic transferences between the AC and DC sides of the converter station may cause what is known as "harmonic instability",

which, evident for a particular installation, must be mitigated by appropriate filter and control modifications [42–44].

2.7 Frequency Range of Interest

In harmonic studies, it is generally sufficient to take into account at most the 50th AC harmonic current (3000 Hz for 60-Hz systems) because the theoretical and field results are in good agreement with each other in this frequency range, and the magnitudes of higher harmonics are reasonably small [12]. With respect to the DC voltage harmonics, although the highest dominant harmonic component corresponds to the 36th order (2160 Hz for 60-Hz systems), the frequency spectrum of interest goes up to 3600 Hz, the higher frequencies accounting for the frequency-dependency characteristics of the transmission line and coupling with the communication systems [35].

2.8 Harmonic Indices

Some indices have been created to define and evaluate harmonic distortion. These indices are also used as an aid to help in the design and assessment of the effectiveness of the measures taken to mitigate the effects of the harmonic components [1,8]. The following indices are considered to be sufficient for the scope of this research and, therefore, telephonic interference factors (TIF) have not been included. Since the following definitions apply to both voltage or current quantities, the variable X will be used.

Effective (or True, or Total) RMS

Also referred to as "True"or "Total" RMS, this index is applicable to a quantity with any periodic waveform, and is determined by the following expression:

$$X = \sqrt{\sum_{h=0}^{50} X_h^2}, \qquad (h \geq 1) \tag{2.5}$$

where X_h is the RMS value of a harmonic component and is given by

$$X_h = \sqrt{\frac{1}{T_h}\int_0^{T_h} x_h^2(t)dt}.$$

where T_h is the period of the harmonic h.

Individual Harmonic Distortion (IHD)

This index is related to a specific harmonic h.

- For an alternating quantity:

$$IHD_h = \frac{X_h}{X_1}, \qquad (h \geq 2) \tag{2.6}$$

- For a direct quantity:

$$IHD_h = \frac{X_h}{X_0}, \qquad (h \geq 1) \tag{2.7}$$

Total Harmonic Distortion (THD)

This index is also referred to as "Total Root Sum Square Distortion".

- For an alternating quantity:

$$THD = \frac{\sqrt{\sum_{h=2}^{50} X_h^2}}{X_1} = \frac{\sqrt{X^2 - X_1^2}}{X_1} \tag{2.8}$$

- For a direct quantity:

$$THD = \frac{\sqrt{\sum_{h=1}^{50} X_h^2}}{X_0} = \frac{\sqrt{X^2 - X_0^2}}{X_0} \tag{2.9}$$

Tables 2.1 and 2.2 show the results of actual measurements of the harmonic contents of two real HVDC systems together with their respective calculated indices (characteristic harmonics are in bold characters) [12,45].

Table 2.1: Typical AC current harmonic content pattern of an HVDC system.

Harmonic Order	Harmonic Current [A_{rms}]	Harmonic Distortion [%]
True RMS	1,933.5	-
1	**1,928.0**	-
2	3.8	0.20
3	5.4	0.28
4	2.4	0.12
5	108.4	5.62
7	61.0	3.16
9	2.7	0.14
10	1.9	0.10
11	**61.0**	**3.16**
12	2.2	0.11
13	**34.3**	**1.78**
15	2.2	0.11
17	4.8	0.25
19	7.7	0.40
21	1.9	0.10
23	**17.2**	**0.89**
25	**15.3**	**0.79**
31	2.2	0.11
35	**6.8**	**0.35**
37	**8.6**	**0.45**
47	**3.1**	**0.16**
49	**3.8**	**0.20**
59	**2.6**	**0.14**
61	**2.3**	**0.12**
71	**1.6**	**0.08**
73	**1.6**	**0.08**
83	**1.2**	**0.06**
THD	-	7.56

Table 2.2: Typical DC voltage harmonic content pattern of an HVDC system

Harmonic Order	Harmonic Voltage [V_{rms}]	Harmonic Distortion [%]
True RMS	250,885	-
0	**250,000**	-
2	764	0.306
4	358	0.143
5	408	0.163
6	582	0.233
10	246	0.098
12	**19,947**	**7.979**
14	509	0.204
16	208	0.083
18	394	0.158
20	389	0.156
22	313	0.125
24	**5,584**	**2.234**
26	486	0.194
28	214	0.086
30	394	0.158
32	330	0.132
34	367	0.147
36	**3,404**	**1.362**
THD	-	8.422

Chapter 3

AC Passive Filters in HVDC Terminals

3.1 Introduction

In industrial applications, as well as in power systems, the traditional way to prevent harmonic currents from being drawn from the AC network is by modifying the "impedance frequency characteristics" of the non-linear load that is causing them. This is done by adequately connecting suitable impedances (AC passive filters) to the system.

The main objective of AC passive filters is, therefore, to limit the values of Individual Harmonic Distortions (IHD) and Total Harmonic Distortion (THD) to levels which satisfy the international or local standards [8]. This involves choosing suitable values for the components to obtain a desired equivalent impedance at the required frequency or frequencies.

As reviewed in Chapter 2, an HVDC converter terminal generates AC as well as DC harmonics. However, since this research involves only AC filters, DC passive filters, which are similarly used on the DC side of the HVDC terminal, will not be discussed. From this point on, "AC filter" or simply "filter" will be used as a short form to designate "AC passive filter" unless it is necessary to avoid confusion.

This chapter continues with the review of the necessary background for under-

standing the problems which are posed to the AC system by the AC passive filters that justified the present research. Some of this background will also be applicable to the design of the active filter, in Chapter 5.

3.2 Point of Connection of the Filter

The point of connection of the AC filters to the AC/DC system in relation to the converter transformer can be at either its primary, secondary, or tertiary windings [34].

The placement of the filters at the secondary (valve-side) winding of the converter transformer would alter the commutation reactance. This would affect the rate of rise of the current during the "turn-on" and the rate of rise of the reverse voltage during the "turn-off", demanding adequate design of the snubber circuits of the valves. Besides, their design would be more complex in order to consider the leakage inductance of the transformer (variable due to the tap changer action if any) together with the AC system or with the filters. Thus, this has not found practical application.

The placement of the filters at a tertiary winding of the converter transformer is attractive because it offers a lower voltage rating. As in the previous option, its design must also consider the transformer leakage inductance. Again, this leakage inductance (usually higher at the tertiary winding [12]) is variable if a tap changer is provided. However, the increased complexity of the design and cost of the converter transformer itself may be offset by the benefits of the lower voltage rating this method provides. In fact, quite a few HVDC systems make use of this arrangement [34].

The placement of the filters at the primary winding of the converter transformer is the only place where the design of the filters would be independent of tap changer operation and of possible resonances between the AC system and the converter transformer impedance. This is, in fact, the most common point of connection.

3.3 Types of AC Passive-Filter Connections

In general, AC passive filters can be connected in series, in parallel or in both ways to the non-linear load with an adequate frequency characteristics as to neutralize the

AC-current harmonic flow.

The AC passive filters perform harmonic flow elimination by connecting passive elements with either high impedance (in the series connection) or with low impedance (in the parallel connection) at specific harmful harmonic frequencies. The circuit diagrams for similar applications of both types of connection are electrical duals.

3.3.1 Series Connection

In this type of connection, the filter acts as a "harmonic isolator", impeding the AC-current harmonic from flowing from the AC system by means of presenting high harmonic impedances.

This type of connection has some disadvantages in HVDC applications: the filter would have to carry the fundamental current, its insulation level should follow the BIL (Basic Insulation Level) of that point in the system and, consequently, in addition, its protection becomes difficult and its reliability compromised. This type of connection would also affect the operation of the HVDC converter as it is known. For these reasons, the series connection seems applicable (in conjunction with parallel-connected filters) only when the required performance of the overall filtering scheme of the HVDC station is very high. Otherwise, the parallel connection has been the preferred arrangement in HVDC systems (see also Section 3.5).

3.3.2 Parallel Connection

The parallel-connected (also referred to as "shunt-connected") type of passive filter, as opposed to the series-connected type, acts as an AC-current-harmonic "diverter" between the AC system and the HVDC terminal by means of presenting low harmonic impedance path to the ground, bypassing the HVDC converter station. An additional and decisive advantage of this type of connection will be shortly seen in Section 3.5.

3.4 Types of AC Filters Used in HVDC Systems

There are two main types of filters that are generally used in HVDC systems: "tuned" and "damped" filters.

3.4.1 Tuned Filters

Tuned filters are aimed at providing low impedance at specific harmonic frequencies only. They can be "single-tuned" filters or "double-tuned" filters, depending on their topology, and, consequently, on their impedance characteristics.

Single-Tuned Filter

This is the simplest of the tuned filters and it is also called a "band-pass filter". Single-tuned filters are designed to filter just one specific harmonic frequency. The circuit diagram of a single-tuned filter is presented in Figure 3.1.

Figure 3.1: Single-tuned filter.

Circuit analysis of the filter branch in the figure yields the expression for the dependency of its impedance on the frequency:

$$Z(f) = R + j\left(2\pi fL - \frac{1}{2\pi fC}\right). \tag{3.1}$$

A small variation of this topology can be the inclusion of a resistor R_p, with a relatively high resistance, in parallel with the inductor and the resistor in series with

it. This is done for improving the effectiveness of the overall filtering scheme of the converter station with respect to TIF (telephonic interference factor) indices [46].

Figure 3.2 shows one example of its corresponding complete frequency characteristic. This characteristic is that of the filter used to suppress the 11th harmonic at the 60-Hz/345-kV inverter station of the Itaipu DC transmission system in Brazil [46].

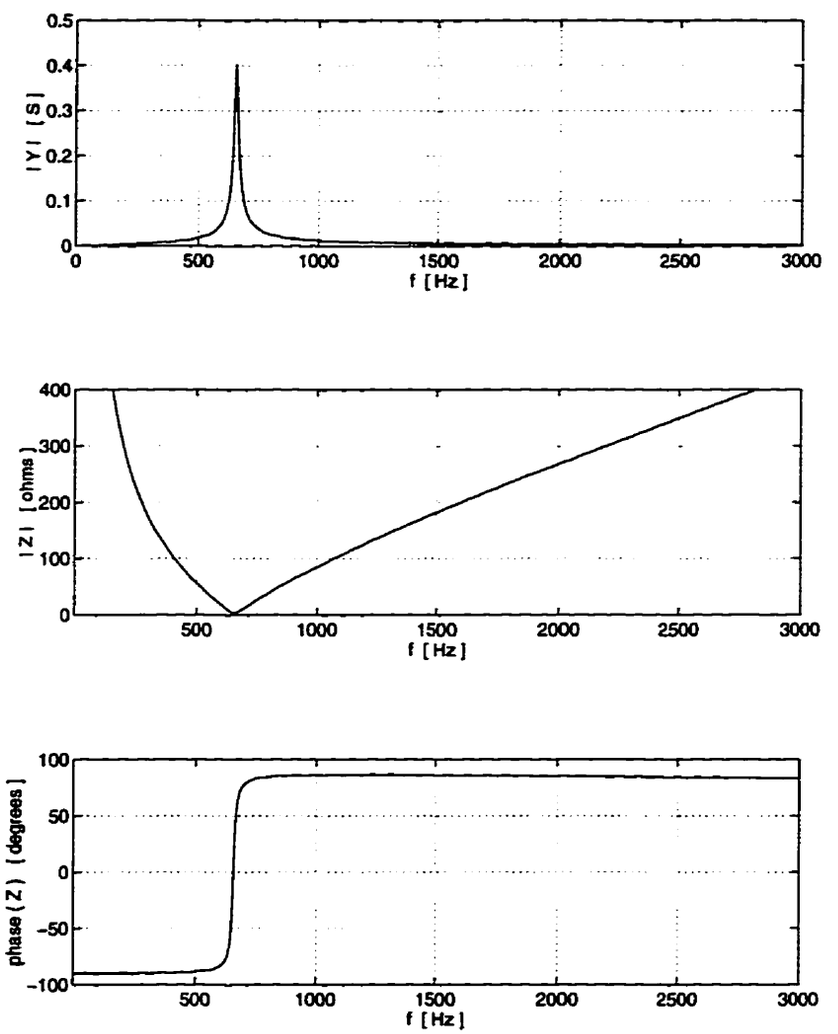

Figure 3.2: Frequency characteristics of a single-tuned filter ($R_p = 3990\ \Omega$, $R = 0\ \Omega$, $L = 24.06$ mH and $C = 2.417\ \mu$F).

The frequency at which it is tuned is very evident from the sharp peak of the admittance magnitude. While it might not be so visually apparent as in Figure 3.2, the impedance magnitude characteristics displays a minimum at the tuned frequency

and the phase characteristics shows that, at the tuned frequency, the behavior of the filter is purely resistive (phase zero). Note that at the fundamental frequency of the system, the filter presents a capacitive behavior.

The lowest possible impedance value is obtained at its resonance frequency (when the values of the inductive and capacitive reactances are equal and cancel each other) and is equal to the value of the resistance. This resonance frequency is determined by

$$f_{res} = \frac{1}{2\pi\sqrt{LC}} \ . \tag{3.2}$$

The value of the reactances at the resonance frequency is given by

$$X_0 = \sqrt{\frac{L}{C}} \ . \tag{3.3}$$

The ratio between the value of the reactances at the resonance frequency and the value of the resistance of the resistor,

$$Q = \frac{X_0}{R}, \tag{3.4}$$

is called the "quality factor" Q of the filter.

The quality factor is an indication of the sharpness of the filter at the resonance frequency. The lower the value of the resistance of the resistor, the sharper the tuning. The usual quality factor values for HVDC applications range from 30 to 60 [35]. The width and precise tuning frequency are therefore two parameters that can be changed for every individual filter. A quantity called "pass-band" is defined as the frequency range defined by the frequencies at which

$$|Z(f)| = \sqrt{2}R \ .$$

That is, at these frequencies, the dominant reactive value equals the resistance and, therefore the impedance phase of the filter is 45°.

Double-Tuned Filter

A double-tuned filter presents low impedance to two specific harmonic frequencies. Double-tuned filters can be designed to have approximately the same filtering characteristics as those determined by the parallel connection of two separate single-tuned

filters as long as their resonance frequencies are reasonably close to each other. Figure 3.3 shows the corresponding circuit diagram.

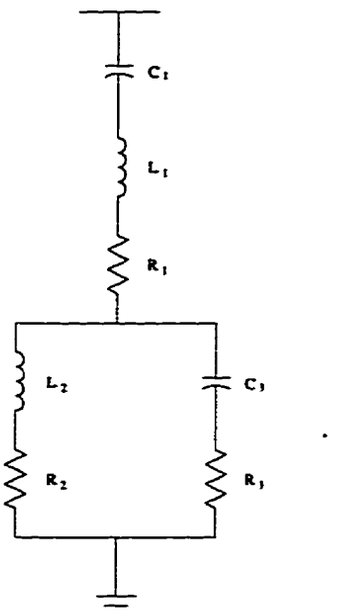

Figure 3.3: Double-tuned filter.

In principle, if other design constraints allow, it might be possible to make use of one double-tuned filter instead of two single-tuned filters. For, example, in the Itaipu system, to avoid a phenomenon called "auto excitation" in the nine 50-Hz generators connected to the rectifier station, a minimum amount of capacitance in the switchyard was imperative. The double-tuned solution was then preferred for its lower capacitance requirement when compared to that of two single-tuned filters.

Also, it is cheaper to replace two single-tuned filters by one double-tuned filter because only one inductor is subjected to full voltage instead of two and its fundamental power loss is less than that in the two individual filters (R_1 is small). By analysis of Figure 3.3, the following expression for the dependency of its impedance on the frequency can be obtained:

$$Z(f) = R_1 + j\left(2\pi f L_1 - \frac{1}{2\pi f C_1}\right) + \frac{(R_2 + j2\pi f L_2)\left(R_3 - j\frac{1}{2\pi f C_3}\right)}{(R_2 + j2\pi f L_2) + \left(R_3 - j\frac{1}{2\pi f C_3}\right)}. \quad (3.5)$$

Although it is possible to design a double-tuned filter which is an exact equivalent of two single-tuned arms in parallel, a better practical method is to design the two

single-tuned filters normally and use them as a prototype considering resistor R_1 as being the resistance of the inductor L_1. Reference [34] shows expressions that yield very good results if the two resonance frequencies are not too close to each other. The impedance near the resonances are practically the same as those of the single-tuned filters. The fact that the impedances at the other frequencies are slightly different from those of the combined single-tuned filters is not usually important. Figure 3.4 shows an example of the complete frequency characteristics of the 11th/13th double-tuned filters at the Itaipu 50-Hz rectifier converter station [46].

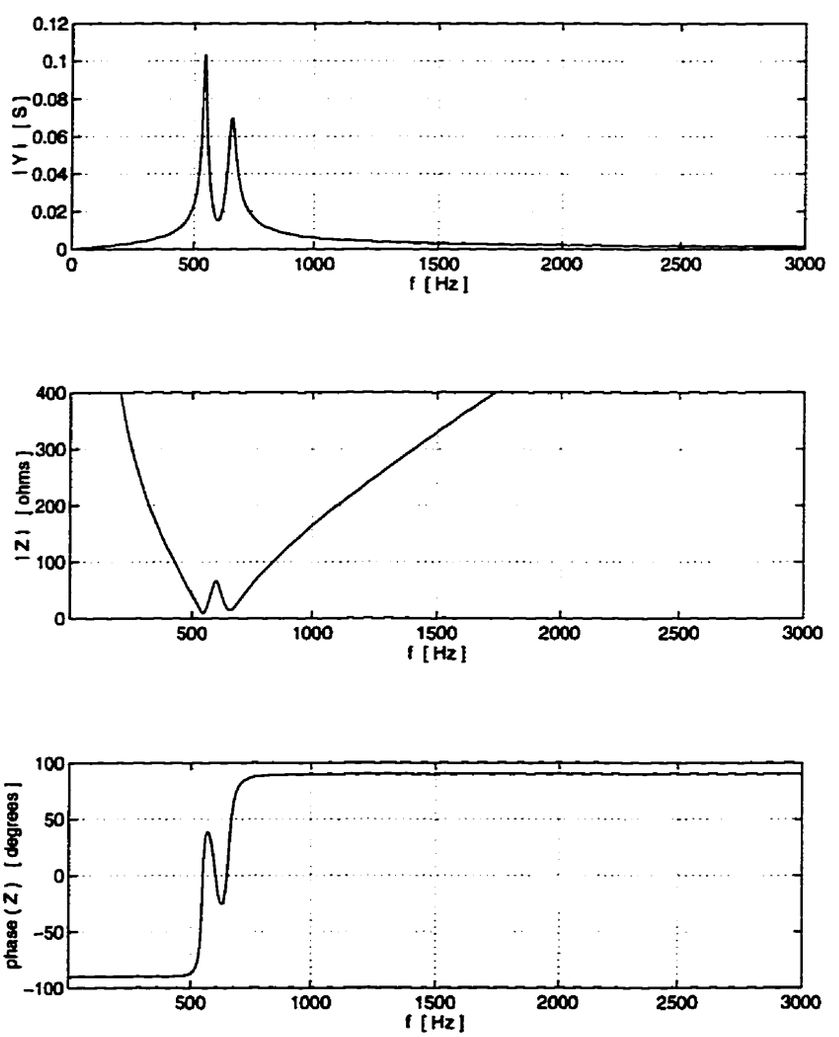

Figure 3.4: Frequency characteristics of a double-tuned filter ($R_1 = 0\ \Omega$, $R_2 = 0\ \Omega$, $R_3 = 0.444\ \Omega$, $L_1 = 41.95$ mH, $L2 = 1.44$ mH, $C_1 = 1.691\ \mu$F and $C_3 = 49.15\ \mu$F).

Although it is also possible to design triple-tuned or higher-ordered multiple-

tuned filters, their use is not practical for the complexity of their expressions and, consequently, their adjustment.

3.4.2 Damped Filters

Damped filters are not aimed exclusively at specific frequencies. Instead, they are designed so as to filter a larger segment of the harmonic frequency, effectively filtering the harmonic frequency it has been tuned to, as well as higher order harmonics. Damped filters are also known as "high-pass filters" and, depending on their topology, provide different impedance characteristics. The simplest type of high-pass filter is the so called "second-order high-pass filter".

Second-Order High-Pass Filter

The circuit configuration of the high-pass filter is sketched in Figure 3.5.

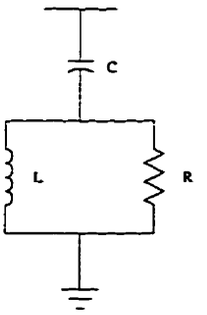

Figure 3.5: Second-Order High-Pass Filter.

The expression for the frequency-dependency characteristics of its impedance is obtained as:

$$Z(f) = \frac{Rj2\pi fL}{R + j2\pi fL} - j\frac{1}{2\pi fC} \ . \tag{3.6}$$

The high-pass filter is also tuned in accordance with equation (3.2). The quality factor for a second-order high-pass filter is defined as

$$Q = \frac{R}{X_0}. \tag{3.7}$$

This is the inverse relationship of that of a single-tuned filter (3.4). However, it is still a measure of sharpness, only, in this case, the higher the value of the resistance of the resistor, the sharper the tuning. In general, a low quality factor (low value of resistance) is chosen to keep the impedance at a low level for frequencies above the resonance frequency. According to reference [35], the typical values for quality factor Q range from 0.7 to 1.4.

On the other hand, considering that the cost of a resistor is proportional to the power it consumes, and that the voltage across resistor R is fairly constant, its resistance can be raised to minimize the fundamental frequency current and, consequently, its power loss.

An example of the corresponding complete frequency characteristics can be seen in Figure 3.6. This is the frequency characteristics of one of the high-pass branches of the Itaipu 60 Hz inverter station.

By modifying the basic configuration of the second-order high-pass filter it is possible to minimize the fundamental power loss and still maintain almost the same characteristics at the higher frequencies. There are two methods largely used, and the modified versions are known as "C-type high-pass filter" and "third-order high-pass filter" (or just "third-order filter").

C-Type High-Pass Filter

This type of high-pass filter (or just "C-type filter") requires a capacitor and a resistor to be installed in series with the inductor forming a single-tuned sub-filter tuned to the fundamental frequency. The function of this sub-filter is to divert the fundamental frequency current from the main resistor. Figure 3.7 shows the circuit diagram.

The following frequency-dependency expression can be extracted from this circuit analysis:

$$Z(f) = \frac{R_1 + j\left(2\pi f L_1 - \frac{1}{2\pi f C_1}\right) R}{R_1 + j\left(2\pi f L_1 - \frac{1}{2\pi f C_1}\right) + R} - j\frac{1}{2\pi f C}. \tag{3.8}$$

Figure 3.8 shows, as an example, the complete frequency characteristics of the c-type filter used in the original CIGRÉ HVDC benchmark system [47–49] (60-Hz

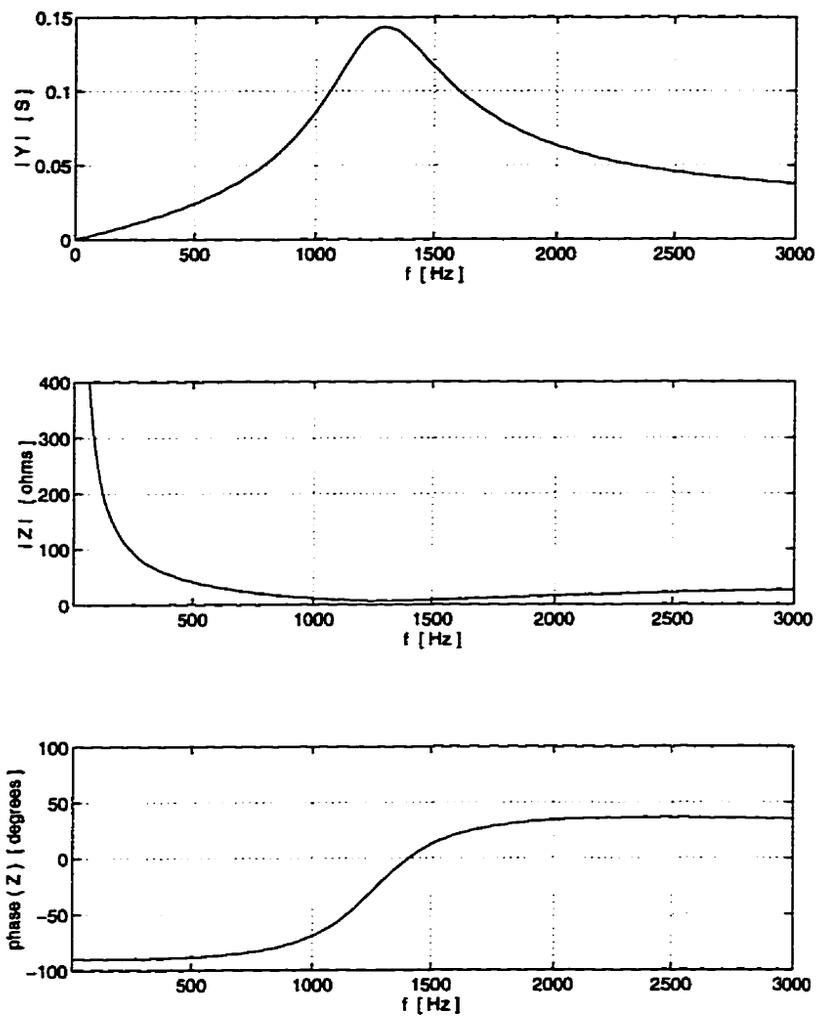

Figure 3.6: Frequency characteristics of a second-order high-pass filter (R=46.76Ω, L = 2.318 mH and C = 6.591 μF).

base-transformed).

Third-Order High-Pass Filter

In this modified version of the second-order high-pass filter, a capacitor is installed in series with the resistor. Therefore, by increasing the impedance in the resistor branch at low frequencies (the fundamental frequency included) the fundamental frequency

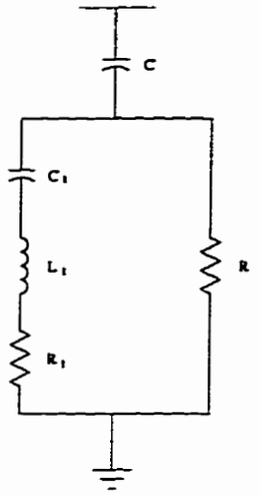

Figure 3.7: C-type high-pass filter.

current is minimized. The circuit of this filter is shown in Figure 3.9.

The expression for the impedance as a function of the frequency becomes

$$Z(f) = \frac{j2\pi fL\left(R - j\frac{1}{2\pi fC_2}\right)}{j2\pi fL + \left(R - j\frac{1}{2\pi fC_2}\right)} - j\frac{1}{2\pi fC_1}. \tag{3.9}$$

Figure 3.10 shows an example of its complete frequency characteristics. This is the impedance characteristics of the 160-MW (200 kV, 800 A) Cross-Channel Lydd Converter Terminal, in England [34]. The advantage of the sharp dip at the resonance frequency may be offset by a broader anti-resonance effect that raises the value of the impedance for higher frequencies just after the resonance frequency. Since the impedance characteristics are usually worse when different values of capacitance are used, C_1 and C_2 often have the same capacitance.

3.5 AC-Filter Reactive-Power Supply

It can be noted that the frequency characteristics of all the AC passive filter impedances seen thus far demonstrate a capacitive behavior at frequencies below their resonance frequencies (this range includes the fundamental frequency).

Therefore, since the operation of an HVDC terminal demands a lagging AC current

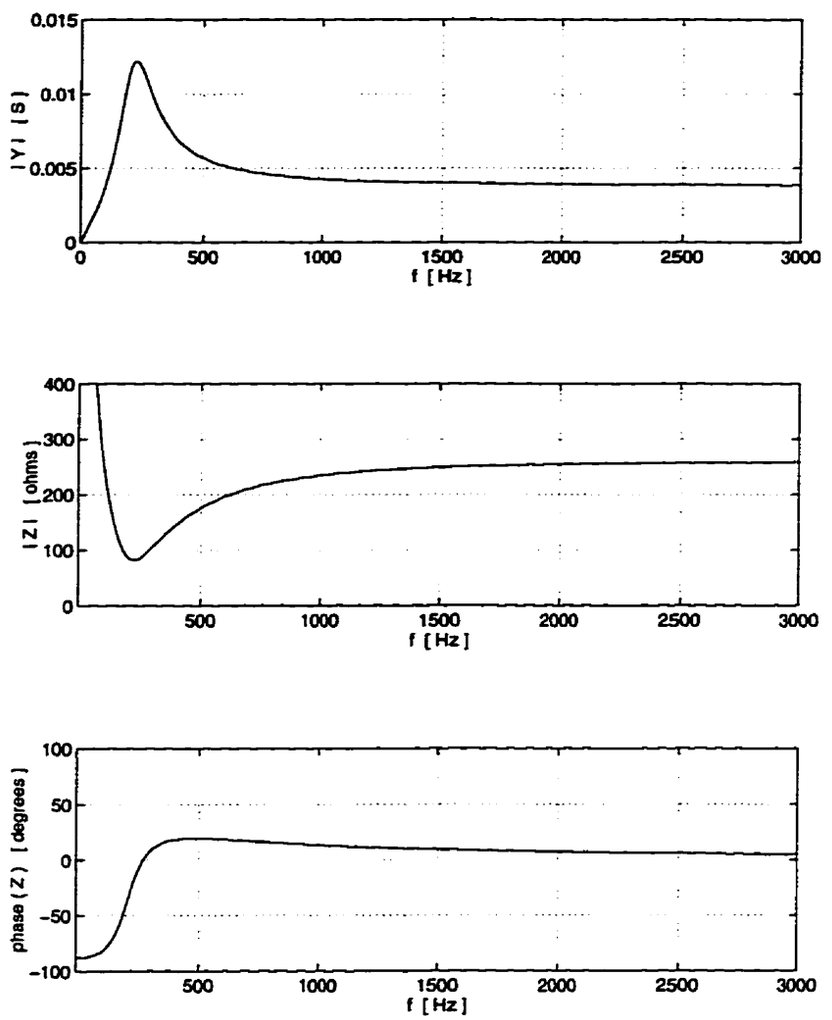

Figure 3.8: Frequency characteristics of a c-type high-pass filter ($C = 5.57\mu$F, $R = 261.87\Omega$, $C_1 = 61.90\mu$F, $L_1 = 113.67$mH and $R_1 = 29.76\Omega$).

due to the delay angle α in the firing of the valves, shunt filters, besides reducing the flow of AC harmonics from the AC system, also reduce the reactive power demand of the station. In fact, the size of a filter is, for practical purposes, defined by the reactive power that the filter supplies at the fundamental frequency. It is essentially equal to the fundamental reactive power supplied by the AC filter capacitors.

Since the required reactive power of an HVDC terminal can be as high as 50% of the station rating, the ability to supply reactive power is the other advantage of parallel-connected AC filters over the series connection. The parallel-connected

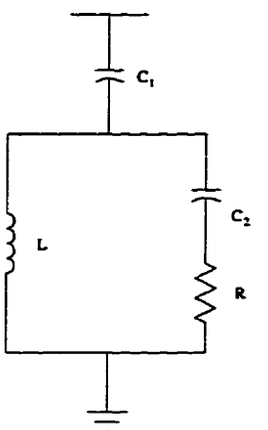

Figure 3.9: Third-order high-pass filter.

filters make a useful contribution to the total reactive power needed, while the series-connected ones, being inductive in the frequency range below their resonance frequency (which includes the fundamental frequency), consume even more reactive power instead.

HVDC schemes are required to operate at near unity power factor over the load range. Therefore, the AC filter operation must be combined with that of the shunt capacitors by means of adequately switching filter and shunt capacitor branches in and out during DC load variations.

The amount of reactive power supplied by the minimum configuration of the passive AC filters should not be larger than the minimum reactive power which is demanded by the converter terminal during light load periods.

3.6 The Design Process

In simple harmonic flow studies in AC/DC systems, assuming the automatic control of DC current, the interaction between one pole of the HVDC terminal and the AC system can be represented in a per-phase-based equivalent circuit like the one shown in Figure 3.11.

In this circuit, the HVDC system is modeled by two current sources in parallel. They represent the fundamental current and the harmonic contents respectively de-

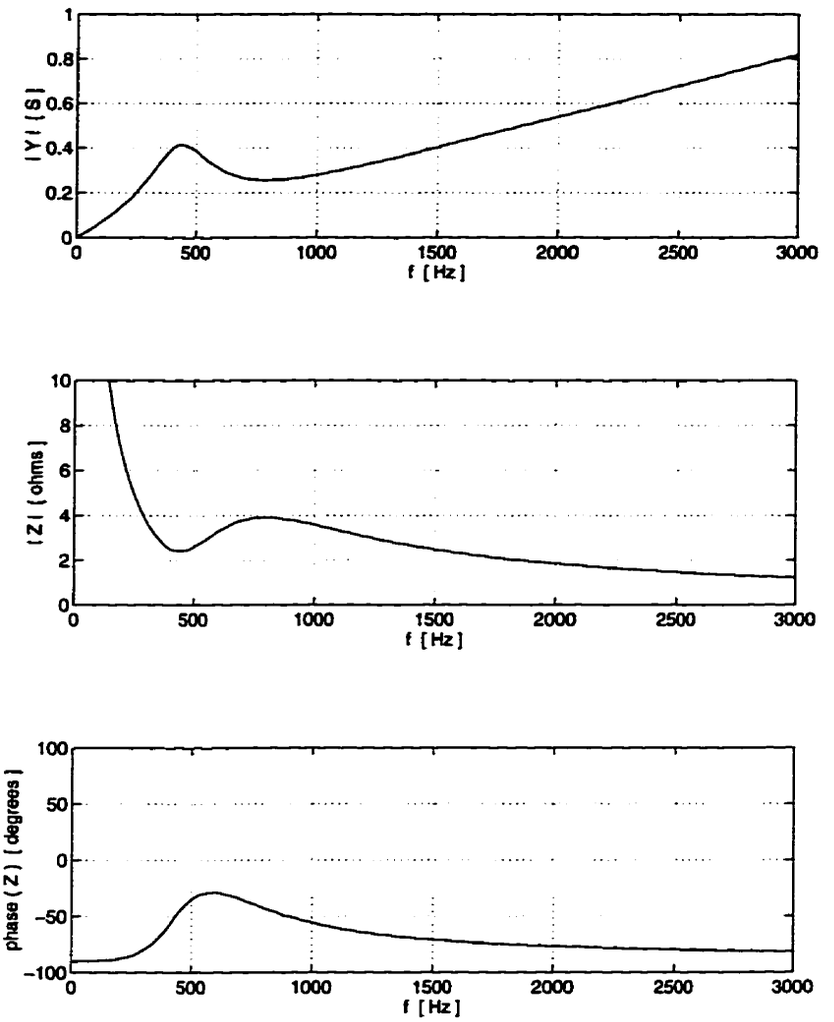

Figure 3.10: Frequency characteristics of a third-order high-pass filter ($R = 2.1\ \Omega$, $L = 0.48$ mH, $C_1 = 108.3\ \mu$F and $C_2 = 108.3\ \mu$F).

manded by the HVDC terminal. All the AC filters are lumped into one impedance Z_f. The shunt capacitor bank (C_{sh}), for reactive power supply, is connected in parallel with the Thevenin impedance (Z_s) of the AC system. The AC system voltage is generated by two series-connected voltage sources. One of them provides the fundamental component, and the other one provides the harmonic "ambient noise" that always exist in a power system.

The main control variables of the design of AC filters for HVDC converter stations are the amount of reactive power demanded by the HVDC converter terminal and

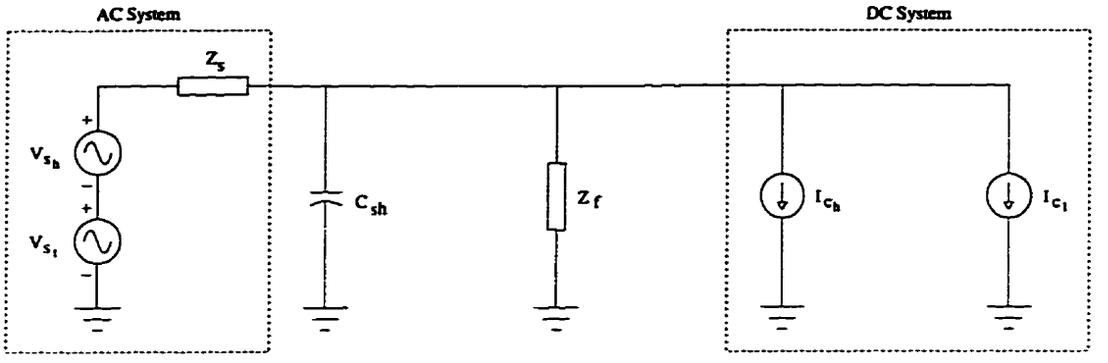

Figure 3.11: Single-phase diagram of an HVDC terminal and connected AC system.

the resonance frequency and sharpness of tuning of each of their different branches. This design process has, basically, three stages [2].

The first one is to derive the harmonic current generation patterns of the converter. The basic input data for this stage are the AC-system voltage, the direct current I_d, the commutating reactance X_c, the firing angle α of the valves and the causes and amount of imbalance with their corresponding harmonic contributions. The validity of the results from this stage is based on the reasonable assumption that the voltage distortion at the HVDC converter terminal will be negligible after the installation of the AC filters.

The second stage is to study the injection of selected harmonic patterns into the AC network in parallel with the filters under all the configurations possible. These filters should be designed to meet the maximum disturbance criteria specified in terms of the disturbance indices presented in Chapter 2 to be applied by the utility.

The final stage would consist of scanning the results of the previous stage to determine the highest amplitude for each harmonic and identify the related operating conditions.

Although a filtering scheme depends on the specific characteristics of the DC and AC systems involved, filtering, for a usual twelve-pulse HVDC system, consists, at least, of two single-tuned filters (one for the 11th harmonic and the other one for the 13th harmonic) and a second-order high-pass filter tuned at or close to the 23rd harmonic. These filters are all split into branches that, during their operation are

individually switched in or out according to the reactive power demanded by the HVDC operation to match load variations.

It is also common for an HVDC scheme to make use of single- or double-tuned 3rd/5th or 5th/7th filters. These are intended to increase the damping of the low-order harmonic overvoltages due to parallel resonance between the AC network and the filter capacitor banks.

3.7 Disadvantages of the Use of AC Passive Filters in HVDC Terminals

Each one of the following subsections presents brief explanations of the main drawbacks in the use of AC passive filters.

3.7.1 Design

Designing AC passive filters is not a trivial task. The problem involves the removal of quantities, based on their differences in amplitude and phase, from relatively much larger quantities. Besides the validity and accuracy of the analytical process, obtaining of the harmonic current patterns, the representation of the AC network and the design of the filter, bring together a large number of alternatives to be considered. This task tends to be so complex that the practical meaning of its results can easily become lost [2].

Each one of the problems described in the following subsections are interdependent and yet, they deal with a certain specific AC system configuration. Unfortunately, due to constant switching operations, there is uncertainty concerning the impedance characteristics of the AC system viewed from the HVDC converter terminals for it can operate under several different topology configurations. Therefore, a solution for a certain resonance problem at a certain frequency, in one configuration, may create a new resonance problem at a different frequency, at the same AC-system configuration or at some other configuration. The fact that the AC system also evolves over the time adds up to the complexity of AC passive filter design and updating.

In addition to covering the steady-state performance, transient studies (faults and switchings) must be carried out to determine ratings and protection measures. A large portion of these studies are performed concurrently with other interrelated investigations. These include the reactive-power balance, voltage fluctuations due to filter switching as well as power factor and risk of auto-excitation of generators.

It is, therefore, clear that a pure mathematical tool for the design of AC passive filters is not possible. Thus, presently, the practical design involves relying on extremes of network layouts and operating conditions, and the final solution is far from being a broad-band solution.

3.7.2 Reactive Power

Since part, or all of the reactive power demanded by the HVDC converter, must be supplied by the AC passive filters, this fact imposes constraints in the free choice of the values of the filter components so as to meet the requirements on AC-current harmonic flow in the AC system. Also, the AC filters may deliver more reactive power than what is actually needed by the HVDC converter at low transmitted DC-power operation, thus, causing sustained fundamental-frequency overvoltages.

The rise in the AC system voltage at low loads is usually prevented by switching some filter units (high-pass) out [46]. In some systems, where harmonic flow constraints are high, it is prevented by switching-in shunt reactors connected to the low-voltage tertiary windings of the converter transformers [21].

3.7.3 AC-System Fundamental-Frequency Variation

The operating frequency of the AC system varies around its nominal value as its loading condition changes and, therefore, the sharpness of the AC filters need to account for these changes. For example, to make provision for a frequency deviation of 1.0 Hz, the value of the capacitance of a third-harmonic AC filter capacitor is 60% greater than that for a frequency deviation of 0.5 Hz [50]. If the filters are not properly designed, a change of as much as 1 Hz in the AC system frequency can lead to serious resonance problems [51].

This problem affects mainly single-tuned filters and, depending on the system, an AC system frequency change as high as 5% could be expected at the design stage [35]. Figure 3.12 shows the frequency deviation information used in the designs of the rectifier and inverter stations of the Itaipu transmission system. The steady-state ranges were considered having the redundant filters disconnected. The transient frequency deviations, lasting at least one minute, were considered with all filters in operation. The lowest possible frequency at the Foz do Iguacu station is only likely to happen in an extreme contingency of the loss of 50% of the capacity of Itaipu's 9 generators [52].

3.7.4 AC-Filter-Component Value Variations

The deviation of the AC fundamental frequency, is compounded by the mistuning of the AC-filter elements. This may arise due to uncertainty in the component values (initial mistuning of the filter due to manufacturing tolerances), internal separately-fused elements failures (capacitors), changes in the values due to changes in the ambient temperature or by self-heating (mainly the capacitors) and the finite size of possible tuning steps (values made available by manufacturers).

All the above effects must be combined to determine the worst detuning conditions. Any error will affect the filter and, hence, its effectiveness, which may cause resonance problems. A 2% change in the values of the inductance or capacitance of a single-tuned filter causes the same detuning as a change of the frequency of the AC system of 1% [35]. The inductance of the filter buses can also contribute to the detuning of the AC filters.

3.7.5 Relative Impedance of the AC Network

It can be noted from Figure 3.11, that the effectiveness of the diversion of the AC-current harmonics by the AC passive filters depends on the impedances of the AC passive filters, at each frequency, when compared to those of the paralleled connection of the shunt capacitor bank and the Thevenin equivalent circuit of the AC system. Therefore, the filtering may not be satisfactory if the harmonic impedance of the AC system is very small.

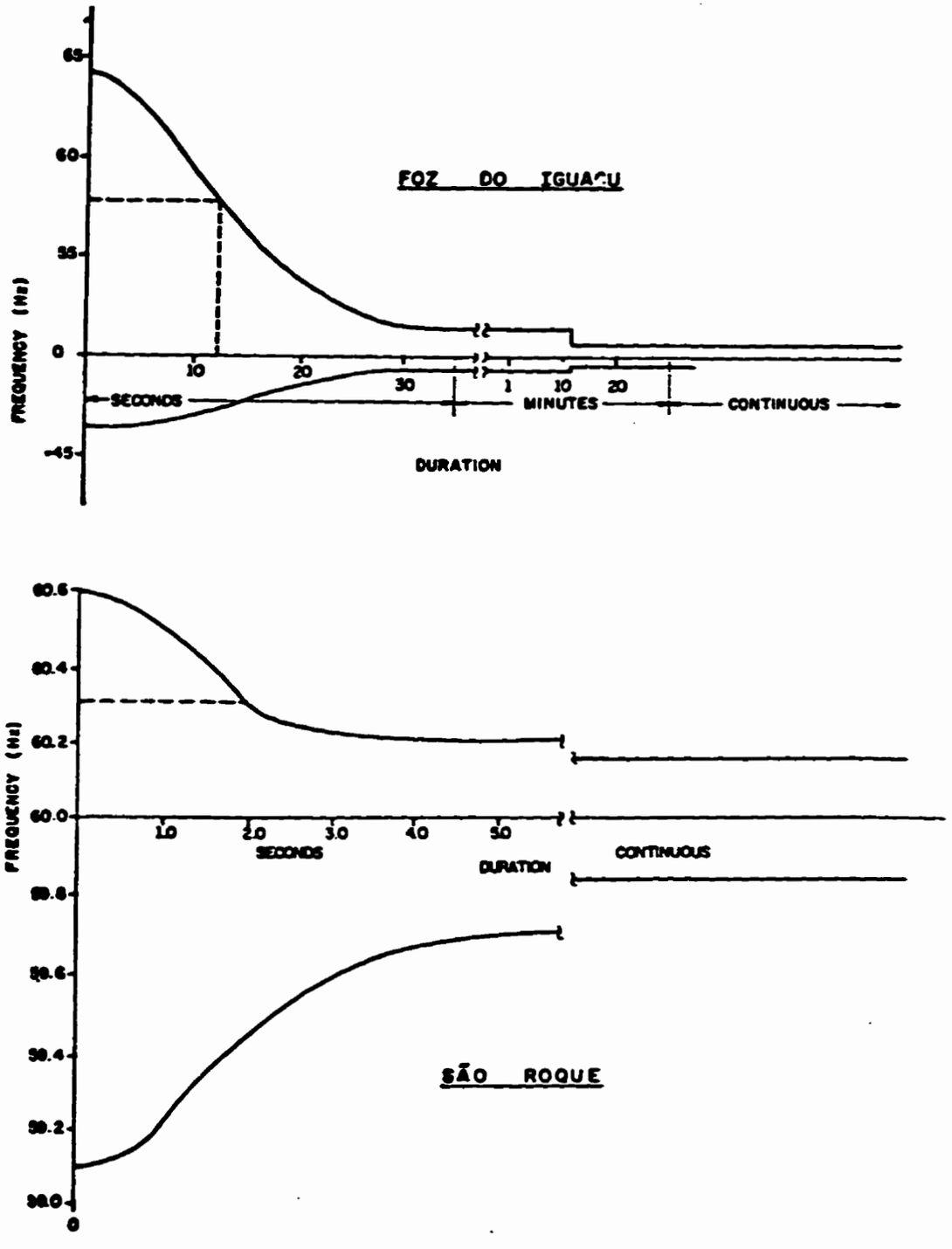

Figure 3.12: Fundamental-frequency deviations considered in the rectifier and inverter terminals of the Itaipu project (extracted from [46]).

3.7.6 Series Resonance

There are several other non-linear loads and equipment (generators, transformers) throughout the AC network that also contribute to ambient AC-current harmonics (especially low ordered ones). If the equivalent series impedance of the AC system, together with the AC passive filters, form a series resonant circuit at a certain frequency, the ambient harmonic currents may be diverted by the AC passive filters and, if not expected at the design stage, these will be overloaded.

In brief, AC passive filters do not discriminate AC-voltage- or current-harmonic sources and may cause a concentration of converging current harmonics to the HVDC station. In one real case, the harmonic current through the filters, with the HVDC converters blocked, was even greater than the one expected due to the HVDC terminal itself [12].

This is closely related to the fault level at the point of filter connection (also referred to as "harmonic driving point impedance"). In filter design, these studies extend over the whole range of harmonic frequencies for which filtering is required.

3.7.7 Parallel Resonance

It has already been mentioned that the impedance behavior of AC passive filters below their resonance frequency is capacitive. Therefore, considering this range of frequency, when the impedance of the AC network is basically inductive, a parallel resonance may occur (see Figure 3.11) with the associated high equivalent impedance. In this case, if the resonance frequency is close enough to any of those of AC-current harmonics drawn by the HVDC converter, harmonic overvoltages are caused.

In this case, harmonic transferences between the AC and DC systems may produce a harmonic feedback loop ("harmonic instability") from which AC overvoltages, magnification of the harmonic currents, and even saturation of the converter transformer core may result [53–56].

Actually, harmonic amplification can arise at nodes widely separated from the HVDC terminal. This puts constraints on the widening of pass-bands (necessary for coupling with AC system frequency changes) and also on the amount of reactive power that can be supplied by the AC passive filters.

A parallel resonance at a frequency lower than the first characteristic harmonic is typical. The resonance problem is usually more significant in the case of AC systems with low short-circuit ratios. Also, the higher the phase angle of the AC system, the less damped the resonance is. Schemes which are directly fed by remote generators without any local load have very little damping from the rest of the AC system on the rectifier side [46].

3.7.8 Physical Area

A considerable area of the switch yard of an HVDC terminal substation is occupied by AC passive filters. This is a critical factor especially in metropolitan areas.

3.7.9 Cost

Among all the components that constitute the AC parallel-connected passive filters, the most expensive ones are the capacitors (approximately 60 % [35]). Therefore, the price of such filters is almost always related to the reactive power which is supplied by them. As a proportion of the total cost of the HVDC terminal, the cost of the AC filters varies from 5% to 15% [35]. However, if unexpected non-characteristic harmonics levels have to be accommodated, the use of additional filters to supplement the original AC passive filters might raise their relative cost to levels as high as 25% [12]. This could indeed affect the economic evaluation of a DC project.

Chapter 4

The HVDC Test System

4.1 The CIGRÉ HVDC Benchmark System

The 50-Hz CIGRÉ HVDC benchmark model [47,48,57], shown in Figure 4.1, has been modified and chosen as the basis for the test system for this thesis. This hypothetical HVDC system has characteristics that represent the factors that cause harmonic instability and other harmonic-related problems. As expected by the CIGRÉ working group 14.02 (Control in HVDC Systems), the deliberate operational difficulties presented by this model provide a very convenient platform on which to test new solution proposals for harmonic-related problems [56].

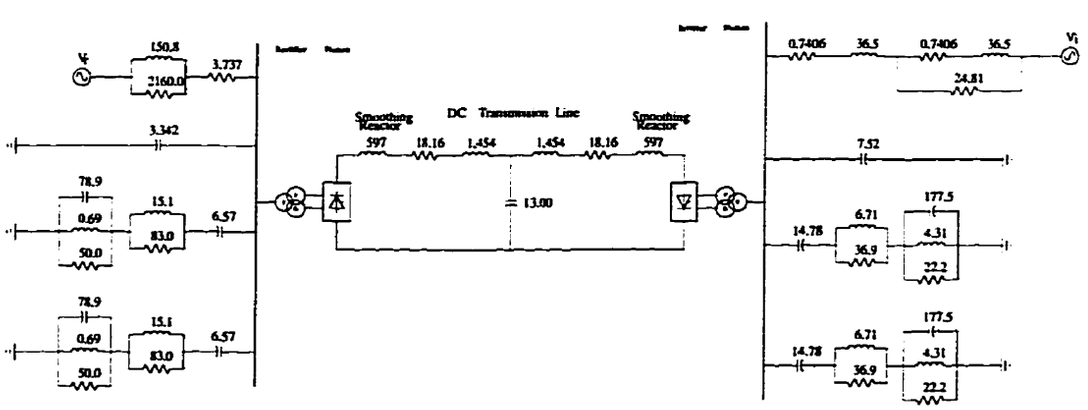

Figure 4.1: The 50-Hz CIGRÉ HVDC benchmark model [Ω, mH, μF].

4.2 The Derivation of the HVDC Test System

Any of the possible control strategies applied at the converter station (DC power, DC voltage, DC current) result in a steady-state operating point at a certain DC current. The transfer functions of the control permit the DC system to be considered as a constant current source for the purposes it has in AC filter evaluation.

Since the scope of this research deals with a basic design of an active AC-filter scheme, the inverter station has been substituted by a fixed ideal DC voltage source. As a consequence, the digital-simulation computation time has been greatly reduced without compromising the validity of the performance of the active filter. The choice for the simplification of the inverter terminal over the rectifier terminal was done in favor of a simpler DC control and a more challenging AC system, which presents a higher parallel resonance and is less damped [47].

This simplification implies that all the dynamic characteristics of the inverter control has been disregarded, i.e., whatever disturbances the DC system experiences, the inverter voltage control will manage to maintain a fixed DC voltage at its end of the DC line. Evidently, this simplification does not allow power reversal or the inverter-current-control mode of operation.

With the objective to fit the test system and the results of this thesis into a North American context, a 60-Hz version of the benchmark system has been derived. Figure 4.2 shows the resulting 60-Hz modified version of the CIGRÉ HVDC benchmark system that has been used in this research.

The inductance and capacitance values of the 60-Hz test system have been obtained by means of frequency base-change operations, and these values are five sixths of those of the 50-Hz system. Although it has been chosen to keep the original values of the resistors unchanged, the consequent fact that the 60-Hz version became slightly more damped than the 50-Hz version does not discredit the design of the AC active filter and avoided the time-consuming task of trimming new resistance values. The main parameters defining the steady-state operation point of the test system are listed in Appendix A.

As required by the nature of the study [49], each converter is modeled by a twelve-pulse bridge as illustrated in Figure 2.2. During normal steady-state operation, the

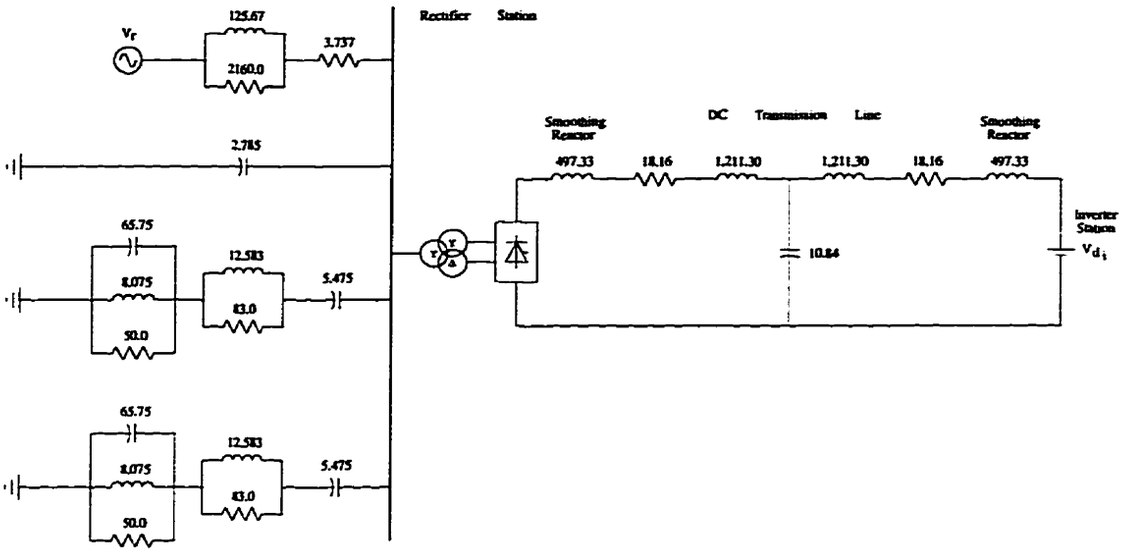

Figure 4.2: The 60-Hz HVDC reference system used in the research [Ω, mH, μF].

theoretical current waveforms are exactly as those previously shown in Figures 2.3 to 2.7. Likewise, the theoretical DC voltage waveforms, are as shown in Figures 2.9 and 2.10.

The DC transmission line model is representative of a 1300-km-long/500-kV overhead line with which the smoothing-reactor/line-capacitance combination produces a DC-side resonance close to the fundamental frequency [57]. The frequency characteristics of the DC side of the HVDC test system is shown in Figure 4.3. A DC-current oscillation at the fundamental frequency on the DC side will cause, by means of the converter operation, DC and 2nd harmonic components in the line current on the AC side, and possibly trigger resonance problems.

The values chosen for the parameters of the converter transformers are typical of HVDC installations and their original data also include their saturation curves [47]. Although this is a convenient feature, since an operation point close to the saturation knee also causes harmonic current flow (mainly at the second harmonic frequency), a linear representation has been selected for the sake of the simplification of the design process and a faster digital simulation.

The AC passive filters consist of 2 identical branches as shown in Figure 4.2.

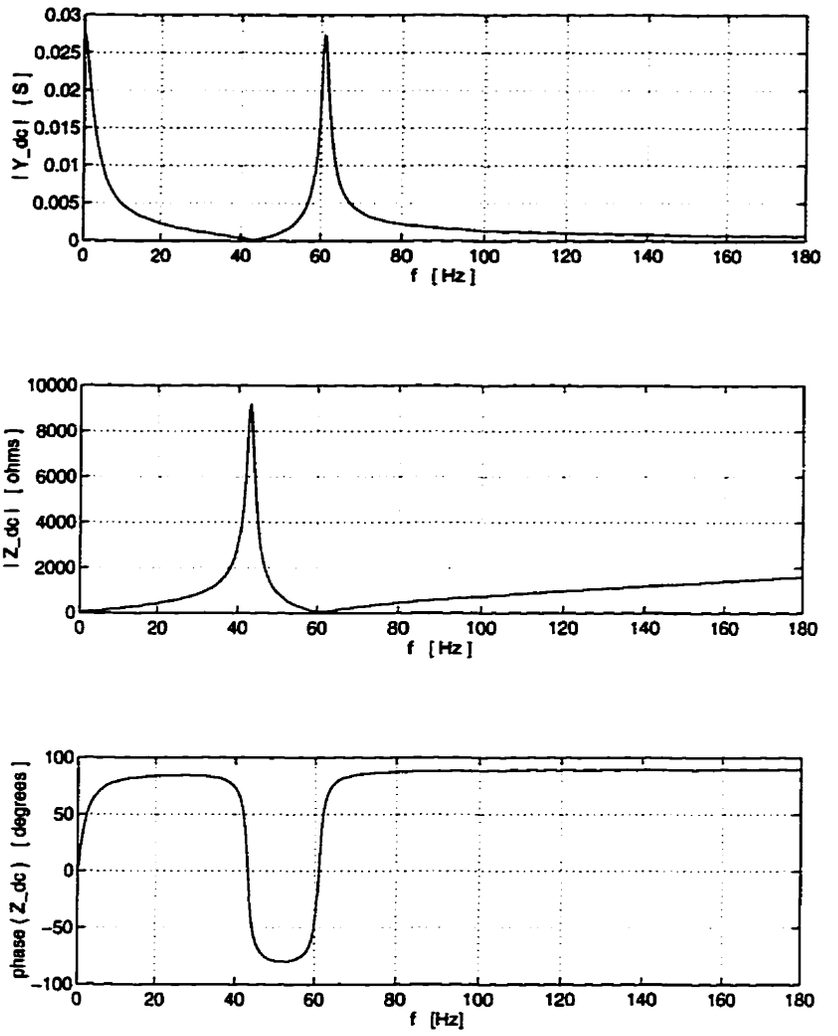

Figure 4.3: Frequency characteristics of the DC-side system.

Figure 4.4 shows the frequency characteristics of the combined connection of both passive-filter arms. As [57] claims, they provide a low impedance path to ground for low-order harmonics as well as for the characteristic ones and are rated at half the nominal DC power.

The reactive power delivered by the AC passive filters corresponds to approximately 93% of the total required reactive power in normal steady-state operation. The shunt capacitor bank, at the rectifier terminal, can respond for up to 23% of the same total reactive power. Therefore, it is possible, if all the shunt capacitor banks are connected, with the passive filters, to supply extra reactive power equal to 16%

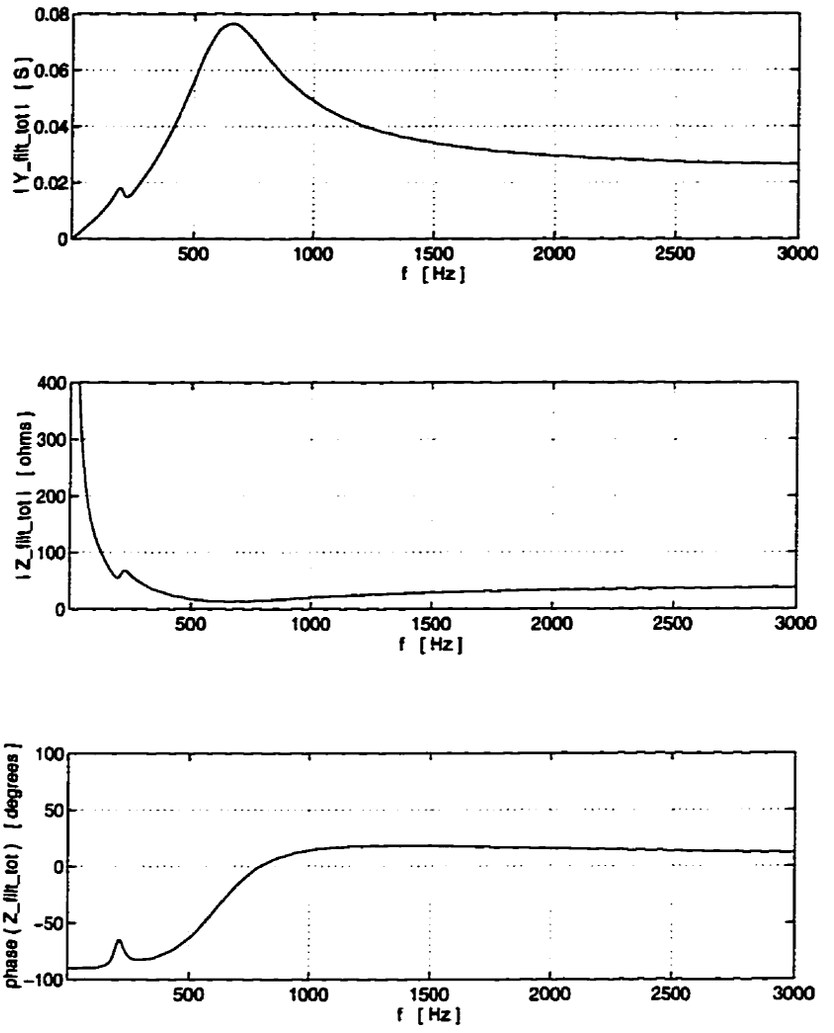

Figure 4.4: Frequency characteristics of the total original AC passive filter.

of the steady-state rated value.

The rectifier AC system is represented by a Thevenin equivalent circuit. The frequency characteristics of the Thevenin impedance is depicted in Figure 4.5. This RRL circuit exhibits the same impedance angle of 84° for the fundamental and third-harmonic frequencies. This is representative of a region in the AC system where power generation is predominant and, therefore, represents a critical case concerning the damping aspect.

The combination of the impedance frequency characteristics of the AC system together with the AC passive filters and shunt capacitor, as seen by the HVDC rectifier

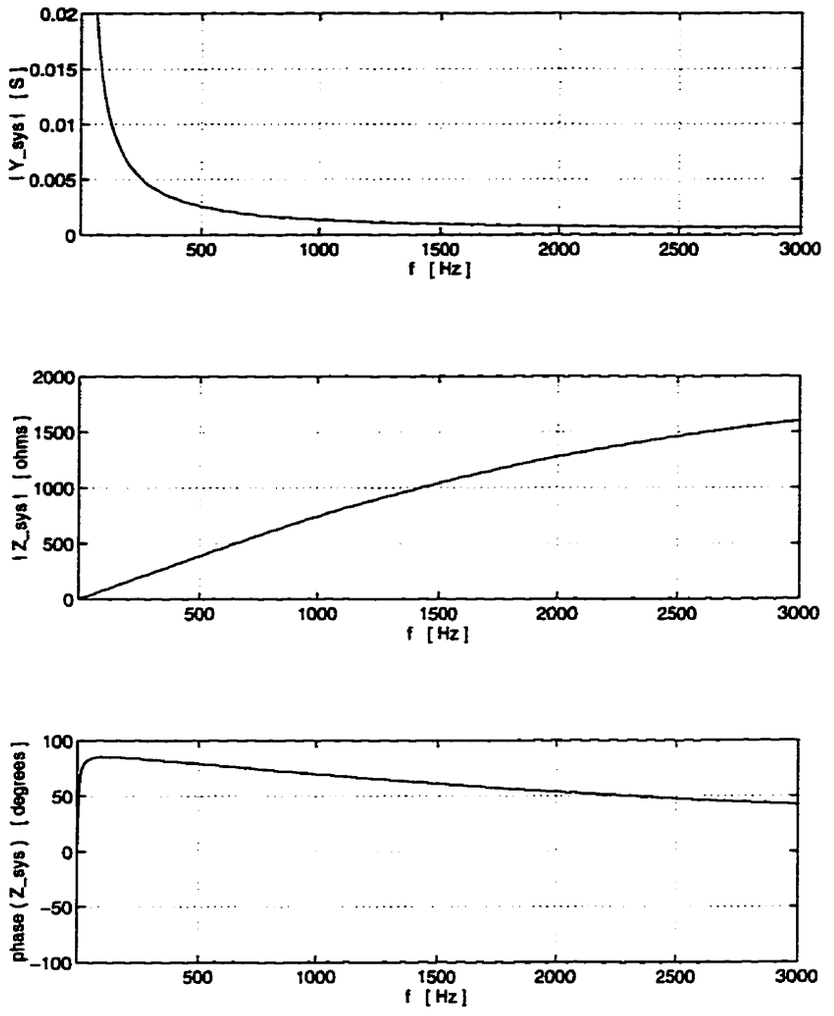

Figure 4.5: Frequency characteristics of the Thevenin equivalent of the AC system.

converter station is shown in Figure 4.6. There is an evident parallel (or anti-) resonance close to the 2nd harmonic frequency. The existence of this parallel resonance at the 2nd harmonic on the AC side and the resonance close to the fundamental frequency on the DC side are peculiarities of the benchmark model that increases its degree of operational difficulty.

The short-circuit ratio (SCR) of the rectifier AC system is 2.5 and the effective ratio (ESCR) is 1.9 (with a damping angle of 70°). These ratios and damping, characterizing a weak rectifier system, impose some degree of difficulty to the HVDC operation in terms of overvoltages, poor recovery from disturbances and voltage and harmonic instabilities.

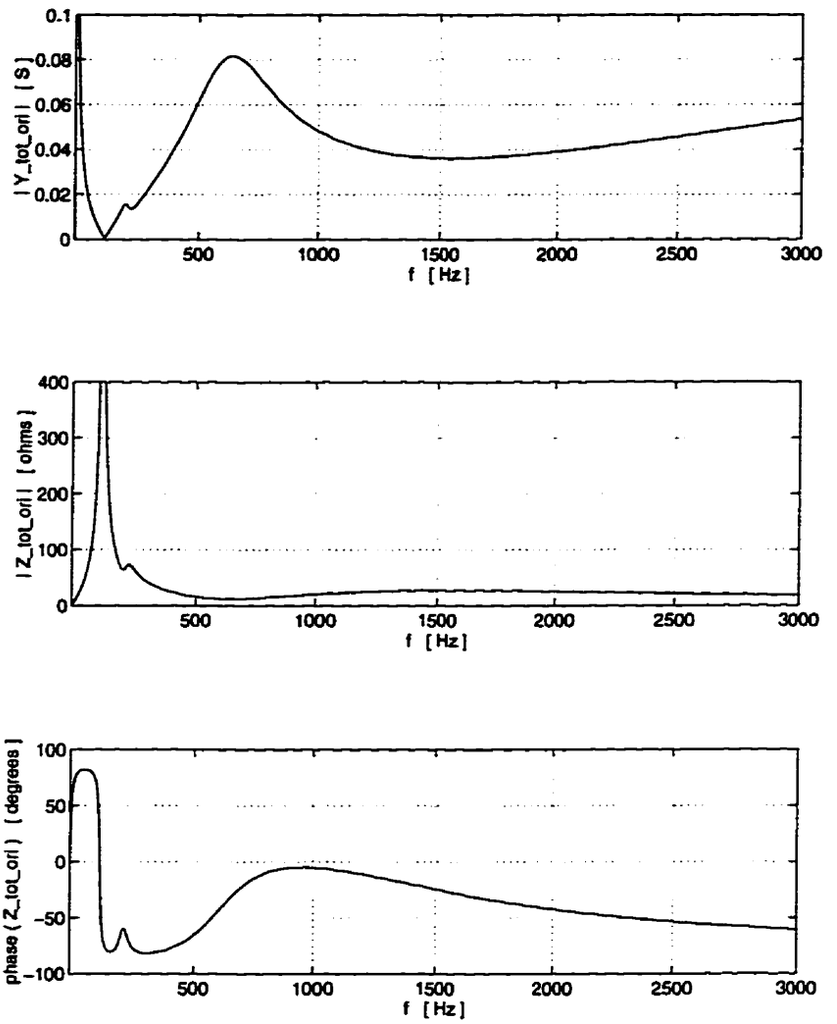

Figure 4.6: Frequency characteristics of the total equivalent AC system.

4.3 The HVDC Test-System Control

The HVDC control system that has been implemented consists of only the basic functions to confer the system with the minimum degree of operability necessary for the purpose of this thesis. Several control functions that are available in real HVDC schemes [52] are not necessary either for the scope and simulation-time scale of this study (e.g., frequency control, tap changing, reactive power control), or due to the small simulation time that the verification of the performance of the active filter requires (e.g. frequency-stability control, overload control and tap-changer control). Therefore, the control scheme that has been incorporated is not significant to

the results of this thesis, and the validation and use of certain incorporated control functions can be deferred to future studies.

The usual quantity to be controlled by a real HVDC system is its transmitted power, and, therefore, a reference P_{d_o} is set for the pole or bipole. Instead, in this thesis, with the objective of simplifying the analysis of the dynamic performance of this initial implementation, a current order I_{d_o} is issued. This value will, ultimately, determine the DC line current in normal steady-state operation. This current order is, initially, used as the input for the voltage-dependent current-order limiter.

4.3.1 The Voltage-Dependent Current-Order Limiter

The weak AC system called for the installation of a control function that could limit the current order to be ultimately forwarded to the current control depending on the DC terminal voltage. This control function is known as voltage-dependent current-order limiting (VDCOL) [52]. The corresponding block diagram can be seen in Figure 4.7.

A sudden DC-voltage drop below a certain level is a consequence of some contingency in the AC or DC systems. In this case, an immediate action to be taken, especially if power is the quantity being controlled, is to reduce the current order. This avoids aggravating the transient problem. Likewise, after the fault is cleared, power must be restored in an orderly manner. This is particularly important when the DC system is connected to weak AC systems. The VDCOL, responsible for these actions, has its block diagram shown in Figure 4.7.

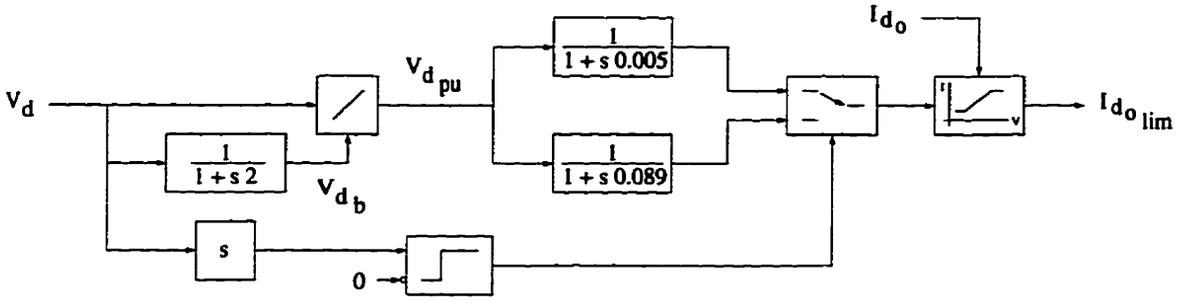

Figure 4.7: Block diagram of the voltage-dependent current-order limiter function.

The normalizing function, implemented by the division of the DC voltage signal

by its filtered value with a long time constant (2 s) allows the VDCOL to operate at different DC voltage levels. The resulting per-unit quantity is then filtered by a high-pass filter with a variable time constant. This time constant assumes two different values, depending on the derivative of the per-unit value. In the case of a fault (negative derivative), the control must act quickly and, therefore, a small time constant is used (5 ms). On the other hand, during the recovery of the fault (positive derivative), the used time constant is larger (89 ms), thus ensuring a cautious re-injection of power into the system.

The actual voltage-dependent current-order limiting function is represented by the last non-linear function block in Figure 4.7. The constraining functions for the possible family of steady-state characteristics are detailed by Figure 4.8. Finally, the original current order is simply scaled by being multiplied by the value in per-unit.

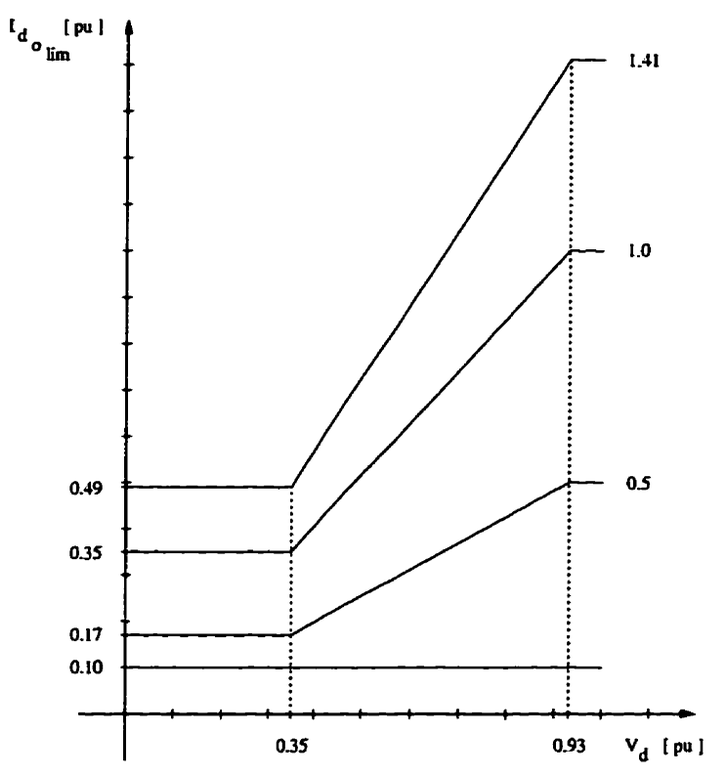

Figure 4.8: Constraining curves of the voltage-dependent current-order limiter function.

4.3.2 The Current Control

The current control is performed by the proportional-integral (PI) type of control displayed in Figure 4.9 [58]. The input for this control is provided by the voltage-dependent current-order limiter previously explained. $I_{d_{o_{lim}}}$ is subtracted from the measured value (in p.u.) of the actual DC current I_d, which generates the error signal I_{d_e}.

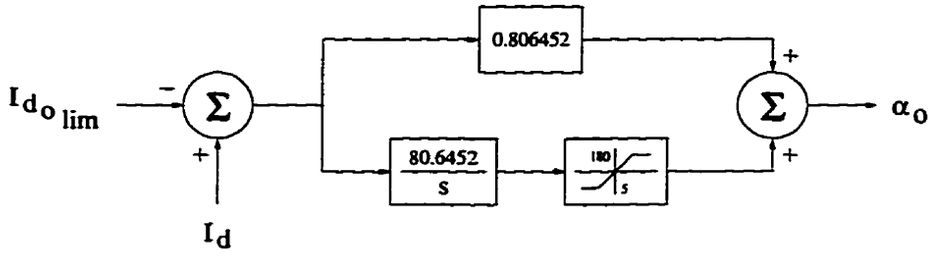

Figure 4.9: Current control.

Once a zero error is achieved, the integral part of the PI controller will be responsible for providing the firing control with a constant value. This output (α_o), is the firing-angle order that will assure an adequately synchronized and time-equidistant firing of the converter valves. A limiting block is placed at the output of the integrator. The lower limit is the minimum firing angle ($\alpha_{min} = 5°$) that assures that there is a sufficient positive voltage across the valves at the moment of firing. This avoids misfirings and consequent overcurrents. The upper limit is the maximum transient firing angle ($\alpha_{max} = 180°$) that prevents the valves from receiving the firing pulse when the voltage across them is negative.

4.3.3 The Firing Control

The firing control is responsible for providing the converter valves with the sequential and time-equidistant firing pulses in normal steady-state operation. The corresponding block diagram of this control is depicted in Figure 4.10.

The firing control consists, basically, in a phase-locked-loop (PLL) oscillator, a commutation-voltage zero-crossing detector and a ring-counter [13]. The measured value of the firing angle α is obtained by sequentially, and synchronously, subtracting

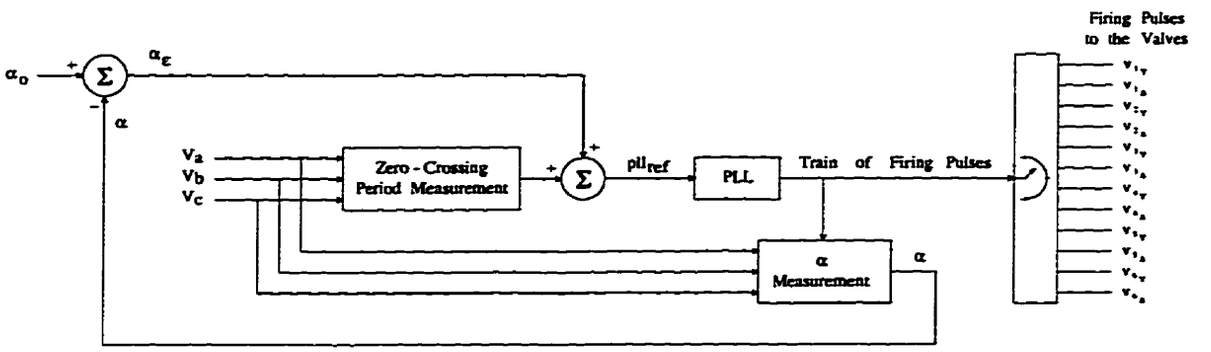

Figure 4.10: Firing control.

the zero-crossing time instant from the firing time instant. This value is filtered, converted to degrees and compared to the ordered firing angle α_o value provided by the current control. The generated error signal α_e then feeds the PLL.

What follows is a brief explanation of the operation of the PLL having Figures 4.10 and 4.11 as references.

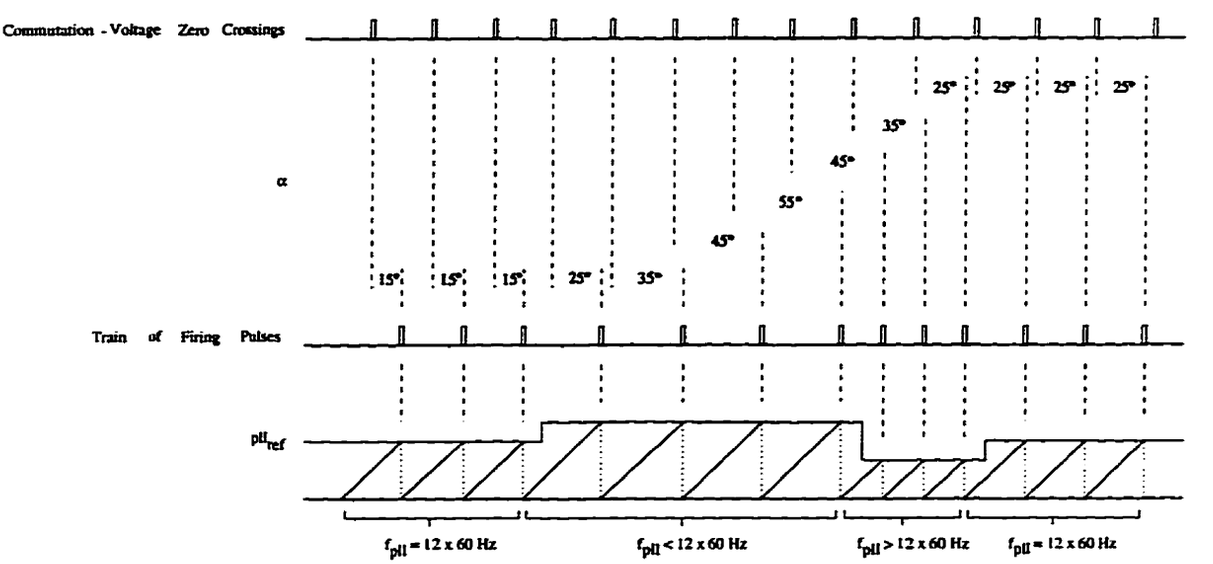

Figure 4.11: Generation of the PLL train-of-pulses in the firing control.

The center frequency of the PLL must be the same as that of the steady-state zero crossings of the commutation voltages. Therefore, it is 12 times the fundamental frequency. Its function is to control the phase of the firing pulses with respect to the zero crossings. If the input α_e is zero, its output is a steady train of time-equidistant pulses. The pulses are generated when the sawtooth waveform is reset after having

the same value as the reference value pll_{ref}.

If the pole control desk determines a decrease in the current order, the PI controller of the current control will increase the order α_o so that the DC line voltage is lowered. The increase of α_o will make the value of α_e positive. The effect that the increase of α_e will have on the train of pulses is determined by the time delay with which the sawtooth waveform is reset. This delay, which means a momentary decrease in the frequency of the train of pulses, will last for as long as the signal α_e exists. It can be noticed that the firing angle keeps increasing while this error exists. This confers an integral characteristic to the PLL. Once this error signal returns to zero, the train of pulses will have the same frequency as the that of the commutation-voltage zero crossings, be time-equidistant, but at a new operating point, shifted by α_e with respect to the original train of pulses. The process following an increase of the DC current order is equivalent. A simplified linear block diagram of the PLL is shown in Figure 4.12.

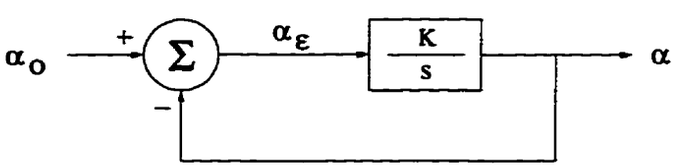

Figure 4.12: Linearized representation of the PLL in the firing control.

Finally, the train of pulses generated by the PLL is sequentially distributed to the respective converter individual valves by means of the 12-stage ring-counter.

Chapter 5

The Active Filter

5.1 Introduction

The need for a better overall performance than that provided by AC passive filters has turned the attention of major power consumers to the use of active filters. AC active-filter units, sometimes under the commercial name of "power line conditioners", are already available in the market for industrial applications [59]. On the other hand, for HVDC terminals, which involve higher voltage and current levels, the cost/benefits ratio has not been completely evaluated.

In contrast to the numerous publications on the industrial applications of active filters [20,22–24,27,28,59–63], few papers [12,21,56,64] have addressed the specific filtering and harmonic problems in HVDC applications. With respect to active filtering in HVDC systems, the main needs are for large capacity, high control capability for better performance and high operating efficiency. No proposal seems to have found practical acceptance yet.

The principle of the operation of active filters can be divided into two stages. The first stage consists of the detection of the amplitudes and phases of the AC current harmonics (or any other system quantity which is associated with them) which are present in the AC line. The second stage is the injection of the appropriate current harmonics or insertion of appropriate voltage harmonics at these frequencies so as to supply the AC current harmonics demanded by the non-linear load locally.

The supply of this harmonic current is accomplished by means of a static converter whose power losses must be provided by the power system. There are, basically, two types of converters that can supply AC currents: cycloconverters, and inverters. The main difference between them is that cycloconverters use power directly from an AC source, while inverters connect to a DC source. Therefore, inverters need one extra power processing stage (rectifying) that cycloconverters do not. Although cycloconverters require one less power processing stage, one recent work [65] suggests that such devices have inherent filtering limitations since they generate a broad spectrum of harmonics of considerable amount. Therefore, the inverter-type converter, together with its DC-power source, has been chosen in this work. They will be referred to as the "active harmonic source" or just "active source" of the active filter.

Regarding its interaction with the AC power system, the active source can operate either as a current source or as a voltage source. The harmonic inverter can use either a voltage source or a current source. Respectively, inverters are then referred to as either a voltage- or a current-fed type of inverter converter bridge. Irrespective of the type of inverter used, since it must be able to generate compensating harmonic currents corresponding to a reference with a minimum time delay, from a control point of view, it can be considered a signal amplifier.

As seen in Chapter 1, the active filter to be implemented in HVDC systems could be connected in series or in parallel to the converter station. As seen in Chapter 3, the main problems associated to the use of series passive filters are the flow of the fundamental current, requirement of high BIL levels, reliability, complexity of protection against short circuits on the HVDC terminal side and consequent costs. Again, the same reasons that led to the traditional use of the parallel connection of the passive filters in HVDC systems will also favor parallel-connected active filters for HVDC systems. The parallel connected active filter would, therefore, prevent the AC harmonic current from flowing from the AC system by operating as an active harmonic-current "diverter".

5.2 The Connection of the Active Source to the AC System - The Path Impedance

Although the direct connection of the active harmonic source to the AC line is feasible in industrial applications [60–63], at an HVDC terminal, it would require either a large number of power semiconductor devices in series to withstand the total AC voltage or to realize the connection through a transformer (as suggested in [22]) to bring the AC voltage down. Still, both options would have to consider the need to connect the power semiconductor devices in a parallel arrangement to be able to accommodate the current. Also, both options would involve configurations whose order of magnitude would be comparable to those of the most expensive parts of an HVDC terminal, which are the converter transformer and the semiconductor bridge. Therefore, due to the very high costs in HVDC applications, the direct connection must be discarded.

A main issue in proposals for active filters in HVDC systems is to reduce the rating of the active source. Proposals for combining arrangements of AC passive filters with different types of active sources, in trying to reduce current and voltage ratings, simply reflect the difficulties that this application imposes on the design of a large capacity active filter.

It is evident that, to reduce the rating of the active harmonic source, its connection to the AC system must be done through an impedance [21, 27, 28]. This impedance, however, must meet certain requirements: it must present a sufficiently high impedance at the fundamental frequency, so that it effectively reduces the AC fundamental-frequency components of voltage and current at the active source; it must also offer a low impedance at harmonic frequencies to provide an economical path for the current being supplied by the active source; it should have low losses. This impedance will be referred to as the "harmonic path-impedance", or simply "path impedance". Figure 5.1 shows the conceptual circuit diagram. This is, essentially, the same circuit as the one shown in Figure 3.11, in Chapter 3, with the passive filter Z_f being substituted by the active filter, composed of the path impedance and the active source.

Another means of further reducing the power rating of the active source is to partially filter some harmonic currents, e.g. high ordered harmonics, by means of

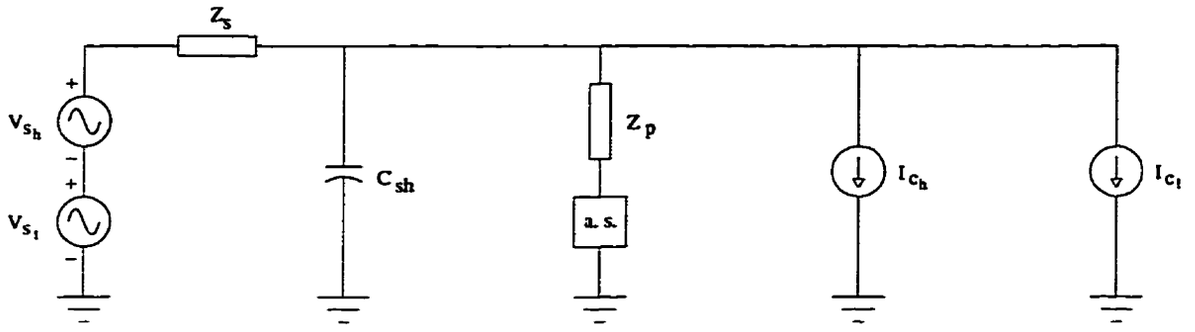

Figure 5.1: Connection of the active filter to the system through an impedance.

passive filtering. This would mean that only the lower order, higher amplitude harmonics, would be actively filtered. Further, besides the reduced rated voltage yielded by the path impedance, the active source would also have its current rating reduced [17,18,21,22,62,63].

Given the required characteristics, the most obvious candidate impedance is the equivalent combination of all the branches of the conventional passive filters themselves [28]. In this case, the active source, in addition to the harmonic current it supplies, would also have to withstand the quadrature current which is determined by the capacitive characteristic of this path impedance at the fundamental frequency. Depending on the percentage of the reactive power demanded by the HVDC terminal to be supplied by the path impedance of the active filter, its rated VAr could have to be as high as 50% of the rated DC power. In a broad and practically feasible solution, the active source should be rated to be able to deliver just the power needed to compensate for the harmonic currents demanded by the HVDC terminal. Therefore, it should not carry any fundamental frequency current or be subjected to fundamental frequency voltage. To accomplish this, the active source can be by-passed by a single-tuned filter providing a low impedance at the fundamental frequency to ground. This approach would be convenient in an eventual application to an already existent system. However, on the other hand, this scheme would impose operational constraints on the ability, which characterizes traditional passive filters, to disconnect some of its branches to control its reactive power compensation during DC-load variations.

Continuing with the effort to devise an active-filter scheme that is suitable for HVDC applications, the use of a band-blocking passive filter, as shown in Figure 5.2, is proposed as the path impedance. The expression for the frequency dependency of

this path impedance is given by

$$Z(f) = \frac{(j2\pi fL)\left(-j\frac{1}{2\pi fC}\right)}{(j2\pi fL) + \left(-j\frac{1}{2\pi fC}\right)}. \tag{5.1}$$

The resonance frequency is given by

$$f_{res} = \frac{1}{2\pi\sqrt{LC}}. \tag{5.2}$$

At the resonance frequency, the magnitude of the reactances is given by

$$X_0 = \sqrt{\frac{L}{C}}. \tag{5.3}$$

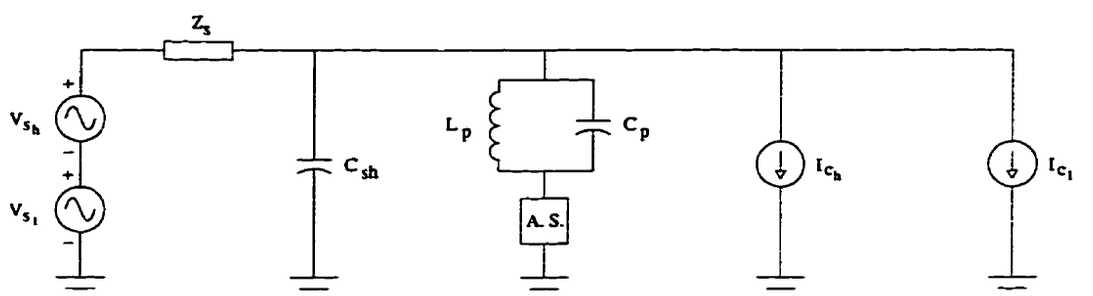

Figure 5.2: Proposed HVDC active-filter path impedance.

This type of path impedance has been used in [66] for lower voltage power distribution systems and had the possibility of its application in high voltage AC systems acknowledged in [67]. Its tuning to the fundamental frequency of the AC system and an adequate choice of the capacitance and inductance values would have the potential to provide an impedance which has good agreement to the desirable characteristics of the path impedance mentioned earlier.

The proposal in this thesis is to totally decouple the filtering of AC harmonics from the reactive power supply for the HVDC terminal. With this arrangement, all the reactive power required by the HVDC terminal would have to be supplied either by extra shunt capacitor banks, by static VAr compensators (SVCs), by synchronous compensators, or by the AC system itself. When compared to the usual HVDC station, this radical proposal has the obvious and significant disadvantage of increasing

the amount of capacitors in the AC filter yard. It is worth noting that both elements are subjected to the line-to-ground AC voltage, it displays an inductive behavior below the fundamental frequency and that, at the fundamental frequency, the reactive power demand of the inductor is totally compensated by the parallel capacitance. Despite the lack of reactive support for the HVDC terminal, the following are some of the advantages that this approach offers:

- This path impedance presents an extremely large impedance magnitude at the fundamental frequency, which causes a *negligible fundamental voltage component across the active source.* In fact, despite the very sharp resonance, the magnitude of the path impedance at frequencies within the usual AC system frequency swing limits [46] is still very high. Therefore, normal AC system frequency variations and/or detuning of capacitance and inductance values in this path impedance have negligible effect on the rating of the active source due to fundamental-frequency components.

- Since the purpose of this impedance is to reduce the rating of the active source, and not exactly filtering, the quality factor can be high (no parallel resistor). Therefore, except for the intrinsic losses of the elements, this path impedance is *lossless.*

- The power rating of the active source of the proposed scheme is only determined by the harmonic current of the HVDC terminal and by the voltage drop this current causes across the path impedance. Considering the percentage of non-characteristic harmonics as being around 7% of the characteristic ones, a rough estimate of the total current through the active source would consider a 10% increase in the rated current due to abnormal harmonics [7]. Since there are no resistors in the path impedance, the only losses are those determined by the efficiency of the active source and those which are inherent to the passive components. The state of the art of PWM amplifiers can ensure *very high efficiency levels* (95% [28], 98% [59]).

- For a given resonance frequency, the higher the inductance, the higher the magnitude of the path impedance at the resonance frequency and the lower the value of the capacitance. It is worth mentioning that for a given VAr rating, the cost

of an inductor is much less than that of a capacitor. Furthermore, *increasing the value of the inductance also decreases the power rating of both the inductor and capacitor.* Bringing the fundamental voltage across the active source to negligible values, since one of the terminals of this device is grounded, is *beneficial to insulation levels.* Decreasing the value of the capacitance increases the value of the magnitude of the path impedance at higher frequencies, which demands, in turn, an increase in the voltage requirement of the active source. Of course, this increase might be negligible when compared to the beneficial decrease obtained at the fundamental voltage.

- The frequency characteristics of the path impedance can naturally provide very low impedances at any harmonic frequency other than the fundamental, and the presently available current and voltage ratings of IGBTs meet the requirements of many HVDC systems. Therefore, it seems that any further reduction of the power rating of the active source by means of additional passive filters (for example, a high-pass filter in parallel with the active source) will under-utilize the *full potential of the active filter.*

- The capacitor would act as a *natural voltage surge protection for the inductor.*

- Traditional passive single-tuned filters present an inductive behavior at high frequencies, and, therefore, pose a high impedance for high-order audible frequencies. The capacitive behavior of the path impedance at high frequencies could improve the *TIF performance* of the overall filter.

- The proposed path impedance can satisfy the requirement of low impedance for injection of frequencies at virtually all super- and sub-harmonics. This characteristic could extend the application of the active filter to a *non-fundamental-frequency control device.* Therefore, sub-synchronous resonance phenomena as well as transient ones generated by switchings or faults could be counteracted.

- Since the active filter and the reactive power supply for the HVDC terminal, under this scheme, would have decoupled operation strategies, it could yield *greater flexibility to the overall operation of the HVDC system.*

- The overall characteristic of the active filter, being decoupled from the reactive power constraints imposed by the HVDC terminal, allows a *higher degree of*

freedom in minimizing the total cost of the active filter. Further freedom would be obtained if a transformer tertiary winding, for example, of a SVC or a synchronous compensator were available. A decrease in the fundamental voltage level across the path impedance, accompanied by a correspondent increase in the current in the active source, could prove to be beneficial to the total cost of the active filter.

- Remedies to unexpected non-characteristic harmonics may add as much as 25% to the original cost of traditional AC filters [21]. This fact justifies consideration of this arrangement aiming at a *broader solution* and with a better performance despite its potential higher installation price.

The factors that influence the decision about the values of the capacitance and the inductance of the proposed path impedance would vary from system to system, with overall cost of the active filter being a determining factor. Unfortunately, although the CIGRÉ HVDC benchmark presents a good basis for performance evaluation, it has not been designed to be a platform on which to compare costs. Therefore, this thesis is confined to comparisons based on filtering performance only.

Since the proposed path impedance does not contribute with reactive power to the CIGRÉ HVDC benchmark system, all the reactive power supplied by the original AC passive filters must be transferred to the shunt capacitor bank. Consequently, the reactive-power control is completely deferred to the shunt capacitance in responding to load changes and contingencies. As a result, the capacitance of the shunt capacitor bank is increased to $C_{sh} = 13.92\mu$F. The capacitance value of the path impedance to be used in this thesis is $C_p = 11.13\ \mu$F. This value delivers the same amount of reactive power as the original filters (166.64 MVAr/phase) and the same amount transferred to the shunt capacitor bank. The value chosen for C_p, together with the fundamental frequency of the AC system, determined the value of the inductance as $L_p = 631.96$ mH. Figure 5.3 shows the frequency characteristics of both the proposed path impedance and the original filters.

It can be noted that the proposed path impedance presents an extremely high impedance at the fundamental frequency (60 Hz) and that, if used passively, it would provide similar filtering characteristics to the original benchmark filters (from the 11th harmonic on). This choice, besides conferring similar frequency characteristic

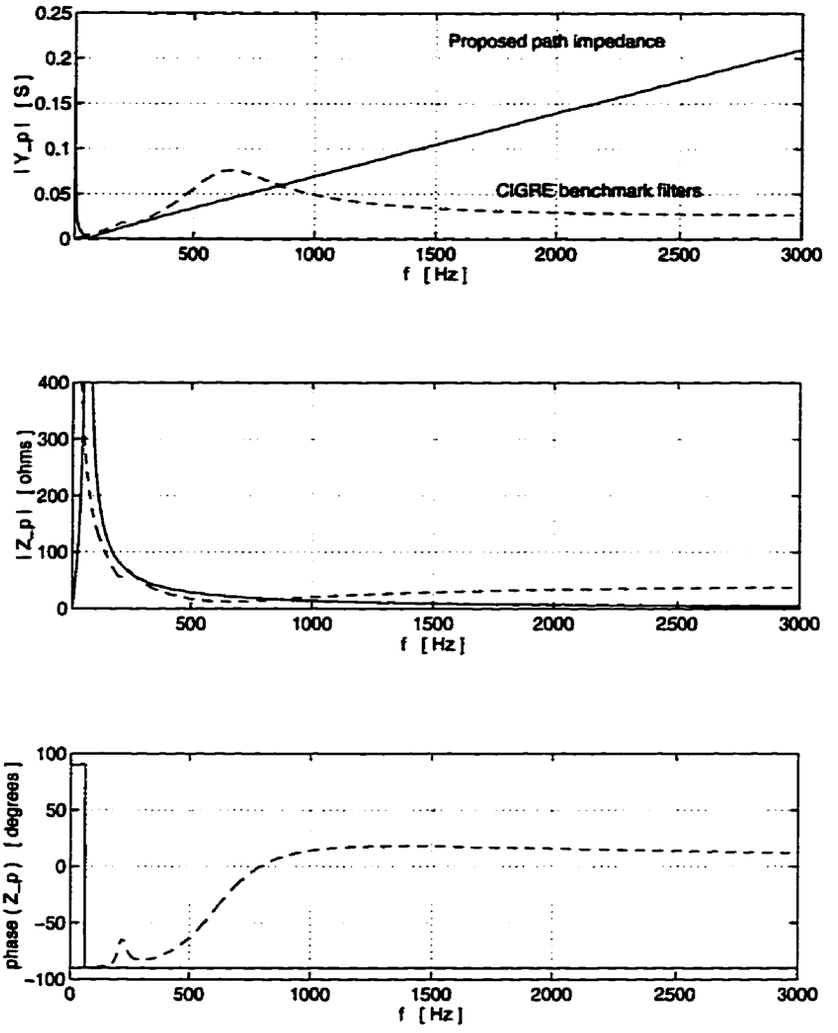

Figure 5.3: Frequency characteristics of the original AC passive filters and of the proposed path impedance (— proposed path-impedance, -- original passive filters).

on the path impedance as the original filters, can, at least qualitatively, allow some hardware comparison between both the original and the proposed arrangements.

5.3 Configuration of the Active Source

As mentioned in Section 5.1, the basic operation of the semiconductor bridge of the active source must be that of an inverter. The active power for the operation of the active source can be supplied from an external DC source or by the AC system itself.

When supplied by the AC system, this active power can be drawn through the path impedance itself, or by means of a rectifier bridge. In the case of the former, energy would then, at each fundamental cycle, be stored in the magnetic field of an inductor, characterizing a DC current-source inverter (CSI) [60–63] or in the electric field of a capacitor, characterizing a DC voltage-source inverter (VSI) [17,18,22].

In the DC current-source inverter, the circuit topology must ensure that there is always a path for the inductor current to flow (a free wheeling path) to avoid overvoltages. In the DC voltage-source inverter, depending on the desired instantaneous harmonic current flow direction, the switching scheme must select the correct terminal of the capacitor to avoid overcurrents.

Since capacitor losses are smaller than those of inductors, the former is usually preferred. In the future, once superconductor materials technology is better established, this tendency may be reversed. In both schemes, the inductor and capacitor losses must be compensated (at fundamental frequency) by an extra control to the active-filtering action so that the DC current, or the DC voltage, of the reactive element is kept at some desired constant level. In this condition, the inverter bridge of the active source should have rectifier operation capability so as to make it possible to draw the active power from the AC system.

Since the proper operation of inverter bridges with passive DC sources depend on the correct charging of the reactive element involved, it is questionable that these types of DC sources could effectively cope with the fast control actions of large amounts of power that involves the operation of HVDC systems. Moreover, since the proposed path impedance does not allow the flow of fundamental-frequency currents, this approach is not possible and, therefore, a rectifier bridge is required to supply the DC power to the inverter of the active source. This rectifier converter is expected to have a much smaller power rating than the main HVDC terminal and therefore, its AC harmonic current demanded from the AC system would easily be filtered by ordinary passive filters. In steady-state operation, the DC-voltage output of the rectifier should be kept at a constant value with the help of an output capacitor. This value is expected to vary whenever the operating point of the HVDC system changes. In this case the voltage level of the rectifier should be accordingly adjusted.

The semiconductor bridge of the active-source inverter could have either a single-

phase or a three-phase configuration. However, since a three-phase configuration would limit the ability of generating unbalanced current harmonics and, in HVDC terminals, due to the levels of power involved, system unbalances should not be disregarded, the proposed inverter bridge configuration should have completely independent phase behavior. Therefore, individual single-phase active filters are proposed to be connected to each one of the phases of the HVDC terminal.

These considerations have led to the single-phase inverter bridge schematically shown in Figure 5.4. This is the basic active source that has been used in this thesis.

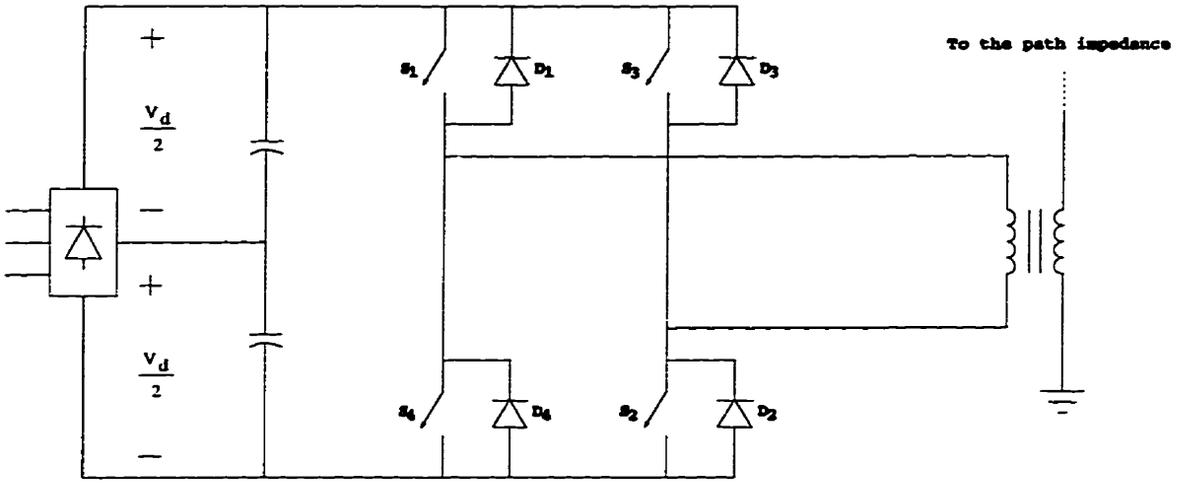

Figure 5.4: The simplified version of the proposed active-source inverter bridge.

The inverter of the active source invokes four power semiconductor devices. The power semiconductor devices in Figure 5.4 are set in a bridge configuration in which only one pair at a time undergoes switching as explained in Section 5.4. The reason for the transformer is to electrically isolate the active source and its load. This electrical isolation causes the load to be "floating" and, therefore, allows for a bipolar output. The load of the active source is the series connection of the path impedance and the parallel combination of the AC system and the new shunt capacitor bank of the HVDC terminal. This can be verified in Figure 5.1. Another use for this transformer is to correctly match the voltage and current levels of the AC system and the devices comprising the active source. For this reason this transformer is also called "matching" transformer. With the objective of simplifying the analysis, and, during the digital simulations, not masking voltage and current levels to which the active-source components will be subjected to, the turn-ratio of the matching

transformer has been chosen to be unity.

5.4 The Sinusoidal-Pulse-Width-Modulation (SPWM) Switching-Control Method

The control of the current output of the active filter could be of either the voltage-controlled-inverter (VCI) type, or of the current-controlled-inverter (CCI) type. Since the current-controlled approach has reportedly presented difficulties in handling transient conditions [17,18,21], the voltage-controlled approach has been preferred in this thesis. While determining the voltage across the active source, this approach allows harmonic currents from other sources in the system to flow freely through the device if no counter action is taken.

The voltage-control method used in this thesis is one of a group known as "pulse-width modulation" (PWM); inverters that operate under this scheme are also known as "PWM power amplifiers". The PWM switching method known as "sinusoidal" (SPWM), which is the most widely used in industrial applications, is illustrated in Figure 5.5 [5]. In this method, a voltage-reference signal, which would be supplied by the control system of the active filter (simply a sinusoidal waveform in this figure), is compared to a triangular carrier wave. The input signals to the power switching devices are generated at the mutual crossing instants of the two waveforms.

Whenever the reference signal is larger than the triangular waveform, power semiconductor devices 3 and 4 are turned off and, immediately after they are extinguished, power semiconductor devices 1 and 2 are turned on. On the other hand, whenever the reference signal is lower than the triangular waveform, power semiconductor devices 1 and 2 are turned off and, immediately after they are extinguished, power semiconductor devices 3 and 4 are turned on. This type of operation obviously requires that the power semiconductor devices have turn-off capability. These devices are usually referred to as "power semiconductor switches" or simply "switches". The simultaneous conduction of switches in series must be prevented by their gate control to avoid short-circuiting the DC source. This is achieved by allowing some time to elapse between these switching actions. This time period during which no switch of the bridge is conducting is known as the "blank time" or "dead time" and should be

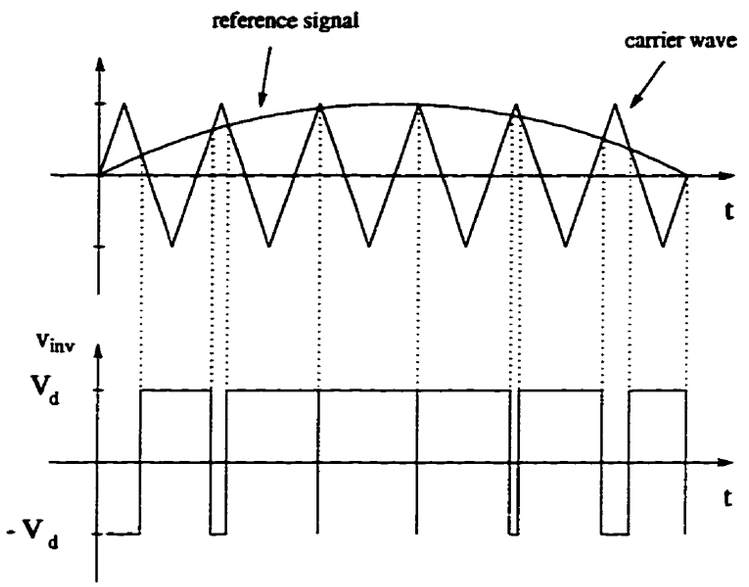

Figure 5.5: Pulse-Width Modulation.

kept to a minimum duration to avoid distortion of the output voltage of the active source [68]. The modulation of the pulse width sent to the switches is inherently, and proportionally, controlled by the time variations of the reference signal. The inverter output is a train of variable-duration pulses which fluctuates between $\pm V_d$, and which reproduce the reference signal when averaged. It is, therefore, a digitally synthesized version of the input signal.

The ratio between the amplitude of the triangular waveform and that of the reference signal is defined as the "amplitude modulation"

$$m_a = \frac{\hat{V}_{signal}}{\hat{V}_{carrier}}. \tag{5.4}$$

The amplitude of the fundamental component of the output of the inverter, provided that $m_a \leq 1$ and that the frequency of the carrier ($f_{carrier}$) is much bigger than the frequency of the reference signal (f_{signal}), is given by

$$\hat{V}_{o_1} = m_a V_d. \tag{5.5}$$

Therefore, the amplitude of the output of the inverter varies linearly with ratio m_a as long as the amplitude of the carrier waveform is greater than that of the reference signal.

The switching frequency of the PWM inverter, determined by the frequency of the triangular carrier waveform, is the average rate at which the circuit develops output pulses. This value must be several times higher than that of the highest aimed harmonic order. In an active-filter application, the higher the switching frequency, the more fidelity to the reference signal is obtained. Unfortunately, there are two factors which impose limits to the switching frequency. The first one is the switching frequency capability of the semiconductor device itself. The second is that the switching losses, being proportional to the switching frequency, and iron losses (eddy current and hysteresis) in the matching transformer, also increase, reducing the circuit efficiency. Another problem that arises as the switching frequency is increased is the electromagnetic interference (EMI). Still, the performance gains obtained from increasing the switching frequency may override these problems, and this is reflected by the fact that the switching frequency of switches will be continually increased by manufacturers [69,70].

5.5 Viability of the Proposal Concerning the Availability of the Switching Device

5.5.1 A Brief Suitability Appraisal of Power Semiconductor Devices

The main requirements determining the choice of the semiconductor switching device in an eventual implementation of any active-filtering system to an HVDC scheme, are the capability of handling the power level demanded by the application, turn-off control capability and a switching frequency which allows a good fidelity in the synthesization of the voltage-reference signal.

Considering the switching characteristics of a generic power semiconductor device, the ideal switch should have large voltage and current ratings, zero conduction drop, zero leakage current in blocking condition, high temperature and radiation withstand capability, high mean time between failures (MTBF), instant turn-on and turn-off characteristics and economical price [70].

Besides the well known devices like the thyristor, GTO, TRIAC, BJT and power

MOSFET which appeared before 1980, some more recent devices like the IGBT (insulated gate bipolar transistor), SIT (static induction transistor), SITH (static induction thyristor) and MCT (mos-controlled thyristor) have been introduced. The IGBT, being the earlier of these (1983), has its applications somewhat more established, and the others, being still at their early stage of development, Among well established power semiconductor switches, the thyristor and the TRIAC, not being endowed with the controllable turn-off characteristic, are not naturally applicable to PWM inverters. Reference [11] presents a detailed comparison of these devices.

Since none of the power semiconductor switches that could be selected for this application (BJTs, MOSFETs, GTOs and IGBTs) is endowed with symmetric-voltage blocking capability, a diode must be connected in anti-parallel to each switch to avoid the reverse voltage (if it is not already provided in the semiconductor package itself). The anti-parallel diodes help to recharge the rectifier output-capacitor and, therefore, keep the DC voltage constant.

Snubber circuits are also required to limit the rates of rise of current during "turn-on", and the rate of rise of voltage during "turn-off". Another use of snubber circuits is to reduce the power loss that occurs during switching.

Figure 5.6 [71] shows the comparative switching frequency and current and voltage ratings of the well established power semiconductor switches.

The state-of-the-art BJT has a very low forward voltage drop, high current ratings and reasonably good switching frequency capability. However, its need for a comparatively higher power requirement for the gating circuitry together with a high leakage current, precludes its application to active filters for HVDC systems. In a PWM inverter application, one of the most important properties of a power semiconductor device is the switching speed and, consequently, its switching frequency capability. This characteristic has immediate influence on the output performance. This requirement also excludes the use of the GTO. Although power MOSFETs have extremely high switching frequency capability and therefore have been extensively used in active filters at industrial power levels, their power rating is too low for HVDC applications. IGBTs, on the other hand, have a sufficient switching frequency capability and yet a much higher power rating. Therefore, among currently available devices, the IGBT appears to be the most promising one for making it possible to take advantage of

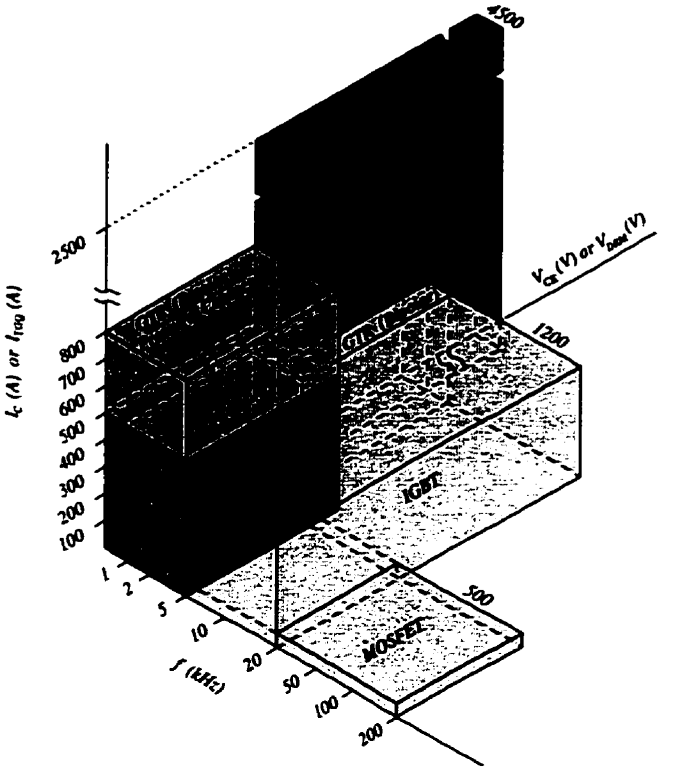

Figure 5.6: Portfolio of currently available power semiconductor devices (extracted from reference [71]).

the high performance of active-filtering techniques in HVDC systems. The general characteristics of the IGBT are highlighted in the next section.

5.5.2 The IGBT

Other commercial names for the IGBT are: MOSIGT (metal oxide semiconductor insulated gate transistor), COMFET (conductivity-modulated FET), GEMFET (gain-modulated FET), IGT (insulated gate transistor) and IGR (insulated gate rectifier). An IGBT is, basically, a hybrid MOS-gated bipolar transistor that combines advantageous input characteristics of a MOSFET (high-input impedance and high speed capabilities) and advantageous output characteristics of a BJT (low saturation voltage characteristics and high power ratings) [72]. Figure 5.7 shows the device symbol for the IGBT and its main characteristics.

Presently commercially available IGBTs, such as from Toshiba, are available at

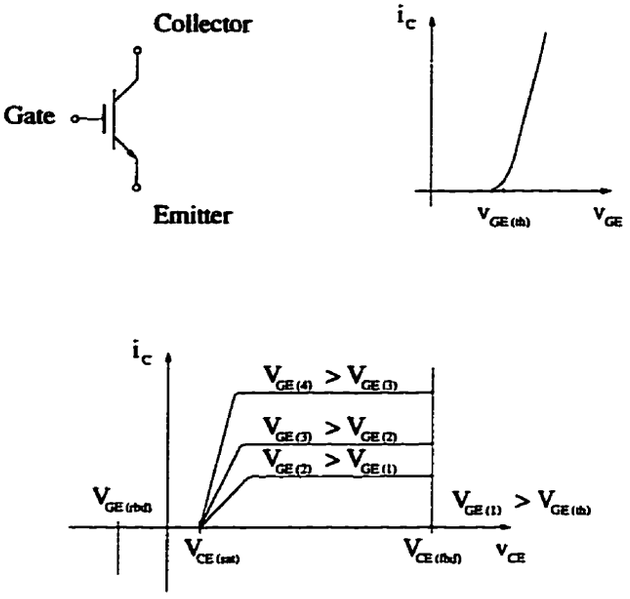

Figure 5.7: IGBT symbol and characteristics.

ratings up to 1600 V/1200 A (non-punch-through-type, NPT) and possess a switching frequency capability of up to 20 kHz (low audible noise) [71]. Such ratings may accommodate HVDC filtering without the need of series or parallel connections of IGBTs in the method proposed in this thesis. Moreover, IGBTs are still under development and IGBTs with power ratings of 3300 V/1200 A have already been announced. The present rate at which improvements are being achieved may soon make IGBTs use in FACTS possible [11, 73].

In practice, the carrier frequency is usually set to one order of magnitude higher than the highest frequency component to be compensated [62]. In this thesis, since harmonics of up to 2940 Hz (49th order harmonic) will be actively filtered, proper reference signal amplification up to this frequency harmonic would require a carrier frequency of at least 30 kHz. This is currently beyond the switching capability of any available device at the required power rating. In maintaining reasonable accuracy with minimum switching loss, the switching frequency has been chosen as 15 kHz. The switching frequency is only around 5 times the highest targeted harmonic of interest (49th), therefore, a high fidelity in the synthesis of the higher-order harmonics of the voltage reference signal should not be expected.

Basic Operation

The IGBT is turned on (collector current flows) by applying a positive voltage from gate to emitter v_{GE} larger than a threshold value $V_{GE(th)}$ (3 - 6 V). The device is turned off by simply reducing the gate voltage to zero or by reversing its polarity, and the drive circuit requires a small power requirement when compared to the other switching devices. The collector current i_C is linearly dependent on v_{GE} according to its transconductance value g_{fs}, and, therefore, the IGBT can be used as a linear amplifier. In switching applications, however, as is the case in this thesis, the device must saturate. The collector-to-emitter saturation voltage ($V_{CE(sat)}$) decreases with an increase in magnitude of i_C. That is, for the lowest values of "on" state voltage, v_{GE} should be much greater than $V_{GE(th)}$ (generally around +15 V). Due to its high input impedance, the IGBT demands minimal gate drive power requirements. The IGBT is an unsymmetrical device, and its reverse blocking capability varies from 10 to 20 V. This characteristic requires the use of the anti-parallel diodes shown in Figure 5.4, which, due to the fast switching required by the application, must be of the fast-recovery type.

Short-Circuit Handling Capability

Both the FBSOA and RBSOA (forward- and reverse-biased safe operating areas) of the IGBT are thermally limited by the junction temperature T_j. The RBSOA, in particular, has a rectangular shape which is limited by the breakdown voltage and the short-circuit current amplitude of the IGBT. These characteristics are very important since it endows the IGBT with short-circuit controlling characteristics. That is, even at high dv/dt and di/dt values, both the turn-on of a transistor to a short-circuit and the application of a short-circuit to a saturated IGBT (the latter one being more critical) may be handled by means of its linear characteristic (high-dissipation active mode). This way, it is possible to turn the IGBT off, without damage, at any instant regardless of current amplitude. Another good characteristic of the IGBT is that the short-circuit current has a negative temperature coefficient, i.e., the short-circuit current drops as the junction temperature of the transistor increases. This means temperature stability during this overload. In fact, IGBTs can withstand full voltage and current ratings for some microseconds. The short circuit strength capability of

the IGBT causes its protective and auxiliary power supply to be less costly.

Losses

Power losses in the IGBT consist of drive losses, conduction losses, off-state losses, and switching losses. Drive losses are inherently negligible in IGBTs. In switching applications, conduction losses are proportional to the duty cycle $D = T_{on}/T_{switching}$, off-state losses are proportional to $1-D$ and, if the ambient temperature extremes are limited, off-state losses are generally insignificant. The switching losses are directly proportional to the switching frequency and are independent of duty cycle or pulse width. In low-frequency applications, where the total switching times are much less than the period, switching losses are also generally negligible.

Although the rise time of the IGBT does not depend on the temperature, the IGBT has a positive temperature coefficient associated with its fall time (approximately 0.27%/°C [72]. A characteristic of the IGBT, sometimes useful, is the ability it provides for controlling the fall time of the collector current. Figure 5.8 shows the characteristic waveform of the current of an IGBT during turn off.

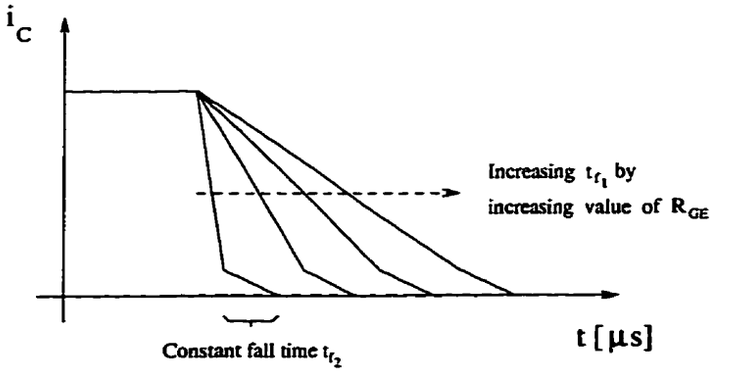

Figure 5.8: Controllability of the fall-time of the IGBT collector current.

The initial fall time (t_{f_1}) can be corrected if a resistor R_{GE} (in fact a thermistor) is connected between the gate and the emitter with a compensating temperature coefficient. This resistor, together with the input capacitance of the gate terminal (a MOSFET characteristic) determines the initial fall time. The final fall time (t_{f_2}) is characteristic to a particular device and is not controllable (a BJT characteristic). Since the turn-off losses depend on t_{f_1} and t_{f_2}, the possibility of controlling t_{f_1} by

means of resistor R_{GE} is a definite advantage. As already mentioned, the usual way to minimize the device over-heating due to switching and protect it from damage, is to install snubber circuits. By delaying the rate of change of the current and/or voltage across the semiconductor switch during switchings, these waveforms are altered so that the product $v_{CE}i_C$ is reduced to values closer to zero [72].

Paralleling of IGBTs

In order to achieve the ambitious goal of actively compensating all the harmonics of an HVDC terminal, depending on the voltage and current levels involved, series and/or parallel connection of IGBTs may have to be considered. The series connection is problematic because IGBTs suffer overvoltage stresses due to different individual switching times. However, nominal voltage matching is preferably solved by a matching transformer with a suitable turns-ratio.

In case the paralleling of IGBTs is required, the main concerns should be the turn-on and turn-off times (more critical as the switching frequency increases) and on-state current balancing. In paralleling IGBTs the characteristics that should be matched are the gate-to-emitter threshold voltage ($V_{GE(th)}$) and the transconductance (g_{fs}). An excellent characteristic of the IGBT (NPT-type) is that, at on-state, for currents greater than a certain value (around 70% of the rated current), it exhibits a positive temperature coefficient of on-resistance and contributes to a stabilization of the current sharing between paralleled IGBTs.

As frequency increases, package inductances and lead resistances can cause switching time unbalances. In this case, all connecting leads should be as short as possible to minimize the resistance effect, and the physical layout of the paralleling should be geometrically accomplished so as to minimize the inductance effect. Use of appropriate individual gate series resistors also correct switching unbalances.

The possibility of having to use paralleled IGBTs should not pose greater problems, since, in fact, the increases in their current rating capabilities by manufacturers have been achieved by internally paralleling IGBT chips.

5.6 The Active-Source Inverter Output Filter

Due to the switching action, the voltage output of the PWM inverter will include high-frequency switching noise. Therefore, an output passive filter is incorporated in the circuit to prevent the corresponding currents these voltage harmonics would create from being injected into the AC system.

The most common applications of PWM inverters deal with the supply of only one single (fundamental) frequency. In this case, the largest harmonics (of order several times higher than the fundamental frequency) are those of the carrier frequency and its multiples [74]. The fundamental component and its multiples are also present in the spectrum frequency around these carrier-frequency harmonics (as side-bands). In the active-filter case, the active source must supply a wide range of voltage harmonic frequencies and, therefore, the frequency spectrum around the switching harmonics is somewhat less predictable.

The source of the harmonics to be passively filtered by the output filter is the active source of the active filter (PWM amplifier), and its load is the series connection of the path impedance and the parallel connection of the AC system and the new shunt capacitor bank of the HVDC terminal. This circuit is shown in Figure 5.9. Note that the voltage sources of the AC system have been short-circuited and the current sources representing the HVDC terminal have been open-circuited (excluded).

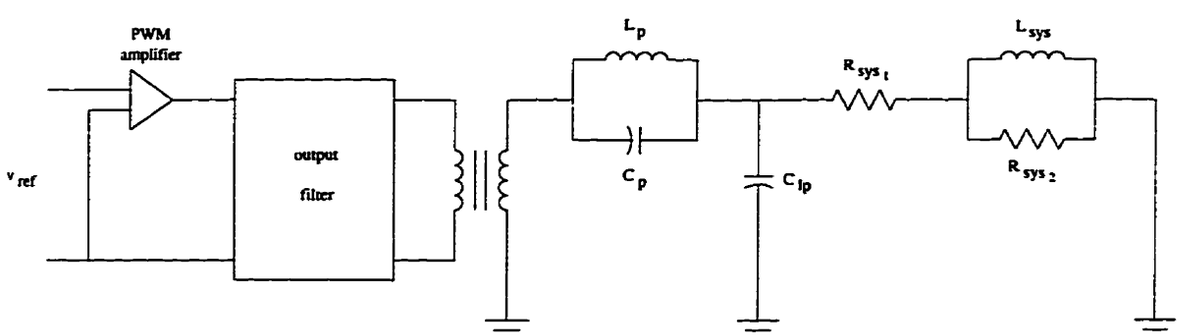

Figure 5.9: Position of the output filter relative to the active source (PWM amplifier) and its load.

The output filter must provide the harmonic source (active source) and its load with the maximum impedance-mismatch possible. This mismatch is obtained by making use of the inherent frequency characteristics of capacitors and inductors. That

is, the impedance of a capacitor decreases with frequency and that of an inductor increases with frequency. Their characteristics determine that capacitors must be connected in parallel to the harmonic source and its load, and that inductors must be connected in series (between) with them.

It is intuitive that the shunt capacitor impedance, if used by itself, must be much smaller than the parallel combination of the source and load impedances to effectively divert the unwanted harmonic current from the load. The same way, as a dual of the shunt capacitor, it is readily apparent that the impedance of a series inductor, if used by itself, must be much larger than the series combination of the source and load impedances to effectively provide an open circuit to the unwanted harmonic voltages from the load. By placing these elements close to the impedances to be mismatched, the attenuation due to both types of ideal elements will efficiently increase with the frequency. In fact, the respective contributions in the real devices to the total attenuation will be limited by parasitic inductances in the capacitors and parasitic capacitances in the inductors. As a consequence, for frequencies above their intrinsic resonance frequencies, their behavior will be those of the their respective parasitic elements.

At this point, considering that the impedance of the active source is expected to be negligible, it is clear that the efficiency of the filter depends, basically, on the active-source load, and, therefore, its frequency characteristics must be known. It can be shown that the maximum power transfer occurs when the source impedance is matched to the load impedance. This should be expected from basic circuit analysis. Since, in the filtering case, the opposite behavior is desired, the best mismatch possible must be sought. The impedance frequency characteristics of the active-source load, as seen from the output filter, is as shown in Figure 5.10. The low impedance characteristic of the load at the active filter frequency range is basically determined by the HVDC shunt capacitor bank and the path-impedance capacitor.

The traditional topology of output filters in single-frequency inverters is the single LC filter cell shown in Figure 5.11. The shunt capacitor, presenting a much lower impedance to high harmonics than the usually inductive loads do, diverts the harmonic currents from the latter. The inductor, in series with the inverter bridge, isolates the low-impedance source from the low-impedance resulting from the parallel connection of the shunt capacitor and the load. This scheme, by itself, has also been

used in all proposals of active filters, where, at most, two HVDC current harmonics were actively filtered and the switching frequency was several times higher than these harmonic frequencies. The chosen switching frequency, being just approximately 5 times the highest HVDC harmonic being actively filtered, makes this mismatch harder to be achieved with the usual LC-cells solutions.

In general, when an LC filter sufficiently attenuates the lowest harmonic present in the output of an inverter, the higher harmonics are automatically adequately reduced to a permissible level. This is because a practical filter is usually designed so that its resonance frequency f_{lp} is below the lowest harmonic to be attenuated. The lower the

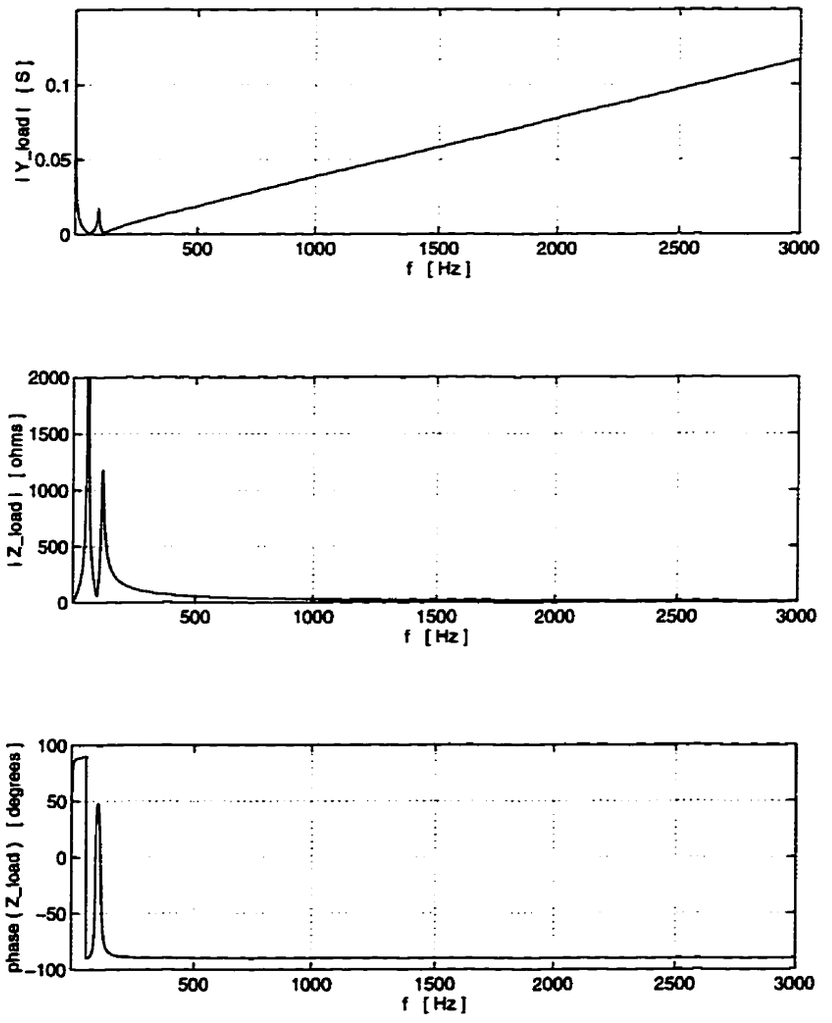

Figure 5.10: Frequency characteristics of the load of the active-source output filter.

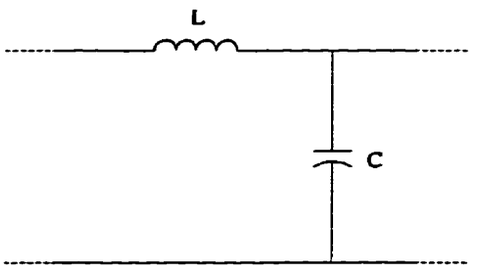

Figure 5.11: LC output filter.

impedance of the source and the higher the impedance of the load at the harmonic frequencies, the better the filter performance.

Two important characteristics of the active source that are affected by the choices of the values of C_{lp} and L_{lp} are the kVA rating of the inverter and its regulation. A large value of the capacitance and a small value of the inductance yields a very good regulation but increases the inverter current to values comparable to the load current. A large value of the inductance and a small value of the capacitance, on the other hand, although it just slightly increases the inverter current, causes an unacceptable voltage drop across the series element.

Both cases will adversely affect the kVA rating of the active source. Therefore, a trade-off is required and there must be a prime consideration for low insertion loss. Therefore, their values, besides the efficiency of the filtering performance, should aim at the minimization of the kVA requirements of the active source. Also, in agreement with this necessity, the inductor must have a high quality factor (low resistance) and the capacitor must have a low value of equivalent series resistance (ESR). Depending on the voltage and current ratings of the semiconductor switching device to be used, increased voltage may prove more desirable than increased current or vice-versa.

The output-filter selectivity required by the application at hand is very severe. This condition is imposed by the large difference between very high harmonic amplitude at the switching frequency and the low amplitude of the highest harmonics of the HVDC terminal to be actively filtered, within a relatively narrow frequency range. If it were not for the high degree of selectivity and the low kVA rating required by the application, just a first-order series inductor would suffice for this source-load impedance combination. The consideration of a commonly-used second-order low-pass LC filter (LC cell) by itself is also discarded. Presenting an extremely low impedance for

the switching frequency harmonics, the load could only be short-circuited by an extremely large shunt capacitor at the output filter. This would be prohibitive due to the large charging demand on the active source. A third order output LCL filter satisfies the mismatch requirement posed by the source and load impedances. However, the required selectivity would require the output filter inductances to be very high. This would imply in the need for a large increase of the required voltage at the active-source rectifier due to the consequent poor regulation.

The adopted solution to the filtering problem is the combined use of an ordinary second-order low-pass LC filter and a block LC filter tuned at the switching frequency, resulting in a fourth-order output filter. The complete output filter can be seen in Figure 5.12

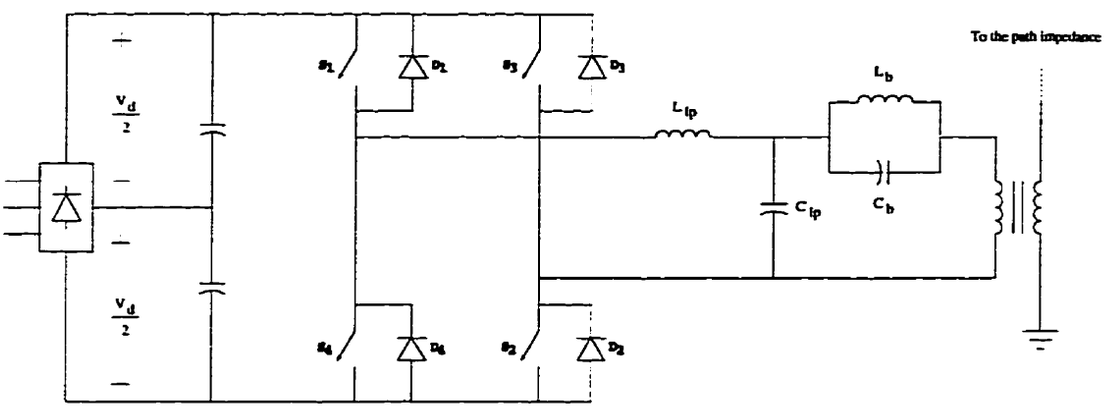

Figure 5.12: Complete output filter of the active source.

The block LC filter presents a very high impedance at the switching frequency against which the the capacitor of the low-pass section can better perform the diversion action. The infinite quality factor and aging deviations of the block filter should not pose problems since the switching frequency of the carrier waveform could be controlled to automatically, and exactly, match the resonance frequency fixed by the block filter.

The design of the block and low-pass sections can be done fairly independently. The main requirement imposed on the block filter is not to adversely affect the regulation of the active source in the range of frequencies to be actively filtered. Therefore the path impedance has been taken as a reference. The criterion adopted is that

the resulting equivalent impedance of the switching-frequency block filter should not significantly increase the impedance of the path impedance at the first two HVDC characteristic harmonic frequencies (660 Hz and 780 Hz). The resulting values are 0.3511 μF and 0.3207 mH. Figure 5.13 shows the frequency characteristics of the switching-frequency block filter, where the parallel resonance can be seen at 15 kHz. Figure 5.14, focusing on the active-filtering frequency range, shows both the block and the path impedances in the same graph for comparison. It can be seen that the impedances of the block filter at the highest characteristic harmonics are of the same order as those of the path impedance. Since the amplitude of these characteristic harmonics are relatively small when compared to the lower order ones, and the impedance of the total circuit is considerably lower at these frequencies, the increase in the voltage requirements of the active source are not significant.

Further to the above considerations, the determination of the values of the capacitance C_{lp} and inductance L_{lp} of the low-pass section of the output filter of the active source should take into account the natural frequencies of oscillation of the complete system. The switching operation of the PWM inverter of the active source excites all the modes of the circuit determined by the load, the output filter and the impedance of the active source. Since the active source is expected to have a negligible impedance, the equivalent circuit, obtained by short-circuiting the active source and disregarding the unitary matching transformer, becomes the one shown in Figure 5.15.

This circuit presents a series connection of 4 parallel LC tuned filters with negligible damping: The AC system and the HVDC shunt capacitor bank at the 2nd harmonic frequency, the path impedance at the fundamental frequency, the block-filter section of the output filter at 15 kHz and the low-pass filter section. This arrangement of parallel resonances also created two series resonance frequencies that could give rise to active-filter control instabilities. The final values are $C_{lp} = 4$ μF and $L_{lp} = 0.24$ mH, which yields $f_{lp} = 5136$ Hz as the resonance frequency of the low-pass section of the output filter. These values have been determined so that the natural frequency occurring within the range of active filtering was placed half way between the 37th and the 47th HVDC harmonics (2520 Hz). This had the objective of reducing the risk of excitation of the natural series resonance of the circuit.

Although damping measures could have been taken at the low-pass filter section, it

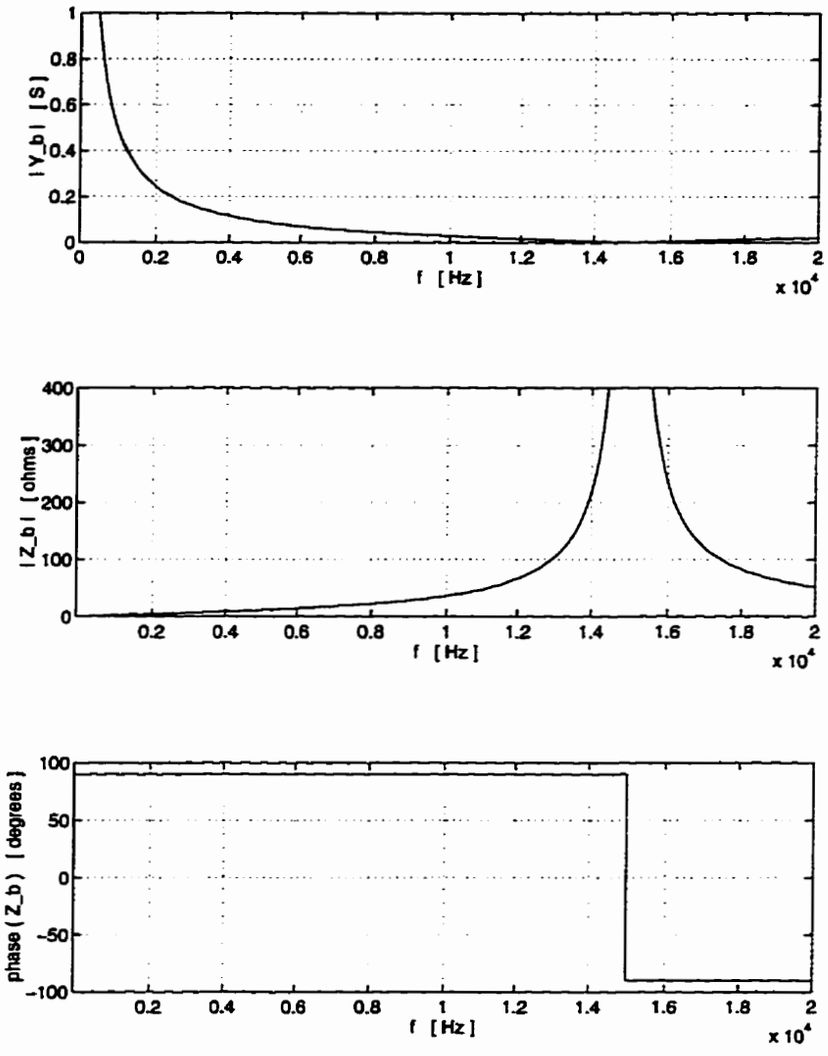

Figure 5.13: Frequency characteristics of the switching-frequency block filter.

is believed that the fact of f_{lp} being well above the highest HVDC harmonic frequency, added to the existence of enough damping in a real system, would be enough to avoid control instabilities due to this parallel resonance. The frequency characteristics of the final circuit is shown in Figure 5.16

As a final result, the compound output filter provides a very effective output filter for the switching frequency harmonics with a moderate rate of roll-off for the remaining undesirable harmonic frequencies, determined by reasonably-sized low-pass filter section elements. Naturally, other main considerations should concern the filter cost, size and weight.

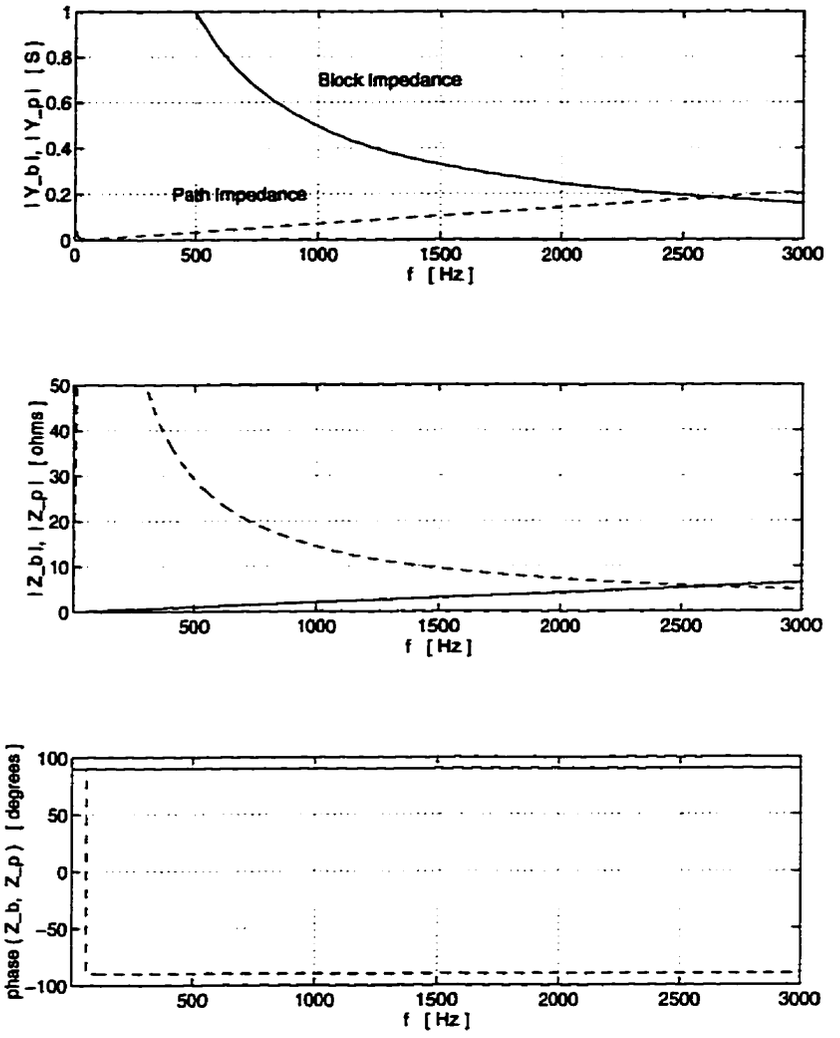

Figure 5.14: Frequency characteristics of the switching-frequency block filter and of the proposed path impedance (— block impedance, --- path-impedance).

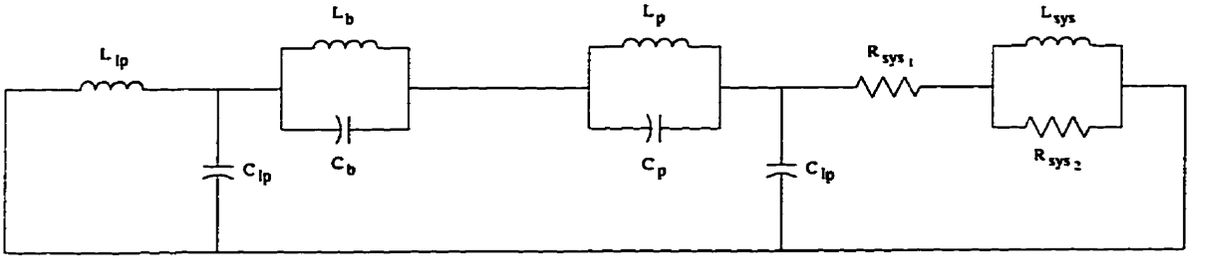

Figure 5.15: Equivalent circuit of the system.

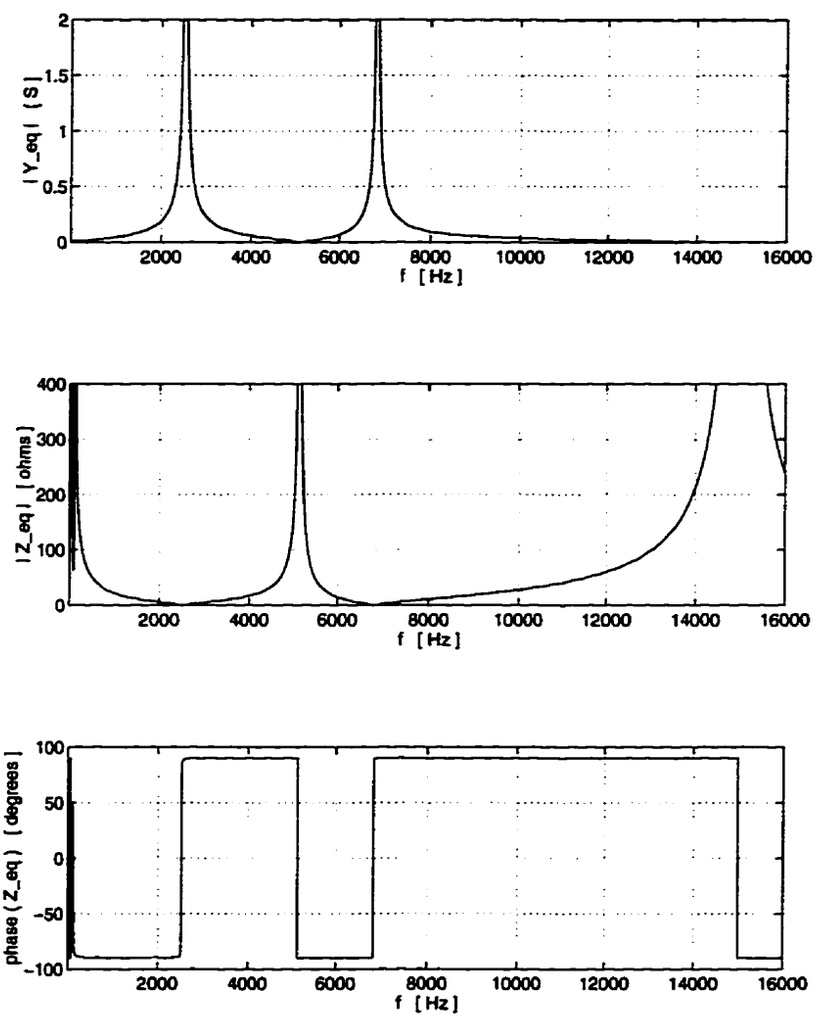

Figure 5.16: Frequency characteristics of the equivalent circuit of the system.

Chapter 6

The Active-Filter Control

6.1 Introduction

In control theory, the two most basic classes of control problems are known as the "servomechanism" and the "regulator" problems. The servomechanism problem is that of designing a control so that the output $\mathbf{y}(t)$ of a system tracks a reference signal $\tilde{\mathbf{y}}(t)$. The regulator problem is a special case of the servomechanism one, where the reference signal to be tracked is identically zero ($\tilde{\mathbf{y}}(t) = \mathbf{0}$), and the task is that of taking an initial state of the plant (due, for example, to a disturbance) to zero. In the case of the active filter, since its active source acts as a voltage source in the presence of the AC/DC system, it is desired that its output tracks the harmonic content of the HVDC converter current that is not diverted from the AC system by the path impedance. The problem at hand is that of a servomechanism design, where the output $\mathbf{y}(t)$ is the current injected by the active filter into the power system, the reference signal $\tilde{\mathbf{y}}(t)$ is the measured harmonic content of the HVDC converter current to be actively filtered, and the control signal $\mathbf{u}(t)$ is the voltage output of the PWM amplifier (or better: the PWM-amplifier harmonic-free reference v_{ref}. In the control systems theory, the PWM amplifier plays the role of the actuator.

There are two basic currents of analysis and design procedure in control theory: (i) classical control and (ii) modern control.

The classical control is usually most successfully applied to linear, time-invariant,

low order, single-input single-output (SISO) systems, and the description of the problem is generally in terms of the system's transfer function. The first concern of this approach must be to stabilize the closed-loop system formed when the output signal (and/or its derivatives) is fedback and used to generate the control signal $\mathbf{u}(t)$. Only then, once the closed loop system has been stabilized, the transient response, bandwidth, and the steady-state error characteristics are tackled. The methods used in the classical approach are basically analytical (Laplace transform, Routh test), graphical (root loci, Nyquist plots, Nichols charts) and, most of all, empirically based knowledge. For high-order systems, as is the case at hand, the designer's ingenuity is indispensable in achieving a satisfactory design.

The modern control theory offers a less "ad-hoc" approach, and the design process is less dependent on practical experience. This reduces the load on the ingenuity of the designer in favor of his or her ability with mathematical tools and widens the classes of problems that can be tackled. The description of the problem is generally in terms of the system's state and output equations.

A category of modern control theory is known as "optimal control" [75–77]. It provides the best possible system of a particular type [78]. Desirable characteristics such as stability, bandwidth and compliance to classical control associated constraints are inherently obtained. If the plant and controllers are assumed linear, the optimal control system is called linear. This is the type of control which has been designed for the active filter and is based mainly based on [76, 79, 80]. The optimal control system will add further desirable characteristics to the final overall system. The main characteristics achieved with the application of a linear optimal control are

- The resulting system is stable, irrespective of the stability of the plant.
- Good gain and phase margins.
- For a broad range of conditions, the resulting control system is equivalent to the reduction of sensitivity to plant parameter variations.
- Very good tolerance to nonlinearities and may be applied to nonlinear systems operating on a small signal basis.
- The solutions are easily computed.

- Provides a framework for the unified study of the control problem studied via classical methods.
- Extends the class of systems for which control designs may be achieved.

6.2 The System's Equations

The circuit diagram relative to the active-filter system (the plant) is shown in Figure 6.1.

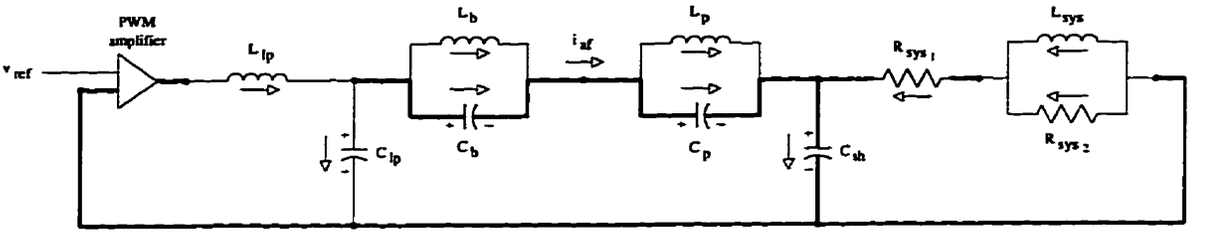

Figure 6.1: Circuit diagram representing the plant, having the active source as input.

This is basically the same circuit presented in Figure 5.12, in Chapter 5, with the secondary-side circuit reflected to the primary side of the matching transformer (unity turns ratio). It is worth noting that the design of the control system ignores the existence of the fundamental components that exist in the actual AC/DC system. This is backed by the fundamental-frequency isolation provided by the path impedance. The AC system is considered free of harmonic sources and the exclusion of the harmonic current source that represents the HVDC converter terminal from the circuit is in accordance with the superposition theorem.

The plant will be represented in terms of its state variables [81–83]. This circuit consists of four capacitors, four inductors and two resistors. The state variables have been chosen to be the voltages across capacitors and currents through inductors. Since any one of the capacitor voltages can be determined from the other three, the order of the circuit becomes the seventh order. Following the basic procedure and terminology for the derivation of the state equations of an electric circuit, the branches and connections with thicker lines in Figure 6.1 have been chosen as the "twigs" that constitute one of the possible "trees" of this circuit. All the other branches are "links" that connect "nodes" of the tree. The derivation of the dynamic and output

equations of the plant follow the order of the numbers associated with the branches whose elements are of the energy-storing type. According to the conventions of voltage polarities and current directions chosen, the state vector of the plant is determined as

$$\mathbf{x} \equiv \begin{bmatrix} x_1 \\ x_2 \\ x_3 \\ x_4 \\ x_5 \\ x_6 \\ x_7 \end{bmatrix} = \begin{bmatrix} v_{C_{sh}} \\ v_{C_p} \\ v_{C_b} \\ i_{L_{sys}} \\ i_{L_p} \\ i_{L_b} \\ i_{L_{lp}} \end{bmatrix}. \tag{6.1}$$

The input $\mathbf{u}(t) \in \mathcal{R}$ is the voltage reference for the PWM amplifier v_{ref} and the output $\mathbf{y}(t) \in \mathcal{R}$ is the current i_{af_h} injected by the active filter into the AC system. The dynamic and output equations become

$$\dot{\mathbf{x}}(t) = \mathbf{A}_{plant}\mathbf{x}(t) + \mathbf{B}_{plant}\mathbf{u}(t) \tag{6.2}$$

$$\mathbf{y}(t) = \mathbf{C}_{plant}\mathbf{x}(t) + \mathbf{D}_{plant}\mathbf{u}(t) \tag{6.3}$$

where

$$\mathbf{A}_{plant} = \begin{bmatrix} -32.5 & 0.0 & 0.0 & 70139.6 & 1979.4 & 62771.8 & 5509.7 \\ 0.9 & 0.0 & 0.0 & -1976.0 & -87340.5 & 78473.2 & 6887.9 \\ 29.0 & 0.0 & 0.0 & -62663.4 & 78473.2 & -359674.8 & 218429.9 \\ -7.9 & 0.0 & 0.0 & -29.7 & 0.0 & 0.0 & 0.0 \\ 0.0 & 1.6 & 0.0 & 0.0 & 0.0 & 0.0 & 0.0 \\ 0.0 & 0.0 & 3118.7 & 0.0 & 0.0 & 0.0 & 0.0 \\ -4166.7 & -4166.7 & -4166.7 & 0.0 & 0.0 & 0.0 & 0.0 \end{bmatrix}$$

$$\mathbf{B}_{plant} = \begin{bmatrix} 0.0 \\ 0.0 \\ 0.0 \\ 0.0 \\ 0.0 \\ 0.0 \\ 4166.7 \end{bmatrix}$$

$$\mathbf{C}_{plant} = \begin{bmatrix} 0.000010 & 0.000000 & 0.000000 & -0.022000 & 0.027552 & 0.873719 & 0.076690 \end{bmatrix}$$

$$\mathbf{D}_{plant} = \begin{bmatrix} 0.0 \end{bmatrix}.$$

The poles of matrix $\mathbf{A}_{plant}$ are at

$$\sigma_{plant} = \begin{bmatrix} -0.7 + j42816.0 \\ -0.7 - j42816.0 \\ -6.3 + j15829.9 \\ -6.3 - j15829.9 \\ -21.5 + j00615.6 \\ -21.5 - j00615.6 \\ -4.9 + j00000.0 \end{bmatrix}. \tag{6.4}$$

Very small real parts confirm the very lightly damped nature (although obviously stable) of the circuit, and the division of the imaginary parts by 2π provides the frequencies, in hertz, at which the plant's modes oscillate (or resonate). These frequencies are easily identifiable in Figure 5.16 in Chapter 5 as the frequencies at which the impedances assume the zero value.

Matrix analysis shows that this plant is completely controllable and completely observable [84]. The complete controllability implies that it is possible, by means of bounded variables and gains, to take any state variable of the plant from an initial value x_i at time t_i to a final value x_f at time t_f in any finite period of time $\Delta t = t_f - t_i$. The complete observability implies that it is possible to identify the contribution of each one of the states to the output.

6.3 The Linear Optimal-Control Design

The design approach is that described by [79]. This approach is based on an initial setting up of the problem as if it were that of a regulator type instead of a servomechanism one. In later steps, the regulator problem will be transformed into one of the servomechanism type, solved, and its results analyzed in light of the transformation performed. Having this in mind, the design method for the regulator problem is now presented.

6.3.1 The Regulator Problem

Considering the state-space representation of a generic system

$$\dot{\mathbf{x}}(t) = \mathbf{A}\mathbf{x}(t) + \mathbf{B}\mathbf{u}(t) \tag{6.5}$$

$$\mathbf{y}(t) = \mathbf{C}\mathbf{x}(t) + \mathbf{D}\mathbf{u}(t), \tag{6.6}$$

the desired control signal $\mathbf{u}(t)$ is a nondynamic function, i.e., an instantaneous function (no derivatives or integrals), of the states $\mathbf{x}(t)$, which are all assumed, at this point, to be available. The control law will be of the form

$$\mathbf{u}(t) \equiv -\mathbf{K}\mathbf{x}(t) \tag{6.7}$$

and the corresponding control arrangement is shown in Figure 6.2.

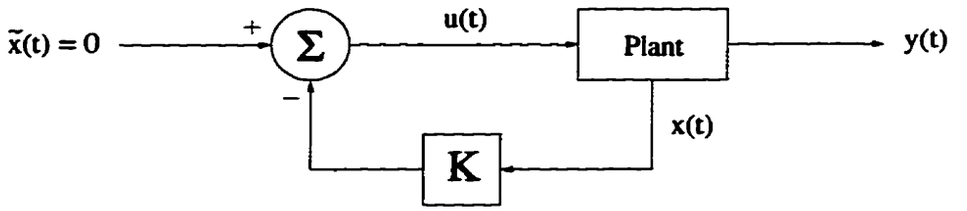

Figure 6.2: Basic block diagram of the regulator problem.

The objective is to perform the control action (take the states to zero) with the least possible amount of control and state energies. With this in mind, the following quadratic performance index is used:

$$V(\mathbf{x}(t_i), \mathbf{u}(\cdot), t_i) = \int_{t_i}^{t_f} [\mathbf{x}(t)^T \mathbf{Q}\mathbf{x}(t) + \mathbf{u}(t)^T \mathbf{R}\mathbf{u}(t)]dt. \tag{6.8}$$

$\mathbf{Q}$ is a symmetric, nonnegative definite, matrix and it prevents the parcel referent to the states energy from being negative. This parcel is allowed to be zero, and, actually, should eventually be zero. $\mathbf{R}$ is a symmetric, positive definite, matrix (in this case, $\mathbf{R} \in \mathcal{R}$) and, therefore, constrains the part corresponding to the control energy to be always positive. Minimizing $V(\mathbf{x}(t_i), \mathbf{u}(\cdot), t_i)$ ensures that $\mathbf{x}(t)$ and $\mathbf{u}(t)$ will be kept small along the time interval $[t_i, t_f]$. Therefore, the solution consists of finding an optimal control law $\mathbf{u}^*(t), t \in [t_i, t_f]$ that minimizes $V(\mathbf{x}(t_i), \mathbf{u}(\cdot), t_i)$ where $\mathbf{x}(t)$ and $\mathbf{u}(t)$ are subjected to the dynamic equation of the plant. The Hamilton-Jacobi

theory [84,85] applied to the regulator problem shows that the optimal performance index has the form

$$V^*(\mathbf{x}(t),t) = \mathbf{x}(t)^T\mathbf{P}(t)\mathbf{x}(t), \tag{6.9}$$

where $\mathbf{P}(t)$ satisfies the differential Riccati equation

$$\frac{d\mathbf{P}(t)}{dt} = \mathbf{P}(t)\mathbf{A} + \mathbf{A}^T\mathbf{P}(t) - \mathbf{P}(t)\mathbf{B}\mathbf{R}^{-1}\mathbf{B}^T\mathbf{P}(t) + \mathbf{Q}, \qquad \mathbf{P}(t_f) = 0. \tag{6.10}$$

The optimal control is

$$\mathbf{u}^*(t) = -\mathbf{R}^{-1}\mathbf{B}^T\mathbf{P}(t)\mathbf{x}(t), \tag{6.11}$$

which is indeed the desired linear feedback law, where

$$\mathbf{K}(t) = \mathbf{R}^{-1}\mathbf{B}^T\mathbf{P}(t). \tag{6.12}$$

Now, since it is interesting that the control action be optimized up to the point when the system reaches steady state, t_f should be made as large as possible, i.e., $t_f \to \infty$. In the case where t_f is finite, $V(\mathbf{x}(t_i),\mathbf{u}(\cdot),t_i)$ is always finite. In the case where $t_f \to \infty$, the requirement that the system is completely controllable is sufficient to ensure that $V(\mathbf{x}(t_i),\mathbf{u}(\cdot),t_i)$ is also finite. Then, if $\mathbf{P}(t,t_i)$ is the solution to the finite case with $\mathbf{P}(t_f,t_f) = \mathbf{0}$, then the constant matrix $\bar{\mathbf{P}} = \lim_{t_f\to\infty}\mathbf{P}(t,t_f)$ (or $\bar{\mathbf{P}} = \lim_{t\to-\infty}\mathbf{P}(t,t_f)$) is the steady-state solution. Moreover, $\bar{\mathbf{P}}$ is also the solution to the algebraic Riccati equation:

$$\mathbf{P}(t)\mathbf{A} + \mathbf{A}^T\mathbf{P}(t) - \mathbf{P}(t)\mathbf{B}\mathbf{R}^{-1}\mathbf{B}^T\mathbf{P}(t) + \mathbf{Q} = \mathbf{0}. \tag{6.13}$$

The optimal performance index has the form

$$V^*(\mathbf{x}(t),t) = \mathbf{x}(t)^T\bar{\mathbf{P}}\mathbf{x}(t). \tag{6.14}$$

The optimal control will be

$$\mathbf{u}^*(t) = -\mathbf{R}^{-1}\mathbf{B}^T\bar{\mathbf{P}}\mathbf{x}(t) \tag{6.15}$$

and the feedback control matrix is

$$\mathbf{K} = \mathbf{R}^{-1}\mathbf{B}^T\bar{\mathbf{P}}. \tag{6.16}$$

The closed loop system is therefore (recall that $\tilde{y}(t) = 0$)

$$\dot{\mathbf{x}}(t) = (\mathbf{A} - \mathbf{BK})\mathbf{x}(t). \tag{6.17}$$

The requirement that the performance-index parcel that is responsible for the energies of the states observes all of the states is sufficient to guarantee that the closed loop system is stable. If the plant is completely observable (which is the case), all the state trajectories are identifiable at the output. This fact can be used favorably if $\mathbf{Q}$ is chosen as $\mathbf{Q} = \mathbf{C}\mathbf{C}^T$. This way, all the trajectories will be represented in the integrand term corresponding to the energy states in the performance index. This will cause $\bar{\mathbf{P}}$ to be positive definite and $V^*(\mathbf{x}(t), t)$ to be a Lyapunov function [86,87]. This choice of matrix $\mathbf{Q}$ has the extra advantage of assigning weights to the states which are proportional to their contribution to the output.

6.3.2 Application of the Internal-Model Principle

The principle of the Internal Model [88, 89] states that, in a regulator problem, the feedback loop must have the same poles as those of the disturbance signal to be neutralized. This principle can be equally applied to servomechanism problems [90, 91]. Therefore, the plant to be controlled must have the same poles as those of the reference signal to be tracked by the output. This signal, if continuous, can be represented as the output of an auxiliary and fictitious system, with no input, and with suitably chosen initial values for its state variables. This so called "reference system" has the form

$$\dot{\mathbf{x}}_{ref}(t) = \mathbf{A}_{ref}\mathbf{x}_{ref}(t), \qquad \mathbf{x}_{ref}(t_i) \tag{6.18}$$

$$\tilde{\mathbf{y}}(t) = \mathbf{C}_{ref}\mathbf{x}_{ref}(t). \tag{6.19}$$

The reference signal $\tilde{\mathbf{y}}(t)$ is the harmonic content of the HVDC converter being drawn from the AC system and is to be actively filtered. The reference signal being the superposition of several harmonic frequencies, with no decaying or increasing exponentials, is theoretically defined as a marginally stable signal. The harmonic frequencies at which the reference signal oscillates are determined by complex conjugate poles with no real parts. Therefore, each harmonic frequency f_h of order h must be represented by a pair of purely imaginary complex conjugate poles $\sigma_h^+ = +j2\pi f_h$ and

$\sigma_h^- = -j2\pi f_h$. It can be checked that matrices $\mathbf{A}_{ref_h}$ and $\mathbf{C}_{ref_h}$, together with the initial state $\mathbf{x}_{ref_h}(t_i)$, given by

$$\mathbf{A}_{ref_h} = \begin{bmatrix} 0 & \sigma_h^+ \\ \sigma_h^- & 0 \end{bmatrix}, \qquad \mathbf{x}_{ref_h}(t_i) = \begin{bmatrix} 1 \\ 0 \end{bmatrix} \tag{6.20}$$

$$\mathbf{C}_{ref_h} = \begin{bmatrix} a_h & b_h \end{bmatrix}, \tag{6.21}$$

where a_h and b_h are the Fourier coefficients of the harmonic component in question, generate the harmonic component of order h. That is, they satisfy

$$\tilde{\mathbf{y}}_h(t) = a_h \cos(2\pi f_h t) + b_h \sin(2\pi f_h t). \tag{6.22}$$

Since the total harmonic content is the superposition of all individual harmonics, the matrices of the system representing the complete reference signal $\tilde{\mathbf{y}}(t)$ have the following forms:

$$\mathbf{A}_{ref} = \begin{bmatrix} \mathbf{A}_{ref_1} & 0 & \cdots & 0 \\ 0 & \mathbf{A}_{ref_2} & \cdots & 0 \\ \vdots & \vdots & \ddots & \vdots \\ 0 & 0 & \cdots & \mathbf{A}_{ref_{h_{max}}} \end{bmatrix}, \tag{6.23}$$

$$\mathbf{C}_{ref} = \begin{bmatrix} \mathbf{C}_{ref_1} & \mathbf{C}_{ref_2} & \cdots & \mathbf{C}_{ref_{h_{max}}} \end{bmatrix}, \tag{6.24}$$

$$\mathbf{x}_{ref} = \begin{bmatrix} \mathbf{x}_{ref_1} \\ \mathbf{x}_{ref_2} \\ \vdots \\ \mathbf{x}_{ref_{h_{max}}} \end{bmatrix}. \tag{6.25}$$

Although the amplitude and phase of the characteristic harmonic currents demanded by the HVDC converter terminal depend on the operating point, the characteristic harmonic frequencies do not change. That is, their characteristic harmonic frequency orders always satisfy

$$h = 12k \pm 1, \qquad \text{for } k = 1, 2, 3, \ldots .$$

In this thesis, however, the plant does not present any poles at frequencies of the characteristic reference signal. In this case, the Internal-Model Principle could have

been satisfied in two ways. The first would be to associate the plant with an auxiliary system with the desired poles in a series (or tandem) connection. This is the principle behind the Repetitive Control approach [90,91]. The second way would be to modify the positions of the plant's poles in the s plane by means of state feedback (pole-placement technique) [92]. The second option is usually preferred to the first for it does not necessarily increase the order of the resulting system. In the case at hand, the plant is a system of the seventh order and the reference signal, considering all the eight characteristic harmonics until the forty-ninth, is of the sixteenth order. This means that it is necessary to make use of both ways to satisfy the Internal Model Principle. Therefore, the six poles of any three of the harmonic frequencies can be built into the plant by means of a state feedback gain matrix $\mathbf{K}_{fb}$. Obviously, the harmonic frequencies whose poles are chosen to be embedded into the plant are those that demand the state feedback gain matrix to have reasonably sized entries. The remaining ten poles of the reference signal are placed in the auxiliary system representing the corresponding harmonic components in series with the modified plant. The modified plant is represented by

$$\dot{\mathbf{x}}(t) = \mathbf{A}_{mod}\mathbf{x}(t) + \mathbf{B}_{mod}\mathbf{u}_{ref_{ser}}(t) \tag{6.26}$$

$$\mathbf{y}(t) = \mathbf{C}_{mod}\mathbf{x}(t) + \mathbf{D}_{mod}\mathbf{u}_{ref_{ser}}(t) \tag{6.27}$$

where

$$\mathbf{A}_{mod} = \mathbf{A}_{plant} - \mathbf{B}_{plant}\mathbf{K}_{fb} \tag{6.28}$$

$$\mathbf{B}_{mod} = \mathbf{B}_{plant} \tag{6.29}$$

$$\mathbf{C}_{mod} = \mathbf{C}_{plant} \tag{6.30}$$

$$\mathbf{D}_{mod} = \mathbf{D}_{plant}. \tag{6.31}$$

The nature of the plant determines that the three first, lowest-order, characteristic-harmonic poles have been placed into the plant. Consequently, the matrices of the tandem system, representing the ten remaining poles of the reference signal are

$$\dot{\mathbf{x}}_{ref_{ser}}(t) = \mathbf{A}_{ref_{ser}}\mathbf{x}_{ref_{ser}}(t) + \mathbf{B}_{ref_{ser}}\mathbf{u}_{ref_{ser}}(t) \tag{6.32}$$

$$\mathbf{y}_{ref_{ser}}(t) = \mathbf{C}_{ref_{ser}}\mathbf{x}_{ref_{ser}}(t) + \mathbf{D}_{ref_{ser}}\mathbf{u}_{ref_{ser}}(t) \tag{6.33}$$

where

$$\mathbf{A}_{ref_{ser}} = \begin{bmatrix} \mathbf{A}_{ref_4} & 0 & \cdots & 0 \\ 0 & \mathbf{A}_{ref_5} & \cdots & 0 \\ \vdots & \vdots & \ddots & \vdots \\ 0 & 0 & \cdots & \mathbf{A}_{ref_{h_8}} \end{bmatrix} \tag{6.34}$$

$$\mathbf{B}_{ref_{ser}} = \begin{bmatrix} 1 & 1 & 1 & 1 & 1 & 1 & 1 & 1 & 1 & 1 \end{bmatrix}^T \tag{6.35}$$

$$\mathbf{C}_{ref_{ser}} = \begin{bmatrix} 1 & 1 & 1 & 1 & 1 & 1 & 1 & 1 & 1 & 1 \end{bmatrix} \tag{6.36}$$

$$\mathbf{D}_{ref_{ser}} = \begin{bmatrix} 0 \end{bmatrix}. \tag{6.37}$$

Therefore, the resulting augmented plant [82] is

$$\dot{\mathbf{x}}_{aug}(t) = \mathbf{A}_{aug}\mathbf{x}_{aug}(t) + \mathbf{B}_{aug}\mathbf{u}_{ref_{ser}}(t) \tag{6.38}$$

$$\mathbf{y}(t) = \mathbf{C}_{aug}\mathbf{x}_{aug}(t) \tag{6.39}$$

where matrices

$$\mathbf{A}_{aug} = \begin{bmatrix} \mathbf{A}_{mod} & \mathbf{B}_{mod}\mathbf{C}_{ref_{ser}} \\ 0 & \mathbf{A}_{ref_{ser}} \end{bmatrix} \tag{6.40}$$

$$\mathbf{B}_{aug} = \begin{bmatrix} 0 \\ \mathbf{B}_{ref_{ser}} \end{bmatrix} \tag{6.41}$$

$$\mathbf{C}_{aug} = \begin{bmatrix} \mathbf{C}_{mod} & 0 \end{bmatrix} \tag{6.42}$$

yield the state vector

$$\mathbf{x}_{aug} = \begin{bmatrix} \mathbf{x} \\ \mathbf{x}_{ref_{ser}} \end{bmatrix}. \tag{6.43}$$

Finally, the block diagram of the regulator problem with the augmented plant is the one shown in Figure 6.3.

6.3.3 The Transformation into a Servomechanism Problem

Now, the transformation of the optimal regulator design into that of a servomechanism one will take place. The augmented plant now has all the poles of the reference signal

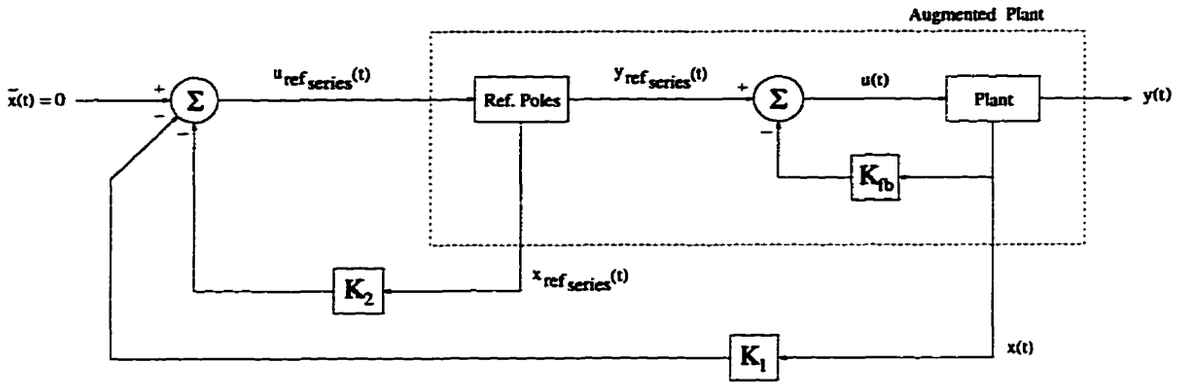

Figure 6.3: Basic block diagram of regulator system for the augmented plant.

$\tilde{\mathbf{y}}(t)$, hence satisfying the Internal-Model Principle. Therefore, provided that a specific $\tilde{\mathbf{x}}_{aug}(t_i)$ is used as the initial state, the reference signal can also be generated by the augmented plant with no input. That is,

$$\dot{\mathbf{x}}_{aug}(t) = \mathbf{A}_{aug}\mathbf{x}_{aug}(t), \qquad \tilde{\mathbf{x}}_{aug}(t_i) \tag{6.44}$$

$$\tilde{\mathbf{y}}(t) = \mathbf{C}_{aug}\mathbf{x}_{aug}(t). \tag{6.45}$$

A performance index that reflects the necessity of reducing the error between the output of the plant and the output of the reference system can be

$$V(\mathbf{x}_{aug}(t_i), \mathbf{u}(\cdot)) = \lim_{t_f \to \infty} \int_{t_i}^{t_f} [[\tilde{\mathbf{y}}(t) - \mathbf{y}(t)]^T \mathbf{Q} [\tilde{\mathbf{y}}(t) - \mathbf{y}(t)] + \mathbf{u}_{ref_{ser}}(t)^T \mathbf{R} \mathbf{u}_{ref_{ser}}(t)] \, dt \tag{6.46}$$

or

$$V(\mathbf{x}_{aug}(t_i), \mathbf{u}(\cdot)) = \lim_{t_f \to \infty} \int_{t_i}^{t_f} [[\tilde{\mathbf{x}}_{aug}(t) - \mathbf{x}_{aug}(t)]^T \mathbf{C}_{aug}^T \mathbf{Q} \mathbf{C}_{aug} [\tilde{\mathbf{x}}_{aug}(t) - \mathbf{x}_{aug}(t)] + \mathbf{u}_{ref_{ser}}(t)^T \mathbf{R} \mathbf{u}_{ref_{ser}}(t)] \, dt \tag{6.47}$$

where

$$\tilde{\mathbf{x}}_{aug}(t) = \mathbf{C}_{aug}^T \begin{bmatrix} \mathbf{C}_{aug} & \mathbf{C}_{aug}^T \end{bmatrix}^{-1} \tilde{\mathbf{y}}(t) \tag{6.48}$$

and $\tilde{\mathbf{x}}_{aug}(t)$ is the reference-state transition that causes the output of the plant to track the output reference $\tilde{\mathbf{y}}(t)$. This last performance index is, therefore, trying to reduce the error, not between the output reference and the output of the plant,

but between the reference-system state vector and the state vector of the augmented plant. This comparison generates the state-vector error.

The response of the active-filter control to system disturbances and to changes to the operating point should be fast and smooth. With the objective of further control on the smoothness of the states and, consequently, also on the output, a extra factor will now be added to the performance index [79], as

$$V(\mathbf{x}_{aug}(t_i), \mathbf{u}(\cdot)) = \lim_{t_f \to \infty} \int_{t_i}^{t_f} \left[\mathbf{x}_{aug}(t)^T \mathbf{Q}_1 \mathbf{x}_{aug}(t) + [\tilde{\mathbf{y}}(t) - \mathbf{y}(t)]^T \mathbf{Q}_2 [\tilde{\mathbf{y}}(t) - \mathbf{y}(t)] + \mathbf{u}_{ref_{ser}}(t)^T \mathbf{R} \mathbf{u}_{ref_{ser}}(t)\right] dt, \tag{6.49}$$

where $\mathbf{Q}_1$ and $\mathbf{Q}_2$ are symmetric and nonnegative definite matrices. Since increased smoothness encourages smaller values of $\mathbf{x}_{aug}(t)$ (and, consequently, of $\mathbf{y}_{aug}(t)$), this may be conflicting with trying to keep the output error small. This is solved as follows. The state vector $\mathbf{x}_{aug}(t)$ is split into two orthogonal components $\mathbf{x}_{aug_1}(t)$ and $\mathbf{x}_{aug_2}(t)$, in the form

$$\mathbf{x}_{aug}(t) = \mathbf{x}_{aug_1}(t) + \mathbf{x}_{aug_2}(t) \tag{6.50}$$

so that one of the components still provides the output

$$\mathbf{C}_{aug} \mathbf{x}_{aug_1}(t) = \mathbf{y}(t), \tag{6.51}$$

and the other one does not contribute to it at all:

$$\mathbf{C}_{aug} \mathbf{x}_{aug_2}(t) = \mathbf{0}. \tag{6.52}$$

For the first component to be responsible for the whole output, it has to be in the range space of $\mathbf{C}_{aug}$. That is, for some vector $\mathbf{v}(t)$,

$$\mathbf{C}_{aug}^T \mathbf{v}(t) = \mathbf{x}_{aug_1}(t). \tag{6.53}$$

It can be checked that this vector is

$$\mathbf{v}(t) = \begin{bmatrix} \mathbf{C}_{aug} & \mathbf{C}_{aug}^T \end{bmatrix}^{-1} \mathbf{C}_{aug} \mathbf{x}_{aug}(t). \tag{6.54}$$

Hence, the orthogonal component can be obtained by simply operating on the real state vector $\mathbf{x}_{aug}(t)$ of the augmented plant

$$\mathbf{x}_{aug_2}(t) = \mathbf{x}_{aug}(t) - \mathbf{x}_{aug_1}(t) = \left[\mathbf{I} - \mathbf{C}_{aug}^T \left(\mathbf{C}_{aug} \mathbf{C}_{aug}^T\right) \mathbf{C}_{aug}\right] \mathbf{x}_{aug}(t). \tag{6.55}$$

Therefore, this relationship can be built into the weighting matrix $\mathbf{Q}_1$

$$\mathbf{Q}_1 = \left[\mathbf{I} - \mathbf{C}_{aug}^T \left(\mathbf{C}_{aug}\mathbf{C}_{aug}^T\right) \mathbf{C}_{aug}\right]^T \mathbf{Q}_3 \left[\mathbf{I} - \mathbf{C}_{aug}^T \left(\mathbf{C}_{aug}\mathbf{C}_{aug}^T\right)^{-1} \mathbf{C}_{aug}\right] \tag{6.56}$$

where $\mathbf{Q}_3$ is an arbitrary nonnegative definite symmetric matrix. This restriction to $\mathbf{Q}_1$ avoids the conflict between the state energy ("smoothness") cost and the error cost.

Since the theory has originally been developed for the regulator problem, it is convenient to maintain the original variables of the performance index, that is, in terms of the state error and control vectors. In this case, it can be shown [79] that the original weighting matrix $\mathbf{Q}$, of the regulator problem is related to $\mathbf{Q}_1$ and $\mathbf{Q}_2$ in the following way:

$$\mathbf{Q} = \mathbf{Q}_1 + \mathbf{C}_{aug}^T \mathbf{Q}_2 \mathbf{C}_{aug} \tag{6.57}$$

To convert the servomechanism problem into a regulator one, the augmented plant is required to be further augmented. The new states are now the differences between the real augmented states and the reference states. Figure 6.4 shows the block diagram of the newly augmented system (the "regulator" system).

The equations now are

$$\dot{\mathbf{x}}_{reg}(t) = \mathbf{A}_{reg}\mathbf{x}_{reg}(t) + \mathbf{B}_{reg}\mathbf{u}_{ref_{ser}}(t), \qquad \mathbf{x}_{reg}(t_i) \tag{6.58}$$

$$\tilde{\mathbf{y}}(t) = \mathbf{C}_{reg}\mathbf{x}_{reg}(t) \tag{6.59}$$

where

$$\mathbf{A}_{reg} = \begin{bmatrix} \mathbf{A}_{aug} & \mathbf{0} \\ \mathbf{0} & \mathbf{A}_{aug} \end{bmatrix} \tag{6.60}$$

$$\mathbf{B}_{reg} = \begin{bmatrix} \mathbf{B}_{aug} \\ \mathbf{0} \end{bmatrix} \tag{6.61}$$

$$\mathbf{C}_{reg} = \begin{bmatrix} \mathbf{C}_{aug} & \mathbf{0} \end{bmatrix} \tag{6.62}$$

$$\mathbf{x}_{reg} = \tilde{\mathbf{x}}_{aug} - \mathbf{x}_{aug}. \tag{6.63}$$

The performance index now becomes

$$V(\mathbf{x}_{reg}(t_i), \mathbf{u}(\cdot)) = \lim_{t_f \to \infty} \int_{t_i}^{t_f} \left[\mathbf{x}_{reg}(t)^T \mathbf{Q}_{reg} \mathbf{x}_{reg}(t) + \mathbf{u}_{ref_{ser}}(t)^T \mathbf{R} \mathbf{u}_{ref_{ser}}(t)\right] dt \tag{6.64}$$

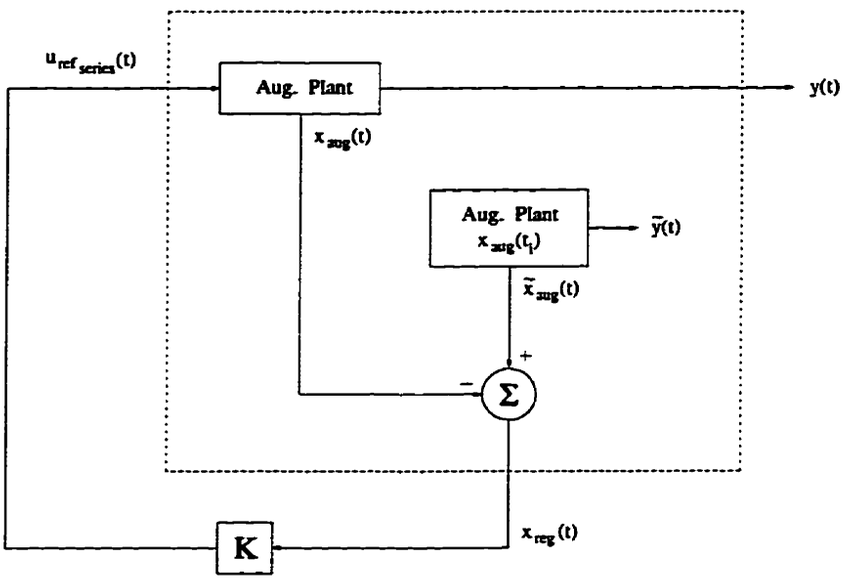

Figure 6.4: Basic block diagram of the servomechanism problem.

where

$$\mathbf{Q}_{reg} = \begin{bmatrix} \mathbf{Q} & -\mathbf{Q} \\ -\mathbf{Q} & \mathbf{Q} \end{bmatrix}. \tag{6.65}$$

Therefore, according to the regulator theory,

$$\mathbf{u}^{*}_{ref_{ser}}(t) = -\mathbf{R}^{-1}\mathbf{B}^{T}_{reg}\mathbf{P}_{reg}\mathbf{x}_{reg}(t) \tag{6.66}$$

where $\mathbf{P}_{reg}$ is the solution of the algebraic Riccati equation

$$\mathbf{P}_{reg}\mathbf{A}_{reg} + \mathbf{A}^{T}_{reg}\mathbf{P}_{reg} - \mathbf{P}_{reg}\mathbf{B}_{reg}\mathbf{R}^{-1}\mathbf{B}^{T}_{reg}\mathbf{P}_{reg} + \mathbf{Q}_{reg} = \mathbf{0}, \tag{6.67}$$

for which, due to the symmetry of the further augmented system [80],

$$\mathbf{P}_{reg} = \begin{bmatrix} \mathbf{P} & -\mathbf{P} \\ -\mathbf{P} & \mathbf{P} \end{bmatrix}. \tag{6.68}$$

The algebraic Riccati equation to be solved becomes

$$\mathbf{P}\mathbf{A}_{aug} + \mathbf{A}^{T}_{aug}\mathbf{P} - \mathbf{P}\mathbf{B}_{aug}\mathbf{R}^{-1}\mathbf{B}^{T}_{aug}\mathbf{P} + \mathbf{Q} = \mathbf{0}, \tag{6.69}$$

and the new optimal control is

$$\mathbf{u}^{*}_{ref_{ser}}(t) = -\mathbf{K}\mathbf{x}_{reg}(t) \tag{6.70}$$

where

$$\mathbf{K} = \mathbf{R}^{-1}\mathbf{B}^{T}_{aug}\mathbf{P}. \tag{6.71}$$

Now the servomechanism problem can be represented in a more familiar block diagram, shown in Figure 6.5.

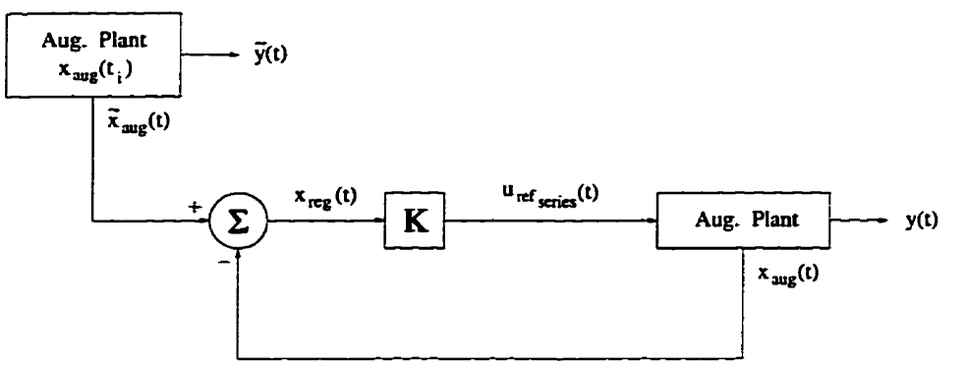

Figure 6.5: Rearranged basic block diagram of the servomechanism problem.

The output reference signal (harmonic content of the converter current which is drawn from the AC system) is composed of the summation of critically stable components (harmonic frequencies). In practice, one way of implementing this control system could be to continuously run a Fast Fourier Transform (FFT) algorithm to obtain the magnitude and phase of each harmonic component, and verify which harmonics exceed the corresponding pre-established maximum allowed values. Given these frequencies (poles), the feedback matrix $\mathbf{K}_{fb}$ and the series system, containing the remaining poles, could be adjusted, and the matrices of the augmented system would be determined. At this point, the algebraic Riccati equation could already be solved, and matrix $\mathbf{K}$ determined. But the problem of an efficient on-line obtainment of the state reference to be followed still remains. That is, there is still a need to find out the trajectories $\tilde{\mathbf{x}}_{aug}(t)$ that the states $\mathbf{x}_{aug}(t)$ must follow so that $\mathbf{y}(t)$ follows the desired output $\tilde{\mathbf{y}}(t)$. An optimal state estimation of this reference signal will therefore be performed (Kalman-Bucy filter) for this purpose.

6.4 The State Estimation of the Reference Signal

This section deals with the generation of the reference states to be tracked by the augmented plant. This procedure is based on the fact that the augmented system has all the poles that characterize the harmonic current to be actively filtered and, therefore, given a suitable initial state-vector value, can generate the required harmonic current.

Obtaining the states of a general linear system through a linear combination of its inputs, outputs and their derivatives is not practical because the presence of noise in these signals will lead to vast errors. A very good property of the Kalman-Bucy state estimator is that it has the same basic form as the system whose states are being estimated (as a model), using both its input $\mathbf{u}(t)$ and output $\mathbf{y}(t)$ as inputs and yielding the on-line-estimated states $\mathbf{x}^*(t)$ as the output. Another property of this state estimator is that it performs optimally in the presence of stationary noise which has the least effect possible. Figure 6.6 shows this scheme conceptually.

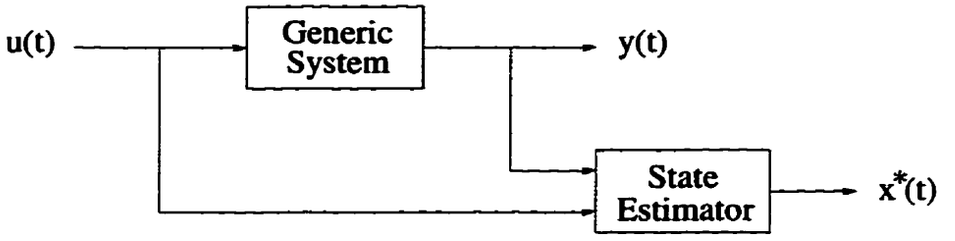

Figure 6.6: Conceptual block diagram of the Kalman-Bucy state estimator.

Having Figure 6.6 as reference, in the case of the active-filter control, the generic system and its input do not exist ($\tilde{\mathbf{u}}(t) = 0$) and the measured reference signal ($\tilde{\mathbf{y}}(t)$), being the only signal available for the estimation of its states, is used as the only input for the state estimator. The equations of the model used for the state estimation of the reference signal are those of the augmented system, which, making use of its full order, is minimally sensitive to noise [79].

Since, from a certain time on, the estimated states of the reference signal $\tilde{\mathbf{x}}^*_{aug}(t)$ should be equal to the states that the augmented plant should follow $\tilde{\mathbf{x}}_{aug}(t, t_i)$, the model of the estimator should be a model of the plant with the addition of a term reflecting the error between the plant output $\tilde{\mathbf{y}}(t)$ (the harmonic content of the converter current being drawn from the AC system) and the output of the estimator

$\tilde{\mathbf{y}}^*(t)$ (the estimated output of the plant). The requirement that the system, that is, the pair $(\mathbf{A}_{aug}, \mathbf{C}_{aug})$, be completely observable is satisfied. Therefore,

$$\Delta\tilde{\mathbf{y}}^*(t) = \mathbf{C}_{aug}\left[\tilde{\mathbf{x}}_{aug}(t) - \tilde{\mathbf{x}}^*_{aug}(t)\right] \tag{6.72}$$

would have the same information as $\tilde{\mathbf{x}}_{aug}(t) - \tilde{\mathbf{x}}^*_{aug}(t)$ in a nonzero time interval and it is a measure of how good the estimation is. This suggests the estimator dynamical and output equations as

$$\dot{\tilde{\mathbf{x}}}^*_{aug}(t) = \mathbf{A}_{aug}\tilde{\mathbf{x}}^*_{aug}(t) + \mathbf{K}_{est}\mathbf{C}_{aug}\left[\tilde{\mathbf{x}}_{aug}(t) - \tilde{\mathbf{x}}^*_{aug}(t)\right] \tag{6.73}$$

$$\tilde{\mathbf{y}}^*(t) = \mathbf{C}_{aug}\tilde{\mathbf{x}}^*_{aug}(t) \tag{6.74}$$

Figure 6.7 shows the block diagram of the corresponding arrangement.

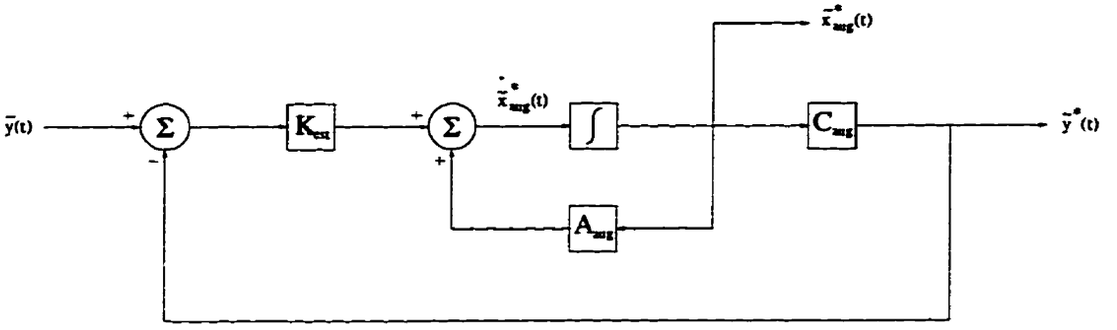

Figure 6.7: Basic block diagram of the reference state estimation.

The dynamical equation can also be written in such a way that puts the state feedback in evidence, as

$$\dot{\tilde{\mathbf{x}}}^*_{aug}(t) = (\mathbf{A}_{aug} - \mathbf{K}_{est}\mathbf{C}_{aug})\tilde{\mathbf{x}}^*_{aug}(t) + \mathbf{K}_{est}\tilde{\mathbf{y}}_{aug}(t). \tag{6.75}$$

$\mathbf{K}_{est}$ could be carefully chosen (by means of pole placement) so that $\tilde{\mathbf{x}}_{aug}(t) - \tilde{\mathbf{x}}^*_{aug}(t)$ becomes smaller, at an exponential rate, as time elapses. That is, so that the eigenvalues of $\mathbf{A}_{aug} - \mathbf{K}_{est}\mathbf{C}_{aug}$ all have negative real parts. If there is any noise associated with $\tilde{\mathbf{y}}(t)$, it will be smoothed. If this is a white noise (uniform power spectrum), it will fall away at high frequencies. In general, the amount of output noise will depend on the choice of $\mathbf{K}_{est}$ but the problem associated with passing noise through a differentiator

is avoided. The speed at which the output of the observer converges to the correct value depends on size of the negative parts of the eigenvalues of $\mathbf{A}_{aug} - \mathbf{K}_{est}\mathbf{C}_{aug}$. Unfortunately, increasing the convergence speed also increases the effective bandwidth of the estimator and, therefore, the noise in $\tilde{\mathbf{x}}^*(t)$ due to the noise in $\tilde{\mathbf{y}}(t)$. Therefore, there is an upper limit on the speed at which $\tilde{\mathbf{x}}^*(t)$ approaches $\tilde{\mathbf{x}}(t)$ and optimal estimators take this into consideration.

The design depends on the probabilistic data concerning the noise associated with the measurement of $\tilde{\mathbf{y}}(t)$. Although the basic problem deals with obtaining the best possible estimator regardless of the noise content, this optimal filtering problem can be converted into one of a deterministic optimal control (regulator) problem (Appendix B describes how this is achieved) as follows.

Assuming that $\mathbf{P}$ is the solution to the algebraic Riccati equation

$$\mathbf{P}\mathbf{A}_{aug}^T + \mathbf{A}_{aug}\mathbf{P} - \mathbf{P}\mathbf{C}_{aug}^T\mathbf{R}^{-1}\mathbf{C}_{aug}\mathbf{P} + \mathbf{Q} = \mathbf{0} \tag{6.76}$$

where $\mathbf{Q}$ is symmetric nonnegative definite, defined by

$$\mathbf{Q} = \mathbf{C}_{aug}^T\mathbf{C}_{aug}, \tag{6.77}$$

and $\mathbf{R}$ is positive definite. The gain of the optimal estimator shown in Figure 6.7 is

$$\mathbf{K}_{est} = -\mathbf{P}\mathbf{C}_{aug}^T\mathbf{R}^{-1} \tag{6.78}$$

The equations of the implemented optimal state-estimator system are given by

$$\dot{\tilde{\mathbf{x}}}_{aug}^*(t) = \mathbf{A}_{aug}\tilde{\mathbf{x}}_{aug}^*(t) + \mathbf{K}_{est}\left[\mathbf{C}_{aug}\tilde{\mathbf{x}}_{aug}^*(t) - \tilde{\mathbf{y}}(t)\right], \tag{6.79}$$

or, explicitly showing the comparison between the measured and estimated outputs

$$\dot{\tilde{\mathbf{x}}}_{aug}^*(t) = \mathbf{A}_{aug}\tilde{\mathbf{x}}_{aug}^*(t) + \mathbf{K}_{est}\left[\tilde{\mathbf{y}}^*(t) - \tilde{\mathbf{y}}(t)\right]. \tag{6.80}$$

6.5 Measurements

6.5.1 Plant State Estimation

The topology of the active filter, together with the control scheme being used, determines that the behavior of the active source of the active filter is that of a voltage

source. This means that currents generated by any other sources in the AC/DC system are allowed to flow freely through the active filter circuit. Therefore, the harmonic current demanded by the HVDC-converter station is passively, and proportionally, shared (current divider) by the parallel connection of the AC system, the shunt capacitor, and the circuit formed by the series connection of the path impedance and the output-filter circuit of the PWM inverter. In the branch formed by the path impedance and the output filter of the PWM inverter, the path followed by these currents is provided by the antiparallel diodes and the output capacitor of the rectifier that feeds the PWM inverter of the active source. It can be verified, in Figure 5.12, in Chapter 5, that diode pairs $D_1\&D_2$ and $D_3\&D_4$, together with the output capacitor of the rectifier of the PWM inverter, alternately provide the harmonic current due to the HVDC converter with paths for the positive and the negative cycles. The fundamental current does not take part in this process due to the high impedance provided by the chosen path impedance.

In normal operation of the active filter, however, all the actual elements of the circuit will experience both harmonic voltages and currents generated by the HVDC converter as well as by the active source of the active filter. It is worth noting that simple measurements would be unable to distinguish voltages and currents components due to the different sources. Further, some of the actual elements of the system will also carry fundamental-frequency components, and the output-filter elements of the PWM inverter will also carry very high switching-frequency components. Therefore, the harmonic content of the states of the plant cannot be measured. Instead, they must be estimated.

The plant model being considered (Figure 6.1) so far is a SISO type of system whose only input is the active source of the active filter, and, consequently, its states do not consider the harmonic current source representing the HVDC-converter terminal or fundamental-frequency sources. Therefore, the estimation of the states, being fed back to match the poles of the plant with those of the reference signal and for use by the optimal-control law, should consider only the active source as the plant input.

Equally, the reference harmonic current to be tracked by the active filter, corresponding to the AC-system harmonic currents (whose states were estimated in Section 6.4) should be estimated from a plant model having only the harmonic current due to the HVDC-converter as input. The actual current that this estimated

current represents must be cancelled by the successful operation of the active filter and, therefore, the measured resulting AC-system harmonic current should be zero.

The estimation of the states of the plant, on the one hand, and of the reference current, on the other hand, have both been simplified to mere on-line simultaneous simulations of two different models of the same AC/DC system.

For the estimation of the states which are fed back and also used in the optimal-control law, the same plant model used in the optimal-control design, having the active-source voltage reference as input and its corresponding active-filter current as output, is simulated. That is, the derivation of these states is executed by a parallel realization of Equations (6.3).

The determination of the component of the harmonic current demanded by the HVDC terminal which passively comes from the AC system is done by means of the on-line simulation of the circuit shown in Figure 6.8. This model uses the measured, and PLL-filtered (Section 6.5.2), AC line current of the HVDC terminal as input and the AC-system harmonic current as output. The states of this model are then forwarded to the reference-signal state estimator.

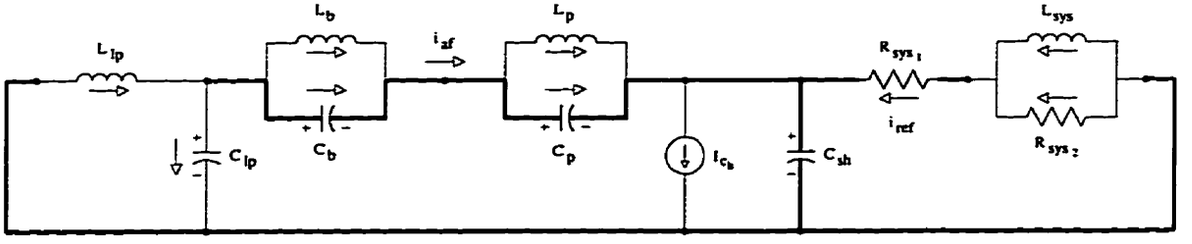

Figure 6.8: Circuit diagram representing the plant, having the HVDC-terminal harmonic-current content as input, for obtainment of i_{ref}.

Being essentially the same plant used for control, the state variable representation of this circuit has the same poles (same matrix $\mathbf{A}_{plant}$) as derived for the control. However, all the other matrices are different from those in Equations (6.3). The dynamic and output equations of this circuit using well known techniques [81–83] and their respective matrix values are as follows.

$$\begin{aligned} \dot{\mathbf{x}}(t) &= \mathbf{A}_{plant}\ \mathbf{x}(t) + \mathbf{B}_{i_h}\mathbf{u}(t) \\ \mathbf{y}(t) &= \mathbf{C}_{i_h}\ \mathbf{x}(t) + \mathbf{D}_{i_h}\mathbf{u}(t) \end{aligned} \tag{6.81}$$

where

$$\mathbf{B}_{i_h} = \begin{bmatrix} -70260.9 \\ 1979.4 \\ 62771.8 \\ 0.0 \\ 0.0 \\ 0.0 \\ 0.0 \end{bmatrix}$$

$$\mathbf{C}_{i_h} = \begin{bmatrix} -0.000010 & 0.000000 & 0.000000 & 0.022000 & -0.027552 & -0.873719 & -0.076690 \end{bmatrix}$$

$$\mathbf{D}_{i_h} = \begin{bmatrix} 0.978000 \end{bmatrix}.$$

6.5.2 Phase-Locked-Loop Fundamental-Component Signal Filter

Another important issue in the derivation of the reference current; is the separation of the harmonic component (I_{c_h}) for the fundamental component of the measured signal i_c. The fundamental component is typically 20 to 30 times larger than the 11th, and largest, characteristic harmonic and they are only 600 Hz apart. Consequently these factors create considerable practical difficulty in removing the fundamental component. An ordinary nth-order high-pass filter is insufficient to provide the conflicting attribute of accuracy (magnitude and phase) and speed. Furthermore, any transient or permanent small change in the system's fundamental frequency would cause loss of tuning and an incorrect reference signal.

Alternatively, a notch filter would provide progressively negligible phase shift and attenuation as frequencies distance themselves from the fundamental frequency. However, it would also be degraded by variations of the fundamental frequency.

The solution has been to utilize a filter based on a phase-locked-loop (PLL) [93–98]. It tracks and compensates for deviation in fundamental frequency. The basic components of the PLL are the phase comparator, the low-pass filter and a voltage-controlled oscillator, as shown in Figure 6.9.

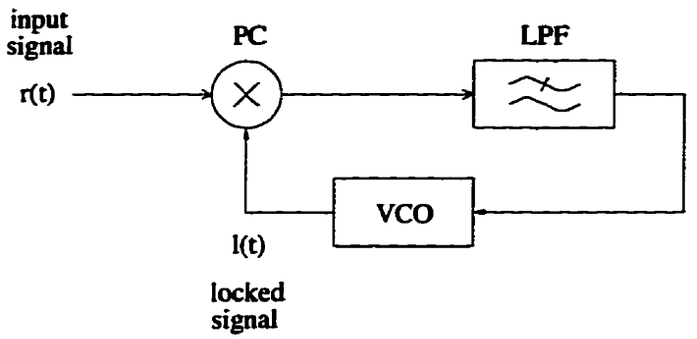

Figure 6.9: Components of a generic phase-locked-loop filter.

A PLL basically synchronizes the frequency of the output of the voltage- controlled oscillator with the frequency of a reference signal. The filtered result of the phase comparison is the error signal that controls the output signal of the VCO. The output of a phase comparator has the following general expression:

$$v_d = K_d f(\Phi_r - \Phi_l). \tag{6.82}$$

Designating v_f as the output of the low-pass filter, the general expression that governs the output frequency of the VCO is

$$f_l = f_0 + K_0 v_f, \tag{6.83}$$

where f_0 is the natural frequency of oscillation of the VCO (with no input).

In power systems, phase changes due to frequency deviations are small and develop slowly, and can be detected by a simple analog multiplier as the phase comparator (PC in Figure 6.9. In the case of the active filter, the reference input is derived from the line current of the HVDC converter terminal. If only the fundamental component of this current were considered, $r(t)$ and $l(t)$ (see Figure 6.2) can be written as

$$\begin{aligned} r(t) &= E_r \cos(\omega_r t + \Phi_r) \\ l(t) &= E_l \cos(\omega_l t + \Phi_l) \end{aligned} \tag{6.84}$$

where

$$\omega_r = 2\pi f_r,$$

and

$$\omega_l = 2\pi f_l.$$

The multiplier output is then given by

$$v_d(t) = K_d\{\cos[(\omega_r - \omega_l)t + \Phi_r - \Phi_l] + cos[(\omega_r + \omega_l)t + \Phi_r + \Phi_l]\}, \tag{6.85}$$

and the output of a perfect low-pass filter by

$$v_f(t) = K_d \cos[(\omega_r - \omega_l)t + \Phi_r - \Phi_l]. \tag{6.86}$$

It can be shown that [98], considering the closed loop in the locked state in which both the reference and the VCO output signals are at the same frequency, the phase difference between these signals must be $\frac{\pi}{2}$ and that the system unlocks (or "skips") if the phase difference equals zero. It can also be shown that the reference angular-frequency range $\Delta\omega_H$, over which the locked PLL, is still able to reduce the phase difference to zero ("hold" range), in response to a frequency deviation, is given by

$$\Delta\omega_H = \omega_0 - K_d K_0 \leq \omega_r \leq \omega_0 + K_d K_0, \tag{6.87}$$

and that the reference angular-frequency "capture" range $\Delta\omega_L$, over which the PLL, if originally unlocked, is able to acquire lock and track to reduce the phase difference between the reference signal and the VCO output to zero, is given by

$$\omega_0 - 2\pi B_L \leq \omega_r \leq \omega_0 + 2\pi B_L, \tag{6.88}$$

where B_L is the low-pass filter bandwidth.

The harmonics in the reference signal will produce jitter in the zero crossings. Since the low-pass filter will damp these oscillations to negligible values, the output of the VCO will continue to track the fundamental component of the reference signal.

The design of a phase-locked loop, ultimately, depends on the design of the low-pass filter. The frequency-domain block diagram of the PLL is shown in Figure 6.10.

Having Figure 6.10 as reference, the following relationships hold:

$$\Theta_e(s) = \Theta_r(s) - \Theta_l(s) \tag{6.89}$$

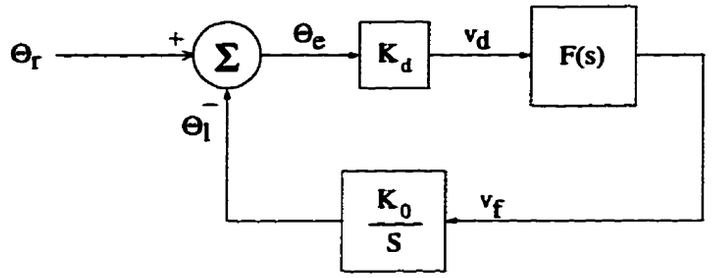

Figure 6.10: Linearized block diagram of a phase-locked-loop filter.

Open-loop transfer function:

$$\frac{\Theta_l(s)}{\Theta_e(s)} = K_d K_0 \frac{F(s)}{s} \tag{6.90}$$

Closed-loop transfer function:

$$\frac{\Theta_l(s)}{\Theta_r(s)} = \frac{K_d K_0 F(s)}{s + K_d K_0 F(s)} \tag{6.91}$$

Characteristic equation:

$$s + K_d K_0 F(s) = 0. \tag{6.92}$$

The majority of the applications of PLL filters (mostly in communications) make use of a first-order low-pass filter. The high-accuracy requirement of the active filter demands the use of a second-order low-pass filter. This causes the closed-loop equation of the PLL filter to be of the third order. The design method of the third-order PLL filter used in this thesis has been the one suggested in [98].

The transfer function of the second-order filter is in the following general form:

$$F(s) = \frac{1 + s\tau_2}{s\tau_1(1 + s\tau_3)}. \tag{6.93}$$

Therefore, for the third-order PLL filter, the following relationships hold:

Open-loop transfer function:

$$T'(s) = \frac{K_d K_0 \tau_2}{\tau_1 \tau_3} \frac{s + \frac{1}{\tau_2}}{s^2\left(s + \frac{1}{\tau_3}\right)} \tag{6.94}$$

Closed-loop transfer function:

$$T(s) = K_d K_0 \left(\frac{\tau_2}{\tau_1 \tau_3}\right) \frac{s + \frac{1}{\tau_2}}{s^3 + \left(\frac{1}{\tau_3}\right) s^2 + \left(\frac{K_d K_0 \tau_2}{\tau_1 \tau_3}\right) s + \frac{K_d K_0}{\tau_1 \tau_3}} \tag{6.95}$$

Characteristic equation:

$$s^3 + \left(\frac{1}{\tau_3}\right) s^2 + \left(\frac{K_d K_0 \tau_2}{\tau_1 \tau_3}\right) s + \frac{K_d K_0}{\tau_1 \tau_3} = 0 \tag{6.96}$$

Routh's stability analysis shows that a condition for the PLL filter to be stable is that

$$\tau_2 > \tau_3. \tag{6.97}$$

It can also be shown that, in order to optimize the phase margin and, consequently, the Bode-stability of the PLL filter, the roots of the characteristic equation should be placed at

$$\begin{aligned} s_1 &= -\omega_n \\ s_2 &= -\zeta\omega_n + j\sqrt{1-\zeta^2}\omega_n \\ s_2 &= -\zeta\omega_n - j\sqrt{1-\zeta^2}\omega_n \end{aligned} \tag{6.98}$$

where ζ is the damping factor and ω_n the natural angular frequency.

These values ensure that the phase margin is maximum, has its value given by

$$\tan \Phi_M = \frac{2\zeta(\zeta+1)}{1+2\zeta}, \tag{6.99}$$

and occurs at the cut-off frequency

$$\omega_M = \sqrt{\frac{1}{\tau_2 \tau_3}} = \omega_n. \tag{6.100}$$

Considering the PLL for the HVDC converter line current, the damping factor has been chosen as $\zeta = \frac{\sqrt{2}}{2}$ to yield, through Equation (6.99), a good phase margin of $\Phi = \Phi_M = 45°$.

The steady-state AC-system frequency has typically a very narrow variation range. K_d and K_0 have both been set at unity. These values, according to Equation (6.87) permit a maximum frequency deviation of $\Delta f_{max} = 0.16$ Hz. This is compatible

with the requirement specified at Itaipu [46]. Trial and error technique resulted in a selected cut-off frequency $f_n = 0.1$ Hz.

The generation of a large second-harmonic component is inherent to the operation of the analog multiplier having sinusoidal signals as inputs (Equation (6.85)). Although this component is considerably reduced by the second-order low-pass filter, the eventual necessity of dealing with the active filtering of second-order current harmonics required the radical reduction of this component by means of the introduction of a notch-filter between the low-pass filter and the VCO tuned at $f_{notch} = 120$ Hz.

The transfer function of the notch filter is given by

$$F_{notch} = \frac{s^2 + (2\pi f_{notch})^2}{s^2 + \left(\frac{2\pi f_{notch}}{Q}\right) s + (2\pi f_{notch})^2}. \tag{6.101}$$

The quality factor that considers the tradeoff between accuracy and speed has been chosen as $Q = 10$. The resulting frequency characteristics plot is given in Figure 6.11.

One last PLL component should now be included. Since the locked state determines that the output of the VCO be shifted by $\frac{\pi}{2}$ radians from the reference signal, a first-order passive phase corrector filter [99] is used to obtain the fundamental component signal which is in phase with the fundamental component of the HVDC converter line current. The transfer function of the phase-corrector filter is given by

$$F_{pc} = \frac{1 - s\frac{1}{(2\pi 60)}}{1 + s\frac{1}{(2\pi 60)}}, \tag{6.102}$$

and its frequency characteristics plot is given in Figure 6.12. The final block diagram of the PLL is shown in Figure 6.13. At this point, it is worth showing the dynamic response of the complete PLL filter. With this in mind, the response to a small but abrupt frequency change in an unitary-amplitude sinusoidal input signal has been simulated in MATLAB. Figure 6.14 shows the corresponding response of error signal PLL_{error}, between the input and the output signals, to a 0.1-Hz step in the frequency of the input signal. The required simulated time of 20 s reflects the low cut-off frequency of the PLL filter.

Finally, the complete block diagram of the active-filter control is shown in Figure 6.15, where each one of its several components can now be easily identified.

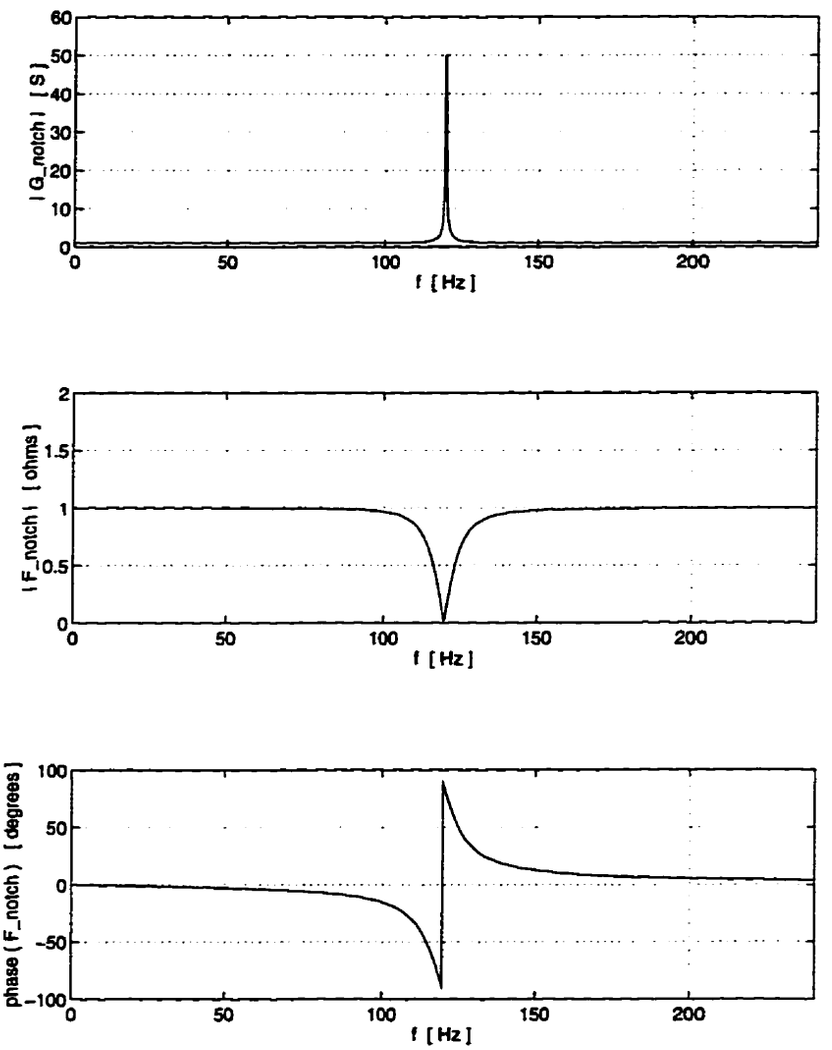

Figure 6.11: Frequency characteristics of the notch filter.

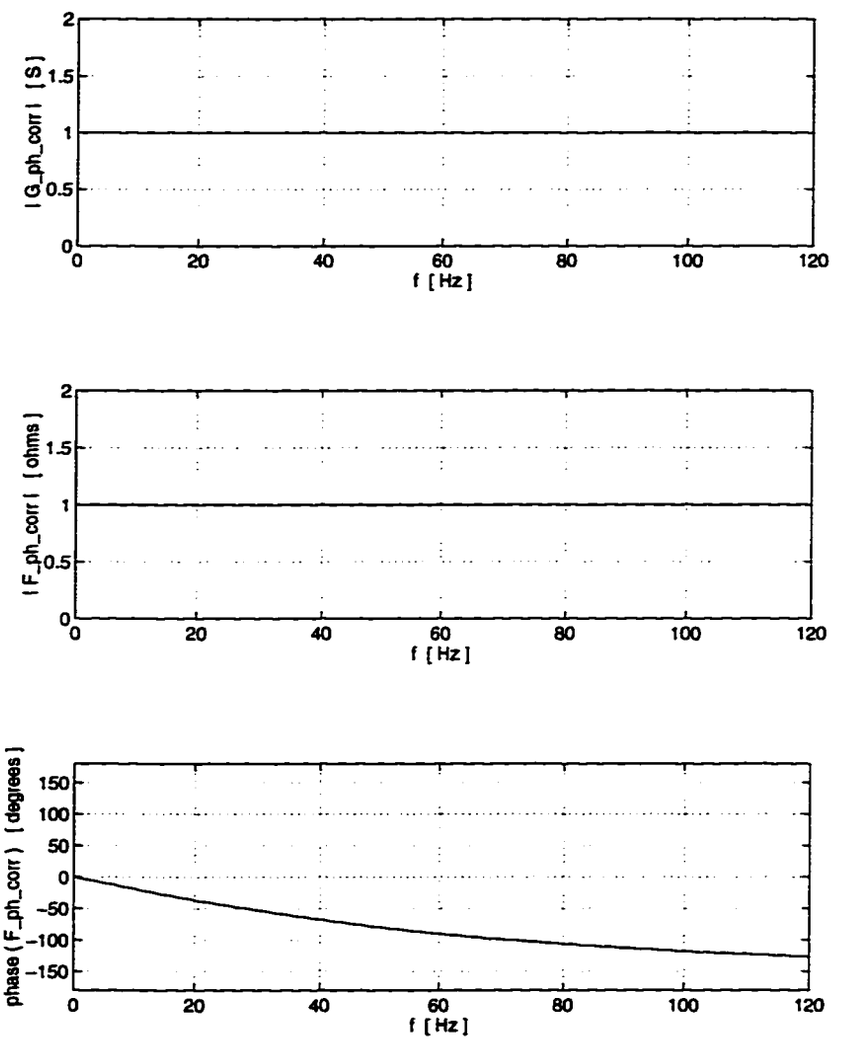

Figure 6.12: Frequency characteristics of the phase-corrector filter.

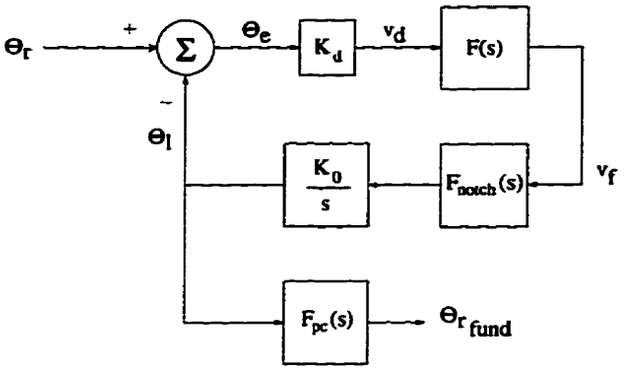

Figure 6.13: Final block diagram of the PLL filter.

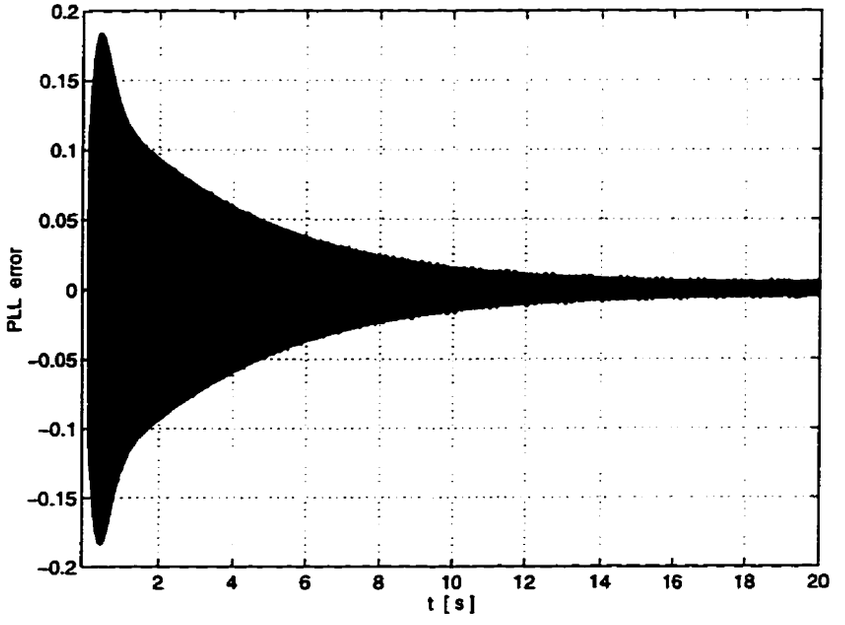

Figure 6.14: PLL-filter dynamic response to a frequency step in the input signal.

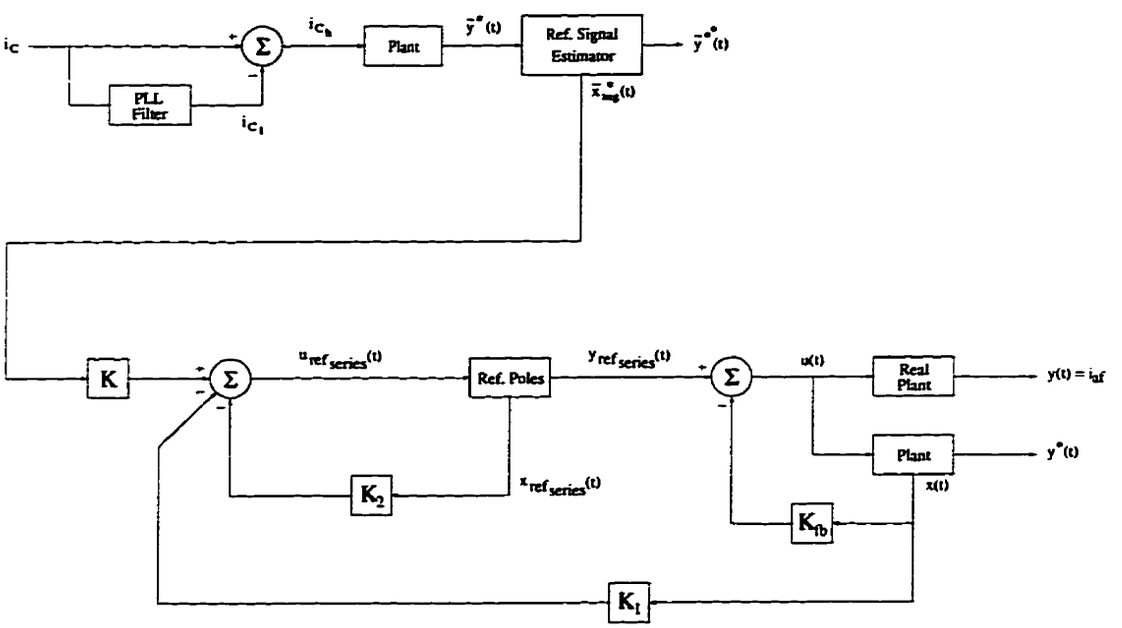

Figure 6.15: Complete block diagram of the active-filter control.

Chapter 7

Dynamic Simulations of the AC/DC System

7.1 Introduction

Although the well known simulation program for power systems, EMTP, was available for this research, another program, SABER, was selected as having the potential to be more amenable to the incorporation of the modeling of the active filter, and its control.

SABER, while not specifically designed for simulating power systems, is a highly sophisticated and state-of-the-art commercial simulation tool. Its use had the promise of providing a very powerful simulation platform while it presented considerable challenge in adapting it to the power system problem at hand. For example, in comparison with EMTP, no power system component models, e.g., semiconductor converter, power transformer, are provided, and these had to be developed from basic elements.

SABER is self-defined as a mixed-signal (continuous and discrete-time variables) simulator [100], and its internal programming includes independent analog and digital algorithms that, when needed, synchronously communicate the interaction between the two types of circuits. It allows the simulation (in the time and frequency domains) of analog systems (continuous with any real value), digital systems (discontinuous, but with a limited set of values), event-driven analog systems (discontinuous, but with

any real value), and mixed modes where analog and digital signals are transmitted between devices.

As to the modeling language, SABER uses a hardware description language, MAST, for modeling analog and mixed-signal devices. This language allows the description of a circuit behavior without having to describe a structure or function to generate that behavior. The characteristics of a device are passed to the simulator as programmatic features that specify control flow and operations on data. Consequently, the implementation of any new device does not require the user to know the integration routines and solution of linear and non-linear equations in the source code (written in C) of the simulator. Besides describing the function of entire analog or digital circuits and systems, MAST also allows measurements during the simulation.

Analog elements are modeled by their algebraic and/or differential equations. The operation of the logic components are approximated, with an acceptable level of accuracy, by modeling functions rather than precise operational characteristics. Digital components are represented by their state Boolean description and time delays, and have no resemblance to the analog circuitry that it models. The state variables are solved at discrete times, and only those functions which are affected by a changed state are computed. This way, the simulation of such systems are made a lot faster than with a pure analog simulator.

The simulation starts from a DC solution for all states (voltages and currents), from which the behavior of the circuit is observed in response to stimuli. SABER offers two options of integration methods: Trapezoidal and Gear (1st and 2nd orders). The 1st-order Gear was the integration method used because of its faster performance for the system studied. SABER allows the user to determine the truncation error to be respected before ending the integration step. The integration time steps can be either fixed or variable, and the minimum and maximum time-step values can also be set. The method used for the solution of the non-linear equations can be chosen from Newton-Raphson (the method used) or Katzenelson (use suggested only when Newton-Raphson fails), and the simulator also accepts an input for the maximum number of iterations.

SABER has been improved for the past ten years, and it now provides extensive libraries of generic components and of real-parts, of different technologies (electrical,

mechanical, hydraulic, thermal), for immediate use. SABER also allows combined use of MATLAB, a widely used mathematical analysis software. Further to this, SABER provides very flexible plotting capabilities which include processing and readings from the resulting waveforms (PLTOOL).

7.2 Simplifications and Implementation Details

7.2.1 HVDC Thyristors

The implementation of accurate nonlinear models of the thyristor valves would be, for the present purpose, unnecessary and an element of complication in the modeling and analysis of the complete system. Therefore, the power semiconductor devices had their ideal models implemented, and the drive circuits and heat sinks, that would be required in a practical implementation, have been neglected.

The implemented HVDC thyristor models change from off-state to on-state whenever the voltage across their terminals is positive and larger than a preset threshold value (set to 1 mV) and a firing pulse is concurrently applied to the gate terminal by the firing control. Once in their on-state, they present a preset value of forward voltage drop (set to 1 mV). On the other hand, the thyristor models will change from the on-state to the off-state whenever the current flowing through the device becomes less than a preset threshold current (set to -1 mA) with a negative derivative. The recovery time, a time period during which a spontaneous reignition can occur in the event of a reapplication of a positive voltage across the terminals, even without the existence of a firing pulse, has not been modeled.

7.2.2 Active-Source IGBTs

A main characteristic of some currently available semiconductor switches is that they present extremely low losses during the conducting state. Therefore, the losses of the active source with such devices, being basically related to the switching actions, are considered proportional to the number of switchings (the switching frequency). A power-loss study would demand a rigorous model of the switching device, and this would consequently imply an extremely long computational time. With the

objective of simplifying the circuit to be analyzed, while retaining the ideal waveforms of voltages and currents associated with the PWM operation, the IGBT switches have been considered as ideal devices, and no snubbers have been used in the active source. They present the same preset value of forward voltage drop, and change from the off-state to the on-state, and vice-versa, the same way as the idealized thyristor models. Further, they also turn off whenever the firing pulse is removed.

Another idealization concerning the PWM operation is that the power semiconductor switches are allowed to turn on and off at any rate. This implies that, at maximum points of the voltage-reference signal which have approximately the same value as the triangular carrier waveform, the IGBT switches would turn on and immediately off, almost instantaneously. This occurrence has intentionally been represented in Figure 5.5 in Chapter 5. In such regions of the voltage-reference signal, a practical implementation would avoid these stresses and switching losses by not allowing the pulse to be removed from the semiconductor's gate until a minimum period of time has elapsed and the reference signal is below a preset value.

7.2.3 Active Source

This thesis has considered a simplified version of the rectifier-converter/outputcapacitor set of the active source. They are represented by one ideal variable DC-voltage source which is instantaneously updated, at the end of each fundamental period, to the highest peak value of the voltage-reference signal (given by the active-filter control) that occurred during the previous period. However, it instantaneously responds to any increase in the voltage-reference signal that surpasses the previous DC voltage level. This simplification reduced the order of the system without affecting the issues of principal concerns in this thesis and saved computation time.

The amplitude of the triangular carrier of the PWM inverter is also updated at the end of each fundamental period to 1% higher than the largest peak-to-peak value of the voltage-reference signal that occurred during the previous fundamental period. Further, at any time, it immediately tracks a rise in the reference signal that surpasses the currently set amplitude of the carrier.

7.2.4 The Phase-Locked-Loop Filter

The PLL filter, which, for the reasons explained in Section 6.5, had to be designed to have a slow time constant, demands a long computation time for reaching the steady-state operation from the initialization point. Furthermore, since the simulations performed would not involve frequency changes, the inclusion of the PLL model in the simulations was inconsequential to the steady-state results. As an illustration, the simulation of a simplified AC/DC test system, without including the active-filter circuits and their controls, required 100 s of simulation time for the PLL to accurately reach its steady-state operation. This simulation was done over a 5-day computation period.

For the purposes of the results presented in this thesis, the required computation time placed a practical limitation in combining the PLL simulation with the active filter. The research was therefore continued to validating the PLL in isolation from the active-filter performance. Since the presented results assume no frequency deviations, instead of the PLL, a single-tuned filter, tuned at the fundamental frequency, and with quality factor $Q = 10$ has been used. The transfer function of this filter is given by

$$F(s) = \frac{0.2653\,s}{7.0362 \times 10^{-6}s^2 + 2.6526 \times 10^{-4}s + 1}. \tag{7.1}$$

7.2.5 Simulation Time and Second-Harmonic Oscillations

SABER is not able to initialize a circuit for a dynamic simulation from a frequency-domain point of view as is usually convenient in power systems applications. Instead, given the voltages across all the capacitors and currents through all the inductors of a circuit, it finds a DC operation point in the time domain. It is worthwhile noting that in a DC-solution scenario, voltage drops across inductances and currents through capacitors are zero. Specifically, the large inductance and reduced resistance of the converter transformers present a very large time constant and posed initialization hurdles.

Therefore, to avoid the prohibitively large amount of simulation time for the system to reach the steady state from a DC solution, a set of initial conditions were required to be crafted in MATLAB and manually input in SABER. All the simulation cases have been run in the same fashion. The DC solution was first obtained from

the set of initial conditions. Then, the AC/DC system was simulated from the DC solution until a reasonably steady state was reached.

The proportional and integral gains of the current control of the HVDC system, being extremely small, require a rather long simulation time until the system is absolutely free from second-harmonic oscillations caused by the initialization process and the AC-system parallel resonance. Therefore, to save computational time, it was decided to tolerate a small amount of second-harmonic oscillations and simulate the AC/DC system for only 18 cycles. In fact, the presence of small second-harmonic oscillations can be seen as an extra stability test posed to active-filter control.

All the waveforms presented in this chapter are those of the last simulated fundamental period (283.33 ms to 300 ms). The observed DC-line voltage and current at the rectifier terminal are in agreement with the theoretical waveforms presented in Chapter 2. The required computational time for the simulation of the complete test system is approximately two and half hours for each fundamental period.

7.3 Simulation of the Original 60-Hz HVDC Benchmark System

The simulation of the steady-state operation of the 60 Hz version of the Modified HVDC Benchmark System, shown in Figure 4.2, in Chapter 4, has been carried out with the objective of allowing a quantitative comparison of the performance of the active filtering against the passive-filtering concept in Sub-Section 7.6.1 of this Chapter.

Figures 7.1 to 7.5 are pertinent to the current balance at the point where the original AC passive-filter branches are connected to the HVDC terminal. Figure 7.1 shows the AC line currents of the HVDC converter, and Table 7.1 presents the corresponding noteworthy harmonic contents and individual harmonic distortions in phase *a*.

The harmonic content is in qualitative agreement with Table 2.1 in Chapter 2. Figure 7.2 shows the total currents diverted to the ground by the AC passive filters. Note that these currents carry a significant amount of fundamental component. This

fundamental component corresponds to the reactive power that is provided by the AC passive-filter branches. This component is also evident in Table 7.2, which presents the harmonic magnitudes and phase angles in phase a, together with their percentages with respect to the fundamental component of the HVDC-converter line current.

The sums of the currents that flow to the HVDC converter terminal and down the original AC passive-filter branches are presented in Figure 7.3. The waveforms are far from pure sinusoids, and this is an inherent characteristic of the passive filtering. The amount of harmonic content that has not been properly filtered by the original passive-filter branches and the corresponding percentage with respect to the fundamental component of the HVDC-converter line current are quantitatively shown in Table 7.3.

This table shows that the amount of fundamental component provided by the AC system and the shunt capacitor bank has been reduced due to the reactive power support provided by the AC passive-filter banks. It is also clear that the amount of compensation of harmonics is far from perfect for the first two characteristic harmonics and deteriorates for the higher-order ones. It is worthwhile noting that this trend follows the frequency characteristics of the total AC passive-filter banks depicted in Figure 4.4 in Chapter 4.

All the harmonic content that has not been filtered must flow through the AC system and the shunt capacitor bank. The percentage of harmonic current that flows through the shunt capacitor bank satisfies the "current divider" rule. Since the shunt capacitor bank provides a much lower impedance at these harmonic frequencies than the AC system, practically all the harmonic currents that the AC passive-filter bank failed to compensate flow through the capacitors. These harmonic currents are highly visible in Figure 7.4 and their existence should be accounted for at the design stage of a real HVDC system. Figure 7.5 confirms that the current flowing from the AC system is practically free from harmonic currents.

Figure 7.6 shows the AC voltage waveform at the HVDC converter terminal (across the shunt capacitor bank). Table 7.4 presents the harmonic distortion indices that, although small, cause the slightly visible waveform distortion.

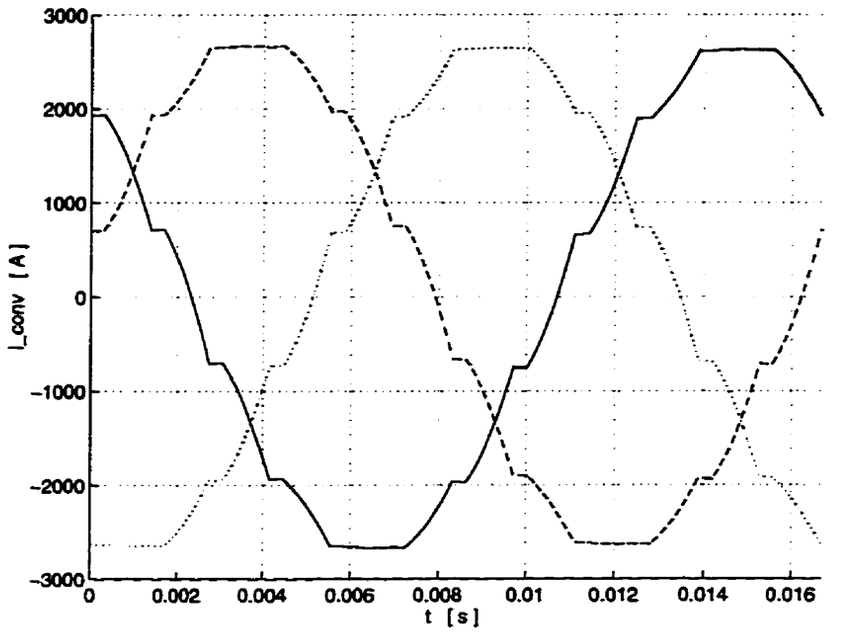

Figure 7.1: HVDC-converter AC line currents with the original AC passive-filter branches (— phase a,— phase b, ··· phase c).

Table 7.1: Harmonic content of the HVDC-converter AC line current in phase a with the original AC passive-filter branches.

Harmonic Order	Amplitude [A]	Phase [°]	IHD [%]
1	2688.07	- 50.12	100.00
2	0.17	169.79	0.00
11	94.49	- 15.49	3.52
13	52.20	- 123.61	1.94
23	24.52	- 29.05	0.91
25	20.00	- 132.62	0.74
35	8.39	- 45.33	0.31
37	8.87	- 151.38	0.33
47	2.51	- 31.42	0.09
49	3.19	- 159.09	0.11

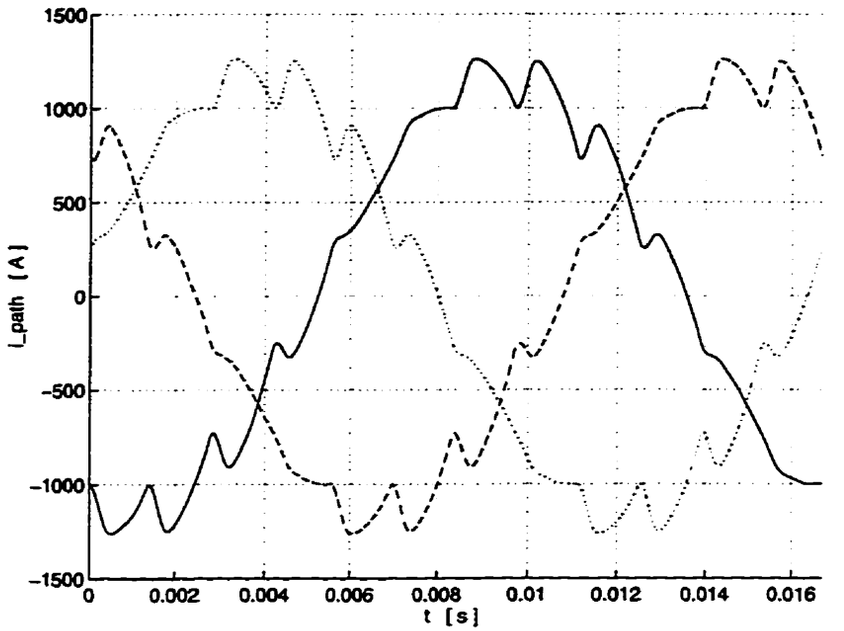

Figure 7.2: Total currents of the original AC passive-filter branches (— phase a,— phase b, ··· phase c).

Table 7.2: Harmonic content of the total current of the original AC passive-filter branches in phase a.

Harmonic Order	Amplitude [A]	Phase [°]	[%]
1	1180.54	68.10	43.92
2	0.65	67.50	0.02
11	88.98	158.43	3.31
13	50.85	46.33	1.89
23	24.07	113.46	0.90
25	18.86	4.72	0.70
35	6.01	73.89	0.22
37	6.00	- 34.51	0.22
47	1.30	77.32	0.05
49	1.59	- 51.27	0.06

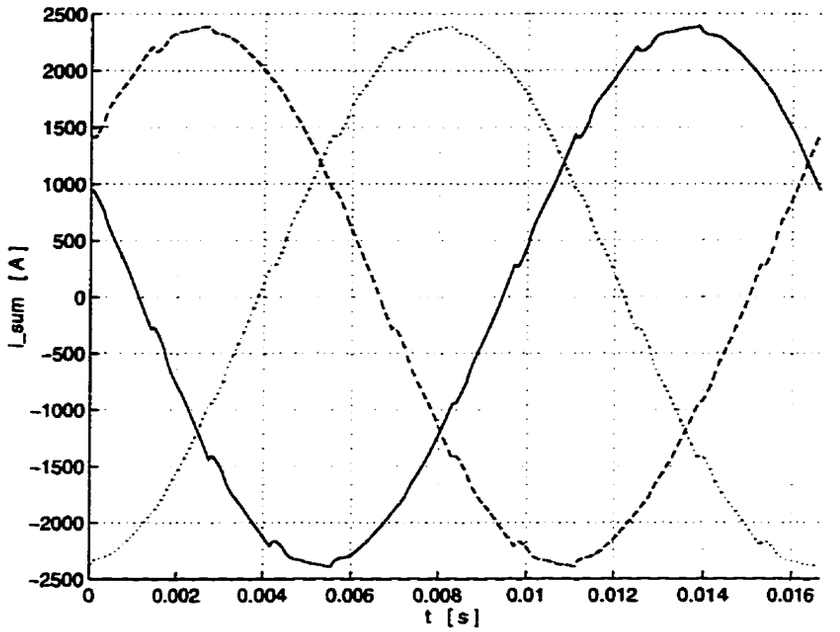

Figure 7.3: HVDC-converter AC line currents which have not been filtered by the original AC passive-filter branches (— phase a,— phase b, ··· phase c).

Table 7.3: Harmonic content of the HVDC-converter AC line current in phase a which has not been filtered by the original AC passive-filter branches.

Harmonic Order	Amplitude [A]	Phase [°]	[%]
1	2370.10	- 24.09	88.17
2	0.64	82.20	0.02
11	11.18	41.97	0.42
13	9.13	- 47.13	0.34
23	15.62	40.67	0.58
25	14.18	- 68.23	0.53
35	7.57	- 1.45	0.28
37	8.16	- 110.37	0.30
47	2.42	- 1.02	0.09
49	3.10	- 129.86	0.12

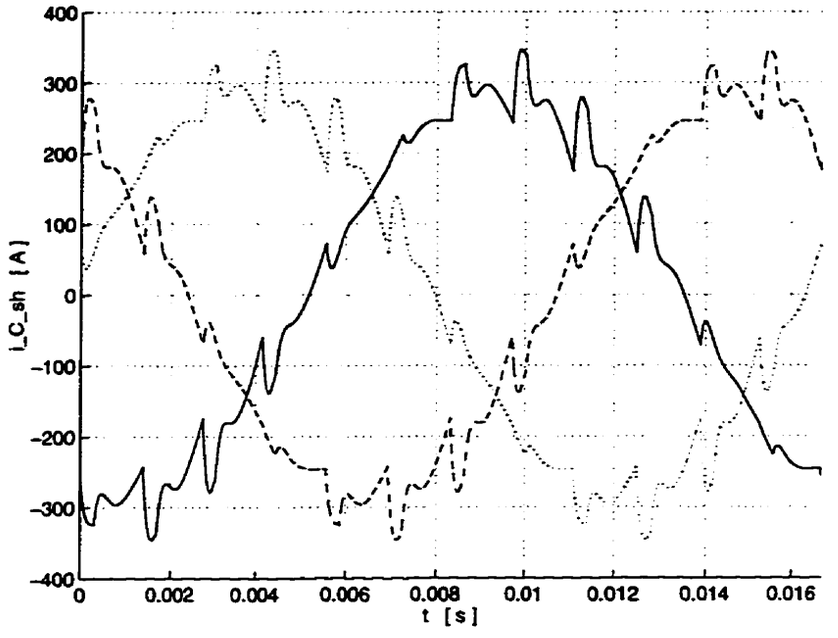

Figure 7.4: Currents through the shunt capacitor banks with the original AC passive-filter branches (— phase a,— phase b, ··· phase c).

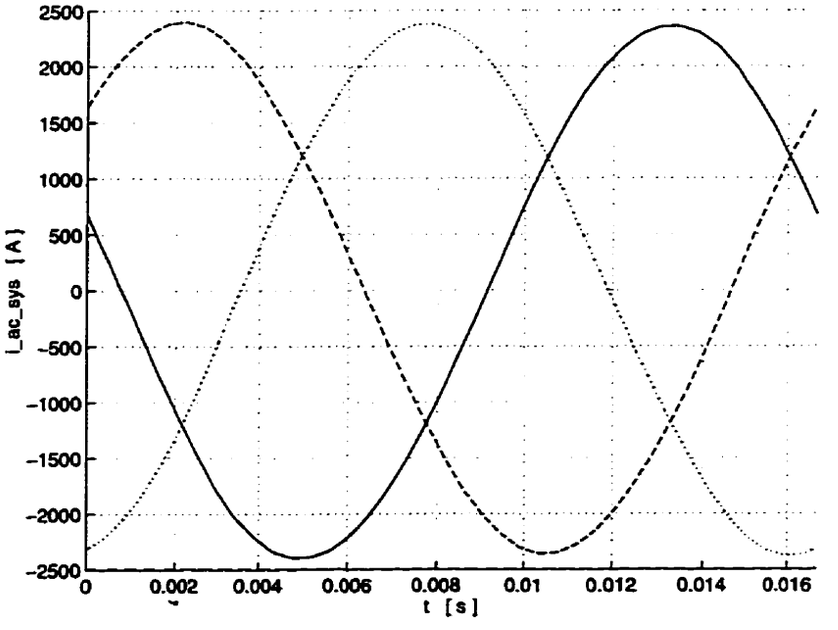

Figure 7.5: AC-system currents with the original AC passive-filter branches (— phase a,— phase b, ··· phase c).

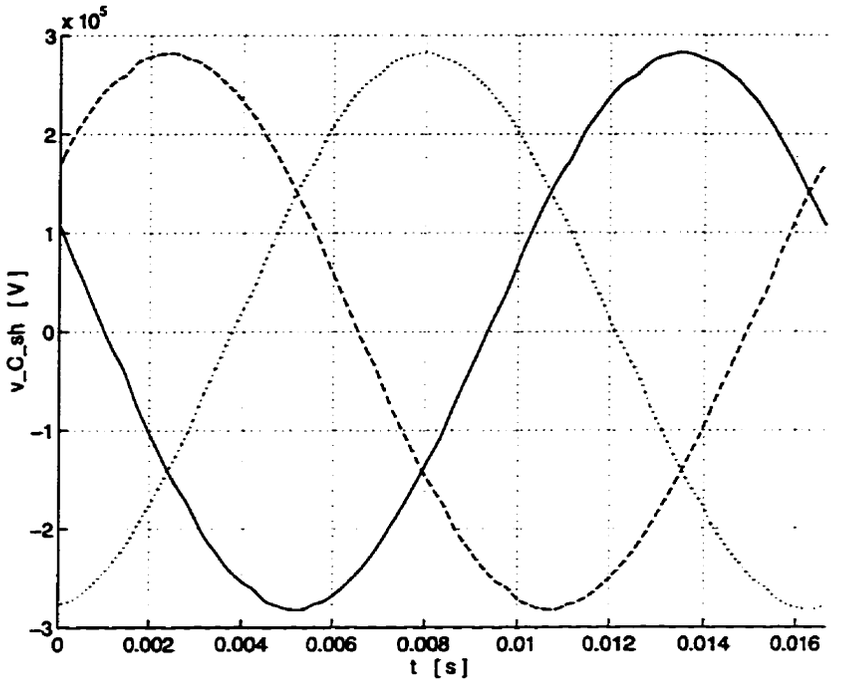

Figure 7.6: AC voltages at the HVDC-converter terminal (across the shunt capacitor banks) with the original AC passive-filter branches (— phase a,— phase b, ··· phase c).

Table 7.4: Harmonic content of the AC voltage in phase a at the HVDC-converter terminal (across the shunt capacitor banks) with the original AC passive-filter branches.

Harmonic Order	Amplitude [V]	Phase [°]	IHD [%]
1	281251.39	- 21.84	100.00
2	71.57	- 22.37	0.03
11	1163.21	134.47	0.41
13	757.17	44.83	0.27
23	669.67	131.49	0.24
25	554.96	22.55	0.20
35	207.32	88.85	0.07
37	211.60	- 20.15	0.08
47	47.66	87.39	0.02
49	61.38	- 41.08	0.02

7.4 Simulation of the Modified 60-Hz HVDC Benchmark System with the Active Filters Disabled

The objective of this section is to demonstrate the effect that the active-filter circuit, when inoperative, has on steady-state operation of the AC/DC system. In this simulation, the complete test system used in this research is modelled. The complete active-filter circuit substitutes the original AC passive filter, and the capacitance of the original shunt capacitor bank is increased as to supply the reactive power that was previously suplied by the original AC passive-filter bank. The new component values are those determined in Chapter 5 and the system can be seen in Figure 7.7.

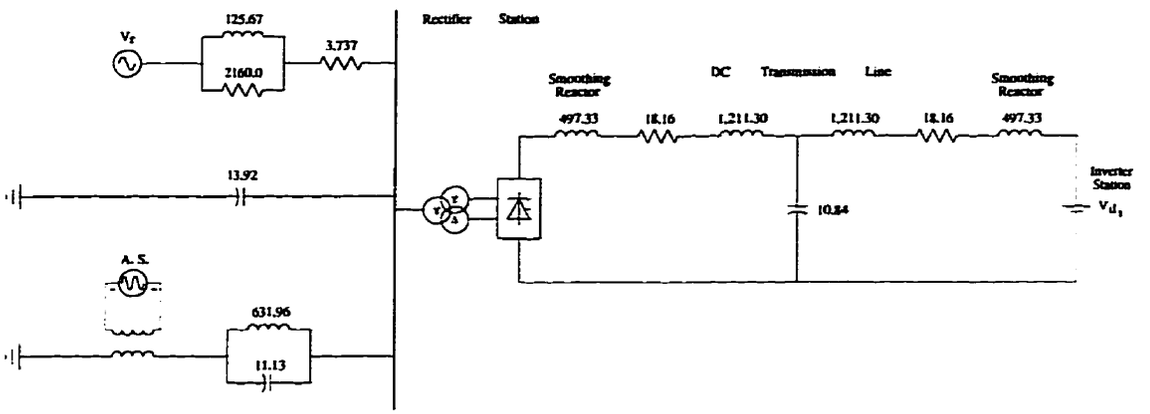

Figure 7.7: The AC/DC test system used in the research [Ω, mH, μF].

Although connected to the system, the active filter is disabled by forcing the voltage reference to the active-source rectifier and PWM inverter (the active source) to zero $v_{ref} = 0$.

Figures 7.8 to 7.12 consider the current balance at the point where the path impedance of the active filter connects to the system. Figure 7.8 illustrates the three AC line currents of the HVDC converter. The noteworthy harmonic components and their corresponding Individual Harmonic Distortion indices pertaining to phase a are presented in Table 7.5 and are in good qualitative agreement with Table 2.1 in Chapter 2.

Figure 7.9 shows the currents that passively flow through the active-filter circuit.

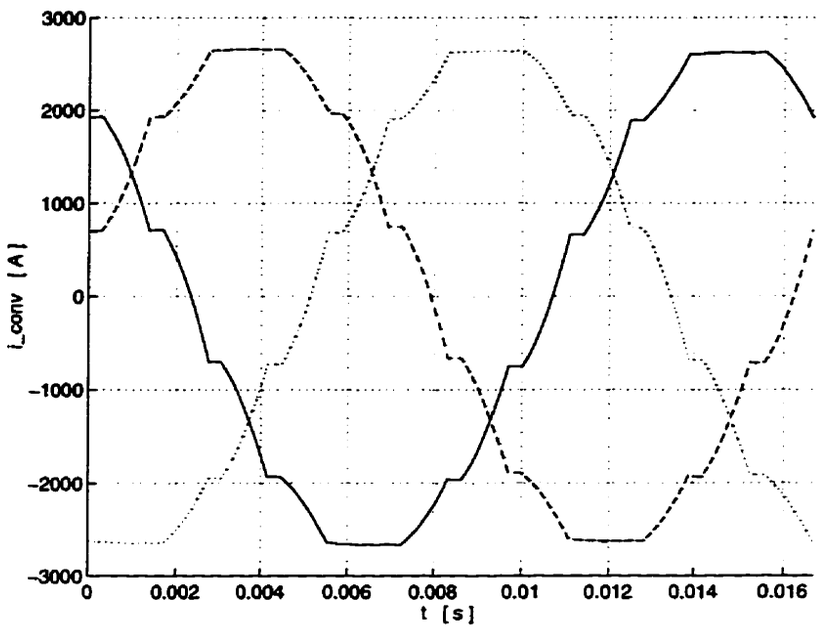

Figure 7.8: HVDC-converter AC line currents with the active filter disabled (— phase a,— phase b, ··· phase c).

Table 7.5: Harmonic content of the HVDC-converter AC line current in phase a with the active filter disabled.

Harmonic Order	Amplitude [A]	Phase [°]	IHD [%]
1	2684.58	- 50.15	100.00
2	0.64	146.58	0.02
11	95.48	- 15.84	3.56
13	53.16	- 123.92	1.98
23	24.46	- 28.60	0.91
25	20.02	- 132.39	0.75
35	8.39	- 42.71	0.31
37	8.84	- 149.25	0.33
47	2.61	- 27.54	0.10
49	3.23	- 155.05	0.12

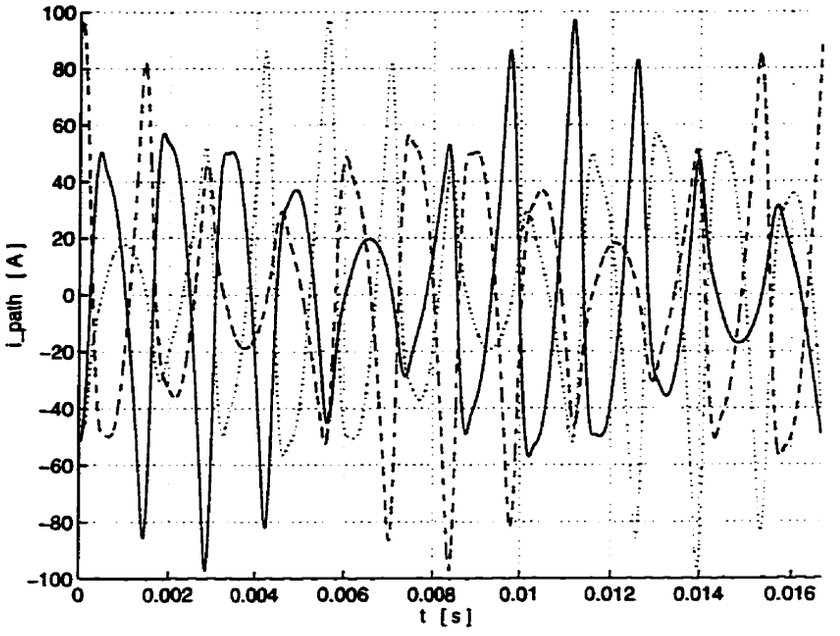

Figure 7.9: Path-impedance currents with the active filter disabled (— phase a,-- phase b, ··· phase c).

Table 7.6: Harmonic content of the path-impedance current in phase a with the active filter disabled.

Harmonic Order	Amplitude [A]	Phase [°]	[%]
1	0.00	- 47.52	0.00
2	0.59	150.50	0.02
11	44.17	- 30.55	1.65
13	24.75	- 141.79	0.92
23	12.10	- 64.93	0.45
25	10.03	- 173.22	0.37
35	4.23	- 111.57	0.16
37	4.37	135.26	0.16
47	0.97	- 136.49	0.03
49	1.10	90.12	0.04

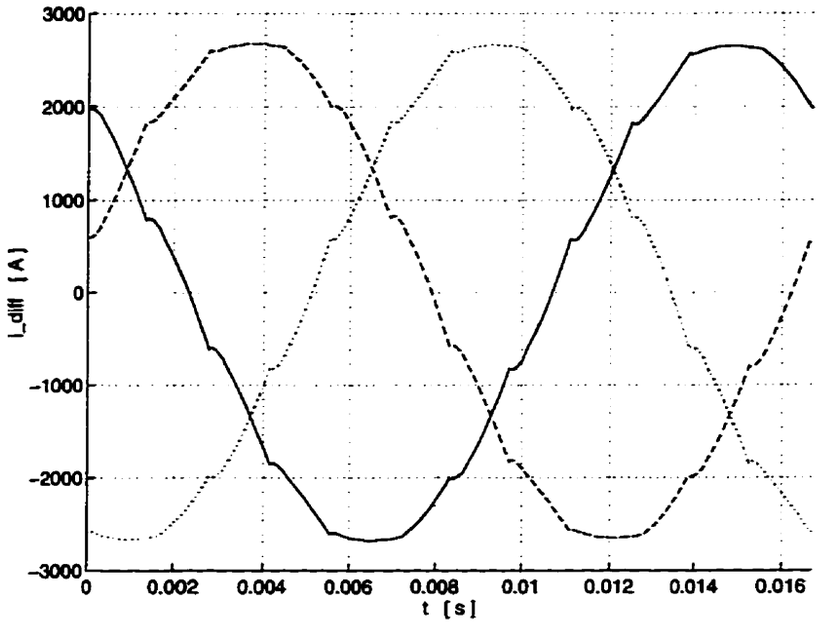

Figure 7.10: HVDC-converter AC line currents which have not been filtered with the active filter disabled (— phase a,— phase b, ··· phase c).

Table 7.7: Harmonic content of the HVDC-converter AC line current in phase a which has not been filtered with the active filter disabled.

Harmonic Order	Amplitude [A]	Phase [°]	[%]
1	2684.59	- 50.15	100.00
2	0.06	103.23	0.00
11	53.93	- 3.84	2.00
13	30.56	- 109.55	1.14
23	16.37	- 2.62	0.61
25	14.06	- 104.59	0.52
35	7.91	- 12.80	0.29
37	8.82	- 120.62	0.33
47	3.07	- 10.06	0.11
49	3.82	- 139.90	0.14

Note that the chosen path impedance prevents these currents from containing any fundamental component. This can be quantitatively confirmed in Table 7.2 which presents the harmonic contents of the current through phase a, and the respective percentages with respect to the fundamental component of the HVDC-converter line current.

The differences (or "errors") between the currents that flow to the HVDC converter terminal and the ones which are passively injected by the active-filter circuit are presented in Figure 7.10. As with the original AC passive filter, the filtering is only partial and these waveforms are not pure sinusoids. Table 7.7 quantizes the amount of harmonic content that has not been properly (passively) filtered by the active-filter circuit. The corresponding percentages with respect to the fundamental component of the HVDC-converter line current are also shown in Table 7.7.

Differently from the original AC passive filter, this circuit leaves the AC fundamental-component current untouched, meaning that the active and reactive fundamental components are being provided by the AC system and the shunt-capacitor bank. It is evident that the overall passive compensation of harmonics done by the active-filter circuit is worse than the one achieved by the original passive filter, specially for the higher-order harmonics. This suggests that the bypassing of the matching transformer of the active filter by a switch should be considered if the active filter is expected to be continuously disabled for long periods of time. The amplification of the two last characteristic harmonics is due to the excitation of the active-filter circuit resonances by the HVDC-converter line currents; however, in practice, the real circuit might be resistive enough to avoid these resonances.

This eventual bypass switching would exclude all the active-source circuit from the system and leave the path impedance directly connected to the ground. By visually analyzing the impedance characteristics of the path impedance and the one of the original passive-filter bank (Figure 5.3 in Chapter 5), it can be expected, based on the simulation of the original system, that, except for the 11th and 13th harmonics, all the other harmonics would be better diverted to the ground, should the matching transformer be bypassed.

The AC system and the shunt capacitor bank proportionally share (according to the "current divider" rule) all the harmonic content that has not been passively fil-

tered by the active-filter circuit. Again, as in the previous simulation, practically all the harmonic currents will flow through the much lower impedance of the shunt capacitor bank. Figure 7.11 displays the harmonic currents distorting the fundamental current component through the shunt capacitor bank. It is also worthwhile noting that the reactive power rating of this shunt capacitor bank is much higher than that of the original bank. Therefore, the unfiltered harmonic current flow through the new shunt capacitor bank constitutes proportionally less harmonic overload than the harmonic overload in the original system. This can be easily verified by comparing Figure 7.11 against Figure 7.4. Figure 7.12 confirms that the current flowing from the AC system is practically free from harmonic currents.

Figure 7.13 shows the AC voltage waveform at the HVDC converter terminal (across the new shunt capacitor bank). An extremely small amount of harmonic distortion can be visually noticed and confirmed by the indices presented in Table 7.8.

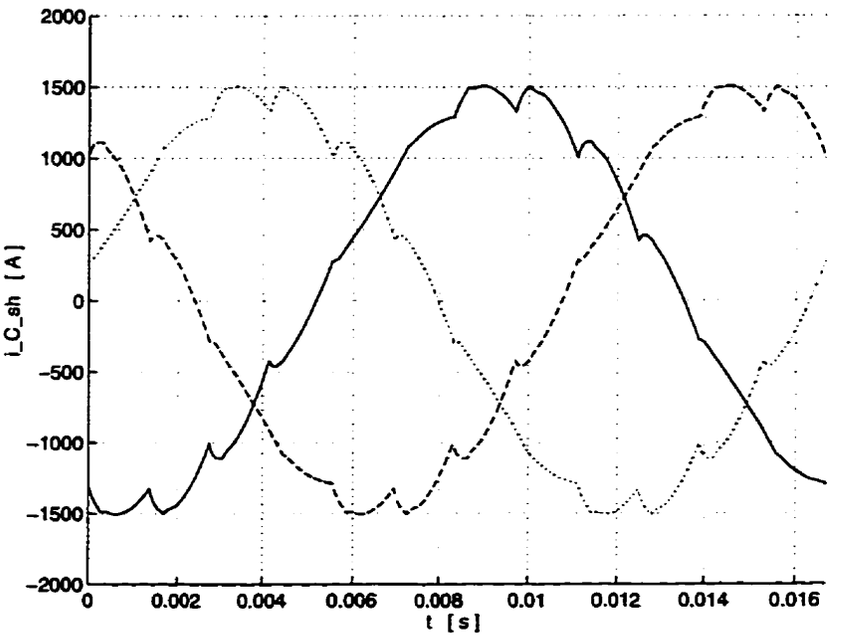

Figure 7.11: Currents through the shunt capacitor banks with the active filter disabled (— phase a,-- phase b, ··· phase c).

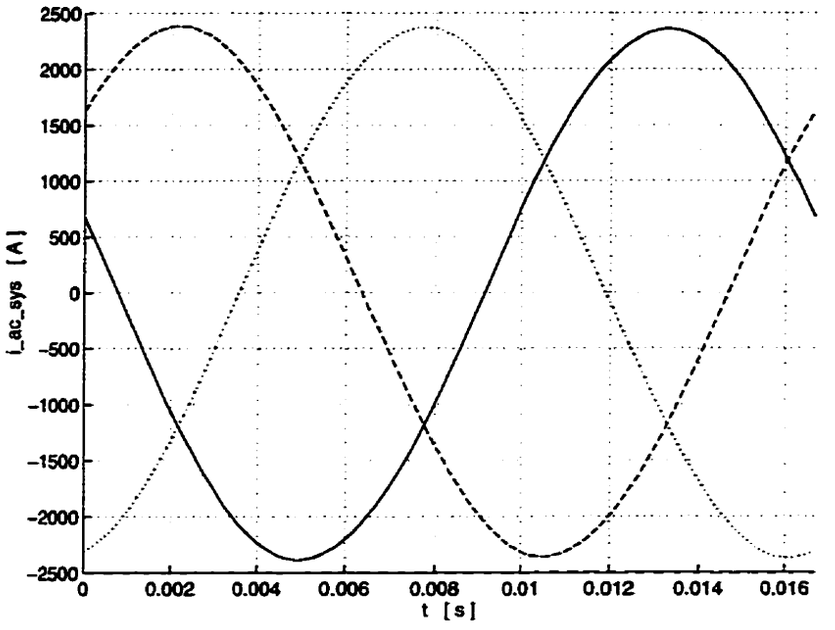

Figure 7.12: AC-system currents with the active filter disabled (— phase a,— phase b, ··· phase c).

7.5 Determination of the Matrices for Control and Estimation

As it has already been mentioned, the characteristic harmonic content of the HVDC-converter line current which is not passively filtered by the active-filter circuit is used as the reference signal for the active-filter control. This waveform is shown in Figure 7.14 and has been obtained by removing the fundamental component from the waveform in Figure 7.10. The individual harmonic content of this waveform is part of Table 7.7 and repeated in Table 7.9. During the operation of the real system, however, this waveform should not be obtained this way. Instead, it must be estimated on-line.

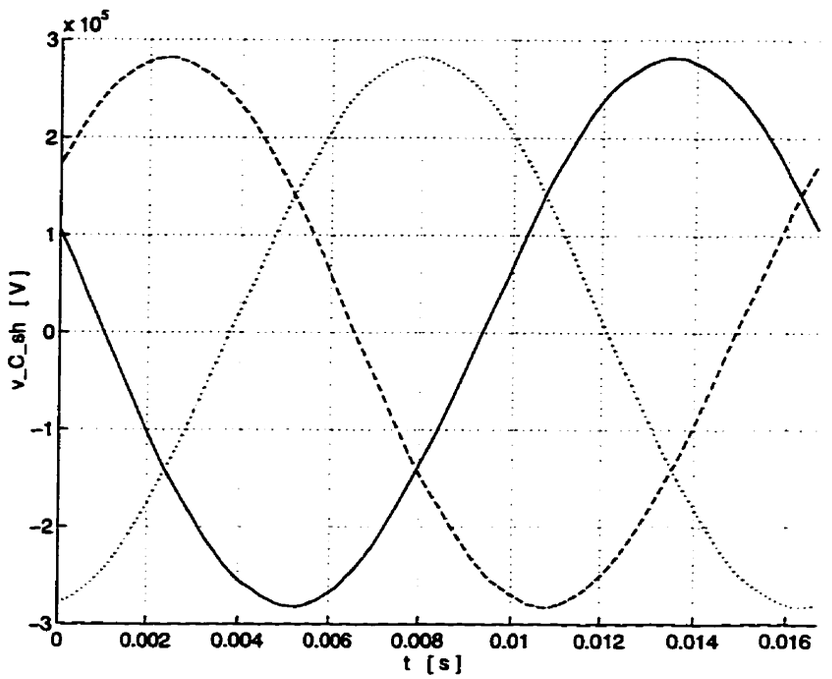

Figure 7.13: AC voltages at the HVDC-converter terminal (across the shunt capacitor banks) with the active filter disabled (— phase a,— phase b, ··· phase c).

Table 7.8: Harmonic content of the AC voltage in phase a at the HVDC-converter terminal (across the shunt capacitor banks) with the active filter disabled.

Harmonic Order	Amplitude [V]	Phase [°]	IHD [%]
1	281338.37	- 21.78	100.00
2	97.34	- 121.48	0.03
11	965.10	86.72	0.34
13	457.29	- 19.32	0.16
23	136.57	87.94	0.05
25	106.93	- 14.46	0.04
35	42.60	76.92	0.02
37	45.52	- 31.40	0.02
47	11.53	71.96	0.00
49	16.47	- 53.71	0.01

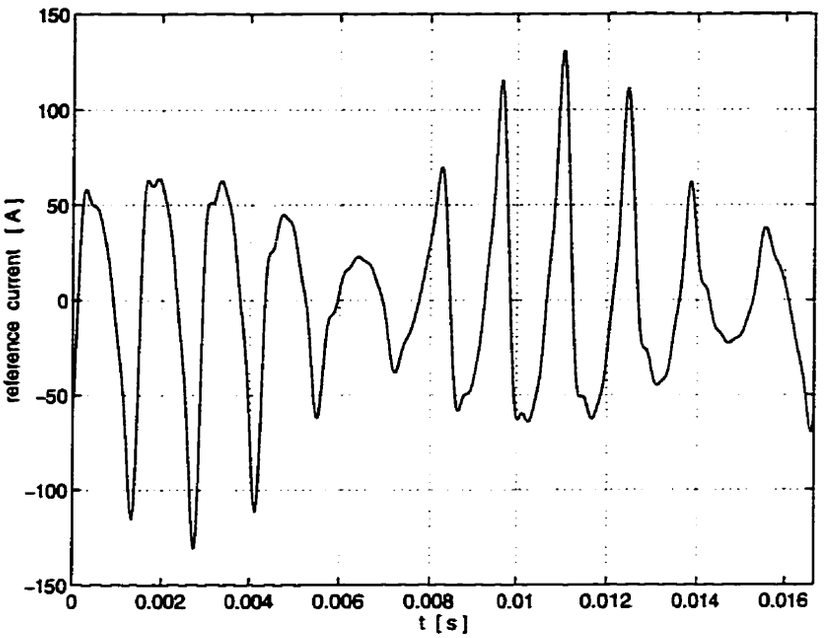

Figure 7.14: Reference-current signal for the active-filter controls.

Table 7.9: Harmonic content of the reference-current signal for the active-filter controls.

Harmonic Order	Amplitude [A]	Phase [°]
11	53.93	- 3.84
13	30.56	- 109.55
23	16.37	- 2.62
25	14.06	- 104.59
35	7.91	- 12.80
37	8.82	- 120.62
47	3.07	- 10.06
49	3.82	- 139.90

The state-variable representation of such signal requires that its poles (the eigenvalues of the characteristic matrix) be at the harmonic angular frequencies. Therefore, these eight pure pairs of pure complex conjugate poles must be

$$\sigma_{ref} = \begin{bmatrix} 0 + j0.4147 \\ 0 - j0.4147 \\ 0 + j0.4901 \\ 0 - j0.4901 \\ 0 + j0.8671 \\ 0 - j0.8671 \\ 0 + j0.9425 \\ 0 - j0.9425 \\ 0 + j1.3195 \\ 0 - j1.3195 \\ 0 + j1.3949 \\ 0 - j1.3949 \\ 0 + j1.7719 \\ 0 - j1.7719 \\ 0 + j1.8473 \\ 0 - j1.8473 \end{bmatrix}. \tag{7.2}$$

As seen in Chapter 6, the plant has six of its original poles displaced onto the six poles corresponding to the first three characteristic harmonics. The state feedback matrix that accomplishes this has been calculated, in MATLAB, by applying the command "place" on matrices $\mathbf{A}_{plant}$ and $\mathbf{B}_{plant}$ used in (6.3), as being

$$\mathbf{K}_{fb} = \begin{bmatrix} -1.3316 & -0.7208 & -2.1058 & 2.6538 & 4.5498 & 0.0226 & -0.0137 \end{bmatrix}. \tag{7.3}$$

The system matrices of the plant, just modified by the new pole placement by state feedback, can now expressed by Equations (6.26) to (6.31). The characteristic matrix of the system that contains the ten reference poles that were not built into

the plant model, and is placed in series with the modified plant, is given by (7.4).

$$\mathbf{A}_{ref_{ser}} =$$

$$\begin{bmatrix}
0.0 & 0.9425 & 0.0 & 0.0 & 0.0 & 0.0 & 0.0 & 0.0 & 0.0 & 0.0 \\
-0.9425 & 0.0 & 0.0 & 0.0 & 0.0 & 0.0 & 0.0 & 0.0 & 0.0 & 0.0 \\
0.0 & 0.0 & 0.0 & 1.3195 & 0.0 & 0.0 & 0.0 & 0.0 & 0.0 & 0.0 \\
0.0 & 0.0 & -1.3195 & 0.0 & 0.0 & 0.0 & 0.0 & 0.0 & 0.0 & 0.0 \\
0.0 & 0.0 & 0.0 & 0.0 & 0.0 & 1.3949 & 0.0 & 0.0 & 0.0 & 0.0 \\
0.0 & 0.0 & 0.0 & 0.0 & -1.3949 & 0.0 & 0.0 & 0.0 & 0.0 & 0.0 \\
0.0 & 0.0 & 0.0 & 0.0 & 0.0 & 0.0 & 0.0 & 1.7719 & 0.0 & 0.0 \\
0.0 & 0.0 & 0.0 & 0.0 & 0.0 & 0.0 & -1.7719 & 0.0 & 0.0 & 0.0 \\
0.0 & 0.0 & 0.0 & 0.0 & 0.0 & 0.0 & 0.0 & 0.0 & 0.0 & 1.8473 \\
0.0 & 0.0 & 0.0 & 0.0 & 0.0 & 0.0 & 0.0 & 0.0 & -1.8473 & 0.0
\end{bmatrix} \tag{7.4}$$

Matrix $\mathbf{A}_{ref_{ser}}$, together with the other unitary vectors $\mathbf{B}_{ref_{ser}}$ in (6.35) and $\mathbf{C}_{ref_{ser}}$ in (6.37) define this series system. The resulting stable augmented system can now be completely expressed by expressions (6.39) to (6.42), and $\mathbf{A}_{aug}$ possesses all of the poles of the reference signal as its eigenvalues:

$$\sigma_{aug} = \begin{bmatrix}
0.0000 + j0.4147 \\
0.0000 - j0.4147 \\
0.0000 + j0.4901 \\
0.0000 - j0.4901 \\
0.0000 + j0.8671 \\
0.0000 - j0.8671 \\
-0.0005 + j0.0000 \\
0.0000 + j0.9425 \\
0.0000 - j0.9425 \\
0.0000 + j1.3195 \\
0.0000 - j1.3195 \\
0.0000 + j1.3949 \\
0.0000 - j1.3949 \\
0.0000 + j1.7719 \\
0.0000 - j1.7719 \\
0.0000 + j1.8473 \\
0.0000 - j1.8473
\end{bmatrix}. \tag{7.5}$$

At this point, the conversion of the problem into one of the regulator type can be done by means of expressions (6.59) to (6.63). The weighting matrices $\mathbf{Q_3}$ in (6.56) (determining $\mathbf{Q_1}$), $\mathbf{Q_2}$ in (6.57) and $\mathbf{R}$ in (6.49) have been derived by means of trial and error during simulation tests to produce an adequate dynamic performance with practically achievable gains, i.e. the final choice of values provided a good settling time after disturbances with reasonable values of entries for the control matrix $\mathbf{K}$.

It has been verified that the dynamic performance of the control is most sensitive, by similar amounts, to the states $v_{C_{sh}}$, v_{C_p} and $i_{L_{lp}}$, and that the sensitivity to the other states is negligible. Therefore, except for the diagonal entries corresponding to the states x_{aug_1}, x_{aug_2} and x_{aug_7}, which are all set to 0.01, all other entries of $\mathbf{Q_3}$ are set to zero.

The value of the weighting matrix responsible for the output-error cost has been set to $\mathbf{Q_2} = 5$. Since the sensitivity of the dynamic performance of the active-filter control to the control energy cost was found to be negligible, $\mathbf{R}$ has been set to 1.

The solution of the Riccati equation in (6.69) with these weighting matrices and (6.70) provide the following control matrix:

$$\mathbf{K} = \begin{bmatrix} \mathbf{K_1} & \mathbf{K_2} \end{bmatrix}$$

$$\mathbf{K_1} = \begin{bmatrix} 237.9508 & -196.0796 & -19.9705 & -968.8383 & -2393.1718 & 207.2800 & -136.3062 \end{bmatrix}$$

$$\mathbf{K_2} = \begin{bmatrix} -806.8024 & -605.6088 & -109.6755 & -206.2305 & -88.6762 \\ & & & & -179.7607 & -37.3100 & -106.7064 & -32.0500 & -98.2373 \end{bmatrix}.$$

The determination of matrix $\mathbf{R}$ in Equation (6.76) for the estimation of the states of the reference signal has also been done by trial and error. A value of $\mathbf{R} = 10^{-11}$ ensured that the reference estimation would be fast enough in relation to the optimal control of the active filter and yield reasonable values for the gain matrix $\mathbf{K}_{est}$. The

resulting gain matrix is

$$\mathbf{K}_{est} = \begin{bmatrix} -6722.0458 \\ -22017.4671 \\ 10144.0406 \\ 8490.9608 \\ 7849.8753 \\ 7927.7023 \\ -65323.3984 \\ -17433.0277 \\ 17631.6736 \\ -22488.9063 \\ 22670.9614 \\ -23181.7846 \\ 23359.1928 \\ -24721.7373 \\ 24870.3574 \\ 24649.2228 \\ -24791.3166 \end{bmatrix}. \tag{7.6}$$

7.6 Simulation Test of the Active Filter

7.6.1 Steady State

This section presents the steady-state operation of the complete AC/DC system including the fully-operative active filter.

Figures 7.15 to 7.22 relate to the current balance at the HVDC converter station bus. Figure 7.15 shows the line currents feeding the HVDC converter station. The harmonic content of the HVDC-converter-station line current in phase a is shown in Table 7.10 together with the IHD indices.

These values are in close agreement with Table 2.1 in Chapter 2. The currents flowing through the path impedances, in each one of the three phases, and injected into the AC/DC system are shown in Figure 7.16. The current in phase a is repeated in Figure 7.17 for clarity.

Figure 7.18 shows the frequency spectrum of the path impedance current in phase *a*. This frequency spectrum is repeated in Figure 7.19 with a reduced range of the amplitude axis.

Figure 7.19 demonstrates that this harmonic content does not include significant amount of harmonics due to the switching frequency of the active source or of any order other than the characteristic HVDC AC harmonics being actively filtered. The amplitudes and phases of the relevant harmonics of the current through the path impedance in phase *a*, as well as their relative errors with respect to the corresponding harmonic content of the HVDC-converter line current, are all quantified in Table 7.11. As expected, due to the decreasing ratio between the switching frequency of the PWM inverter and the frequencies of the higher-order harmonics, the active-filter performance, although still better than the original passive-filter banks, deteriorates both in magnitude and phase as the harmonic frequency increases.

The differences between the HVDC converter line currents and the currents injected through the path impedances reflect the error of the active-filter output. These waveforms, which should ideally be pure sinusoids, are presented in Figure 7.20. Table 7.12 demonstrates that the harmonic content that is not properly cancelled is far less than that obtained in the original system with passive-filter banks.

Finalizing the harmonic-current balance analysis, Figures 7.21 and 7.22 respectively show the currents that flow into the new capacitor bank and from the AC system. All the negligible harmonic content which has not been successfully canceled by the active filter is drawn by the shunt capacitor. This harmonic content by no means overloads the shunt capacitors. In Figure 7.22, it can be noticed that the line currents flowing from the AC system are, for practical effects, pure sinusoids.

Figure 7.23 shows the practically clean phase voltages at the HVDC-converter bus. This is credited to the fact that, besides the excellent performance of the active filter, no harmonic sources have been represented in the AC system. Table 7.13 confirms the extremely low harmonic content of the bus in question.

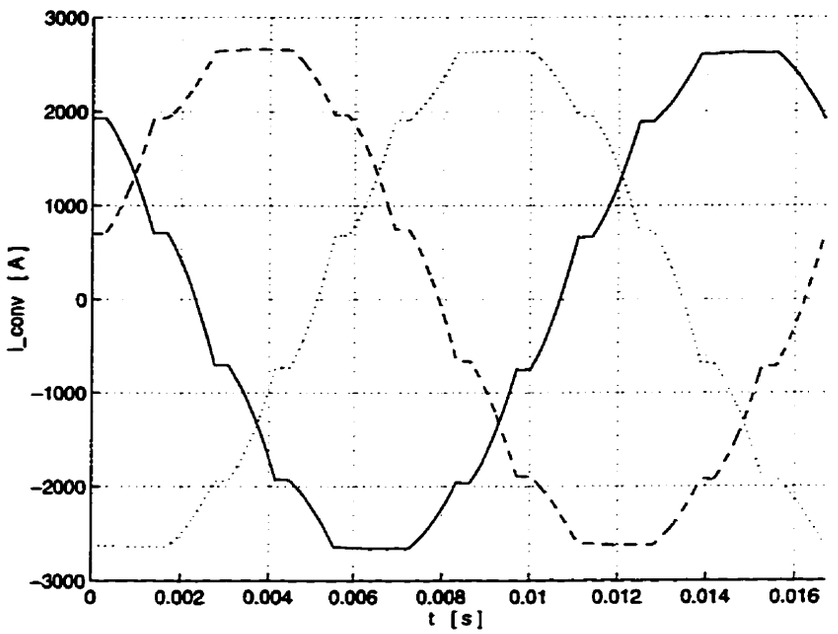

Figure 7.15: HVDC-converter AC line currents with the active filter enabled (— phase a, — phase b, ··· phase c).

Table 7.10: Harmonic content of the HVDC-converter AC line current in phase a with the active filter enabled.

Harmonic Order	Amplitude [A]	Phase [°]	IHD [%]
1	2690.88	- 49.93	100.00
2	1.34	- 32.18	0.05
11	98.04	- 16.86	3.64
13	54.29	-127.66	2.02
23	28.97	- 31.53	1.08
25	22.65	-141.17	0.84
35	13.61	- 51.16	0.51
37	11.64	-169.03	0.43
47	6.80	- 74.65	0.25
49	5.13	161.94	0.19

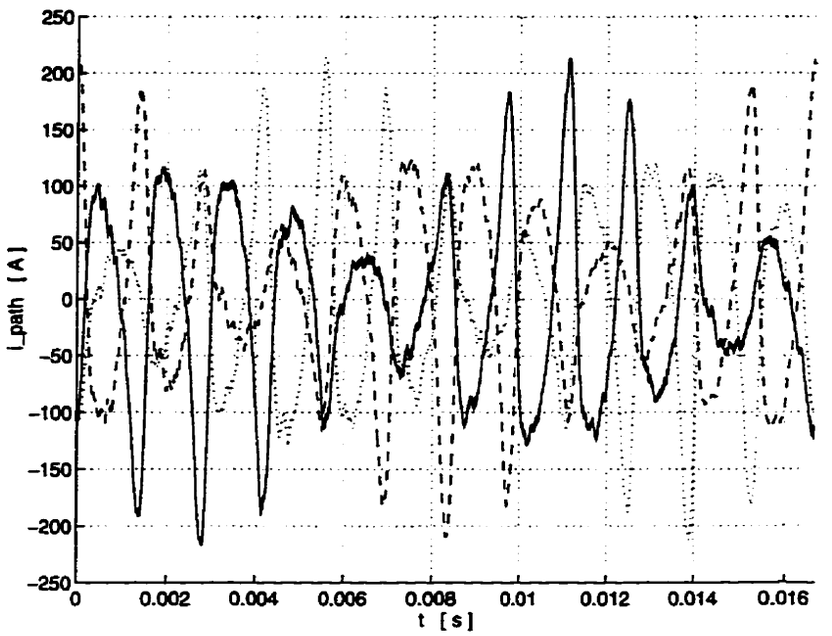

Figure 7.16: Path-impedance currents with the active filter enabled (— phase a, — phase b, ··· phase c).

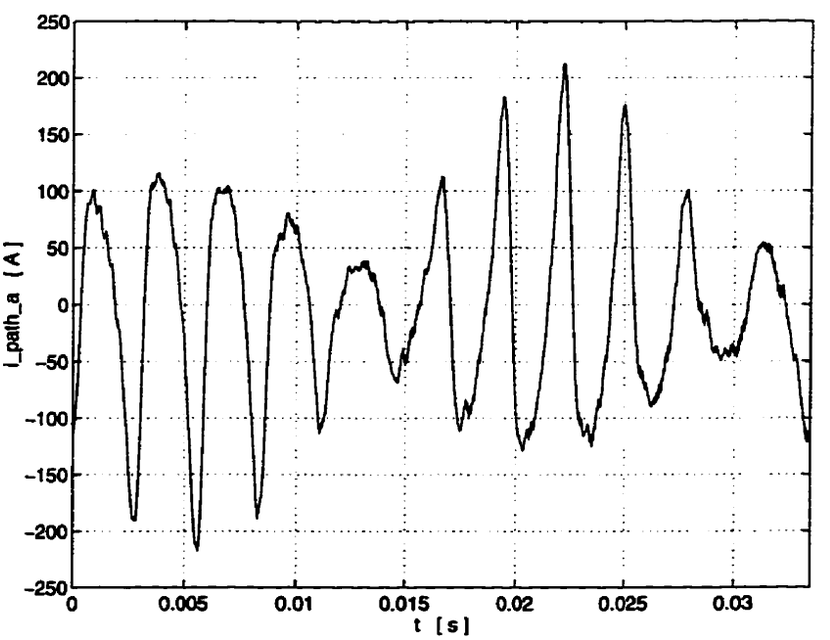

Figure 7.17: Path-impedance current in phase a with the active filter enabled.

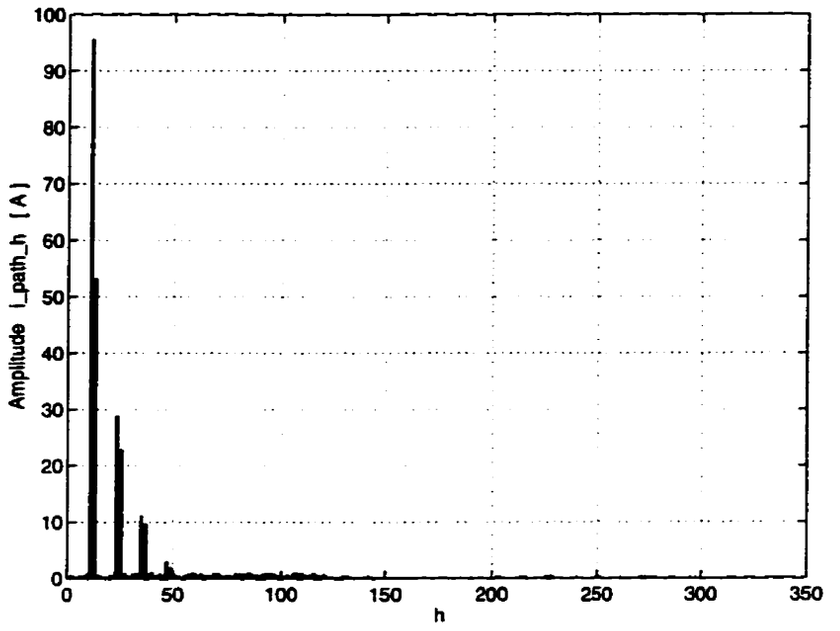

Figure 7.18: Frequency spectrum of the path-impedance current in phase a with the active filter enabled.

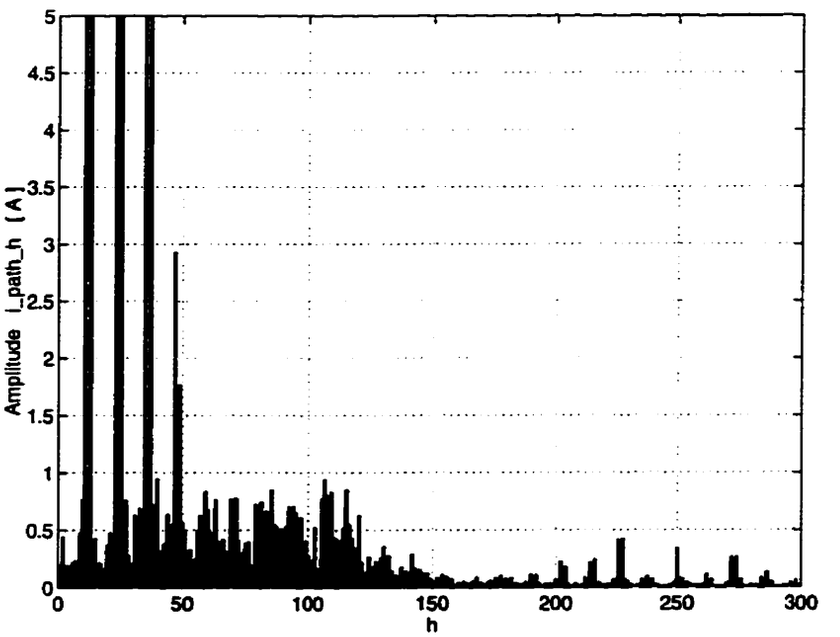

Figure 7.19: Frequency spectrum of the path-impedance current in phase a with the active filter enabled (reduced range of the amplitude axis).

Table 7.11: Harmonic content of the path-impedance current in phase *a* with the active filter enabled.

Harmonic Order	Amplitude [*A*]	Amplitude Error [%]	Phase [°]	Phase Error [%]	[%]
1	0.19	–	- 52.98	–	0.01
2	0.44	–	161.47	–	0.02
11	95.51	- 2.58	- 17.50	3.79	3.54
13	53.09	- 2.21	-128.75	0.85	1.97
23	28.70	- 0.93	- 35.14	11.45	1.07
25	22.68	0.13	-144.23	2.17	0.84
35	10.97	- 19.40	- 56.78	10.99	0.41
37	9.63	- 17.27	-174.16	3.03	0.36
47	2.93	- 56.91	- 98.85	32.41	0.11
49	1.77	- 73.97	128.02	- 20.95	0.07
250	0.29	–	46.28	–	0.01

Figures 7.24 to 7.27 display waveforms concerning the active-source rectifier and PWM inverter connected to phase a. Figure 7.24 shows the PWM voltage-reference signal generated by the optimal control. The maximum peak of this signal determines the DC voltage of the rectifier of the active source. The envelope formed by the hundreds of pulses that occur during one fundamental period is presented in Figure 7.25. From this figure, it can be concluded that the voltage level which the IGBT switches must be able to withstand in steady state is 3,097 V. The current waveforms that flow through the IGBT switches and the anti-parallel diodes are in Figures 7.26 and 7.27 respectively. Their respective RMS values are 83.74 A and 68.02 A. These RMS values can be used as guides to the required current ratings of these semiconductor devices.

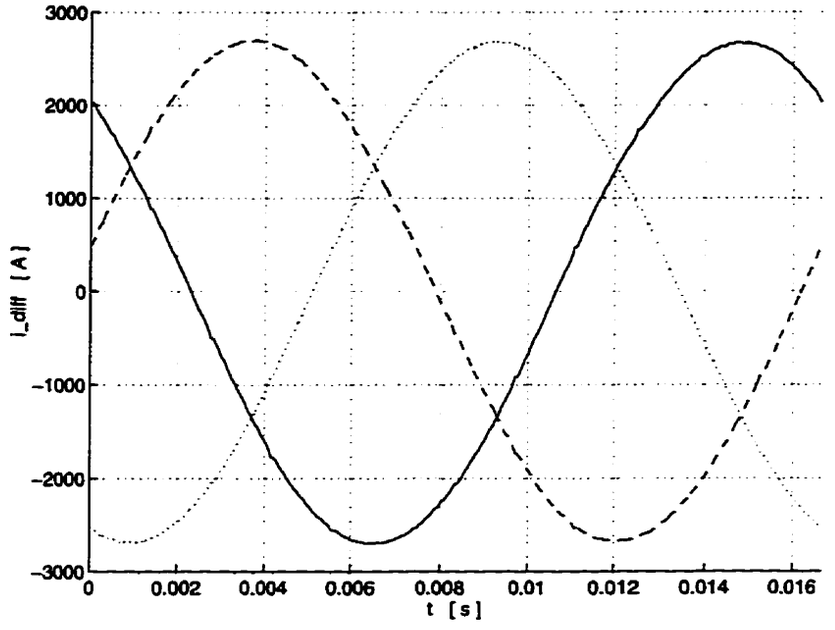

Figure 7.20: HVDC-converter AC line currents which have not not been filtered with the active filter enabled (— phase a, — phase b, ··· phase c).

Table 7.12: Harmonic content of the HVDC-converter AC line current in phase a which has not been filtered with the active filter enabled.

Harmonic Order	Amplitude [A]	Phase [°]	[%]
1	2691.07	- 49.93	100.00
2	1.77	- 28.82	0.07
11	2.75	6.15	0.10
13	1.58	- 87.84	0.06
23	1.84	48.20	0.07
25	1.21	- 51.33	0.04
35	2.90	- 29.32	0.11
37	2.22	-146.33	0.08
47	4.30	- 58.47	0.16
49	3.80	176.99	0.14

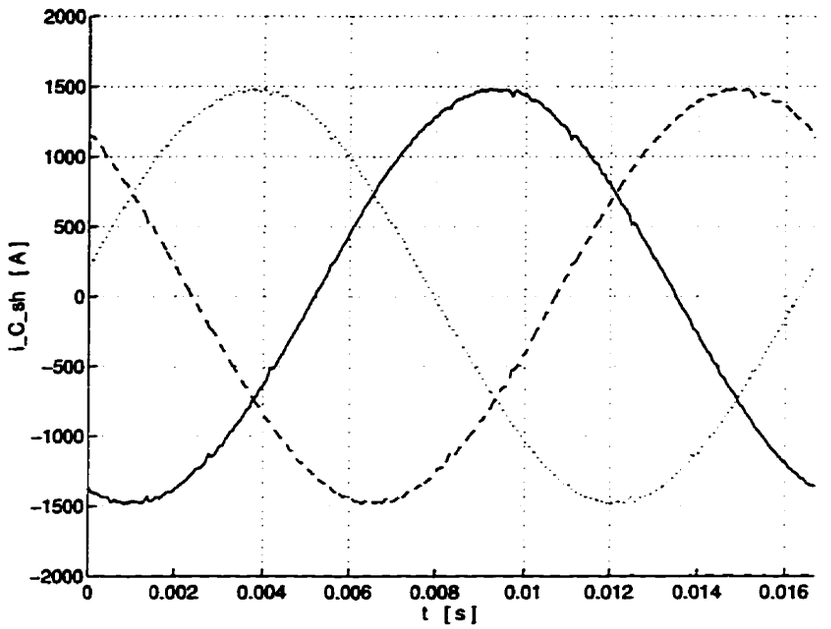

Figure 7.21: Currents through the shunt capacitor banks with the active filter enabled (— phase a, — phase b, ··· phase c).

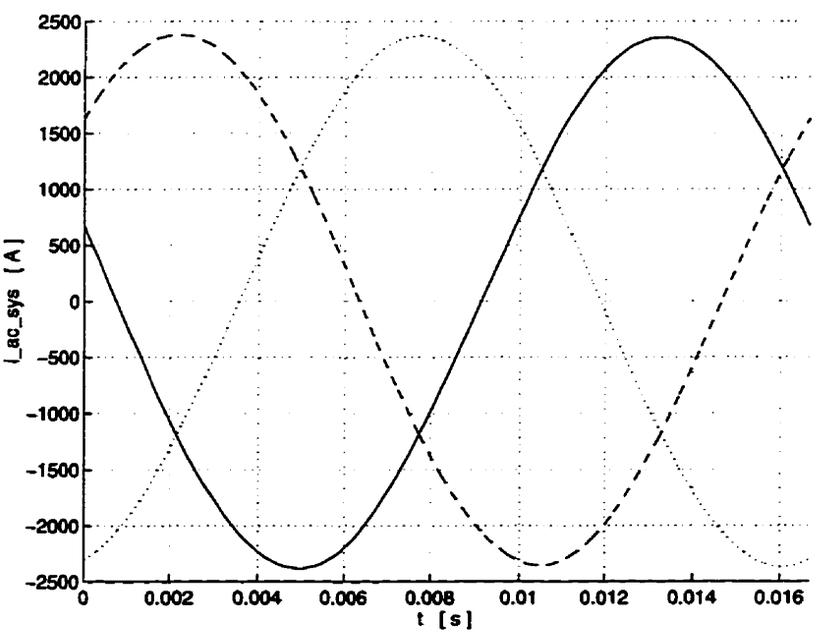

Figure 7.22: AC-system currents with the active filter enabled (— phase a, — phase b, ··· phase c).

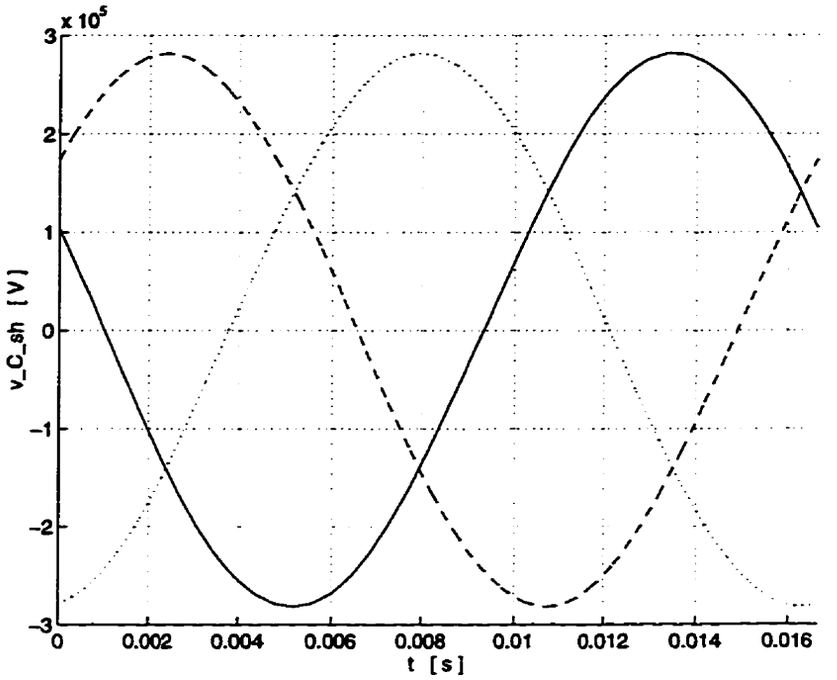

Figure 7.23: AC voltage at the HVDC-converter terminal (across the shunt capacitor banks) with the active filter enabled (— phase a, — phase b, ··· phase c).

Table 7.13: Harmonic content of the AC voltage in phase a at the HVDC-converter terminal (across the shunt capacitor banks) with the active filter enabled.

Harmonic Order	Amplitude [V]	Phase [°]	IHD [%]
1	281327.36	- 21.63	100.00
2	221.66	- 33.82	0.07
11	51.14	68.76	0.02
13	53.38	4.11	0.02
23	3.44	67.49	0.00
25	15.92	18.89	0.01
35	20.40	38.89	0.01
37	16.13	- 17.44	0.01
47	13.80	36.23	0.00
49	11.12	- 29.39	0.00

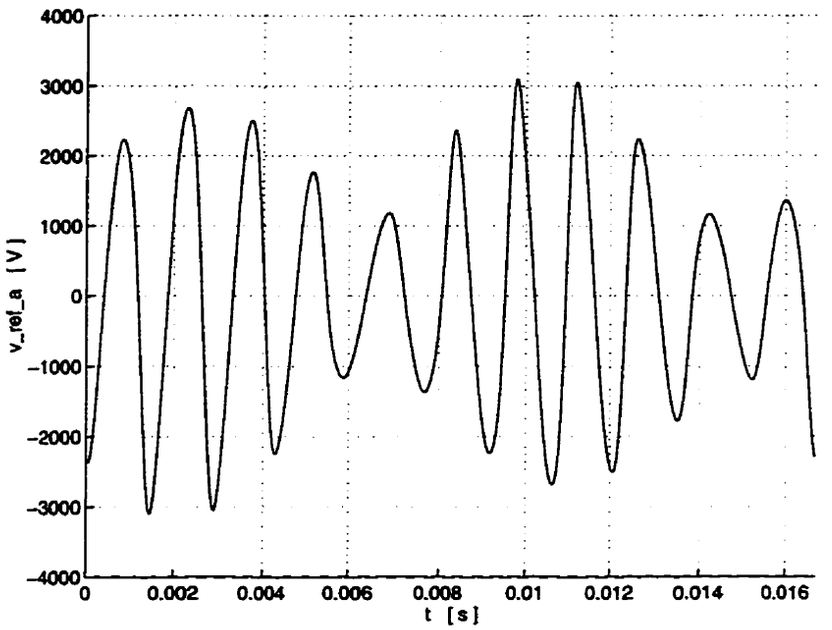

Figure 7.24: PWM voltage-reference signal for active filter in phase a.

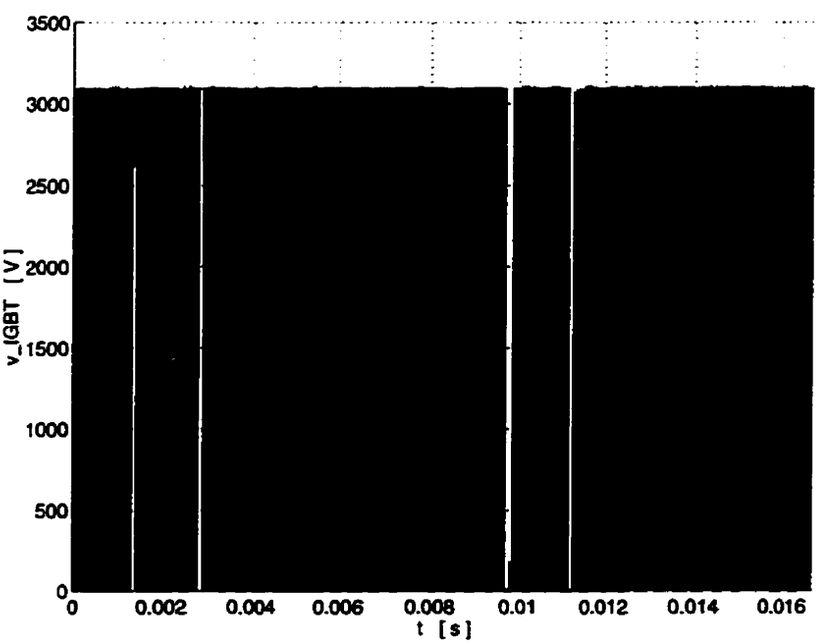

Figure 7.25: Voltage across IGBT #1 in active source in phase a.

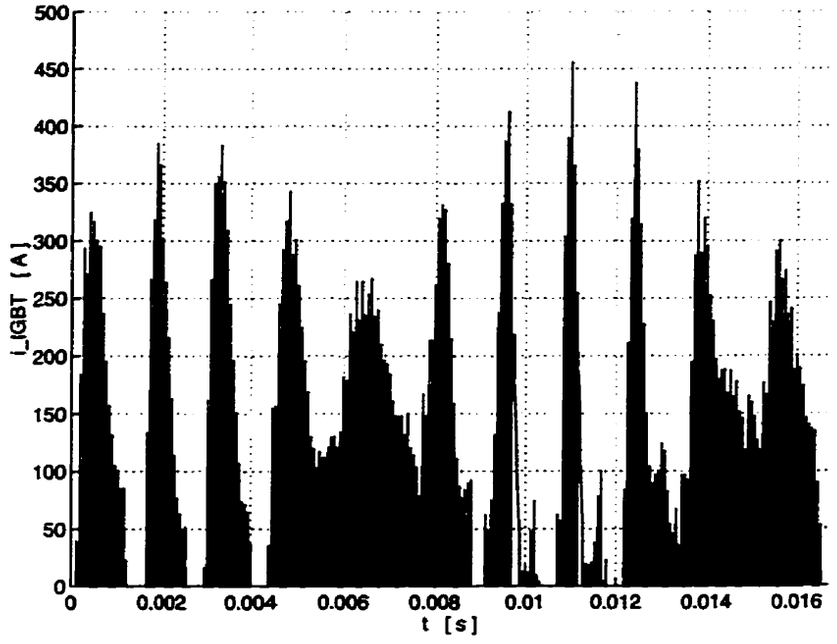

Figure 7.26: Current through IGBT #1 in active source in phase a.

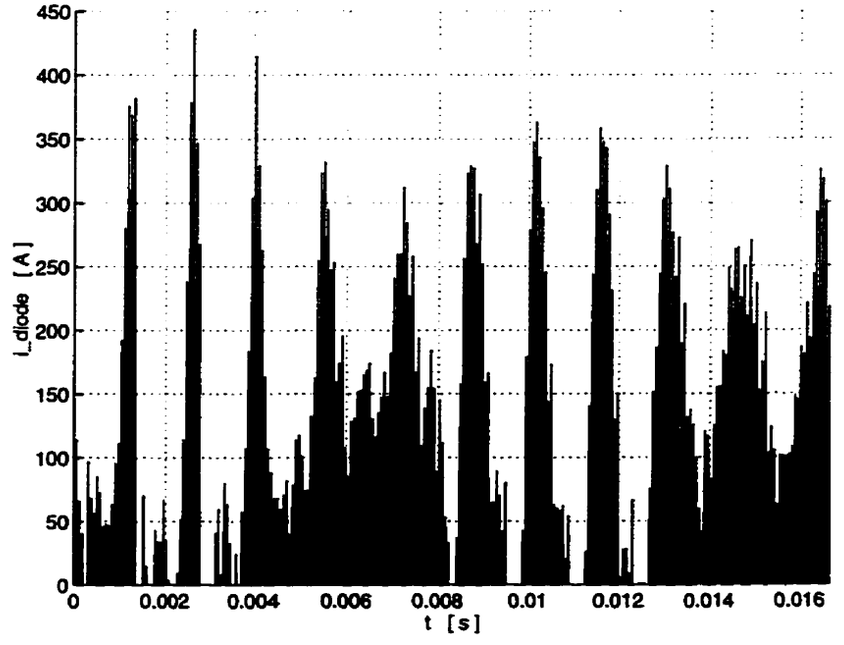

Figure 7.27: Current through anti-parallel diode #1 in active source in phase a.

7.6.2 10%-Step of the DC-line Current Order

Further to the accuracy evaluation provided by the steady-state simulation, it is necessary to evaluate the dynamic performance of the active filter when subjected to changes in the operating point. With this objective, a 10%-step is applied to the current order I_{d_o} of the current control of the DC pole. Although the same circuit modeled in the steady-state simulation is used in this simulation, the gains of the PI control, in the current control, are increased so that the change in the DC line occurs significantly fast, for a proper active-filter control evaluation. The PI gains for this simulation have been set at $K_p = 30$ and $K_i = 3000$. The increasing of these gains also provided the additional benefit of reducing the required simulation time.

The 10%-step case is simulated using the final conditions of the steady-state case as initial conditions, and the step in the current order takes place at $t = 1$ μs into the simulation. The increase in the transmitted DC power (active power) is completely supported by the unregulated AC system, and, therefore, this causes the magnitude of the voltage at the HVDC terminal and, consequently, the shunt capacitor bank currents, to be reduced. The system is simulated for 100 ms, enough time to show the performance of the active filter during the most critical period. Figure 7.28 shows that the 10%-increase in the line currents of the HVDC converter is almost fully accomplished at the end of the simulation.

The increase in the current in the converter transformers causes the overlap angle μ to increase as well. As theoretically expected from Figure 2.7, in Chapter 2, the increase of the overlap angle causes the shape of the AC line currents to be close to those of pure sinusoids, and, therefore, reduce their harmonic content. This reduction is detected by the active-filter control, which reduces the voltage reference to the PWM inverter of the active source. Figure 7.29 shows this reference v_{ref} only in phase a for clarity, and Figure 7.30 presents the resulting change in the current through the corresponding path impedance.

The active filters in phases b and c present the same behavior as the one in phase a. The unfiltered currents in the three phases are shown in Figure 7.31. The optimal-control and reference-signal state estimation gains have been calculated from a AC line current with a different harmonic content. Therefore, although the poles of the reference signal still remain at the same frequencies, the fact that the individual

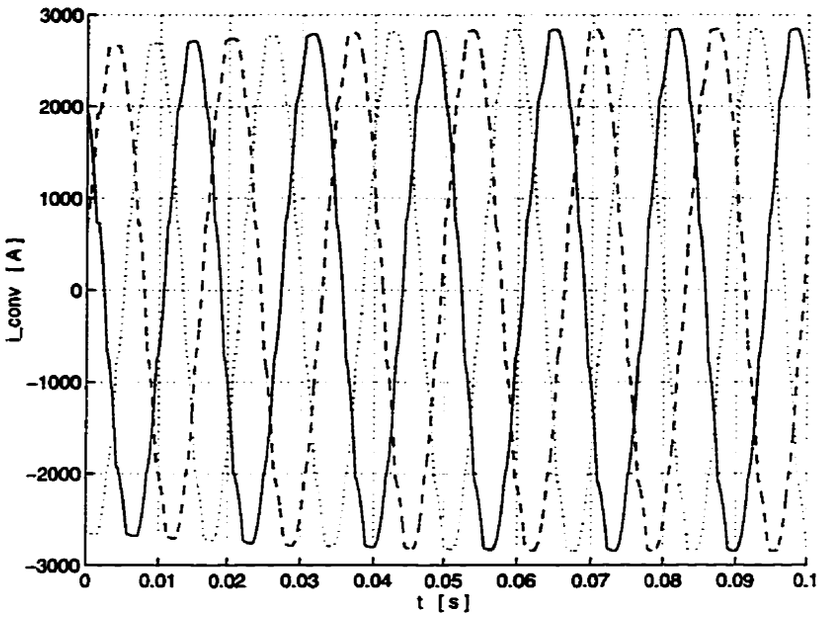

Figure 7.28: HVDC-converter AC line currents - Response to a 10%-step in the current order of the HVDC system (— phase a, — phase b, ··· phase c).

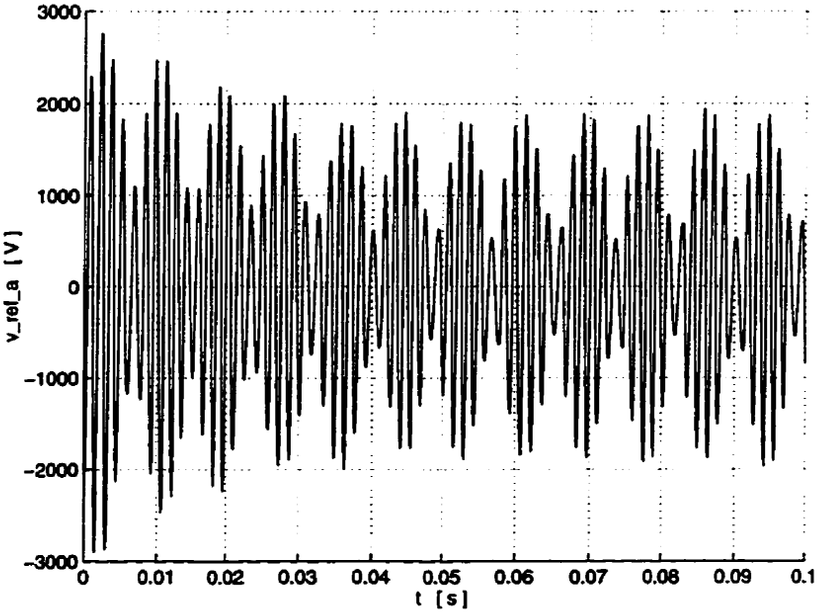

Figure 7.29: PWM voltage-reference signal for active filter in phase a - Response to a 10%-step in the current order of the HVDC system.

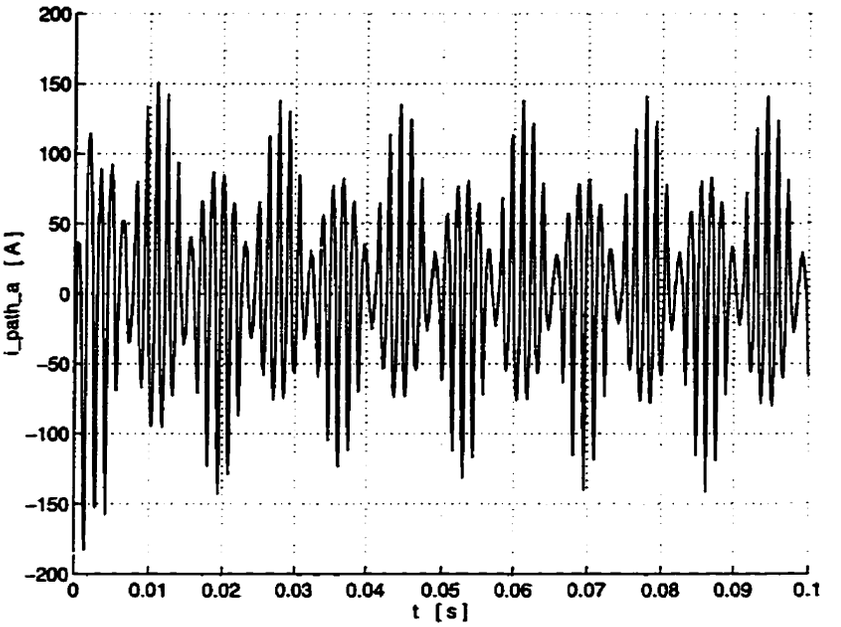

Figure 7.30: Path-impedance current in phase a - Response to a 10%-step in the current order of the HVDC system.

harmonic amplitudes and phases have changed, causes the gains to be now sub-optimal. Therefore, once the new operating point is completely established, a FFT of the reference signal should be run, and new optimal gains calculated. However, it can be noticed from Figure 7.31 that, although the active filtering is not as accurate during the change in the operating point as it is during the steady-state operation, the active filters still perform satisfactorily. Furthermore, Figure 7.32 shows that the shunt capacitor bank is never overloaded by the active filter, and Figure 7.33 attests that the AC-system currents do not present any significant harmonic content. The practically harmonic-free HVDC-converter-terminal voltage waveforms are shown in Figure 7.34.

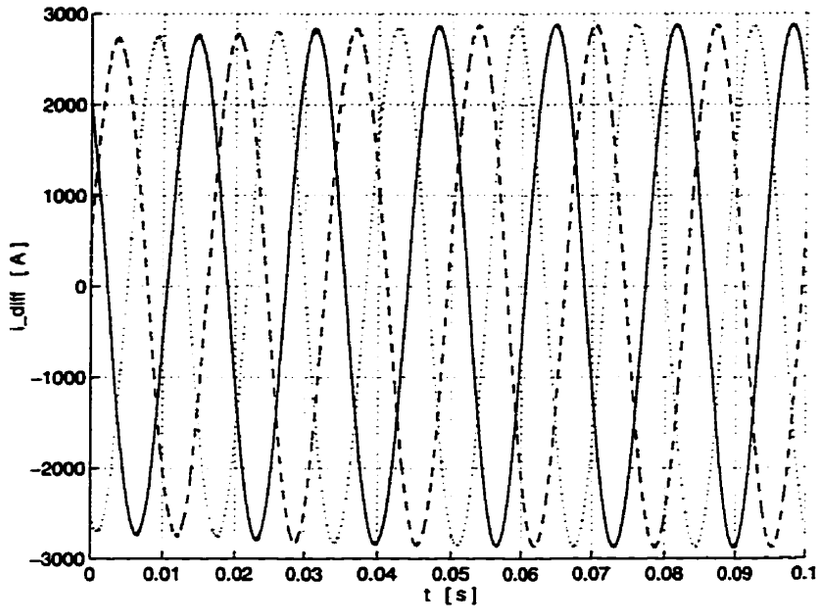

Figure 7.31: HVDC-converter AC line currents which have not been filtered - Response to a 10%-step in the current order of the HVDC system (— phase a, — phase b, ··· phase c).

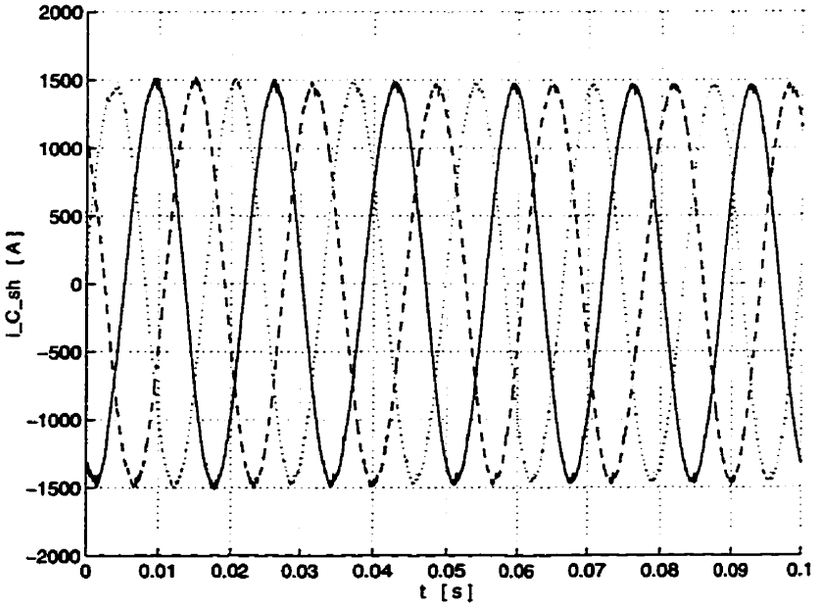

Figure 7.32: Currents through the shunt capacitor banks - Response to a 10%-step in the current order of the HVDC system (— phase a, — phase b, ··· phase c).

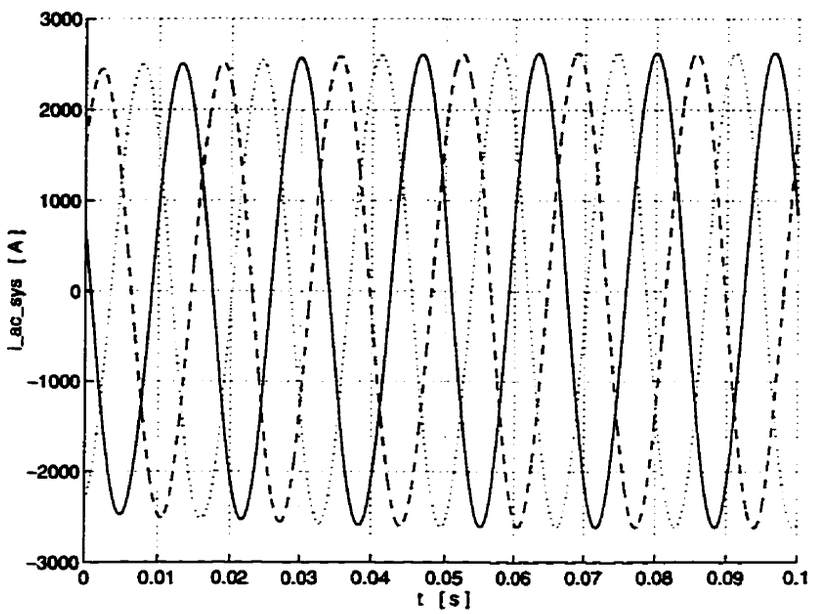

Figure 7.33: AC-system currents - Response to a 10%-step in the current order of the HVDC system (— phase a, -- phase b, ··· phase c).

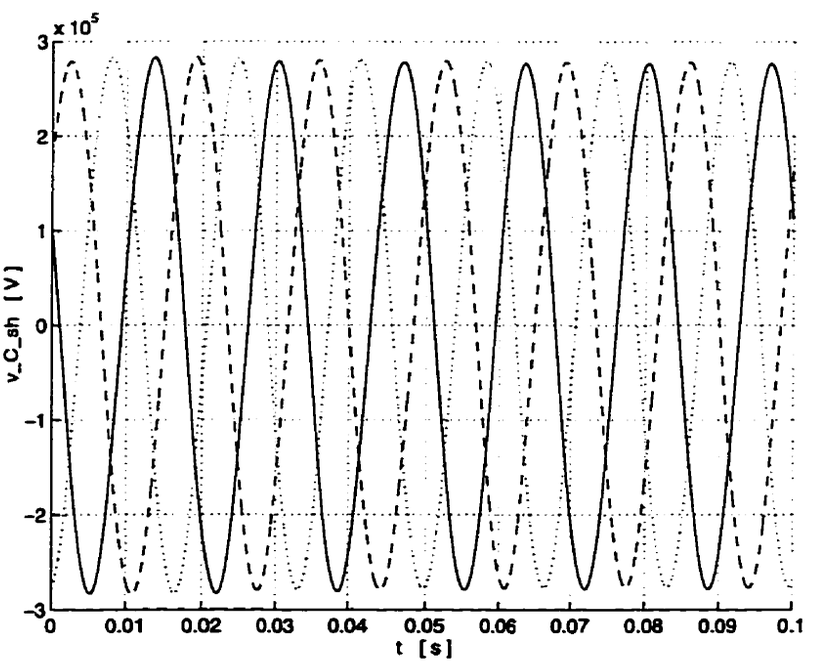

Figure 7.34: AC voltages at the HVDC-converter terminal (across the shunt capacitor banks) - Response to a 10%-step in the current order of the HVDC system (— phase a, -- phase b, ··· phase c).

Chapter 8

Conclusions

The main objective of this research has been to devise a new AC active-filter scheme that is suitable for HVDC applications. In the light of the different drawbacks, presented in some previously proposed schemes and concepts, the active filtering topology and control scheme for this thesis have been successfully demonstrated as a contribution in AC filtering for HVDC systems. The research has concentrated on the fundamental theoretical problems rather than the hardware implementation and economics. The simulations included in this thesis may be considered as an improvement on the previous works for having considered a considerably accurate model of the HVDC converter station, together with its most important basic controls, and a reasonably complex (from the operation point-of-view) AC system. Specific conclusions are as follows:

- The proposed path impedance successfully reduced the rating requirements of the active source to only voltage and current levels specifically required by the harmonic active filtering and provided an electrically inexpensive path for the injected harmonic currents. The level required by the application to the CIGRÉ benchmark HVDC system is possible to be met by a single connection of presently available IGBT switches if a low turns-ratio matching transformer is used (e.g., $a = N_1/N_2 = 5$). Higher current ratings can be obtained by using parallel connected IGBTs. The ongoing developments in power semiconductor devices will soon allow more relaxed voltage and current rating constraints for the power level required by this application. Differently from previous proposals,

the topology, together with the estimation-based control-scheme implemented, conferred the active filter a voltage-source characteristics. Besides providing means to smoothly respond to abrupt changes in the operating point of the HVDC system, the voltage-source characteristics of the active filter also allowed further reduction in the voltage and current ratings of the active source.

- It has been shown that the proposed active filter can accurately reduce the amount of harmonics supplied by the AC system to negligible values, displaying a far superior performance than that of passive filtering. Yet, the injected current has negligible switching frequency harmonics and does not overload the HVDC-converter-station shunt capacitor in steady-state operation or during changes in the operating point as has been reported on previous work.

- Although only the characteristic harmonics have been actively filtered, the topology and the control scheme implemented present a wide bandwidth. The topological and control concepts, being able to include filtering capability of virtually any non-characteristic harmonics by means of modifications concerning only software parameters, can also be considered as an improvement on previous works.

- The research has revealed that active filtering for AC-side HVDC harmonics is more complicated than simple classical feedback control for compensation of individual harmonics. Where multiple harmonic elimination is to be achieved, it has been concluded that proper filtering, dynamic response and stability are more demanding and lead to a multi-variable state-space approach.

- In common with other potential applications of modern feedback control to power systems, the issue of practical feasibility and robustness are of concern. This thesis has concentrated on exploring the effectiveness of this new approach, achieved significant theoretical improvement on previous proposals, and does put it in the context of a practical method of connection to the DC system. For the limited test cases achieved, the active-filter concept has been shown to be effective, sufficiently encouraging for practical implementation to be explored.

- The optimal-control strategy is robust in that it naturally rejects disturbances in any oscillation modes other than those determined by the harmonics being

actively filtered, and that it can be used with a path impedance exhibiting different impedance characteristics. The response to a step in the current order of DC-line current of the HVDC link is smooth and does not cause overvoltages or overcurrents in any of the elements of the active filter or the HVDC bus terminal. The controllability of this active device has the important potential to provide an enhancement of the system stability during the occurrence of any non-fundamental-frequency dynamic phenomenon. Furthermore, the temporary use of the lossy linear region of the IGBT's characteristic may also be considered during contingent operations.

- In an eventual practical implementation, measuring devices and microprocessors must meet the speed and accuracy requirements of the control scheme. The most demanding task of the control scheme is the Fourier analysis of the reference signal and the solution of the algebraic Riccati equation. Since the alterations in the state of the AC/DC system happen in a relatively large time span, the microprocessors time constraints are very relaxed. The fact that the control gains might have sub-optimal values between these calculations does not pose problems. Equally, all the state estimations can be accomplished with simple functions like integrators, adders and multipliers.

- The nature of the control scheme demands that the states of the AC-system network be estimated. This would imply that further real-time processing should be responsible for the topology and state estimation of the AC system. This is not a significant processing requirement because the AC-network topology changes happen at a relatively slower rate than the control process.

- Since the chosen switching rate is only about five times larger than the 47th and 49th harmonics, these cannot be accurately actively filtered. It is also probable that an increase of the PWM switching, and consequent losses, would not compensate for the accurate filtering of these negligible harmonics. Although this situation might change with further increase of the power levels of HVDC systems, these two harmonic currents could well be left to be passively filtered by the station shunt capacitor bank, instead of providing the circuit with an extra impedance to the ground, in parallel with the matching transformer, as in previous work.

- The proposed scheme does not require any specially-designed converter transformer (as in the earliest proposal), and the necessary measuring devices are already available in an HVDC converter terminal.

- Unlike all previous proposals, the passive elements of the active filter do not include resistors, and, except for inherent element losses, the switching losses are the only ones to supplied by the AC system. It is believed that the use of a rectifier as the means for supplying the active-filter losses provides a better dynamic performance than the energy-storing devices proposed in some of previous works.

- The obvious drawback of the proposed path impedance is the requirement to increase the amount of capacitors in the filter yard of the HVDC converter station. However, future operation performance requirements and lower harmonic generation limits in power systems will lead to considering the higher performance provided by active filters in the design of AC filters for HVDC converter stations. As exposed in Chapter 5, all the flexibilities and better performance that come with the decoupling of the filtering and reactive supply tasks might be worth a potential increase in the initial cost. Further, the probable use of unity-power-factor converters in the future would exempt the use of the shunt capacitor bank and also encourage the use of the proposed path impedance.

- Transient variations in the AC-system frequency would cause the phase corrector filter in the PLL to be mistuned. Therefore, in practice, a second VCO, with the same dynamic characteristic as the one which output has its phase compared to the reference signal, but with its output relatively shifted by $\frac{\pi}{2}$ radians from the main one, should be preferred.

Suggestions for Future Work

The proposed decoupling of the filtering and reactive power support gives rise to many different studies relating these two functions. What follows are just the most immediate visions.

- The performance of the proposed control scheme should be tested with the occurrence of non-characteristic harmonics, and special attention should be paid to the potential AC/DC harmonic instability presented by the CIGRÉ HVDC benchmark system.

- Additional control loops could be added to the active filter to have its ability to counteract the so called "ambient" harmonics tested.

- The use of the proposed active-filter topology, being well suited for sub-harmonic frequencies, could prove to be very useful for counteracting subsynchronous oscillations.

- The active-filter capability of delivering control actions in any non-fundamental frequency should be explored. These studies could, for example, verify its ability to minimize the effects of some switching transients like those of capacitors and transformers.

Appendix A

The Test-System Data

The DC System

Nominal DC voltage:	$V_d = 500$ kV
Nominal DC current:	$I_d = 2$ kA
Nominal firing angle:	$\alpha = 15°$
Nominal overlap angle:	$\mu = 23.1745°$
Smoothing reactance:	$L_s = 497.33$ mH
Nominal Active Power:	$P_d = 1000$ MW
Nominal Reactive Power:	$Q_d = 535.21$ MVAr

DC line

Length:	1,300 km
Resistance:	0.027936 mΩ/km
Inductance:	1.863544 mH/km
Capacitance:	0.008337 μF/km

Converter Transformers (Linear Single-Phase Units)

Nominal power: $S = 199.3333$ MVA

Nominal primary voltage: $V_1 = 199.1858$ kV

Nominal primary current: $I_1 = 1.0007$ kA

Leakage reactance: $X_{leak} = 0.18$ p.u.

Coupling coefficient: 0.9991

Excitation current: $i_{exc} = 0.01$ p.u.

Y-Y bank

Nominal secondary voltage: $V_2 = 121.9652$ kV

Nominal secondary current: $I_2 = 1.6343$ kA

Nominal turns ratio: $a = \frac{N_2}{N_1} = 0.6123$

Y-Δ bank

Nominal secondary voltage: $V_2 = 211.2500$ kV

Nominal secondary current: $I_2 = 0.9436$ kA

Nominal turns ratio: $a = \frac{N_2}{N_1} = 1.0606$

The AC System

Nominal converter line voltage: $V_{l_{conv}} = 345.110$ kV

Nominal converter line current: $I_{l_{conv}} = 1.8975$ kA

$\theta_{conv} = -28.1561°$

Nominal AC-system line voltage: $V_{l_{sys}} = 373.319$ kV

Appendix B

State Estimation as an Optimization Problem

Suppose the noise $w(t)$ in the measured signal is white (uncorrelated from instant to instant), gaussian (all the probabilistic information about the noise is given in the covariance of the noise) and has zero mean (as is usual in practice). This means that

$$E[w(t)] = 0 \qquad \text{for all } t \tag{B.1}$$

$$E[w(t)w(\sigma)^T] = S\delta(t-\sigma) \qquad \text{for all } t \text{ and } \sigma, \tag{B.2}$$

where S is a constant positive scalar (stationary noise). It is also assumed that $\tilde{\mathbf{x}}_{aug}(t_i)$ is a gaussian random variable with zero mean, covariance P_i and independent of $w(t)$:

$$E[\tilde{\mathbf{x}}_{aug}(t_0)] = 0 \tag{B.3}$$

$$E[\tilde{\mathbf{x}}_{aug}(t_0)\tilde{\mathbf{x}}_{aug}(t_0)^T] = P_0 \tag{B.4}$$

$$E[\tilde{\mathbf{x}}_{aug}(t_0)\mathbf{w}(t)^T] = 0 \qquad \text{for all } t. \tag{B.5}$$

The optimal estimator will be aiming for the least variance of the estimated state (and, consequently, output). That is, for a given state, a measurement β of the output $\tilde{\mathbf{y}}(t)$, $t_i \leq t \leq t_f$, is desired such that

$$E\left\{[b\tilde{\mathbf{x}}_{aug}(t_1) - \beta]^2\right\} = 0 \tag{B.6}$$

is minimum. Then β is the minimum variance estimate of $b\tilde{\mathbf{x}}_{aug}(t_f)$. It can be shown that, since all the random variables involved are gaussian with zero mean, β is the

result of linear operations on $\tilde{\mathbf{y}}(t)$:

$$\beta = \int_{t_i}^{t_f} [s(t; b, t_f)\tilde{\mathbf{y}}(t)]dt. \tag{B.7}$$

Therefore, for arbitrary b and $t_f \geq t_i \geq -\infty$, the problem is that of finding a function of time $s(t; b, t_f)$ such that

$$E\left\{\left[b\tilde{\mathbf{x}}_{aug}(t_f) - \int_{t_i}^{t_f} [s(t; b, t_f)\tilde{\mathbf{y}}(t)]dt\right]^2\right\} = 0 \tag{B.8}$$

is minimized. Then, once $s(t; b, t_f)$ has been found, a minimum variance of $b\tilde{\mathbf{x}}_{aug}(t_f)$ will be exactly

$$\int_{t_i}^{t_f} [s(t; b, t_f)\tilde{\mathbf{y}}(t)]dt, \tag{B.9}$$

which makes use of signal measurements until $t = t_f$. To be able to achieve this as an on line procedure, this problem will be transformed into one of an optimal regulator problem. The expected value can be shown to be able to be written as the following quadratic performance index:

$$E\left\{\left[b\tilde{\mathbf{x}}_{aug}(t_f) - \int_{t_i}^{t_f} [s(t; b, t_f)\mathbf{y}(t)]dt\right]^2\right\} = \mathbf{r}(t_i)^T P_i \mathbf{r}(t_i) + \int_{t_i}^{t_f} [\mathbf{r}(t)^T \mathbf{Q}\mathbf{r}(t) + \mathbf{s}(t)^T \mathbf{R}\mathbf{s}(t)]dt, \tag{B.10}$$

where the right-hand side, opposed to the left-hand side, is completely deterministic. Matrices $\mathbf{P}_i$ and $\mathbf{Q}$ are symmetric, nonnegative definite, and $\mathbf{R}$ is positive definite, $\mathbf{s}(t)$ is arbitrary, and $\mathbf{r}(t)$ has the same dimension as $\tilde{\mathbf{x}}_{aug}(t)$ and is given by

$$\dot{\mathbf{r}}(t) = -\mathbf{A}_{aug}^T \mathbf{r}(t) + \mathbf{C}_{aug}^T \mathbf{s}(t), \qquad \mathbf{r}(t_f) = b. \tag{B.11}$$

Therefore, the problem of chosing $s(\cdot)$ to minimize the left side of B.10 is the same as the deterministic problem of chosing it to minimize the right side subjected to (B.11). However, regarding the optimal regulator problem, there is in this case, a backward time characteristic. That is, the boundary condition on $\mathbf{r}(t)$ occurs at the final time t_f instead of at the initial time t_i and the first term of the right side of the

equality is at the initial time, as opposed to that of the regulator problem, where it could be used to define the final value (usually close to zero) of the states. Creating the auxiliary variable $\hat{t} = -t$ and defining new vectors $\hat{\mathbf{s}}(\hat{t}) = \mathbf{s}(t)$, $\hat{\mathbf{r}}(\hat{t}) = \mathbf{r}(t)$ the performance index becomes

$$V = \hat{\mathbf{r}}(\hat{t}_i)^T \mathbf{P}_i \hat{\mathbf{r}}(\hat{t}_i) + \int_{\hat{t}_f}^{\hat{t}_i} [\hat{\mathbf{r}}(\hat{t})^T \mathbf{Q} \hat{\mathbf{r}}(\hat{t}) + \hat{\mathbf{s}}(\hat{t})^T \mathbf{R} \hat{\mathbf{s}}(\hat{t})] d\hat{t}, \tag{B.12}$$

where $\hat{t}_f \leq \hat{t}_i$ and the constraint equation is

$$\dot{\hat{\mathbf{r}}}(\hat{t}) = \mathbf{A}_{aug}^T \hat{\mathbf{r}}(\hat{t}) - \mathbf{C}_{aug}^T \hat{\mathbf{s}}(\hat{t}), \qquad \hat{\mathbf{r}}(\hat{t}_f) = b. \tag{B.13}$$

If $\hat{\mathbf{P}}(\hat{t})$ is the solution for the differential Riccati equation

$$-\frac{d\hat{\mathbf{P}}(\hat{t})}{d\hat{t}} = \hat{\mathbf{P}}(\hat{t}) \mathbf{A}_{aug}^T + \mathbf{A}_{aug} \hat{\mathbf{P}}(\hat{t}) - \hat{\mathbf{P}}(\hat{t}) \mathbf{C}_{aug}^T \mathbf{R}^{-1} \mathbf{C}_{aug} \hat{\mathbf{P}}(\hat{t}) + \mathbf{Q}, \qquad \hat{\mathbf{P}}(\hat{t}_i) = \mathbf{P}_i, \tag{B.14}$$

the following optimal control law achieves the minimization of the Performance Index B.12 subjected to B.13:

$$\hat{\mathbf{s}}(\hat{t}) = \mathbf{R}^{-1} \mathbf{C}_{aug} \hat{\mathbf{P}}(\hat{t}) \hat{\mathbf{r}}(\hat{t}) \tag{B.15}$$

Since matrices $\hat{\mathbf{P}}(\hat{t})$ and $\mathbf{Q}$ are nonnegative definite and $\mathbf{R}$ is positive definite, from the regulator theory, $\hat{\mathbf{P}}(\hat{t})$ exists for all $\hat{t} \leq \hat{t}_i$, is symmetric and nonnegative definite. Now, defining $\mathbf{P}(t) = \hat{\mathbf{P}}(\hat{t})$ when $\hat{t} = -t$, implies that $\mathbf{P}(t)$ is the solution for the following Riccati differential equation for all $\hat{t} \geq \hat{t}_i$ and is also symmetric and nonnegative definite:

$$-\frac{d\mathbf{P}(t)}{dt} = \mathbf{P}(t) \mathbf{A}_{aug}^T + \mathbf{A}_{aug} \mathbf{P}(t) - \mathbf{P}(t) \mathbf{C}_{aug}^T \mathbf{R}^{-1} \mathbf{C}_{aug} \mathbf{P}(t) + \mathbf{Q}, \qquad \mathbf{P}(t_f) = \mathbf{P}_i \tag{B.16}$$

consequently,

$$\mathbf{s}(t) = \mathbf{R}^{-1} \mathbf{C}_{aug} \mathbf{P}(t) \mathbf{r}(t). \tag{B.17}$$

Now, substituting this second expression for function $\mathbf{s}(t)$ into the the originally stated interdependence between $\mathbf{s}(t)$ and $\mathbf{r}(t)$ (equation B.11) yields

$$\dot{\mathbf{r}}(t) = -\mathbf{A}_{cst}^T(t) \mathbf{r}(t), \qquad \mathbf{r}(t_f) = \mathbf{b}, \tag{B.18}$$

where

$$\mathbf{A}_{est} = \mathbf{A}_{aug} - \mathbf{P}(t)\mathbf{C}_{aug}^T\mathbf{R}^{-1}\mathbf{C}_{aug}. \tag{B.19}$$

Therefore an expression for $\mathbf{r}(t)$ is

$$\mathbf{r}(t) = \boldsymbol{\phi}_{est}^T(t_f, t)\mathbf{b}, \tag{B.20}$$

where $\boldsymbol{\phi}_{est}(t_f, t)$ is the associated transition matrix. Consequently, from the second expression relating $\mathbf{s}(t)$ and $\mathbf{r}(t)$ the final shape of function $\mathbf{s}(t)$ is explicitly

$$\mathbf{s}(t) = \mathbf{R}^{-1}\mathbf{C}_{aug}\mathbf{P}(t)\boldsymbol{\phi}_{est}^T(t_f, t)\mathbf{b}. \tag{B.21}$$

This function $\mathbf{s}(\cdot)$, finally, minimizes the probabilistic problem and satisfies the above expression given that $\mathbf{P}(t)$ is the solution of the last differential Riccati equation.

It can be shown that the minimum value of the deterministic problem (right side of equation B.10) is $\mathbf{b}^T\mathbf{P}(t_f)$. Once function $\mathbf{s}(t)$ has been obtained,

$$\int_{t_i}^{t_f} [\mathbf{s}(t)\tilde{\mathbf{y}}(t)]dt = \mathbf{b}\tilde{\mathbf{x}}^*(t_f), \tag{B.22}$$

the minimized expected value is

$$E\left\{\left[\mathbf{b}\tilde{\mathbf{x}}_{aug}(t_f) - \mathbf{b}\tilde{\mathbf{x}}_{aug}^*(t_f)\right]^2\right\} = \mathbf{b}\mathbf{P}(t_f)\mathbf{b}, \tag{B.23}$$

and since $\mathbf{b}$ is arbitrary, it ultimately yields

$$E\left\{\left[\tilde{\mathbf{x}}_{aug}(t_f) - \tilde{\mathbf{x}}_{aug}^*(t_f)\right]\left[\tilde{\mathbf{x}}_{aug}(t_f) - \tilde{\mathbf{x}}_{aug}^*(t_f)\right]^T\right\} = \mathbf{P}(t_f). \tag{B.24}$$

Therefore, $\mathbf{P}(t_f)$ is a measure of the error between $\tilde{\mathbf{x}}_{aug}(t_f)$ and its estimated value $\tilde{\mathbf{x}}_{aug}^*(t_f)$ (error covariance). Again, it is the steady state condition that is relevant to the filtering problem, that is, $t_i \to -\infty$. Since the plant and noise are time invariant, the value of $\mathbf{P}(t)$ as $t_i \to -\infty$ is time invariant and can be computed as $\bar{\mathbf{P}} = \lim_{t\to-\infty}\mathbf{P}(t)$ where $\mathbf{P}(t)$ satisfies the differential Riccati equation (equation B.14) with initial condition $\mathbf{P}(0) = \mathbf{0}$ and $\mathbf{P}$ is the solution to the algebraic Riccati equation

$$\mathbf{P}\mathbf{A}_{aug}^T + \mathbf{A}_{aug}\mathbf{P} - \mathbf{P}\mathbf{C}_{aug}^T\mathbf{R}^{-1}\mathbf{C}_{aug}\mathbf{P} + \mathbf{Q} = \mathbf{0}. \tag{B.25}$$

The gain of the optimal estimator is also constant:

$$\mathbf{K}_{est} = -\mathbf{P}\mathbf{C}_{aug}^{T}\mathbf{R}^{-1}. \tag{B.26}$$

The optimal estimator system is then a time invariant system with the following form:

$$\dot{\tilde{\mathbf{x}}}_{aug}^{*}(t) = \mathbf{A}_{aug}\tilde{\mathbf{x}}_{aug}^{*}(t) + \mathbf{K}_{est}\left[\mathbf{C}_{aug}^{T}\tilde{\mathbf{x}}_{aug}^{*}(t) - \tilde{\mathbf{y}}(t)\right], \tag{B.27}$$

or

$$\dot{\tilde{\mathbf{x}}}_{aug}^{*}(t) = \mathbf{A}_{aug}\tilde{\mathbf{x}}_{aug}^{*}(t) - \mathbf{K}_{est}\tilde{\mathbf{y}}(t). \tag{B.28}$$

It can be shown that the requirements that the pair $\left(\mathbf{A}_{aug}, \mathbf{C}_{aug}^{T}\right)$ be completely observable and that $\mathbf{Q}$ be chosen as $\mathbf{Q} = \mathbf{C}_{aug}^{T}\mathbf{C}_{aug}$ ensure this system is asymptotically stable (eigenvalues of $\mathbf{A}_{est}$ with negative real parts).

References

[1] J. Arrilaga, D. A. Bradley, and P. S. Bodger, *Power System Harmonics*. John Willey & Sons, 1985.

[2] T. E. Calvery and C. H. Stanley, "AC filter calculations particuarly regarding non-characteristic harmonics," in *International Symposium on HVDC Technology - Sharing the Brazilian Experience*, no. 2-2, (Rio de Janeiro, RJ, Brazil), March 20th - 25th, 1983.

[3] M. Etezadi-Amoli and T. Florence, "Voltage and current harmonic content of a utility system - a summary of 1120 test measurements," *IEEE Transactions on Power Delivery*, vol. 5, no. 3, pp. 1552 – 1557, July, 1990.

[4] T. C. Shuter, H. T. Vollkommer Jr., and T. L. Kirkpatrick, "Survey of harmonic levels on the American electric power distribution system," *IEEE Transactions on Power Delivery*, vol. 4, no. 4, pp. 2204 – 2213, October, 1989.

[5] B. K. Bose, *Modern Power Electronics - Evolution, Technology, and Applications*. John Willey & Sons, 1992.

[6] A. Domijan, "Formation of a strategy for energy development and utilization with power electronic conversion technologies: A southeast U.S.A. regional approach," *IEEE Transactions on Energy Conversion*, vol. 7, no. 1, pp. 49 – 56, March, 1992.

[7] K. Reichert and B. E. Wirth, "Analysis of harmonics and their effect on power systems," *Brown Boveri Review*, no. 1/2, pp. 41 – 46, 1984.

[8] C. K. Duffey and R. P. Stratford, "Update of harmonic standard IEEE-519 IEEE recommended practices and requirements for harmonic control in elec-

tric power systems," in *Annual Petroleum and Chemical Industry Conference*, no. PCIC-88-7, (Dallas, TX, USA), pp. 1618 – 1624, September 12th - 14th, 1988.

[9] A. V. Johansson and A. Ekstrom, "Telephone interference criteria for HVDC transmission lines," *IEEE Transactions on Power Delivery*, vol. 4, no. 2, pp. 1408 – 1421, April, 1989.

[10] A. Robert, "Connection of harmonic producing installation in AC high voltage networks with particular reference to HVDC," *Electra*, no. 149, pp. 73 – 86, 1993.

[11] CIGRÉ Working Group 14.17 - "Semiconduntor Power Devices", "Semiconductor power devices for use in HVDC and FACTS controllers," *Draft*, no. D SC14, June, 1996.

[12] H. Sasaki and T. Machida, "A new method to eliminate AC harmonic currents by magnetic flux compensation - considerations on basic design," *IEEE Transactions on Power Apparatus and Systems*, vol. PAS - 90, no. 5, pp. 2009 – 2019, September/October 1971.

[13] J. Arrilaga, *High Voltage Direct Current Transmission.* Peter Peregrinus Ltd., 1983.

[14] H. Sasaki and T. Machida, "Transient analysis of harmonic curent elimination by magnetic flux compensation," *IEEE Transactions on Power Apparatus and Systems*, vol. PAS-93, pp. 669 – 675, March/April, 1975.

[15] H. Sasaki and T. Machida, "An economic evaluation of the AC harmonic curent elimination method by magnetic flux compensation," *IEEE Summer Meeting*, 1978.

[16] L. Gyugyi and E. C. Strycula, "Active AC power filters," *IEEE Industry Applications Society Annual Meeting*, pp. 529 – 535, 1976.

[17] N. Mohan, H. A. Peterson, W. F. Long, G. R. Dreifuerst, and J. J. Vithayathil, "Active filters for AC harmonic suppression," *IEEE/PES Winter Meeting*, vol. PAS-96, no. A 77 026-8, pp. 1068–1069, July/August, 1977.

[18] G. R. Dreifuerst, *AC Harmonic Filtering Using Controlled Current Injection.* PhD thesis, University of Wisconsin-Madison, 1981.

[19] N. Mohan, "Modified high-pass filters for HVDC converter terminals," in *IEEE/PES Summer Meeting*, no. A 79 423-5, (Vancouver, BC, Canada), July 15 - 20, 1979.

[20] F. Z. Peng, H. Akagi, and A. Nabae, "A new approach to harmonic compensation in power systems - a combined system of series active and shunt passive filters," *Electrical Engineering in Japan*, vol. 110, no. 5, pp. 88 – 99, 1990.

[21] C. Wong, N. Mohan, S. E. Wright, and K. N. Mortensen, "Feasibility study of AC and DC active filters for HVDC converter terminals," *IEEE Transactions on Power Delivery*, vol. 4, no. 4, pp. 2067 – 2075, October, 1989.

[22] T.-N. Le, M. Pereira, K. Renz, and G. Vaupel, "Active damping of resonances in power systems," *IEEE Transactions on Power Delivery*, vol. 9, no. 2, pp. 1001 – 1008, 1994.

[23] F. Z. Peng, H. Akagi, and A. Nabae, "A combined system of shunt passive and series active filters - stability and compensation characteristics," *Electrical Engineering in Japan*, vol. 110, no. 5, pp. 122 – 130, 1990.

[24] F. Z. Peng, H. Akagi, and A. Nabae, "A new approach to harmonic compensation in power systems - a combined system of shunt passive and series active filters," *IEEE Transactions on Industry Applications*, vol. 26, no. 6, pp. 983 – 950, November/December 1990.

[25] H. Fugita and H. Akagi, "Combined system of a series active filter and a shunt passive filter - an optimum design of the shunt passive filter," *Electrical Engineering in Japan*, vol. 113, no. 2, pp. 91 – 101, 1993.

[26] H. Akagi, Y. Kanazawa, and A. Nabae, "Generalized theory of the instantaneous reactive power in three-phase circuits," in *Proceedings J. I. E. E. IPEC (International Power Electronics Conference)*, (Tokyo), pp. 1375 – 1386, 1983.

[27] H. Fugita and Y. Akagi, "A practical approach to harmonic compensation in power systems - series connection of passive and active filters," in *IEEE Industry*

Applications Society Annual Meeting, vol. 2, (Seattle, WA, USA), pp. 1107 – 1112, October 7th - 12th, 1990.

[28] H. Fugita, Y. Akagi, and A. Nabae, "Control schemes and compensation characteristics of an active filter connected in series to a passive filter," *Electrical Engineering in Japan*, vol. 110, no. 5, pp. 131 – 140, 1990.

[29] I. Takahashi and Y. Omura, "High-power active filter using LC-tuned filter," *Electrical Engineering in Japan*, vol. 113, no. 3, pp. 135 – 143, 1993.

[30] E. H. Watanabe and L. A. S. Pilotto, "Series active filter for the DC side of HVDC transmission systems," *Proceedings J. I. E. E. IPEC (International Power Electronics Conference)*, no. Tokyo, Japan, pp. 1024 – 1030, April, 1990.

[31] W. Zhang, G. Asplund, A. Aberg, U. Jonsson, and O. Loof, "A test installation in the Konti-Skan DC link at Lindome converter station," *IEEE Transactions on Power Delivery*, vol. 8, no. 3, pp. 1599 – 1606, July, 1993.

[32] W. Zhang and G. Asplund, "Active DC filter for HVDC systems," *IEEE Computer Applications in Power*, pp. 40 – 44, January 1994.

[33] M. Pereira, K. Sadek, N. Christl, P. Luetzelberg, and H. Huang, "Active filtering of DC-side harmonics of HVDC systems with passive elements," in *ICPST*, (Beijing, China), October, 1994.

[34] B. J. Cory (editor), *High Voltage Direct Current Convertors and Systems*. Macdonald & Co. Ltd., 1965.

[35] E. W. Kimbark, *Direct Current Transmission*, vol. 1. Willey-Interscience, 1971.

[36] E. Uhlmann, *Power Transmission by Direct Current*. Springer-Verlag, Berlin/ Heidelberg, 1975.

[37] R. Witzmann, W. Schultz, K. Krueger, S. Koetschau, and A. Mukherjee, "Analysis of non-characteristic harmonics of a large HVDC transmission system and comparison with site tests," in *AC and DC Power Transmission*, no. 345, (London, UK), pp. 384 – 389, September 17th - 20h, 1991.

[38] K. H. Kruger and B. Kulicke, "Non-characteristic harmonics in a high voltage direct current-converter station caused by system and firing angle asymetry," *Siemens Forsch. - u. Entwickl. - Ber*, vol. 11, no. 5, pp. 241 – 244, 1992.

[39] J. Reeve and P. C. S. Krishnayya, "Unusual current harmonics arising from high-voltage DC transmission," *IEEE Transactions on Power Apparatus and Systems*, vol. PAS-87, no. 3, pp. 883 – 893, March, 1968.

[40] J. Reeve and J. Baron, "Harmonic DC line voltages arising from HVDC power conversion," *IEEE Transactions on Power Apparatus and Systems*, vol. PAS-89, no. 7, pp. 1619 – 453, September/October, 1970.

[41] N. L. Shore, G. Andersson, A. P. Canelhas, and G. Asplund, "A three-pulse model of DC-side harmonic flow in HVDC systems," *IEEE Transactions on Power Delivery*, vol. 4, no. 3, pp. 1945 – 1954, July, 1989.

[42] J. D. Ainsworth, "Harmonic instability between controlled static converters and AC networks," *Proceedings of the IEE (London)*, vol. 114, pp. 949 – 957, July, 1957.

[43] L. Hu and R. Yacamini, "Harmonic transfer through converters and HVDC links," *IEEE Transactions on Power Electronics*, vol. 7, no. 3, pp. 514 – 525, July, 1992.

[44] E. V. Larsen, D. H. Baker, and J. C. McIver, "Low-order harmonic interactions on AC/DC systems," *IEEE Transactions on Power Delivery*, vol. 4, no. 1, pp. 493 – 501, January, 1989.

[45] R. H. Lasseter, F. W. Kelley Jr., and C. B. Lindh, "DC filter design methods for HVDC systems," *IEEE Transactions on Power Apparatus and Systems*, vol. PAS-96, no. 2, pp. 571 – 578, March/April, 1977.

[46] A. P. Canelhas, S. de Azevedo Morais, B. Bergdahl, and M. Drumond, "AC filter design of the Itaipu HVDC converter stations," in *International Symposium on HVDC Technology - Sharing the Brazilian Experience*, no. 2-5, (Rio de Janeiro, RJ, Brazil), March 20th - 25th, 1983.

[47] M. Szechtman, T. Wess, and C. V. Thio, "First benchmark model for HVDC control studies," *Electra*, no. 135, pp. 54 – 73, April, 1991.

[48] M. Szechtman, T. Wess, and C. V. Thio, "A benchmark model for HVDC system studies," in *AC and DC Power Transmission*, no. 345, (London, UK), pp. 374 – 378, September 17th - 20th, 1991.

[49] J. Rittiger, "Digital simulation of HVDC transmission and its correlation to simulator studies," in *AC and DC Power Transmission*, no. 345, (London, UK), pp. 414 – 416, September 17th - 20th, 1991.

[50] T. T. Nguyen, "Optimal harmonic filter design procedure," *Electric Power Systems Research - Switzerland*, vol. 23, no. 3, pp. 217 – 226, May, 1992.

[51] N. Gothelf, P. Lundin, and M. Rubinstein, "X-filter - a computer program for optimizing filter circuits," *ABB Review - Switzerland*, no. 5, pp. 31 – 38, May, 91.

[52] S. Lefebvre, "HVDC controls for system dynamic performance," *IEEE Transactions on Power Systems*, vol. 6, no. 2, pp. 743 – 752, May, 1991.

[53] J. Reeve and J. A. Baron, "Harmonic interaction between HVDC converters and AC power systems," *IEEE Transactions on Power Apparatus and Systems*, vol. PAS-90, no. 6, pp. 2785 – 2793, November/December, 1971.

[54] J. Reeve and T. S. Rao, "Dynamic analysis of harmonic interaction between AC and DC power systems," *IEEE Transactions on Power Apparatus and Systems*, vol. PAS-93, no. 2, pp. 640 – 646, March/April, 1974.

[55] A. E. Hammad, "Analysis of second-harmonic instability for the Chateauguay HVDC/SVC scheme," *IEEE Transactions on Power Delivery*, vol. 7, no. 1, pp. 410 – 415, January, 1992.

[56] X. Jiang and A. M. Gole, "An energy recovery filter for HVDC systems," in *IEEE/PES Winter Meeting*, (Columbus, OH, USA), January 31st - February 5th, 1993.

[57] M. Szechtman, T. Wess, and C. V. Thio, "The CIGRÉ benchmark model - a new proposal with revised parameters," *Electra*, no. 157, December, 1994.

[58] P. F. de Toledo, H. Porangaba, M. Z. Taam, F. S. de Oliveira Frontin, D. Menzies, and K. Eriksson, "Itaipu HVDC transmission system - dynamic performance of bipole I," in *CIGRÉ Symposium*, no. 200-09, (Boston, USA), pp. 699 – 741, 1987.

[59] R. S. Burwen, "Kilowatts on order," *IEEE Spectrum*, pp. 32 – 37, February, 1993.

[60] G.-H. Choe and M.-H. Park, "A new injection method for AC harmonic elimination by active power filter," *IEEE Transactions on Industrial Electronics*, vol. 35, no. 1, pp. 141 – 147, February, 1988.

[61] H. Kawahira, T.Nakamura, S.Nakazawa, and M.Nomura, "Active power filter," in *Proceedings J. I. E. E. IPEC (International Power Electronics Conference) - IEE Japan*, vol. 2, (Tokyo, Japan), pp. 981 – 992, March 27th - 31st, 1983.

[62] S. M. Williams and R. G. Hoft, "Implementation of current source inverter for power line conditioning," in *IEEE Industry Applications Society Annual Meeting*, vol. 2, (Seatle, WA, USA), pp. 1073 – 1080, October 7th - 12th , 1990.

[63] S. Fokuda and M. Yamaji, "Design and characteristics of active power filter using current source converter," in *IEEE Industry Applications Society Annual Meeting*, vol. 2, (Seattle, WA, USA), pp. 965–970, October 7th - 12th , 1990.

[64] H. Sasaki and T. Machida, "Transient analysis of harmonic current elimination method by AC magnetic flux compensation," in *IEEE/PES Summer Meeting*, no. T 73 412-4, (Vancouver, BC, Canada), pp. 669 – 675, July 15th - 20th, 1973.

[65] S. Madangopal and J. J. Cathey, "Supression of converter introduced harmonic currents using a forced-commutated cycloconverter," *IEEE Transactions on Energy Conversion*, vol. 5, no. 4, pp. 632 – 639, December, 1990.

[66] V. Rajagopalan, A. Jacob, A. Sevigny, T. N. Nguy, and L. Audy, "Harmonic currents compensation scheme for electrical distribution systems," in *International Federation of Automatic Control - IFAC*, (Lausanne, Switzerland), pp. 683 – 690, September 12th - 14th, 1983.

[67] V. C. Fitermann, F. Hillenbrand, and C. Landgraf, "Ein regelverfahren zur aktiven filterung in der starkstromtechnik," *Regelungtechnik*, vol. 8, pp. 263 – 270, 1982.

[68] R. C. Dodson, P. D. Evans, H. T. Yazdi, and S. C. Harley, "Compensating for dead-time degradation of PWM inverter waveforms," *Proceedings of the IEE (London)*, vol. 137, no. 2, pp. 73 – 81, 1990.

[69] B. K. Bose, "Recent advances in power electronics," *IEEE Transactions on Power Electronics*, vol. 7, no. 1, pp. 2 – 16, January, 1992.

[70] B. K. Bose, "Evaluation of modern power semiconductor devices and future trends of converters," *IEEE Transactions on Industry Applications*, vol. 28, no. 2, pp. 403 – 413, March/April, 1992.

[71] Toshiba Coorporation - Semiconductor Group, "GTR module (IGBT)," *Data Book*, vol. 3506D-A, 1992.

[72] B. J. Baliga, M. Chang, P. Shafer, and M. W. Smith, "The insulated gate transistor (IGT) - a new power switching device," *IEEE / IAS Annual Meeting Conference Records*, pp. 794 – 803, 1983.

[73] G. Kaplan, "Industrial electronics - 1997 technology analysis & forecast," *IEEE Spectrum*, pp. 79 – 83, January, 1997.

[74] F. Brichant, *Force-commutated inverters : design and industrial applications.* Oxford : North Oxford Academic, 1984.

[75] M. Athans and P. L. Falb, *Optimal Control - An Introduction to the Theory and Its Applications.* MacGraw-Hill, Inc., 1966.

[76] B. D. O. Anderson, "Design of feedback laws for linear control systems," in *National Radio and Electronics Engineering Convention*, (Sidney, Australia), pp. 4 – 5, 1967.

[77] A. P. Sage, *Optimum Systems Control.* Prentice Hall, Inc., 1977.

[78] R. E. Kalman, "When is a linear control system optimal?," *Journal of Basic Engineering*, pp. 51 – 60, March, 1964.

[79] B. D. O. Anderson and J. B. Moore, *Design of Feedback Laws for Linear Control Systems.* Prentice Hall, Inc., 1971.

[80] E. Kreindler, "On the linear optimal servo problem," *International Journal on Control*, vol. 9, no. 4, pp. 465 – 472, 1969.

[81] M. F. Moad, "A simple approach to obtaining network state equations," *Proceedings of the IEEE*, pp. 80 – 81, January, 1971.

[82] C.-T. Chen, *Linear System Theory and Design.* Holt, Rinehart and Winston, Inc., 1984.

[83] V. Rajagopalan, *Computer-Aided Analysis of Power Electronic Systems.* New York : Dekker, 1987.

[84] R. E. Kalman, "Mathematical description of linear dynamical systems," *SIAM Journal on Control*, vol. 1, no. 2, pp. 152 – 193, 1963.

[85] R. E. Kalman, "Contributions to the theory of optimal control," in *Bol. Soc. Matem.*, (Mexico), pp. 102 – 119, 1960.

[86] R. E. Kalman and J. R. Bertram, "Control system analysis and design by the second method of Lyapunov," *Journal of Basic Engineering*, vol. 82, no. 2, pp. 371 – 400, June, 1960.

[87] LaSalle and S. Lefschetz, *Stability by Lyapunov's Direct Method with Applications.* Academic Press Inc., New York, 1961.

[88] B. A. Francis, O. A. Sebakhy, and W. M. Wonham, "Synthesis of multivariable regulators: The internal model principle," *Applied Mathematics & Optimization*, vol. 1, no. 1, pp. 64 – 86, 1974.

[89] B. A. Francis and W. M. Wonham, "The internal model principle for multivariable regulators," *Applied Mathematics & Optimization*, vol. 2, no. 2, pp. 170 – 194, 1975.

[90] S. Hara, Y. Yamamoto, T. Omata, and M. Nakano, "Repetitive control system: A new type servo system for periodic exogenous signals," *IEEE Transactions on Automatic Control*, vol. 33, no. 7, pp. 659 – 668, July, 1988.

[91] T. Egami and T. Tsuchiya, "PWM inverter control by system control theory," in *International Federation of Automatic Control - IFAC*, (Tallinn, Estonia, USSR), pp. 527 – 532, 1990.

[92] J. J. D'Azzo and C. H. Houpis, *Linear Control System Analysis and Design: Conventional and Modern.* MacGraw-Hill, Inc., 1988.

[93] M. A. Appleton, "The automatic synchronization of triode oscillators," *Cambridge Philosophical Society Proceedings*, vol. 21, pp. 231 – 249, 1922 - 1923.

[94] S. G. Margolis, "The response of a phase-locked loop to a sinusoid plus noise," *Institution of Radio and Electronics Transactions*, no. IT 3, p. 136, June, 1957.

[95] J. D. Ainsworth, "The phase-locked oscillator - a new control system for controlled static converters," *IEEE Transactions on Power Apparatus and Systems*, vol. PAS-87, no. 3, pp. 859 – 865, March, 1968.

[96] S. C. Gupta, "Phase-locked loops," *Proceedings of the IEEE*, vol. 63, no. 2, pp. 291 – 306, February, 1975.

[97] R. E. Best, *Phase-Locked Loops: Theory, Design and Applications.* MacGraw-Hill, Inc., 1984.

[98] J. B. Encinas, *Phase-Locked Loops.* Chapman and Hall, 1993.

[99] M. Hasler and J. Neirynck, *Electric Filters.* Artech House, Inc., 1986.

[100] Analogy, Inc., *SABER Manual.* release 2.2, Analogy, Inc., 1989.